Application of artificial intelligence methods for the design and development of aircraft flight control laws

by

Seyed Mohammad HOSSEINI

MANUSCRIPT-BASED THESIS PRESENTED TO ÉCOLE DE TECHNOLOGIE SUPÉRIEURE IN PARTIAL FULFILLMENT FOR THE DEGREE OF DOCTOR OF PHILOSOPHY
PH.D.

MONTREAL, JANUARY 29, 2025

ÉCOLE DE TECHNOLOGIE SUPÉRIEURE
UNIVERSITÉ DU QUÉBEC

BOARD OF EXAMINERS

THIS THESIS HAS BEEN EVALUATED

BY THE FOLLOWING BOARD OF EXAMINERS

Ms. Ruxandra Botez, Thesis Supervisor
Department of Systems Engineering at École de technologie supérieure

Mr. Georges Ghazi, Thesis Co-supervisor
Department of Systems Engineering at École de technologie supérieure

Mr. René Jr Landry, President of the Board of Examiners
Department of Electrical Engineering at École de technologie supérieure

Mr. Tony Wong, Member of the jury
Department of Systems Engineering at École de technologie supérieure

Mr. Adrian Hiliuta, External independent evaluator
CMC Electronic

THIS THESIS WAS PRENSENTED AND DEFENDED

IN THE PRESENCE OF A BOARD OF EXAMINERS AND PUBLIC

JANUARY 17, 2025

AT ÉCOLE DE TECHNOLOGIE SUPÉRIEURE

ACKNOWLEDGMENT

I would like to express my deepest gratitude to those who assisted me in completing this Ph.D. journey.

First and foremost, I would like to express my deepest gratitude to my esteemed supervisor, Professor Ruxandra Botez. Her exceptional supervision and guidance at the Research Laboratory of Applied Research in Active Controls, Avionics, and Aeroservoelasticity (LARCASE) have been instrumental in my Ph.D. studies. Her support, invaluable insights, and patience have been pivotal for my research. Her confidence in my potential and continuous encouragement have not only enriched my academic experience but have also significantly contributed to my personal growth. I am profoundly thankful for all her mentorship, for every piece of advice, and for believing in me.

I would also like to extend my heartfelt thanks to my co-supervisor, Professor Georges Ghazi. Beyond being an exceptional supervisor, he has been a true friend who has guided me through my challenges. His invaluable insights, thoughtful feedback, and continuous encouragement have significantly enriched this thesis. His commitment to providing a robust academic environment and your readiness to assist me have been greatly appreciated. Thank you so much for always being there to support me.

Special thanks also go to Professor René Jr Landry and Professor Tony Wong. Their insightful comments and constructive feedback on my research proposal (Ph.D. exam) have been instrumental in realizing my research goals. Their guidance has significantly contributed to the quality and depth of this work.

To my family, words cannot express the depth of my gratitude for their unwavering support and love. To my parents, their sacrifices, patience, endless encouragement, and believes in my dreams have been my most significant source of strength. To my brother, his constant

cheer and understanding have been vital to this journey. This accomplishment would not have been possible without their support and faith in me.

Thanks are dues to the Canada Research Chair of Aircraft Modelling and New Simulation Technologies for funding this research, which greatly helped me during my Ph.D., as Professor Ruxandra Botez is the Canada Research Chair Tier 1 Holder in Aircraft Modeling and New Simulation Technologies. I appreciate the CAE Inc. team and Mr. Oscar Carranza Moyao for their support in the development of the Research Aircraft Flight Simulator (RAFS) of the Cessna Citation X at the LARCASE laboratory. Many Thanks to Odette Lacasse of the ETS for her support.

Lastly, I acknowledge all those who have contributed, directly or indirectly, to this thesis. Their support, whether through discussions, feedback, or simply being there, has been essential in this academic endeavor.

Thank you all for being an integral part of this journey.

Application des méthodes d'intelligence artificielle pour la conception et le développement des lois de commande de vol des aéronefs

Seyed Mohammad HOSSEINI

RESUMÉ

Le développement des systèmes de commande de vol a toujours été le sujet principal de nombreuses études. Dans l'aviation affaires, il est essentiel d'assurer la stabilité, la robustesse et la précision des performances de suivi de l'avion pour garantir la sécurité et le confort des passagers pendant toute la durée du vol, en particulier pendant la phase de croisière et dans différents environnements de vol. Bien que les contrôleurs conventionnels aient révélé des performances précises, l'intégration de méthodologies basées sur l'intelligence artificielle peut offrir de nouvelles caractéristiques et capacités pour concevoir la prochaine génération de systèmes de commande de vol. Ces contrôleurs peuvent être développés sans connaissance explicite du modèle de l'avion, gérer efficacement les incertitudes et contrôler l'avion avec une configuration de paramètres fixes pour toutes les conditions de vol tout en présentant des caractéristiques adaptatives améliorées.

Le premier article présente d'une méthodologie de contrôle constituée d'un système de logique floue adaptative de type 1 (T1AFLS) et d'un système de contrôle à mode glissant (SMC), pour contrôler le taux de tangage de l'avion et la vitesse vraie (TAS) pendant la croisière. Le T1FLS calcule la dynamique inconnue, qui est mises à jour à l'aide de lois d'adaptation conçues par le théorème de Lyapunov. Ensuite, les fonctions approximées sont intégrées dans le système SMC afin de garantir les performances de suivi de l'avion et d'assurer sa stabilité et sa robustesse.

Dans la deuxième étude, le T1FLS a été transformé en un système de logique floue de type 2 amélioré à l'aide d'un nouvel algorithme de réduction de son type. Cet approximateur bidimensionnel peut gérer un plus grand nombre d'incertitudes. Les résultats de la simulation pour cette combinaison du T2FLS, du système de contrôle adaptatif et du système SMC ont été comparés à ceux du système T1AFSMC. Cette comparaison a révélé que les performances du T2AFSMC étaient légèrement supérieures à celles du T1AFSMC. Les deux systèmes T2AFSMC, utilisés à la fois pour le système de contrôle du taux de tangage et de la TAS, ont pu répondre aux exigences de stabilité, de robustesse et de performance de suivi de l'avion pendant la croisière.

La troisième étude porte sur le développement d'un système de commande pour le mouvement latéral de l'avion. Le T2AFLS a été utilisé pour calculer la dynamique de l'avion pendant le vol. Cet approximateur a été utilisé dans un système de commande à mode glissant super-torsion, amélioré par des lois d'adaptation et par l'algorithme d'optimisation par essaims particulaires (PSO) pour trouver les valeurs des paramètres de la commande à mode glissant. Pour traiter la dynamique couplée du roulis et du lacet, un contrôleur intégral

agissant sur l'angle de dérapage de l'avion a été utilisé pour stabiliser indirectement la vitesse de lacet. Ces méthodologies ont été évaluées pour s'assurer que les performances de l'aéronef étaient appropriées, et le mode de glissant adaptatif à super-torsion a donné de meilleurs résultats que le contrôle optimisé du mode de glissement par le PSO.

Dans la quatrième étude, un système de commande de pilote automatique a été développé en utilisant une combinaison de réseaux neuronaux récurrents flous (FRNN) et des systèmes SMC. Dans ce système de pilotage automatique, deux réseaux neuronaux récurrents flous distincts ont été développés pour les modes de vitesse verticale et de maintien de l'altitude, ce qui a permis d'obtenir une très bonne approximation de la dynamique de l'avion. De plus, deux contrôleurs à mode glissant ont été appliqués pour permettre à l'avion de suivre les signaux de référence dans chaque mode. Ce système de pilotage automatique utilise un nouvel algorithme de transition flou pour passer d'un mode à l'autre.

Les méthodologies proposées ont été validées l’aide d’une plateforme de simulation non linéaire, développée par les données de vol provenant d'un simulateur de vol d'avion de recherche de niveau D pour l'avion Cessna Citation X au LARCASE, dans différentes conditions de vol.

Mots-clés: Système de contrôle de vol, Avionique, Système Flou, Commande par mode glissant, Commande adaptative, FLS, Réseaux neuronaux récurrents, FRNN, Cessna Citation X, Turbulence, PSO, Lyapunov

Application of artificial intelligence methods for the design and development of aircraft flight control laws

Seyed Mohammad HOSSEINI

ABSTRACT

The development of flight control systems has always been the main topic of many studies. In commercial aviation, it is essential to address the aircraft stability, robustness, and precise tracking performance for ensuring passengers safety and comfort during the entire flight, especially during the cruise phase and in different flight environments. While conventional controllers revealed accurate performance, integrating Artificial Intelligence (AI)-based methodologies can offer new features and capabilities to shape the next generation of flight control systems. These controllers can be developed without explicit knowledge of the aircraft model, effectively handle uncertainties, and control the aircraft with a fixed parameter configuration for all flight conditions with enhanced adaptive characteristics.

The first article discusses a control methodology constructed by a Type One Adaptive Fuzzy Logic System (T1AFLS) and a Sliding Mode Control system (SMC), to control the aircraft pitch rate and True AirSpeed (TAS) during cruise. The T1FLS approximates the unknown dynamics, which are updated using adaptation laws designed by the Lyapunov theorem. Subsequently, the approximated functions are integrated into the SMC system to guarantee the aircraft tracking performance and ensure its stability and robustness.

In the second article, the T1FLS was converted to an enhanced Type Two FLS using a new Type Reduction algorithm. This two-dimensional approximator can handle a larger number of uncertainties. The simulation results for this combination of the T2FLS, Adaptive Control, and SMC systems were compared with those of the T1AFSMC system. The comparison revealed that the T2AFSMC performed slightly better than the T1AFSMC. Both T2AFSMC systems, employed for both pitch rate and TAS control systems, could meet the requirements of aircraft stability, robustness, and tracking performance during the cruise.

The third study focused on developing a control system for the aircraft lateral motion. The T2AFLS was employed to approximate the unknown aircraft dynamics during flight. This approximator was employed within a super-twisting sliding mode control system, enhanced with adaptation laws, and with the Particle Swarm Optimization (PSO) algorithm to find parameter values of the sliding mode controller. To address the coupled roll and yaw dynamics modes, an Integral controller acting on the aircraft sideslip angle, was used to stabilize the yaw rate indirectly. These methodologies were evaluated to ensure the aircraft appropriate performance, and the Adaptive super-twisting sliding mode performed better than the PSO-based sliding mode control.

In the fourth paper, an autopilot control system was developed using a combination of Fuzzy Recurrent Neural Network (FRNN) and SMC systems. In this autopilot system, two separate FRNNs were developed for both Vertical Speed and Altitude Hold modes, which dynamically approximate the aircraft dynamics. Moreover, two sliding mode controllers were applied to allow the aircraft to track the reference signals in each mode. This autopilot system employed a new fuzzy transition algorithm to switch between these modes.

The proposed methodologies were validated by a nonlinear simulation platform, developed using flight data from a Level D research aircraft flight simulator for the Cessna Citation X aircraft at the LARCASE in different flight conditions.

Keywords: Flight control system, Avionics, Fuzzy System, Sliding Mode Control, Adaptive Control, FLS, Recurrent Neural Network, FRNN, Cessna Citation X, Turbulence, PSO, Lyapunov

TABLE OF CONTENTS

Page

LIST OF TABLES

Page

LIST OF FIGURES

Page

LIST OF ABREVIATIONS

AOA	Angle Of Attack
MSE	Mean Squared Error
RMSE	Root Mean Squared Error
MAE	Mean Absolute Error
ISE	Integral Squared Error

LIST OF SYMBOLS

a	Angle of attack (deg)
α_{damp}	Inertia damping parameter in the PSO
A, B, M, N	Unknown Function
$\hat{A}, \hat{B}, \widehat{M}, \widehat{N}$	Approximated functions
c_1	Personal acceleration in the PSO
c_2	Social acceleration in the PSO
C_h, C_d	Positive constants
C_f, C_g	Positive constants
C	Positive design parameter
$D(t), d(t)$	Turbulence
$e_{q,v,p}$	Tracking errors
$e_{(vs\ h)}$	Tracking errors
$\hat{F}_{(vs\ h)}$	Functions approximated by the MFRNN
$\tilde{F}_{(vs\ h)}$	Approximation error

$F_{(vs\,h)}, G_{(vs\,h)}$	Unknown nonlinear functions
$\hat{f}_{q,v}, \hat{g}_{q,v}$	Approximated functions
F_A , G_{Bmax}	Positive constants
$g_{(h\,vs)}$	Positive constant
g	Adaptation gain
G_b	Global best in the PSO algorithm
h_{trans}	Transition Altitude (ft)
h	Altitude (ft)
h_{ref}	Desired altitude (ft)
$h(x)$	Unknown dynamics function
$\hat{h}(x)$	Approximated dynamics function
H	Switching (reaching) term gains
$\tilde{I}_{1:m}^{n}$	Fuzzy sets
I	Positive Constant
$k_{(h\,vs)}$	Gains of the switching control laws

k_s	Scaling factor for the particle's velocity in the PSO
k	Integral control gain
L	Switching (reaching) term gains
L_D	Turbulence bound
$L_{(h\ vs)}$	Postive design parameters
L_m	Positive design parameter
L_1, L_2	Positive gains in the super twisting switching control law
m	Positive Constant
$m_{(h\ vs)}$	Mode transition coefficients
m_1, m_2	Uncertain functions
$n(x,t)$	Uncertain function
N	Positive design parameters
N_{up}, N_{lo}	Positive design parameters
p	Roll rate (Degree per second)
p_{ref}	Roll rate reference (Degree per second)

P_{b_r}	Personal best in the PSO algorithm
q	Aircraft pitch rate (deg/s)
q_{ref}, q_d	Aircraft pitch rate reference (deg/s)
r	Yaw rate (Degree per second)
r_1	Positive gain in the super twisting switching control law
R	Minimum approximation errors
$S_{q,v}$	Sliding surfaces
S_l	Sliding surface for the lateral motion
$S_{(h,vs)}$	Sliding surfaces
u_{ail}	Ailerons command signal (Degree)
u_{rud}	Rudder command signal (Degree)
u_{eq}	Equivalent control law
u_{sw}	Switching control law
$u_{eq_{(h\,vs)}}$	Equivalent control laws
$u_{sw_{(h\,vs)}}$	Switching control laws

$u_{(h\ vs)}$	Control laws for the altitude hold (h) and vertical speed (vs) modes (deg/sec)
u_{AT}	Ultimate autopilot control law (deg/sec)
U_q^{eq}, U_q^{sw}	Equivalent and switching Control laws for pitch rate control
$U_{sp}^{eq},, U_{sp}^{sw}$	Equivalent and switching Control laws for speed control
U_q^{Final}, U_{sp}	Pitch rate and speed control inputs
v	Aircraft speed (mps or m/s)
v_{ref}	True AirSpeed reference (mps or m/s)
V_t	Proposed Lyapunov candidate
V_{fuzzy}	Lyapunov term for the Type-Two Adaptive Fuzzy System
V_{sw}	Lyapunov term for the adaptive super twisting switching control law
$V(t)$	Aircraft True AirSpeed (TAS) (mps or m/s)
$V_d(t)$	Aircraft True AirSpeed (TAS) Reference (mps or m/s)
VS	Vertical Speed (ft/s)
VS_{ref}	Desired Vertical Speed (ft/s)
w	Minimum Approximation function

w_{damp}	Damping inertia in the PSO
W	Weights of the MFRNN
x	Aircraft state vector
$x_{(vs,h)}$	Inputs of the Mulitplayer Fuzzy Recurrent Neural Network (MFRNN)
X_{cg}	Center of Gravity (%)
X_{lo}, X_{up}	Lower/ Upper bounds of the Searching Range
y_{lo}, y_{up}	Lowest and highest bounds of decision variables
Z	Minimum approximation egrrors

Greek Alphabets

β	Sideslip angle (Degree)
ϵ	Minimum approximation error
$\mu_{M_i^r}$	Membership Function
$\mu_{1m}(x)\ \mu_{2n}(x)$	Gaussian membership functions
μ_{NHE}	Membership function of the Negative High Error (NHE) linguistic term
μ_{ME}	Membership function of the Medium Error (ME) linguistic term

μ_{NHE}	Membership function of the Positive High Error (PHE) linguistic term
$\mu_i^n(x_i)$	Fuzzy membership function
Λ_1	Positive design parameter
ξ	Positive design parameter
δ_1, δ_2	Arbitrary positive finite boundaries for m_1 and m_2
Ω_1,Ω_2	Acceleration parameters in the PSO
$\psi_{f_{q,v},g_{q,v}}$	Fuzzy Basis Function (FBF)
$\Psi_{up}(x)\ \Psi_{lo}(x)$	Fuzzy Basis Functions (FBF)
ρ	Positive Constants
$\theta^*_{f_{q,v},g_{q,v}}$	Optimal Adjustable Parameters
$\theta_{f_{q,v},g_{q,v}}$	Vectors of Adjustable Parameters
$\theta_{up}^T\ \theta_{lo}^T$	Fuzzy adjustable parameters vector
Θ	Adjustable parameters
$\eta_{1,2}$	Control inputs
$\eta_{sw1,2}$	Switching (reaching) control terms

$\eta_{eq1,2}$	Equivalent control terms
$\sigma_{f,g}$	Constants of adaptation laws
σ	Sliding manifold
$\sigma_{f,g}$	Constants of adaptation laws
$\gamma_{f,g}$	Gains of adaptation laws
Δ	Design parameter

Subscripts

h	Altitude
J	Number of swarm particles
l	Lateral motion
m	Number of input variables to fuzzy logic system
n	Number of fuzzy rules
p	Roll rate
p_{max}	Swarm Size in the PSO
q	Pitch rate

s	Iterations in the PSO
v	Speed
vs	Vertical Speed
lo	Lower bound
up	Upper bound
ref	Reference or desired
eq	Equivalent term
sw	Switching term
cg	Center Of Gravity

INTRODUCTION

This section is dedicated to presenting the flight control systems and their evolution over the time and then to the explanation of the problem statement which will be addressed by the solutions suggested in this research.

0.1 Evolution of the Flight Control Systems

Basically, a pilot controls the motions of an aircraft by giving appropriate commands to the control surfaces. These control surfaces can be classified into two parts: primary control surfaces (ailerons – roll motion about the longitudinal axis, elevators – pitch motion about the lateral axis, and rudder – yaw motion about the vertical axis) and secondary control surfaces, such as wing flaps, leading-edge devices, spoilers, and trim systems (Federal Aviation Administration, 2016).

Over the time, different flight control systems were developed as an interface and connection between the pilot and the control surfaces, and each of them will be briefly presented in this section.

The first generation of aircraft was equipped with mechanical flight control systems. In these systems, the yoke (or column) and the pedals were directly connected to the specific control surfaces with rods, levers, cables, and pulleys (Fielding, Varga, Bennani, & Selier, 2002). As a result, the aircraft maneuverability was highly dependent on the pilots' strength (Pratt, 2000). However, this type of flight control system is very complicated to implement and is also heavy. These two aspects are all more constraining as they increase considerably with the size and functionality of the aircraft (Atul Garg, Rezawana Islam Linda, & Tonoy Chowdhury, 2013).

Over the years, mechanical flight control systems became less and less efficient as aircraft became larger. These systems required considerable effort from the pilots to move the control surfaces, which were subject to very high aerodynamic loads, especially at high speeds.

However, the introduction of the hydro-mechanical flight control system was a significant innovation that aimed to solve these inefficiencies (Hunt, Vaughan, & Warring, 1996). This system, composed of a mechanical part to move the control surface and a hydraulic part to assist the pilot, marked a significant enhancement in the evolution of flight control systems (Edwards, Lombaerts, & Smaili, 2010 ; Hunt et al., 1996).

Since the hydro-mechanical flight control system could not effectively reduce the pilot's workload, designers have proposed to apply the Fly-by-Wire (FBW) technology in aircraft. In these systems, all pilot commands are transformed into electrical signals. These signals, sent through wires, are processed by flight control computers to command the displacement of the actuators mounted on each control surface (Atul Garg et al., 2013). Moreover, it is possible in FBW systems to automatically process the command signals from flight control computers without the pilot's intention to keep the aircraft in an equilibrium and stable position (Atul Garg et al., 2013). As stated in (Al-Lami et al., 2015 ; Collinson, 2011), the FBW system allows wing optimal performance under high aerodynamic loads without structural damage.

Moreover, since fewer mechanical and hydromechanical connections exist, drag and weight are significantly reduced. Furthermore, the FBW systems computers are responsible for checking the aircraft maneuvers during flight to keep them within authorized limits. Thus, the pilot's workload is significantly reduced. In addition to the above factors, the development of FBW systems has enabled aircraft to be controlled by flight control laws based on the pilot's command and the corresponding surface position, aircraft altitude, and airspeed to produce sufficient lift forces for a balanced flight. The controllers developed in this research will be designed for the Cessna Citation X business jet aircraft, which is equipped with Fly-By-Wire (FBW) systems.

0.2 Problem Statement

In the previous section, the evolution of the flight control systems was explained in detail. These constant developments illustrate that the aviation industry continuously seeks new solutions to enhance flight safety and efficiency. The application of Artificial Intelligence (AI) based control systems in modern aviation systems has a great potential to enhance the safety, performance, and stability of commercial aircraft. This study is dedicated to the development of AI-based control systems for the Cessna Citation X business jet aircraft, to ensure its stability and robustness, while reducing the pilot's workload under all flight conditions within the aircraft flight envelope in different motions. Reducing the pilot's workload is important because it is directly related to the occurrence of human errors, leading to aircraft accidents and incidents.

According to statistics provided by William Rankin, Ph.D., a member of Boeing's technical staff, in the early 19th century, 80% of flight accidents were caused by machine failure, and only 20% resulted from human factors (William Rankin, Ph.D., 2007). Today, these proportions have been reversed, with 80% of accidents mainly due to human errors. The reduction in machine failures demonstrates that aircraft systems have evolved considerably over time to become more reliable and efficient. However, this advancement in aircraft systems increases the complexity of the pilot's tasks to control an aircraft, due to the limitations of human perception and information processing to make appropriate decisions during flights (Maurino & Salas, 2010).

Furthermore, dealing with uncertainties is another critical issue considered in this study, which can affect aircraft performance. The term "uncertainty" in control systems refers to the lack of system information, and environmental conditions. This aspect becomes more important when a complex system such as an aircraft has to be controlled. In this case, it may be difficult to explain system performance when unexpected dynamics changes and variations occur due to environmental phenomena. In addition, uncertainties can be classified into parametric (structural) and functional (non-structural) uncertainties.

As discussed in (Åström, 2000), a control system must satisfy three main concepts:

- "Observability", which means how a system state can be determined from the measured outputs.
- "Controllability", which defines the ability to move from an initial state to a desired state in a finite time,
- "Stability" refers to the ability to achieve a bounded system output from a bounded input and to return to the equilibrium state after a disturbance.

In fact, the existing uncertainties can directly influence these three factors. These uncertainties in an aircraft system occur from the estimated model parameters, unknown and unmodeled dynamics, control surface failures, variations in operational conditions, nonlinearities linearization, aerodynamic parameter variations, and unanticipated external disturbances that adversely affect the aircraft performance (Herzallah, 2005).

As a control objective, the observability, controllability, and stability of an aircraft must be preserved while dealing with uncertainties in the design of flight control laws. This issue can be challenging due to the different operational modes of the aircraft, as they can change the pole positions in the system and, consequently, unstabilize the system in a closed loop (Resnick, 1991).

0.3 Research Motivations

To ensure aircraft stability and robustness in different maneuvers, various conventional methods have been applied to control different aircraft types over the past few years. Although these methods have produced accurate results and stable maneuvers, these controllers depend highly on the aircraft dynamics. As a result, any variation in the aircraft dynamics can affect their performance. Moreover, the recent technological advances in aircraft systems have increased the pilots' workload, which can increase the rate of errors in their decision-making.

Therefore, the sophisticated nature of aircraft automated systems and the fact that pilots must interact alone with all these systems underscore the importance of further studies on the development of intelligent control systems in aircraft.
In contrast with traditional aircraft control systems, AI-based controllers require no prior knowledge of the system, and they can learn and handle a large number of uncertainties with a single configuration in different flight conditions and environments, while conventional controllers need to switch their configurations by changing the gains and design parameters to control the aircraft in different maneuvers.

In addition, due to their generalized nature, AI-based systems can be excellent methods for designing controllers suitable for various types of aircraft. Moreover, by using AI-based control systems such as fuzzy logic systems, we can also apply human perception and knowledge to control system design by choosing appropriate linguistic variables.

On the other hand, the Neural Network based controllers are more fault tolerant as they can easily cope with small changes in the inputs, and they can be developed by considering the aircraft model as a black box.

Furthermore, as another research motivation, this research aims to ensure the stability and robustness of an aircraft in the presence of atmospheric turbulence, which are the foremost issues that need to be discussed. In control system design, turbulence has always been considered a significant challenge to achieving smooth maneuvers that satisfy both aircraft safety and passengers' comfort.

0.4 Thesis Organization

This thesis is structured in six Chapters to guide the reader through the description of the research topic and its specific contributions.

In Chapter 1, a comprehensive literature review is presented, covering the methodologies applied to various aircraft systems, starting from conventional flight control systems. The chapter concludes with the application of AI-based control systems for different aircraft types. In Chapter 2, the research objectives for this thesis are defined. The chapter provides a brief explanation of the research objectives and the related methodologies. In addition, the main contributions of each article are summarized in detail.

Chapter 3 presents the research article entitled “Novel Controller Methodology for the Cessna Citation X under Turbulence during Cruise”, published in the “Journal of Aerospace Information Systems”. This article describes the application of Type One Adaptive Fuzzy Sliding Mode Control systems designed for the longitudinal motion of the Cessna Citation X (CCX) aircraft. Chapter 4 introduces the full manuscript, "New Type-II Fuzzy Logic-Based Control System for the Cessna Citation X," also published in the *Journal of Aerospace Information Systems*. This methodology was developed for the control of the longitudinal motion of the CCX aircraft, completing the first sub-objective of this research.

Chapter 5 summarizes the application of a combination of a Type Two Adaptive Fuzzy Logic System and an enhanced Super-twisting Sliding Mode Control system for the lateral motion of the CCX aircraft, addressing the second sub-objective of this research. This article was published in the “Aerospace” journal.

Chapter 6 is dedicated to the development of an autopilot system using a Fuzzy Recurrent Neural Network (FRNN) based Sliding Mode Control system, submitted in the Aeroautical Journal.

Finally, the thesis concludes with a discussion of the results, followed by a conclusion regarding the achieved objectives and outcomes.

CHAPTER 1

Literature Review

1.1 Conventional Control Systems

The application of classical, optimal, modern, and robust control systems in aviation spans a wide range of aircraft. The methodologies introduced below were well-established to ensure reliable performance, safety, and stability of aircraft.

1.1.1 PID and Optimal Control Systems

(Deepa & Sudha, 2016) used a Proportional-Integral-Derivative (PID) control system for the pitch control of a general aviation aircraft. The gains of this PID controller were tuned with different techniques, including Zeigler–Nichols (ZN), Modified Zeigler–Nichols, Tyreus–Luyben and Astrom–Hagglund methods. A comparison of the performances of these techniques showed that the Zeigler–Nichols algorithm performed the best in determining accurate gain values to ensure aircraft stability.

(Ingabire & Sklyarov, 2019a) compared the performances of a Linear Quadratic Regulator (LQR), Linear Quadratic Gaussian (LQG), and a nonlinear control system for the pitch control of a fixed-wing Unmanned Air Vehicle (UAV). All these controllers demonstrated great performances in terms of stability margins and robustness. However, the nonlinear control system outperformed the LQR and LQG controllers in this application. (Vishal & Ohri, 2014a) suggested using the Genetic Algorithm (GA) to adjust the parameter values of the PID and LQR controllers. They showed that applying the GA to optimize the LQR controller was a more effective method for stabilizing the aircraft pitch than using the GA-based PID controller. (Chrif & Kadda, 2014) stated that using a Kalman filter as a state estimator can improve the performance of LQR and LQG control techniques in the output-feedback control of the aircraft pitch, roll and sideslip angles. By comparing the LQR and

LQG controllers, they showed that the LQG performed better under noisy conditions for controlling the longitudinal motion of the A340 aircraft.

According to (Sir Elkhatem, Engin, Pasha, Rahman, & Pillai, 2021), an LQR control system and a fractional-order integral controller, which were optimized by a simultaneous Particle Swarm Optimization (PSO) algorithm, can perform appropriately as a full-state feedback controller, achieving both robustness and stability under different levels of failures in an aircraft actuation system. This controller was developed for the pitch control of Boeing 747 aircraft, which features a non-minimum phase pitch angle dynamic. In order to control the non-minimum phase dynamics of a Planar Vertical Takeoff and Landing (PVTOL) aircraft, (Xin & Pan, 2010) employed the $\theta - D$ method instead of the state dependent Riccati equation to design a robust optimal control system to reduce the computational load. This approach effectively addressed the altitude and roll angle tracking problem while also ensuring robustness and stability.

(Yamina Boughari, Georges Ghazi, Ruxandra Mihaela Botez, & Florian Theel, 2017) optimized a Linear Quadratic Regulator (LQR) modern control system used for the Stability Augmentation System (SAS) and a Proportional-Integral (PI) controller developed for the Control Augmentation System (CAS) by a Differential Evolution (DE) algorithm for controlling the Cessna Citation X (CCX) aircraft with a minimum cost while satisfying the flight handling qualities. These authors also validated this control methodology in (Yamina, Georges, Ruxandra Mihaela, & Florian, 2017a) to obtain the linear stability margins of roll and pitch motions. In addition, the aircraft performance was evaluated using different commands such as pull-push, step, ramp inputs, and fast roll to ensure that the CCX aircraft flew within the safety limits.

1.1.2 Robust Control Systems

(Kodhanda, Kolhe, Zeru, & Talole, 2017) applied a combined control system developed using an Uncertainty and Disturbance Estimation (UDE) approach to estimate the

uncertainties and a robust input-output linearization technique to achieve the closed-loop stability of a high-performance aircraft in the presence of disturbances. This methodology allows for controlling the aircraft without having a precise aircraft model or prior knowledge about the different types of uncertainties and disturbances. In addition, (Qian Wang & Stengel, 2005) successfully implemented a stochastic robust nonlinear control system design on a high-incidence aircraft model, with the aim to encounter critical flight conditions at large angles of attack and addressing the nonlinearities inherent in the aircraft model.

(S. Li, Wang, & Tan, 2017) studied the tracking performance of a Quadrotor using an adaptive robust control system to smoothly and robustly follow the commanded trajectory. This control system could successfully deal with external disturbances and actuator saturations. Another solution for attenuating the effects of disturbance on a quadcopter was suggested by (Lu Wang & Su, 2015) who used a combination of Robust Disturbance Observer (DOB) control theory, and nonlinear feedback control system to handle the model uncertainties such as its mass, inertia, actuation system parameters and compound aerodynamics disturbances, and to stabilize a quadcopter while following the given attitude reference signal. As a fault-tolerant control system, (Trifonov, Prochazka, & Krüger, 2019) have designed a flight control system based on an H_∞ robust control system to deal with unmodeled aerodynamics uncertainties, severe faults and failures in the actuation systems, and also turbulence. This robust controller was tested on a nonlinear model of an ADMIRE aircraft.

Flying near the buildings over crowds presents challenges for UAVs and quadcopters due to adverse wind conditions. For this purpose, (Jasim & Veres, 2020) proposed to apply a robust nonlinear dynamic inversion methodology to control the attitude of a quadrotor, and a feedback position controller in the outer loop to control its lateral and vertical motions. The development of a hybrid controller, including an adaptive dynamic inversion system and robust control system for an Osprey aircraft, was evaluated by (MacKunis, Patre, Kaiser, & Dixon, 2010). High-fidelity simulation results showed that the proposed controller could handle parametric uncertainties and unknown disturbances, which led to achieving

asymptotical tracking performance. As another solution for handling the model uncertainties, (Raza, Malik, Khan, Mazhar, & Ullah, 2020) applied a feedback linearization state control system in the inner loop, and a robust controller in the outer loop along with a high-gain observer to ensure robustness against the aerodynamic uncertainties in the fixed-wing aircraft model.

To address the variations of the mass and Center of Gravity (CG) due to the fuel consumption in the linear model of the CCX aircraft, (Yamina Boughari, Botez, Ghazi, & Theel, 2017) have employed an optimized control system using the Genetic Algorithm (GA) and the Differential Evolution (DE) algorithm to achieve both robustness and stability in the longitudinal and lateral motions, with an acceptable level of handling qualities for the CCX aircraft.

To control the CCX pitch rate, (Ghazi, Rezk, & Botez, 2016) developed a two loops flight control system based on the PID methodology. In this controller, Guardian Maps theory was applied to determine the appropriate gains. Despite the simplicity of this control approach, the methodology successfully met the handling qualities required for the longitudinal motion of the CCX. Furthermore, (Ghazi & Botez, 2015b) showed that the LQR control system combined with Guardian Maps theory can satisfy robustness against the variations of aircraft Center of Gravity (CG) and mass while meeting handling qualities of the CCX lateral motion with very good results. On the other hand, (Ghazi & Botez, 2014) have found that both the Genetic algorithm and the guardian map theory are valid methodologies to obtain the optimal weighting matrices. This control methodology not only achieved robustness but also successfully met handling quality requirements for both the Lynx and CCX aircraft.

1.1.3 Sliding Mode Control System

(Lixin Wang et al., 2024) proposed a new flight control system constructed by use of several sliding mode controllers employed in two loops to achieve tracking performance of different state variables such as roll, pitch and yaw rates in the inner loop, and roll angle in the speed

axis, as well as the Angle of Attack (AOA) and sideslip angle in the outer loop. This flight control system also employed a trajectory Proportional-Integral-Derivative (PID) based control system in the outermost loop to manage the flight altitude and speed. This methodology successfully satisfied the stability margin of the closed loop system of an oblique wing aircraft during the wing skewing procedure.

(Ventura, Morales, Oliver, & Quesada, 2023) developed a dynamic sliding mode control based on the PID sliding surface for each of the altitude, directional, longitudinal, and lateral hexacopter sub-systems to guarantee its Ultimate Uniform Bound (UUB) stability using an Attractive Ellipsoid method and without an accurate knowledge about the dynamics model in the presence of bounded disturbances.

(Xiu, Liu, & Xu, 2018) improved the design of a global sliding mode control system by integrating an exponential attenuation function in the sliding surface to satisfy the robustness and to achieve a rapid rate of response in controlling the position and attitude of a rectangular four-rotor aircraft as an underactuated system containing different uncertainties.

(P. Singh, Salahudden, Giri, & Ghosh, 2022) proposed employing a sliding mode control system with a power-reaching control law developed to stabilize a Hansa-3 research aircraft across its flight envelope and to achieve its attitude control with perturbation. Using this methodology, the states reaching phase can be accelerated, and system robustness was obtained in real scenarios.

Furthermore, (Sadik Aboud, S. Abd Al-Amir, A. Alhamdany, & M. Kadhim, 2023) have shown that by optimizing the parameters of the Sliding Mode Control system using the Particle Swarm Optimization (PSO) algorithm, the tracking performances, as well as the angular positions and velocities in a Vertical Take-Off and Landing (VTOL) aircraft, could be achieved in the presence of uncertainties, while eliminating chattering. In this article, the Lyapunov and Routh methods were incorporated to prove the stability of the proposed controller.

(Bist & Sondhi, 2022) introduced a Fractional-Order Sliding Mode Controller (FOSMC) for an Unmanned Aerial Vehicle (UAV) to achieve position and speed tracking performance and to guarantee its closed-loop stability with asymptotical convergence and a minimum time delay using the Lyapunov–Razumikhin theorem. In this methodology, state variables were reconstructed by a delayed observer.

(P. Singh, Giri, & Ghosh, 2023) showed that a combination of backstepping and sliding mode control systems can effectively control both longitudinal and lateral-directional motions. This methodology incorporates a smooth switching term to stabilize the highly maneuverable both with and without side winds, while also reducing chattering.

(Zhuang, Sun, Chen, & Zeng, 2021) employed an adaptive sliding mode control system integrated with a backstepping control methodology to control the attitude of a simplified nonlinear model Boing-747 aircraft with six degrees of freedom. In this methodology, the adaptation laws were used to compensate for the disadvantages of the Sliding Mode Control (SMC) system dealing with uncertainties and disturbance. As demonstrated in the paper, this technique was effective in eliminating chattering.

To control a F-18 fighter that flies at high angles of attack and achieves smooth pitch angle and pitch rate tracking, (M. Rouyan, Varatharajoo, Eshghi, Junita Abdullah, & Suzuki, 2018) developed a linear integral SMC system for the F-18 nonlinear longitudinal model. It was found that this controller can operate better than the Integral SMC and can guarantee the aircraft global stability during the specified maneuver.

(Ijaz, Fuyang, Hamayun, & Anwaar, 2021) developed a control methodology based on a Nonlinear Dynamics Inversion method and an Adaptive Integral Sliding Mode Control (AISMC) system. This article aims at maintaining optimal flight quality at high angles of attack and it deals with disturbances and aerodynamics uncertainties. This control architecture includes an outer loop for controlling angle-of-attack, side-slip angle, and

aircraft velocity and an inner loop for the Euler angular rates, thus guaranteeing the robustness and internal dynamics stability of the aircraft. In this control system, an iterative re-weighted least square system was developed based a real-time wind tunnel data to estimate the aircraft aerodynamic forces and moments.

(Hassani, Mansouri, & Ahaitouf, 2024) developed a new attitude control system for a quadrotor based on a non-singular integral terminal sliding mode control system equipped with a super-twisting switching term and a backstepping control system to handle uncertainties and reduce the effects of perturbations. The finite-time convergence of state variables and the system stability were proven by the Lyapunov theory and experimental tests. Moreover, (Yan, Dai, Liu, Xing, & Liu, 2019) proposed a new methodology based on an adaptive super-twisting sliding mode control system to meet the trajectory tracking performance using the longitudinal model of a wing-sweep morphing aircraft. This control system robustly handled variations due to drastic changes in aerodynamic parameters, mass distribution, aerodynamic perturbations, and unknown disturbances, effectively reducing chattering. This research also revealed that the phugoid variables vary with greater values at low sweep morphing speed, while short period variables are higher at high sweep morphing speed.

Furthermore, (Matouk, Abdessemed, Gherouat, & Terchi, 2020) suggested an enhanced second-order sliding mode control system using a super twisting algorithm to obtain trajectory tracking performance and stabilization of a quadcopter. In this modified control approach, six separate control laws were developed for each roll, pitch, and yaw motion for the quadcopter position and attitude. (J. Liu, Sun, Chen, & Sun, 2020) integrated a super twisting sliding mode control system with a finite time extended state observer and a thrust vector method to control a fighter aircraft flying at a high angle of attack. By applying this methodology, the finite time system state error convergence was achieved while dealing with coupling effects, aerodynamic uncertainties, and unknown disturbances.

On the other hand, (Labbadi, Boukal, & Cherkaoui, 2020) demonstrated that integrating the fractional-order control approach into the super-twisting sliding mode flight control system can improve the performance of quadrotors. This enhancement was tested in various complex position and attitude tracking scenarios, resulting in appropriate tracking performance with rapid convergence and high robustness against stochastic perturbations, while effectively addressing uncertainties.

1.2 Artificial Intelligence (AI) Based Control Systems

The application of AI-based control systems in an aircraft was the main topic of many articles. This section mainly discusses the applications of two AI-based control methodologies such as 1) Neural Network control systems and 2) Fuzzy Logic controllers.

1.2.1 Neural Network based Control Systems

(S. Kamalasadan & Ghandakly, 2011) proposed the application of Radial Basis Function Neural Networks (RBFNN) in model reference adaptive controllers to achieve pitch rate tracking performance using a nonlinear model of a F-16 aircraft. This controller was able to robustly handle the dynamics variations and ensure the stability of the aircraft while providing highly tracking performance. (Suresh, Omkar, Mani, & Sundararajan, 2006) presented a direct adaptive neural network controller for the F-8 fighter aircraft. This control system enhanced the accuracy of the pilot's control input with both offline and online learning methods. The Neural Networks described in this article approximated the variations of the aerodynamic coefficients and control surface malfunctions.

(J. Lee & Kim, 2020) addressed variations of aerodynamics and mass properties due to the span variations in a morphing aircraft. In this article, they applied a feedforward Neural network-based nonlinear dynamic inversion control system to stabilize the aircraft by considering handling quality requirements while maintaining performance under varying conditions.

(L. Zhou, Liu, Cheng, Wang, & Fan, 2020) explained that system uncertainties and disturbances in a hypersonic aircraft model can be effectively handled using an attitude control system developed by use of an adaptive dynamic surface control and Radial Basis Function Neural Networks (RBFNNs). Using this methodology, robustness was achieved in the tracking performance of the aircraft. Morevoer, the semi-globally Uniformly Ultimate Boundedness (UUB) of this control methodology has been proven by the Lyapunov theorem.

On the other hand, to primarily address internal and external disturbances, (Shen & Xu, 2021) developed an active disturbance rejection methodology using the Adaptive Radial Basis Function (ARBF) neural network to improve the trajectory tracking performance of unmanned helicopters. This approach improved the adaptive properties of the controller, which could not be fully achieved using the extended state estimator of the classical Active Disturbance Rejection (ADR) system.

In addition, (P. Singh, Giri, & Ghosh, 2022) proposed new attitude and altitude control methodologies for a high fidelity aircraft based on RBFNN approximator and backstepping SMC system. These methodologies could guarantee the semi-global uniformly bounded stability with a minimum knowledge of the aircraft aerodynamics parameters while dealing with fast flight conditions variations.

Furthermore, (Deng, Huang, Xu, & Tao, 2023) addressed the challenges such as dealing with external disturbances and unknown nonlinear dynamics in controlling of a Vertical Take-Off and Landing (VTOL) aircraft. In their article, the VTOL nonlinearities and dynamics were approximated by RBFNNs, and the approximations were integrated into a global fast terminal sliding mode control system and adaptive control laws to obtain the tracking performance for the control of the VTOL position, and its roll angle. In order to control and guarantee the stability of a Planar Vertical Take-Off and Landing (PVTOL) aircraft in the presence of disturbances, (Zheng & Yang, 2020) proposed an enhanced Adaptive Neural Network system combined with backstepping control system. In this control system, the

neural network was trained by gradient descent algorithm to approximate the PVTOL dynamics. The gradient descent training algorithm applied in this article had a more accurate dynamics approximation than the σ-modification technique.

For the design of an event-triggered control system, (Lu et al., 2022) suggested employing a high-gain state observer, and a dynamic surface control system using neural networks to approximate the dynamics of a quadrotor. Moreover, the results of hardware-in-loop evaluations showed that robustness and tracking performance were achieved while the energy consumption and communication volume were reduced. (Oktay & Kose, 2021) investigated the operational aspects of a combined methodology using an Adaptive Deep Neural Network (ADNN) and a Proportional-Intergal-Derivative (PID) control system to address the changes in the hexacopter model dynamics and morphing states.

(Rojo Princy Andrianantara, Ghazi, & Botez, 2023) integrated an Adaptive Neural Network (ANN) controller, an online Recursive Least Squares (RLS) based dynamics inversion approximator, and a PID control system to ensure the pitch rate tracking of the CCX aircraft in different flight conditions. Similarly, (Quintin, Andrianantara, Ghazi, & Botez, 2024) showed that the same methodology may be applied to stabilize and control the lateral motion of the CCX aircraft. In addition, (Rojo P. Andrianantara, Ghazi, & Botez, 2024) also integrated a Single Hidden Layer feedforward ANN with a Model Reference Adaptive Controller (MRAC) and a Recursive Least Square (RLS) state estimator to control the pitch rate of the CCX aircraft during the cruise.

Existing literature has shown the efficiencies of the ANNs and RBFNNs in controlling different types of air vehicles. However, Recurrent Neural Networks (RNNs) offer new potentials over the traditional control systems based on ANNs and RBFNNs, such as handling time-dependent data, etc., to enhance aircraft stability and safety in aviation. Hence, a brief explanation of previous research articles is presented on the development of the RNNs, as follows:

(Juang, Chiou, & Chien, 2008) proposed to replace a classical PID controller with a real-time RNN control system for an aircraft autopilot landing system. This controller employed a Genetic Algorithm (GA) to find its optimal control parameter values. The performance of this controller was validated in the presence of severe turbulence. The controller was claimed to perform similarly to an experienced pilot during the landing of a commercial aircraft.

As another controller for the auto-landing system, (Lin & Boldbaatar, 2015) developed a Recurrent Wavelet Elman Neural Network (RWENN) for the control of a conventional aircraft. This controller incorporated a gradient descent algorithm equipped with an adaptive learning rate. This control system could handle both turbulence and partial loss of elevator surface during landing.

On the other hand, (Lin & Hsu, 2002) illustrated that a hybrid RNN-based adaptive control system, can efficiently handle the dynamics variations of wing rock motion, and it can guarantee its stability. (C.-T. Lee & Tsai, 2010) showed that Recurrent Neural Networks (RNNs) can also serve as approximators for the coupling effects of forces and moments of the ADS33 helicopter in the slalom maneuver. This RNN-based approximator was integrated into an adaptive backstepping control system to guarantee its stability and robustness in the presence of uncertainties, and to achieve tracking performance in different maneuvers. (Nivison & Khargonekar, 2017a) introduced a new training algorithm for a RNN control system of a nonlinear agile aircraft. This algorithm could satisfy the system robustness against disturbances, deal with uncertainties in aircraft aerodynamics by minimizing the amplitude of the control command signals. (S. Hosseini, Inga, Ghazi, & Botez, 2023) developed a model reference-based control system for the longitudinal motion of the CCX aircraft. In this control system, a Single Hidden Layer RNN inverse dynamics approximator was proposed whose weights were updated by two adaptation laws in order to enhance the CCX pitch rate tracking performance across different flight conditions. In addition, to reduce the steady state error, the authors suggested using a PID control system to generate an elevator command signal.

1.2.2 Fuzzy Logic based Control Systems

In many articles, fuzzy logic systems were used alone as controllers or integrated with other control methodologies to enhance aircraft performance, safety, and fault tolerance properties.

(Khan, Grigorie, Botez, Mamou, & Mébarki, 2019a) developed a three-loop control system for the actuators of a morphing wing, aimed at extending the laminar airflow, reducing the drag, and consequently reducing fuel consumption. Three control laws were developed using a combination of a PID control system and a fuzzy logic system for each actuator's position, speed, and current. Furthermore, with the same research motivation to create a novel morphing mechanism, (Iqbal, Teodor, Botez, & Andrei, 2012) proposed a control methodology based on Proportional-Derivative (PD) and fuzzy logic system. The methodologies presented in (Iqbal et al., 2012 ; Khan et al., 2019a) were validated through various wind tunnel experiments.

(Cervantes & Castillo, 2015) considered applying type 2 fuzzy control systems in a hierarchical design for controlling all control surfaces of a conventional aircraft. This methodology revealed that the aircraft was robust against uncertainties in its flight dynamics model, including turbulence. In this article, a flight simulator was used to simulate various real-world scenarios. (Castillo & Cervantes, 2014) integrated a Genetic Algorithm (GA) into Type One (T1) and Type Two (T2) Fuzzy Logic Systems (FLSs) for the pitch attitude control of a F-14 aircraft in its longitudinal motion. This research indicated that the T2 Fuzzy Logic Control System (T2FLCS) operated better than the PID and the T1FLS controllers in all simulation scenarios, especially in the presence of turbulence.

Furthermore, (X. Jiao & Jiang, 2016) suggested combining an Interval Type-Two Fuzzy Logic System (IT2FLS) with a sliding mode control system to handle the uncertainties and severe disturbances at high-speed maneuvers in the longitudinal motion of a hypersonic aircraft. Similarly, (D. J. Singh, Verma, Ghosh, & Malagaudanavar, 2022) presented a model-based Interval Type-2 Takagi–Sugeno FLS to control the longitudinal motion of a

generic research aircraft known as X-29A, which led to an improved transient performance in comparison with a Fuzzy LQR control system and an LQR control system.

The combination of a Takagi–Sugeno FLS with an adaptive control system was also employed by (Seyed Mohammad Hashemi, Botez, & Grigorie, 2020) to control an insect-inspired nano air vehicle to minimize its energy consumption in a resonance-based click mechanism. This was achieved by using Lyapunov-based adaptation laws to obtain tracking performance and to cope with the chaotic dynamics. (Swain & Sarathi, 2017) combined three control methodologies, including a fuzzy logic system, an adaptive control system, and a Proportional-Intergral (PI) control system, to achieve appropriate Angle of Attack (AOA) tracking performance in the longitudinal FOXTROT aircraft. This control methodology yielded excellent results in comparison with the conventional controllers designed using the Ziegler-Nichols (ZN), Tyreus Luyben (TL), and Extended Skogestad Internal Model (ESIMC) methods.

(Tao et al., 2016) developed a methodology using a combination of PID and fuzzy logic systems to improve the adaptability and anti-jamming capabilities of a Parrot AR Drone 2.0 quadrotor equipped with a target color detector using OpenCV. The performance characteristics of this control system were validated in the presence of wind gusts. (Khalid, Zeb, & Haider, 2019) compared the performance of a PID controller, Sliding Mode control system, and Fuzzy-PID control system for the aircraft pitch control system. This comparison demonstrated that a Fuzzy logic-based PID controller performs better in terms of signal characteristics and robustness.

On the other hand, (Pan, Zhou, Sun, & Er, 2013) proved that an adaptive fuzzy H^{∞} control system can guarantee the convergence of the tracking error to zero in an aircraft wing rock suppression. In this methodology, the composite adaptation system was employed to avoid performance degradation of fuzzy logic approximator due to the H^{∞} control system. (Sukumar Kamalasadan & Ghandakly, 2007) employed a set of Fuzzy Reference Model

Adaptive Control systems to control the pitch rate of a high-performance F-16 aircraft without the need for explicit system identification.

Fault-tolerant control is another important topic that has been studied in many articles to guarantee aircraft safety under fault conditions.

To address the faults such as loss-of-effectiveness in actuation system, (Ziquan Yu et al., 2022) proposed using a fixed-time prescribed performance function for each unmanned airship (UA) in a formation group to transform the synchronization errors into new tracking errors. These error variables were used in the fractional order-based sliding-mode control system combined with Recurrent Fuzzy Neural Network (RFNN) systems to learn the unknown dynamics of multiple UAs. The experimental results obtained from a hardware-in-loop evaluation demonstrated the enhanced control performance of the proposed methodology. This research methodology was further extended by (Ziquan Yu, Yang, et al., 2023) incorporating an Adaptive Fractional Order-based Type Two Recurrent Fuzzy Neural Network equipped with an event-triggered system to reduce the communication load in a group of UAVs.

Furthermore, a combination of Fuzzy Logic and Adaptive Control systems was successfully developed for controlling hypersonic and business aircraft. (Hušek & Narenathreyas, 2016) showed that the good tracking performance in longitudinal motion can be achieved by the use of a Takagi–Sugeno fuzzy system for a LET L410 aircraft in the presence of its model uncertainties and disturbances, such as turbulence.

To deal with a wide range of uncertainties, such as control uncertainties, external disturbances, and errors existing in the dynamics model, (S.M. Hashemi & Botez, 2022) integrated a model referenced LQR control system, a robust adaptive control system, with a Takagi-Sugeno Fuzzy Logic system to guarantee the very good tracking performance of the Hydra Technologies UAS-S4 Ehecatl.

In addition, (X. Jiao & Jiang, 2015) the X-24 B longitudinal motion was controlled using a combination of Type-2 Takagi–Sugeno–Kang (TSK) fuzzy logic and sliding mode control. This control system guaranteed the aircraft's stability and generated smooth control input signals during the cruise.

(Rong, Han, & Zhao, 2014) proposed two direct and indirect control methodologies, including adaptive fuzzy control systems, for managing the wing rock motion of an aircraft at high angles of attack. These controllers employed an Extended Sequential Adaptive Fuzzy Inference System (ESAFIS), which approximated the aircraft dynamics on-line in the indirect control system. In contrast, the ESAFIS estimated the ideal control law in the direct control system. The authors also integrated a sliding mode control system to reduce the modeling error in both the direct and indirect methodologies.

The capabilities of the fuzzy logic system to guarantee the robustness and stability of an aircraft during landing were also evaluated, as follows:

Controlling an aircraft under severe wind is very important during landing, especially in the presence of a failure in the actuation system. To address this issue, (Hai-Jun Rong, Guang-Bin Huang, Sundararajan, & Saratchandran, 2006) combined a TSK fuzzy neural network (TSK-FNN) model with 4 classical feedback control systems to control the aircraft altitude, airspeed, heading angle, and sideslip rate. The TSK-FNN was trained using an Online Sequential Fuzzy Extreme Learning Machine methodology. Moreover, (Xing & Ai, 2023) developed a fault-tolerant adaptive fuzzy sliding mode to deal with both disturbance and dynamics variations during the landing of a carrier-based hypersonic aircraft. Similarly, (H. Li, Su, & Jiang, 2015) presented an asymmetric variable universe adaptive fuzzy control system, that achieved an accurate and stable landing maneuver of a carrier-based aircraft. (Y. Q. Li & Lei, 2014) compared the performance of multiple methods such as PID, Takagi-Sugeno (T-S) Fuzzy, and adaptive fuzzy controllers for an aircraft model designed by dynamics equations. This article showed that the adaptive fuzzy controller performed better

than the other controllers in terms of robustness, and stability, particularly in handling parameter variations and disturbance.

(Chwa, 2015) evaluated the functionality of an adaptive fuzzy control system applied to a VTOL aircraft to ensure tracking performance in the presence of uncertainties and disturbances. The Adaptive Fuzzy System in this paper was used to estimate unknown parameters and disturbances and was combined with robust output feedback to increase the accuracy of the aircraft trajectory tracking performance and guarantee its boundedness under various uncertain conditions. (Zhilong Yu et al., 2024) proposed a new control system to robustly track the reference attitude. This controller was developed by using a fixed-time sliding mode differentiator and a fuzzy logic system to reject external disturbances and handle model uncertainties. This control methodology showed its capability to manage actuator faults in tailless aircraft.

Previously, it was discussed that various combinations of Neural Network systems and Fuzzy Logic systems were efficient for compensating for system failures in aircraft. (Melin & Castillo, 1999) integrated Adaptive Neural Networks, Fuzzy Logic systems, and Fractal Theory to improve the robustness and adaptability of an aircraft in the presence of its dynamic variations. (Zhu & Yang, 2019) integrated a dynamic recurrent fuzzy neural network into an adaptive sliding mode control system for the automatic longitudinal motion of a carrier-based aircraft landing system. In this control system, the FRNN compensated for system failures. The stability and robustness of the aircraft longitudinal landing system, equipped with this FRNN-based controller, were validated under the effects of disturbance to achieve ideal glide slope tracking.

CHAPTER 2

Research Objectives, Methodologies and Contributions

2.1 Research Objectives, Methodologies and Contributions

With respect to the explained research motivation and problem statement above, the main objective of this thesis can be summarized by the following sentence:

"Application of Artificial Intelligence Methods for the Design and Development of Aircraft Flight Control Laws."

The main objective of this thesis is to introduce new flight control systems using AI-based methods, aiming to reduce the pilot's workload and handle uncertainties during flight. Additionally, the proposed methodologies will be validated both in the presence and absence of turbulence, covering all flight conditions across the aircraft flight envelope. To achieve this, four AI-based control methodologies will be developed, each addressing specific aspects of the system. The sub-objectives include developing new AI- based control systems for the longitudinal and lateral motions of the aircraft, followed by the design of an autopilot system.

2.1.1 Sub-objective 1 - Control System for Aircraft Longitudinal Motion

In this first sub-objective, two novel control systems were developed for the longitudinal motion of the Cessna Citation X (CCX) aircraft. One controller was designed for the CCX pitch rate, and another was designed for stabilizing the CCX True Airspeed. Each of these methodologies and their contributions are described below.

2.1.1.1 The first Methodology

For the first sub-objective, primarily, a novel combination of three control methodologies was developed using the Type One Fuzzy Logic System (T1FLS), Sliding Mode Control

(SMC) system, and Adaptive Control system to guarantee the aircraft robustness and stability with accurate tracking performance. In this methodology, the aircraft unknown nonlinear functions were approximated using the T1FLS to deal with the existing uncertainties. It is worth noting that these approximations were updated using adaptive control laws during the model simulation. Then, these approximated functions were integrated into the Sliding Mode Control (SMC) system. The performance of this methodology was compared with that of a Model Reference based Adaptive Recurrent Neural Network (MARNN) control system. This comparison showed better tracking performance was obtained using the T1AFLSMC instead of the MARNN system. This superior performance was illustrated using different tracking error metrics such as AMSE, ARMSE, AMAE, and AISE across the entire CCX flight envelope in the presence and absence of turbulence.

2.1.1.2 Contributions

The main contributions of this study are described as follows:

- The novel application of the Type One Adaptive Fuzzy Sliding Mode Control system with a modified switching control term for a commercial aircraft such as the Cessna Citation X (CCX) business jet aircraft. This methodology was developed with no prior knowledge, and it controls the aircraft in all flight conditions distributed over the whole CCX flight envelope. All gains and control parameters are constant in all flight conditions.
- The validation of this methodology using a simulation platform developed based on the flight data obtained from a Level D Research Aircraft Flight Simulator (RAFS)
- A separate T1AFSMC was employed to maintain and stabilize the True AirSpeed of the CCX at its trimmed value, especially in the presence of medium-intensity turbulence, in order to improve the tracking performance.
- To simulate the turbulence effects, the Dryden turbulence model was used for the design of this control methodology. This atmospheric disturbance model is one of the most accurate turbulence models available in the Matlab/Simulink library.

- In this research, in addition to all operational aspects, it was considered that the elevator control inputs remained smooth in all flight conditions. This criterion is important to be considered since any drastic variations and sudden motions of the elevators may cause mechanical damage to their actuators.
- The Lyapunov theorem was used to prove the model stability and calculate the adaptation laws to update the approximated function by the T1FLS in real time to deal with uncertainties and parameter variations during the simulation. In addition, to reduce the pitch rate steady-state errors, an integral control term was added to the developed control law. The boundedness of this term was proved using the "Heine-Cantor" Theorem.

These methodologies and their results were thoroughly explained and discussed in two conference papers, and in one journal paper that was submitted to the Journal of Aerospace Information Systems:

- **Conference Paper 1:**
  Hosseini, S., Inga, C., Ghazi, G., and Botez, R. M., "Model-Referenced Adaptive Flight Controller Based on Recurrent Neural Network for the Longitudinal Motion of Cessna Citation X," presented at the AIAA AVIATION 2023 Forum, San Diego, CA and Online,2023, Published on the AIAA Aviation 2023 Forum website: https://doi.org/10.2514/6.2023-3797.

- **Conference Paper 2:**
  Hosseini, S., Ghazi, G., and Botez, R. M., "Application of Type One Adaptive Fuzzy Sliding Mode Control System for the Longitudinal Motion of the Cessna Citation X," presented at the AIAA AVIATION 2023 Forum, San Diego, CA and Online, 2023, Published on the AIAA Aviation 2023 Forum website: https://doi.org/10.2514/6.2023-3801 .

- **Journal Article 1:**
  Hosseini, S. M., Ghazi, G., & Botez, R. M. (2024). Novel Controller Methodology for the Cessna Citation X Under Turbulence During Cruise. Journal of Aerospace Information Systems, 21(11), 892-905. https://doi.org/10.2514/1.I011374

2.1.1.3 The second Methodology

This methodology employed a Type-2 Adaptive Fuzzy Sliding Mode Control (T2AFSMC) to control the pitch rate of the CCX aircraft and addressed the probable inherent control limitations. Although the T1AFSMC gave a promising performance in handling the uncertainties, nonlinearities, and turbulence in the aircraft longitudinal motion control, it was also necessary to compare its performances with those of the T2AFSMC. In this methodology, the T2FLS approximated the unknown nonlinear functions existing in the state-space representation of the CCX aircraft. These approximations were integrated with both sliding mode control and adaptive control systems to ensure not only the stability of the aircraft but also its robustness against uncertainties and turbulence, considered as a critical environmental flight condition.

2.1.1.4 Contributions

- This control design study is novel regarding its application on business aircraft, such as the Cessna Citation X aircraft. According to the presented literature review in Chapter 1, few studies were dedicated to the design of this type of controller for such an aircraft. In the presence of a Dryden turbulence model, the stability and robustness of the proposed control methodology were also ensured, showing that the proposed controller can operate in different environmental flight conditions.
- Similar to the T1AFSMC, approximating aircraft dynamics using the T2FLS does not require any previous knowledge about the aircraft model, and its parameters, etc. Therefore, this methodology can be used for any type of aircraft model with a minimum number of measured state variables. In the literature, the T2FLS was mainly implemented for the design of the switching term in the sliding mode control system, while this article employed it as an approximator for aircraft dynamics. Due

to the fact that the type two fuzzy membership function has a lower and an upper bound, it can handle more uncertainties compared to the T1FLS.

- Similarly, in the T2AFLSMC methodology, the smoothness of the elevator control input signals was guaranteed, which was essential for the safety of the aircraft actuation system.
- The approximated functions by the T2AFLS were updated by the adaptation laws obtained using the Lyapunov theorem. These adaptation laws could effectively deal with the variations in the aircraft dynamics model and its parameters due to turbulence and changes in flight conditions. This T2AFSMC methodology eliminates the need for a training process, which is required for the design of Neural Network systems.
- Previously, different Type Reduction (TR) methods, such as the Center Of Sets (COS) method and Karnik-Mendel (KM) algorithms (Zeghlache et al., 2019 ; Zeghlache, Ghellab, & Bouguerra, 2017 ; Zeghlache, Kara, & Saigaa, 2015) were applied in the literature for the T2FLS design.

  In our study, the Nagar-Bardini (NB) algorithm (Chen, 2019 ; El-Nagar & El-Bardini, 2014) was employed, which combined the Type Reduction and defuzzification components into one process. This methodology can significantly reduce the computational execution time.
- By applying the T2AFSMC in both pitch rate and airspeed control systems, aircraft stability was ensured, and tracking error convergence was achieved, giving very good results in both ideal and turbulent flight conditions. Furthermore, the Lyapunov Theorem ensured the stability and boundedness of the tracking errors.

This methodology and its results were thoroughly explained and discussed in two conference papers, and in one journal paper submitted to the Journal of Aerospace Information Systems:

- **Conference Paper 3:**

  Hosseini, S., Ghazi, G., and Botez, R. M., “Design of a Type Two Fuzzy-based system to Control the Pitch Rate of the Cessna Citation X,” presented at the AIAA

AVIATION 2023 Forum, San Diego, CA and Online, 2023, Published on the AIAA Aviation 2023 Forum website https://doi.org/10.2514/6.2023-3802.

- **Conference Paper 4:**
  Hosseini, S., Ghazi, G., and Botez, R. M., "Design of a Nonlinear Adaptive Fuzzy Logic System for Cessna Citation X Speed Control," presented at the AIAA SCITECH 2024 Forum, Orlando, FL, 2024, Published on the AIAA SCITECH 2024 Forum website: https://doi.org/10.2514/6.2024-0119.

- **Journal Article 2:**
  Hosseini, S. M., Ghazi, G., & Botez, R. M. (2024a). New Type-2-Fuzzy-Logic-Based Control System for the Cessna Citation X. Journal of Aerospace Information Systems, 21(10), 846-864. https://doi.org/10.2514/1.I011398

2.1.2 Sub-objective 2: Control System for Aircraft Lateral Motion

In the next step of this research, another controller was designed for the lateral motion of the aircraft, which is a complex maneuver whose stability is very important in different flight phases, such as cruise (the longest phase). The same criteria were chosen as the ones defined for Sub-objective 1 (regarding the handling qualities and the smoothness of the command signal). In this control system, the aircraft roll rate was controlled by the T2FLS, while stabilizing the yaw rate was stabilized using an Integral control system.
Therefore, to obtain a stable turning maneuver during the cruise phase, the methodology described in the next sub-section was employed:

2.1.2.1 Methodology

Concerning the sub-objective defined above, a new combination of these control methodologies was proposed, including a Type Two Fuzzy Logic System (T2FLS), an

Adaptive Control system, and an Adaptive Super-Twisting Sliding Mode Control system for the lateral motion of the CCX aircraft.

The results of this hybrid control system were compared with those of a PSO-based Type Two Adaptive Fuzzy Super Twisting Sliding Mode Control, in which the gains of the Super Twisting Sliding Mode Control were obtained by use of the Particle Swarm Optimization (PSO) algorithm.

2.1.2.2 Contribution

- In the literature, different control methodologies were developed for the control of the longitudinal motion of the aircraft, and few research topics investigated the design of flight control systems for aircraft lateral motion, which is more complex due to the coupled dynamics between the roll and yaw motions.
- The combination of the T2FLS logic system and adaptive control laws obtained from the Lyapunov theorem contributed to update the approximated real-time dynamics. This approximator can handle a larger number structured and unstructured uncertainties, which directly and indirectly affect the aircraft performance and stability.
- A Dryden Turbulence model was employed to simulate environmental disturbances to ensure the aircraft performance in different flight conditions. In order to guarantee the aircraft robustness and stability, two different types of Super-Twisting Sliding Mode Control (STSMC) systems were proposed: firstly, the Adaptive STSMC whose adaptation laws were derived from the Lyapunov theorem (Shtessel, Taleb, & Plestan, 2012 ; Yan et al., 2019) and secondly, the Particle Swarm Optimization (PSO) algorithm. Moreover, the finite time convergence and boundedness were proven for both methods. The performance of each methodology was obtained in all flight conditions in the CCX flight envelope with and without turbulence.
- From a theoretical aspect, this methodology is new, as the combination of the Adaptive and PSO-based Super Twisting Sliding Mode control system with the T2AFLS was not previously considered in the literature; in fact, the T2AFLS was used to find the gains of the switching control law, whereas this research employed it

as an approximator for the aircraft dynamics. Moreover, in the design of the PSO algorithm, the introduced cost function could successfully find the values of three design parameters with a minimum number of iterations.

- From an application point of view, this research is pioneering the development of this special type of Type 2 fuzzy Logic-based control system for business aircraft.
- These control methodologies were validated across all flight conditions distributed over the CCX flight envelope, using a nonlinear simulation platform developed for the CCX aircraft at LARCASE.

This methodology and its results were thoroughly explained and discussed in one conference and one journal paper published in the "Aerospace" journal:

- **Conference Paper 5:**
  Hosseini SM, Bematol I, Ghazi G, Botez RM, "A Novel Particle Swarm Optimization based Fuzzy Super-Twisting Sliding Mode Control System for the Lateral Motion of Cessna Citation X," presented at the AIAA AVIATION 2024 Forum, Las Vegas, NV, 2024, Published on the AIAA SCITECH 2024 Forum website: https://doi.org/10.2514/6.2024-4256.

- **Journal Article 3:**
  Hosseini SM, Bematol I, Ghazi G, Botez RM, "Enhanced Fuzzy-Based Super-Twisting Sliding-Mode Control System for the Cessna Citation X Lateral Motion". Aerospace. 2024; 11(7):549. https://doi.org/10.3390/aerospace11070549.

2.1.3 Sub-objective 3 – Autopilot Control System Design

After designing control systems for both the longitudinal and lateral motion of the aircraft, a new autopilot control system was proposed to achieve both climbing and descending maneuvers at different flight conditions.

2.1.3.1 Methodology

This research contributed to designing an autopilot control system for the aircraft longitudinal motion, including two separate control systems developed for each Altitude Hold (AH) and Vertical Speed (VS) mode.

Initially, the aircraft dynamics in both AH and VS autopilot modes were calculated using two PSO-based Multilayer Fuzzy Recurrent Neural Networks (MFRNN) systems. In this methodology, the weights of the MFRNN systems were initialized using the PSO algorithm, and then the weights acting in the last layer were updated on-line using the backpropagation algorithm, while the other weights acting on the layers remained constant. These approximators were integrated into two sliding mode controllers to satisfy the aircraft robustness, stability, and tracking performances to reach the commanded altitude and vertical speed at different flight conditions in ideal environmental conditions, and in turbulence.

2.1.3.2 Contributions

- This study proposed a new dynamics method based on the MFRNN system to calculate the existing nonlinear dynamics of the aircraft for both AH and VS modes. These MFRNNs were implemented based on the concepts described in (Fei, Wang, Liang, Feng, & Xue, 2022). However, this methodology was improved by applying the PSO algorithm applied for the weight initialization, and then by updating the weights of the last layer in an online process by use of the backpropagation technique.

- The combination of the sliding mode control system and the FRNN methodology and its application for the design of an autopilot control system is novel, as it has not been considered in the Unmanned Air Vehicles (UAVs) articles (Ahsan, Shafique, Mansoor, & Mushtaq, 2013 ; Cárdenas, Boschetti, & Celi, 2012 ; Darwish et al., 2021 ; Feng & Liu, 2023 ; K., G., & N., 2014 ; S. Lee, Kim, Baik, & Cho, 2022 ; H. Liu et al., 2015 ; M. Liu, Egan, & Santoso, 2015 ; Mansoor Ahsan & Ali Hanif, 2014 ; Qi, Zhu, Wang, Shan, & Liu, 2021 ; Qian & Liu, 2020 ; Santoso, Liu, & Egan, 2008 ; Win, Nyunt, & Tun, 2019 ; Zareb, Nouibat, Bestaoui, Ayad, & Bouzid, 2019 ;

W. Zhang et al., 2023 ; Zhao, Duan, Yu, Qu, & Zhang, 2021 ; R. Zhou, Wang, Yu, & Zhang, 2023), hypersonics (T. Dong, Qin, Song, Wang, & Lei, 2022 ; Fenfen, Xubo, Haiming, & Tong, 2020 ; H. Gao et al., 2020 ; Hiliuta, Botez, & Brenner, 2005b ; Napolitano & Kincheloe, 1995 ; Park et al., 2023 ; Perez, Moncayo, Moguel, Perhinschi, Al Azzawi, et al., 2014 ; Perez, Moncayo, Perhinschi, Al Azzawi, & Togayev, 2015 ; Sahbon, Jacewicz, Lichota, & Strzelecka, 2023 ; Taha, Bayuomi, El-Bayoumi, & Hassan, 2009) and even commercial aircrafts (Barros Dos Santos & De Oliveira, 2011 ; Islam, Alam, Laskar, & Garg, 2016 ; Juang & Chiou, 2006 ; Nivison & Khargonekar, 2017a ; Qiu, Delshad, Zhu, Nibouche, & Yao, 2017 ; Solomon Raj & Kumar, 2015 ; Theis, Ossmann, Thielecke, & Pfifer, 2018), showing a significant contribution and advancement in the aerospace field. These control systems operated adequately and gave excellent results in all flight conditions across the flight envelope of the CCX aircraft in ideal and turbulent environments.

- This research proposes a new fuzzy logic-based transition algorithm to switch between the AH and VS modes in the autopilot control system for the first time. This methodology was based on a transition algorithm proposed in (Ghazi, 2014). In comparison with the algorithm described in (Ghazi, 2014), where three (AC, AH, VS) modes were used, only two (AH and VS) modes were considered, and no separate controller for the Altitude Capture mode was required in the autopilot system.

- This study is based also on a Type One Adaptive Fuzzy Sliding Mode Control System already developed by us in (Seyed Mohammad Hosseini, Ghazi, & Botez, 2024b) for the pitch rate of the CCX aircraft.

- The CCX stability using the proposed control methodologies were proven using the Lyapunov theorem to ensure that the tracking errors converge to zero in a finite time.

This methodology and its results were thoroughly explained and discussed in one journal paper submitted to the “Aeronuatical” journal.

- **Journal Article 4:** Hosseini SM, Ghazi G, Botez RM, “New Fuzzy-RNN Autopilot System for Cessna Citation X Aircraft with a Fuzzy Transition Algorithm”. the Aeronautical journal. Submitted, 2024.

2.2 Results Validation

An essential step in the design of control systems for an aircraft is to ensure the performance, stability, and validation of applied methodologies. To examine the performances of the Artificial Intelligence (AI) based control systems described earlier in all previous sub-objectives, and for different flight conditions, these controllers were validated using a nonlinear simulation platform developed for the Cessna Citation X aircraft at the LARCASE. This simulation platform was developed using real flight data obtained from the Level-D Research Aircraft Flight Simulators (RAFS) available at the LARCASE. The Level-D term refers to the highest level of certification that can be issued by the FAA (Federal Administration Aviation) for the aircraft flight simulators. The RAFS was developed by the well-known aerospace companies CAE and Cessna to be used for research needs at the LARCASE.

CHAPTER 3

NOVEL CONTROLLER METHODOLOGY FOR THE CESSNA CITATION X UNDER TURBULENCE DURING CRUISE

S.M. Hosseini, G. Ghazi, and R.M. Botez

Research Laboratory in Active Controls, Avionics and AeroServoElasticity (LARCASE),
Department of Systems Engineering, École de Technologie Supérieure,
1100 Notre-Dame West, Montreal, Quebec, Canada H3C 1K3

Paper published in *Journal of Aerospace Information Systems*, October 2024

Resumé: La conception d'une nouvelle approche de contrôle pour le mouvement longitudinal du Cessna Citation X pendant la croisière est réalisée en utilisant une combinaison de contrôle de mode glissant (SMC), de logique floue de type un (T1FLS) et de systèmes de contrôle adaptatifs. Cette méthodologie est présentée pour 1) contrôler le taux de tangage de l'avion et 2) stabiliser la vitesse de l'avion pendant les turbulences. Le modèle non linéaire de l'avion a été généré à l'aide d'une plate-forme de simulation, qui a été conçue sur la base des données de vol obtenues à partir du plus haut simulateur de vol d'avion de recherche de niveau D certifié par la FAA. Le système de logique floue adaptative de type 1 a été mis en œuvre pour approximer les fonctions inconnues afin de construire la partie équivalente du système de commande à mode glissant qui gère les effets des incertitudes et des turbulences. Les lois d'adaptation, dérivées du théorème de Lyapounov, ont été utilisées pour mettre à jour les fonctions approximatives dans la loi de commande à chaque condition de vol et itération de simulation. En utilisant la combinaison des systèmes de contrôle, le taux de tangage pouvait suivre le signal de référence donné, tandis que la vitesse de l'avion restait à une valeur de référence avec et sans turbulences dans l'ensemble de l'enveloppe de vol. Les résultats ont montré que les contrôleurs proposés satisfaisaient aux performances de suivi tout en générant un braquage régulier de la gouverne de profondeur, deux éléments importants pour les applications aéronautiques réelles.

Abstract: The design of a new control approach for the longitudinal motion of the Cessna Citation X during cruise is performed using a combination of Sliding Mode Control (SMC), Type One Fuzzy Logic (T1FLS), and Adaptive Control Systems. This methodology is presented for 1) controlling the aircraft pitch rate and 2) stabilizing the aircraft speed during turbulence. The nonlinear model of the aircraft was generated using a simulation platform, which was designed based on flight data obtained from the highest FAA certified Level-D Research Aircraft Flight Simulator. The Type One Adaptive Fuzzy Logic system was implemented to approximate unknown functions for constructing the equivalent part of the Sliding Mode Control system which handled the effects of uncertainties and turbulence. The adaptation laws, derived from the Lyapunov theorem, were used to update the approximated functions in the control law at each flight condition and simulation iteration. Using the control systems combination, the pitch rate could follow the given reference signal, while the aircraft speed remained at a reference value with and without turbulence across the whole flight envelope. Results have shown that the proposed controllers satisfied tracking performance while generating smooth elevator deflection, both of which are important for real-aircraft applications.

3.1 Introduction

This article is devoted to the development of Type One Adaptive Fuzzy Sliding Mode Control systems for both pitch rate and True AirSpeed (TAS) of an aircraft during cruise.

According to (William Rankin, Ph.D., 2007), recent statistics reveal that human errors account for 80% of aviation accidents. Moreover, the advancement in aircraft systems has also increased the complexity of flight operations, requiring pilots to maintain high levels of concentration and awareness during the flight. These aspects have led us to design Fuzzy logic-based control systems to reduce the pilot’s workload.

In addition, this rapid development in aeronautical and aerospace technologies has increased the importance of high-performance, robust, and precise control systems needed to ensure safe and balanced flight in an aircraft seen as a complex system, which means the aircraft control systems must maintain stability and maneuverability under various flight conditions while minimizing the effects of external disturbances and uncertainties.

Previously, various types of classical and advanced control systems have been designed to address the aforementioned challenges. These systems have yielded precise and accurate performance, showing that they are reliable for real-world applications in the Aerospace and Aviation industry.

A controller was designed in (Kanokmedhakul, Pholdee, Bureerat, & Panagant, 2019) for the pitch of an aircraft by combining a Proportional-Integral-Derivative (PID) with a Linear Quadratic Regulator (LQR) controller. The controller parameters were fine-tuned using a Differential Evolution (DE) algorithm. Similarly, a set of multivariable PID controllers and an LQR -based altitude controller were suggested in (Guardeño, López, & Sánchez, 2019) to guarantee the robustness of a DJI-F450 quadrotor under the influence of uncertainties and disturbances. In (Fan, Liu, & Kwong, 2017), an effective gain scheduling-based Fault-Tolerant Control (FTC) system was proposed for flexible aircraft using a Linear Parameter Varying (LPV) approach. This system addressed critical problems such as actuator saturation and control surface blocking. The control gains in this methodology were obtained with a set of set-invariant conditions constrained by Linear Matrix Inequalities (LMI). In another study (Q. Zhang & Liu, 2018b), to achieve optimal tracking performance in aircraft close formation under various maneuvers, a new controller design was suggested based on a command-filtered backstepping methodology. This controller had an estimator for uncertainties in formation aerodynamics due to trailing vortices of the leader aircraft. This methodology was validated on two UAVs.

A hybrid non-linear feedback control methodology was developed in (P. Singh et al., 2023) using backstepping and sliding mode control systems for the aircraft lateral-directional motion to improve its maneuverability while satisfying a set of handling qualities.

Despite the appropriate performance of controllers obtained with classical and advanced control techniques, they may not operate adequately in environmental critical conditions, external disturbances, and system failures. These methodologies also may not be efficient in dealing with uncertainties and varying flight conditions. In (Snyder, Zhao, & Hovakimyan, 2021), an adaptive control system was introduced for linear parameter-varying (LPV) systems to deal with time-varying uncertainties and disturbances on the longitudinal dynamics of a conceptual Urban Air Mobility aircraft.

An aerodynamic model-based robust adaptive control was proposed in (Q. Zhang & Liu, 2018a), using an online formation aerodynamic model that predicts and counteracts unknown aerodynamic effects, ensuring precise tracking performance between follower and leader aircraft, along with robustness against external disturbances.

AI-based control systems offer adaptive characteristics and learning capabilities that classical and advanced control systems may lack. As a result, these controllers have recently gained significant attention in various research studies as follows:

In research (Perez, Moncayo, Moguel, Perhinschi, Azzawi, et al., 2014) and (Perez et al., 2015), adaptive fault-tolerant control systems were developed to stabilize fighter aircraft during actuator and structural failures. The controllers utilized bio-inspired artificial immune algorithms, nonlinear dynamic inversion, and model-reference adaptive control systems. The optimal parameters in the artificial immune algorithm were determined using genetic algorithms.

Authors in (Ziquan Yu, Li, et al., 2023) proposed using prescribed performance functions to modify UAV tracking errors. An actor-critic neural networks-based Reinforcement Learning

was developed to learn unknown nonlinearities, with nonlinear disturbance observers designed to improve fault-tolerant formation control capabilities and minimize RL errors.

The work in (Cervantes & Castillo, 2015) presents the design of three separate fuzzy controllers to control the longitudinal, lateral, and directional motions of an aircraft using a genetic algorithm to help the fuzzy logic-based models perform effectively in the presence of disturbances. To guarantee the trajectory tracking performance of various types of UAVs, a fuzzy logic-based controller was developed, whose gains were tuned using an enhanced genetic algorithm (K. Wilburn, G. Perhinschi, & N. Wilburn, 2014).

In (Castillo & Cervantes, 2014), researchers proposed combining a fuzzy logic methodology with a genetic algorithm to optimize the membership functions for the longitudinal control of an F-14 aircraft. In (Y. Gao, Liu, Wang, & Wu, 2019), an interval type-two fuzzy neural network was applied with and without quantization to control the speed and altitude in order to guarantee the tracking performance of a hypersonic flight vehicle. In (Ziquan Yu et al., 2022), a fault-tolerant controller was proposed for unmanned airships (UAs) with actuator faults by using fractional calculus, sliding mode control, and fixed-time prescribed performance functions (PPFs). This controller employed Recurrent Fuzzy Neural Networks (RFNNs) to enhance the synchronization tracking performance for multiple UAVs.

The authors applied in (Hušek & Narenathreyas, 2016) a Takagi-Sugeno-based Parallel Distributed Compensation control technique to manage the longitudinal motion of a LET L410 aircraft, aiming to achieve closed-loop stability and asymptotic reference tracking of the pitch rate in the presence of parametric uncertainties and disturbances. The Authors in (X. Jiao & Jiang, 2016) implemented an interval type-two fuzzy sliding mode controller to achieve tracking performance and robustness of a hypersonic aircraft with white noise and uncertainties, while a general fuzzy logic based controller could satisfying the aforementioned criteria for a B747 aircraft in (Tavoosi, 2020). Moreover, an AFSMC methodology was proposed in (Y. Wang, Wu, & Liu, 2017) to control an aircraft nonaffine Dutch-Roll System.

According to (Ghosh Roy & Peyada, 2017), the integration of an Artificial Bee Colony (ABC) optimizer in an Adaptive Neuro-Fuzzy System (ANFIS) may improve the efficiency of the control system in estimating the nonlinear parameters in the models of two aircraft: HFB-320 and the Advanced Technologies Testing Aircraft System (ATTAS). Furthermore, in (Ziquan Yu, Yang, et al., 2023), a novel approach combining Type Two Fuzzy Neural Networks and Fractional Order Control methodologies was introduced. This efficient fault-tolerant tracking control technique not only reduces the communication load but also ensures synchronized UAV tracking.

In (S. M. Hashemi & Botez, 2022), the authors proposed a flight dynamics controller for the Hydra Technologies UAS-S4 Ehécatl based on a robust adaptive fuzzy logic system. In this research, the UAS-S4 model was developed using a Takagi-Sugeno fuzzy logic system, with adaptive gains to handle the uncertainties. Similarly, in (Khan, Grigorie, Botez, Mamou, & Mébarki, 2019b), a fuzzy logic-based control technique was proposed for the morphing wing actuation system equipped with Brushless DC (BLDC) motors. This technique was validated through numerical simulations, and experimental bench and wind tunnel tests in both LARCASE Price-Païdoussis and NRC wind tunnels. In (Seyed Mohammad Hashemi et al., 2020), a novel approach for the resonance based click mechanism was proposed using a fuzzy control system, that created a powerful flapping propulsion system to reduce the energy consumption.

In addition to the previous articles, at the Laboratory of Applied Research in Active Controls, Avionics and AeroServoElasticity (LARCASE), researchers have applied different conventional methodologies for developing of classical, modern, optimal and robust control systems for the longitudinal and lateral motions of the Cessna Citation X aircraft (Y. Boughari, Ghazi, Theel, & Botez, 2013 ; Yamina Boughari, Georges Ghazi, et al., 2017 ; Ghazi et al., 2016).

In (Yamina Boughari, Botez, et al., 2017), a robust control system (H^{∞}) was suggested for the Cessna Citation X aircraft using two metaheuristic algorithms. This technique was

implemented to satisfy a set of flight handling qualities criteria, using genetic and differential evolution algorithms to determine the weighting functions of the H^{∞} controller. Moreover, in (Ghazi & Botez, 2015b), the authors presented an enhanced flight control system for the lateral motion of this aircraft, comprising two main components: a Stability Augmentation System (SAS) and a Control Augmented System (CAS) designed by using the optimal control theory, along with a Guardian map algorithm to verify the robustness of the controller. A Genetic algorithm was also applied to adjust their gains. For the design of an autopilot in (Ghazi & Botez, 2014), the authors applied a Linear Quadratic Regulator (LQR) and a Genetic algorithm with the Guardian Map theory to assess the accuracy of handling qualities while meeting the robustness criteria for the Lynx helicopter and the Cessna Citation X.

Respectively, several AI-based methodologies were applied for the Cessna Citation X aircraft at the LARCASE. To control the pitch rate, a combination of a Model Predictive Controller (MPC), and an Adaptive Neural Network (ANN) controller in (Rojo P. Andrianantara et al., 2024), a Type One and a Type Two Adaptive Fuzzy Logic based control system in (S. Hosseini, Ghazi, & Botez, 2023a, 2023b) were employed for the Cessna Citation X during the cruise in ideal flight conditions. Furthermore, a new control methodology was described in (Zohreh Nejad, Aillot, Henry, Ghazi, & Botez, 2024) for ground speed control using Reinforcement Learning trained on a nonlinear longitudinal ground dynamics model of a Cessna Citation X aircraft.

Based on this literature review, the performances of conventional methods are limited, and they face some unexpected drawbacks due to their structural characteristics. Accordingly, conventional methodologies can only be used under certain operational conditions. Therefore, if the flight condition varies, or the dynamics of a system changes, the structure of conventional control systems must be changed. Otherwise, an aircraft would need to alternate the use of one controller another, which is not desirable for an aircraft modelled as a nonlinear system. It must be mentioned that this problem may worsen when facing unpredicted conditions in the presence of uncertainties.

The main contribution of this research lies in the development and application of an AI-based flight control system for the Cessna Citation X business aircraft. The novelty of this research is the application of an ensemble of three complementary control methodologies, combining a type one fuzzy logic methodology as an AI-based control system with two other advanced control systems, such as adaptive and sliding mode control systems. Although this methodology was applied to hypersonic aircraft (Castillo & Cervantes, 2014 ; Y. Gao et al., 2019 ; X. Jiao & Jiang, 2016) or Unmanned Air Vehicles (UAVs) (Babaei, Mortazavi, & Moradi, 2011 ; S. M. Hashemi & Botez, 2022 ; Ziquan Yu et al., 2022 ; Ziquan Yu, Yang, et al., 2023), there are few (Tavoosi, 2020 ; Y. Wang et al., 2017), if any, articles that have validated this AI-based control system for business aircraft types, such as the Cessna Citation X aircraft. We tested this control methodology on an accurate simulation platform designed for the Cessna Citation X business aircraft validated by flight data obtained from a Level-D Research Flight Simulator (RAFS). In addition, the performance of the controller was evaluated in the presence of turbulence, which was not considered in (Castillo & Cervantes, 2014 ; Y. Gao et al., 2019 ; X. Jiao & Jiang, 2016). The combination of these methodologies enabled the design of a single controller that ensures optimal aircraft performance under various flight conditions across the whole flight envelope during cruise without the need of prior knowledge of the aircraft nonlinear model. Simulation results highlighted that our novel flight control law, which uses a distinct switching control term as denoted by η_T in Eq. (25), effectively mitigated steady-state errors in the pitch rate. Our proposed control law not only guarantees the stability of the aircraft but also ensures that the pitch rate tracking error convergence to zero. Furthermore, this study introduces an additional type-one adaptive fuzzy sliding mode control system to stabilize the aircraft true airspeed. Using a second controller for the cruise speed had some advantages and disadvantages. The turbulence drastically affects the true airspeed, which may prevent the pitch rate from tracking the reference signal. Therefore, using a single pitch rate control system could hardly meet the tracking performance in the presence of turbulence. Meanwhile, the aircraft speed control system helped to reduce the amplitudes of the aircraft airspeed variations and keep them within a specific range around the aircraft trimmed cruise speed. This issue not only

stabilized the aircraft speed but also assisted in achieving the tracking performance of the aircraft pitch rate. However, the main drawback of using these two control systems operating in parallel is that they may cause high-frequency oscillations with small amplitudes induced to the pitch rate, which was resolved by choosing appropriate design parameters in the sliding surface, and by switching control law in both controllers. To underpin the system efficacy and stability, a Lyapunov candidate was used. This approach provided a mathematical proof for aircraft stability, and it was used to calculate the adaptation laws. These laws are essential for updating the approximated functions determined by the Type-One Fuzzy Logic system for different flight conditions during simulation.

This paper proposes the application of a Type-One Adaptive Fuzzy Sliding Mode Control System for the Cessna Citation X aircraft, which is organized into four sections. The aircraft model and the applied Type One Fuzzy Logic System are discussed in Section 3.2.1. The theoretical aspects of each aircraft pitch rate and speed control systems are explained in Sections 3.2.2 et 3.2.3. Section 3.2 ends with a basic description of the Dryden turbulence model. Based on the analysis of the results provided in Section 3.3, this research is concluded in Section 3.4. The details of the proof of stability for the aircraft speed control system is presented in the Appendix. I.

3.2 Methodology

This research presents the design of two separate controllers, one for the pitch rate, and one for the True Airspeed (TAS), based on the Type One Adaptive Fuzzy Sliding Mode Control (T1AFSMC) approach for the Cessna Citation X aircraft.

3.2.1 Aircraft Longitudinal Model

The suggested controllers in this article were designed for the nonlinear longitudinal model of aircraft. This nonlinear mode represents the aircraft dynamics using several differential equations. These equations depict the relationships between the forces and moments applied

to the aircraft (S. M. Hashemi & Botez, 2022). In general, the aircraft dynamics can be modeled with a state-space equation as follows:

$$x^{(n)}(t) = F(x,t) + G(x,t)\eta + d(t) \tag{3.1}$$

Where, η is the control input, and n denotes the order of derivative in Eq. (3.1). This Equation shows the state-space model of aircraft with respect to the state variables $x = [u, w, q, \theta]^T$ for controlling the longitudinal motion, given that $F(x.t)$ and $G(x.t)$ are the unknown functions which are considered to be approximated by the Type One Fuzzy Logic System (T1FLS) presented in this article. These two functions contain all nonlinearities and variables that can be controlled using η as the control law, and $d(t)$ is the external disturbance such as turbulence.

In this article, a simulation platform was employed to create the nonlinear model of the Cessna Citation X business aircraft. This platform was developed in MATLAB/Simulink at the LARCASE based on the flight data derived from a Level-D Research Aircraft Flight Simulator (RAFS) for the Cessna Citation X business jet aircraft manufactured by CAE as shown in Fig. 3.1 (Ghazi & Botez, 2015a). The Level-D represents the highest level of certification issued by the Federal Aviation Administration (FAA) for flight simulators.

Figure 3.1 Level-D Flight Simulator for the Cessna Citation X Aircraft

Two assumptions have been considered for the proof of stability to simplify the aircraft dynamics and ensure the applicability of the mathematical tools used for stability analysis as described separately in Assumptions 1 (Slotine & Li, 1991 ; C.-H. Wang, Liu, & Lin, 2002 ; L.-X. Wang, 1997), and 2 (C.-H. Wang et al., 2002). It is also essential to recognize that the assumptions used in the proof of stability must be plausible and representative of the actual behavior of the aircraft. It is also crucial to examine aircraft robustness under different flight conditions and turbulence.

Assumption 1 ((Slotine & Li, 1991 ; C.-H. Wang et al., 2002 ; L.-X. Wang, 1997)). For the unknown dynamics functions $F(x.t)$, $G(x.t)$ and $d(t)$ the following conditions are applied:

$$|F(x,t)| \leq F < \infty \tag{3.2}$$

$$, 0 < g_{min} \leq G(x.t) \leq g_{max} \text{ while } g_{min} \neq 0$$

$$\text{and } |d(t)| \leq T$$

Where F, g_{min} , g_{max} , and T are positive values. If x is a subset of R^n (n is the dimension of the subset) and lies in a compact set Q_x, then $\|x\| \leq k_x < \infty$, which means that the $F(x.t)$, $G(x.t)$ and $d(t)$ terms are bounded. This assumption also implies that the $G(x.t)$ characterizing the influence of the control command denoted by η in Eq. (3.1) on the system dynamics, is confined within a known range and does not vanish completely.

Assumption 2 ((C.-H. Wang et al., 2002)). It is assumed that the ϱ_f and ϱ_g are two parameters that reside in the compact sets $\Omega_f = \{\varrho_f \in R^Q, \|\varrho_f\| \leq z_f\}$, and $\Omega_g = \{\varrho_g \in R^Q, \|\varrho_g\| \leq z_g\}$, respectively. Here, Q represents the dimension of the subset while z_f and z_g are the finite positive constants.

The next sub-section is dedicated to the brief description of the Type-One Fuzzy Logic System used as an approximator in the designed control system whose structure will be discussed in Section 3.2.1.1 as follows.

3.2.1.1 Design of the Type-One Fuzzy Logic System

In aircraft control, approximating unknown functions in an aircraft state-space model, such as $F(x,t)$ and $G(x,t)$ presented in Eq. (3.1), is common. As a simplified representation of flight dynamics, aircraft models may contain uncertainties due to assumptions and variations in environmental conditions during flight, which can change the aircraft dynamics. To handle these uncertainties and to improve aircraft performance and safety against dynamics variations, a T1FLS was developed as an approximator in this article for two unknown functions, $F(x,t)$ and $G(x,t)$.

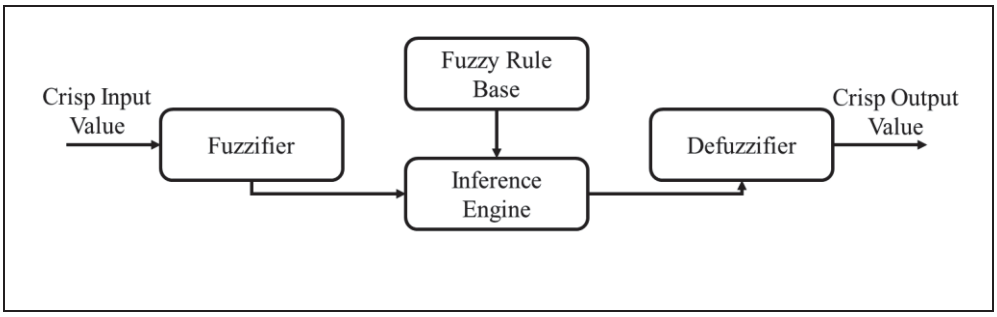

Figure 3.2 Components of a Type-One Fuzzy Logic System

Fig. 3.2 presents a typical schematic of a Type-One Fuzzy Logic system. Basically, a Type-One Fuzzy Logic System includes four main components: a Fuzzifier, a Fuzzy Rules base, a Fuzzy Inference Engine, and a Defuzzifier whose roles were discussed in (L.-X. Wang, 1997). Respectively, the Fuzzifier takes the crisp inputs and transforms them into fuzzy values (degrees of membership) between [0,1] using a membership function; then, the fuzzified inputs are passed to the Inference Engine. The fuzzy rule base contains set of If-Then rules expressing the relationship between the inputs and outputs using fuzzy logic; these fuzzy rules are accommodated in the Fuzzy Rule Base. The Inference Engine identifies the applicable fuzzy rules by evaluating the linguistic terms and applies the related rule on the fuzzified inputs and then aggregates the outputs of these rules to produce a fuzzy output set for each output variable. Ultimately, the Defuzzifer takes the outputs of the Inference engine and transforms the fuzzy outputs into crisp output values (L.-X. Wang, 1997).

As described in (L.-X. Wang, 1997), the output of a T1FLS can be represented by $\hat{P}(x)$ as follows:

$$\hat{P}(x) = \theta^T \psi(x) \tag{3.3}$$

Where, $\theta^T = [p_1, \ldots\ldots, p_r]$ is a vector of free parameters for r rules which can be updated using the designed adaptation laws described in Section 3.2.2. Furthermore, $\psi^T(x) = [\psi_1(x), \ldots., \psi_r(x)]$ are the Fuzzy Basis Functions (FBF) that are calculated using Eq. (3.7). This term defines the relationships between the uncertain inputs and outputs. Here, r shows

the number of rules in this fuzzy Logic-based model. To calculate the approximated function in Eq. (3.3), it is required to choose i measured variables $x = [x_1, \dots, x_i]$ as inputs of the Fuzzy Logic Based-Control System (FLCS).

Respectively, a membership function associated with a fuzzy set expresses how the input values are mapped to a membership degree; Fig 3.3 (Ref. (J. Zhou, Yang, & Wang, 2016)) illustrates the Gaussian membership function used in this study whose formula is given in Eq. (3.4).

$$\mu_{M_i^r}(x) = e^{\frac{-1}{2}\left[\frac{x-b}{a}\right]^2} \tag{3.4}$$

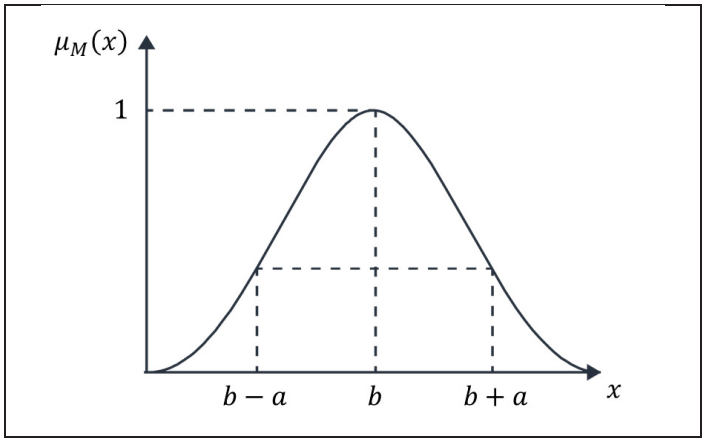

Figure 3.3 Gaussian Membership Function Scheme

The relationship between the fuzzy sets can be represented by r fuzzy rules in the IF input THEN output structure as shown in Eq. (3.5), where p_r is the fuzzy singleton output to calculate $\hat{P}$ in each rule.

$$If\ x_1\ is\ M_1^r\ and \dots and\ x_i\ is\ M_i^r\ then\ \hat{P}\ is\ p_r \tag{3.5}$$

It should be stated that the degree of membership of each element such as $x_1, \dots, x_i$ to a fuzzy set $(M_1^r, \dots, M_i^r)$ in the r^{th} rule can be defined by a membership function shown by $\mu_{M_i^r}(x)$. Accordingly, in this paper, the singleton fuzzifier, the product inference engine, and the

centroid (center-average) defuzzifer were used to calculate the approximated function $\hat{P}(x)$ as follows (Roopaei, Zolghadri, & Meshksar, 2009):

$$\hat{P}(x) = \sum_{1}^{r} p_r \left[\prod_{1}^{i} \mu_{M_i^r}(x) \right] / \sum_{1}^{r} \left[\prod_{1}^{i} \mu_{M_i^r}(x) \right] \tag{3.6}$$

Here, $\hat{P}$ denotes the output of the Fuzzy Logic System, and $\psi(x)$ are the Fuzzy Basis Functions (FBFs) as shown in Eq. (3.7). In this article, $\psi(x)$ was calculated separately for approximating both unknown functions $F(x,t)$ and $G(x,t)$, expressed by $\psi_{f_q}(x)$ and $\psi_{g_q}(x)$, respectively in the pitch rate control system and by $\psi_{f_v}(x)$ and $\psi_{g_v}(x)$ in the aircraft true airspeed control system.

$$\psi(x) = \prod_{1}^{i} \mu_{M_i^r}(x) / \sum_{1}^{r} \left[\prod_{1}^{i} \mu_{M_i^r}(x) \right] \tag{3.7}$$

The denominator of Eq. (3.7) is always positive and non-zero, and at each iteration of the simulation, and at least one rule is always active as $\sum_1^r [\prod_1^i \mu_{M_i^r}(x)] > 0$. Also, in Eqs. (3.6) and (3.7), $\prod_1^i \mu_{M_i^r}(x) = \mu_{M_1^r}(x) \times \mu_{M_2^r}(x) \times ... \times \mu_{M_i^r}(x)$ is the t-norm or product inference engine (L.-X. Wang, 1997).

The methodology used for obtaining $\hat{P}(x)$ using Eq. (3.6), will be applied to approximate the unknown functions denoted by $F(x.t)$ and $G(x.t)$ in the aircraft nonlinear model expressed by Eq. (3.1). This technique will be applied to both aircraft pitch rate and speed control systems, to obtain the approximated functions $\hat{f}_q(x.\theta_{f_q})$, $\hat{g}_q(x.\theta_{g_q})$, $\hat{f}_v(x.\theta_{f_v})$ and $\hat{g}_v(x.\theta_{g_v})$, in Sections 3.2.2 and 3.2.3.

For this purpose, five Gaussian membership functions were selected as shown in Eq. (3.4) for the pitch rate, its reference signal in the pitch rate control system, and for TAS and Angle of

Attach (AOA) for the design of aircraft speed control system; the linguistic terms for each of these variables are presented in Table 3.1.

Table 3.1 Linguistic Terms and Configurations of Membership Functions

Variables	Linguistic Terms				
q (deg/s)	Too Small	Small	Medium	Large	Too Large
	Parameter values				
	$b = -0.5$, $a^2 = 2$	$b = 0.75$, $a^2 = 2$	$b = 2$, $a^2 = 2$	$b = 3.25$, $a^2 = 2$	$b = 4.5$, $a^2 = 2$
q_d (deg/s)	Linguistic Terms				
	Too Small	Small	Medium	Large	Too Large
	Parameter values				
	$b = -0.5$, $a^2 = 2$	$b = 0.75$, $a^2 = 2$	$b = 2$, $a^2 = 2$	$b = 3.25$, $a^2 = 2$	$b = 4.5$, $a^2 = 2$
TAS (m/s or mps)	Linguistic Terms				
	Too Slow	Slow	Moderate	Fast	Too Fast
	Parameter values				
	$b = 0$, $a^2 = 2500$	$b = 75$, $a^2 = 2500$	$b = 150$, $a^2 = 2500$	$b = 225$, $a^2 = 2500$	$b = 300$, $a^2 = 2500$
AOA (deg)	Linguistic Terms				
	Very Low	Low	Average	High	Very High
	Parameter values				
	$b = 0$, $a^2 = 25$	$b = 5$, $a^2 = 25$	$b = 10$, $a^2 = 25$	$b = 15$, $a^2 = 25$	$b = 20$, $a^2 = 25$

Therefore, the ensemble of 25 fuzzy rules were defined for each pitch rate, and speed control system in Tables 3.2, and 3.3, respectively:

Table 3.2 Fuzzy Rules for the Pitch Rate Control System

q_d / q	Too Small	Small	Medium	Large	Too Large
Too Small	p^1_{f,g_q}	p^2_{f,g_q}	p^3_{f,g_q}	p^4_{f,g_q}	p^5_{f,g_q}
Small	p^6_{f,g_q}	p^7_{f,g_q}	p^8_{f,g_q}	p^9_{f,g_q}	p^{10}_{f,g_q}
Medium	p^{11}_{f,g_q}	p^{12}_{f,g_q}	p^{13}_{f,g_q}	p^{14}_{f,g_q}	p^{15}_{f,g_q}
Large	p^{16}_{f,g_q}	p^{17}_{f,g_q}	p^{18}_{f,g_q}	p^{19}_{f,g_q}	$p^{20}_{f\ g_q}$
Too Large	p^{21}_{f,g_q}	p^{22}_{f,g_q}	p^{23}_{f,g_q}	p^{24}_{f,g_q}	p^{25}_{f,g_q}

Table 3.3 Fuzzy Inference Rules for the Aircraft Speed Control System

AOA / TAS	Very Low	Low	Average	High	Very High
Too Slow	p^1_{f,g_v}	p^2_{f,g_v}	p^3_{f,g_v}	p^4_{f,g_v}	p^5_{f,g_v}
Slow	p^6_{f,g_v}	p^7_{f,g_v}	p^8_{f,g_v}	p^9_{f,g_v}	p^{10}_{f,g_v}
Moderate	p^{11}_{f,g_v}	p^{12}_{f,g_v}	p^{13}_{f,g_v}	p^{14}_{f,g_v}	p^{15}_{f,g_v}
Fast	p^{16}_{f,g_v}	p^{17}_{f,g_v}	p^{18}_{f,g_v}	p^{19}_{f,g_v}	$p^{20}_{f\ g_v}$
Too Fast	p^{21}_{f,g_v}	p^{22}_{f,g_v}	p^{23}_{f,g_v}	p^{24}_{f,g_v}	p^{25}_{f,g_v}

To calculate the values of $p^{r=1:25}_{f.g_q}$ and $p^{r=1:25}_{f.g_v}$ in Tables 3.2 and 3.3, using adaptation laws in Eqs. (3.18) and (3.27), $\theta^T = [p_1, \ldots\ldots, p_r]$ were initialized with random values. These adaptation laws improve the accuracy of the approximated functions as the aircraft dynamics may vary in different flight conditions. The following sections explain the design of pitch rate and aircraft speed control systems.

3.2.2 Pitch Rate Control System

The pitch rate control system is essential for achieving aircraft stabilization and maneuverability (Nelson, 1998). With this regard, the T1FLS approximator was combined with sliding mode control and adaptive control methodologies for controlling the aircraft pitch rate in this section.

Sliding mode control system is an advanced control methodology commonly used for stabilizing and controlling nonlinear and dynamic systems (Utkin, Poznyak, Orlov, & Polyakov, 2020). This controller can drive the tracking error towards zero while improving the stability and robustness against uncertainties and rejecting turbulence by ensuring that the aircraft dynamics converge to a cross-section of the equilibrium state called as sliding surface.

Generally, adaptive control enhances the performance of fuzzy logic-based models by its dynamic adjustment and tuning of parameters (Mohammadzadeh et al., 2023). This adaptation laws allow T1FLS approximator to become effectively versatile and robust even in different flight conditions or in the presence of uncertainties, disturbances, and aircraft dynamics variations.

Using the aircraft state-space model in Eq. (3.1), the tracking error $e_q(t) = q(t) - q_d(t)$, and its derivative as $\dot{e}_q = \dot{q}(t) - \dot{q}_d(t)$, the sliding surface was selected as follows (Sun, Gong, & Yang, 2020):

$$S_q(t) = \dot{e}_q(t) + Ce_q(t) = \dot{q}(t) - \dot{q}_d(t) + Ce_q(t) \tag{3.8}$$

Where, $C > 0$. By taking the time derivative of the sliding surface in Eq. (3.8), and knowing $\ddot{q}(t) = f_q(x,t) + g_q(x,t)\eta + d(t)$ from Eq. (3.1), $\dot{S}_q(t)$ can be written as follows (Roopaei et al., 2009):

$$\dot{S}_q(t) = \ddot{e}_q(t) + C\dot{e}_q(t) = \ddot{q}(t) - \ddot{q}_d(t) + C\dot{e}(t) = f_q(x.t) + g_q(x.t)\eta - \ddot{q}_d(t) + C\dot{e}(t) + d(t) \quad (3.9a)$$

$$\dot{S}_q(t) = [f_q(x,t) - \hat{f}_q(x,\theta^*_{f_q})] + \hat{f}_q(x,\theta^*_{f_q}) + [g_q(x,t) - \hat{g}_q(x,\theta^*_{g_q})]\eta + \hat{g}_q(x,\theta^*_{g_q})\eta - \ddot{q}_d(t) + C\dot{e}(t) + d(t) \quad (3.9b)$$

Having $\dot{S}_q(t)$ in Eq. (3.9a), the equivalent control law denoted by η_{eq1} can be simply obtained by $\dot{S}_q(t) = 0$ (Roopaei et al., 2009), then:

$$\eta_{eq1} = \left(\frac{1}{g_q(x,t)}\right)\left[-f_q(x,t) + \ddot{q}_d(t) - C\dot{e}_q(t) - d(t)\right] \quad (3.10)$$

Adding and subtracting $\hat{f}_q(x.\theta^*_{f_q})$ as presented in Eq. (3.9b), the minimum approximation error can be defined as $w = f_q(x,t) - \hat{f}_q(x.\theta^*_{f_q}) + \left(g_q(x,t) - \hat{g}_q(x.\theta^*_{g_q})\right)\eta$. Replacing w in Eq. (3.9b) leads to (Roopaei et al., 2009):

$$\dot{S}_q(t) = w + \hat{f}_q(x,\theta^*_{f_q}) + \hat{g}_q(x,\theta^*_{g_q})\eta - \ddot{q}_d(t) + C\dot{e}_q(t) + d(t) \quad (3.11)$$

According to the universal approximation theory in (X, 1994), $\theta^*_{f,g}$ can be defined in Eq. (3.12) as the optimal values of $\theta_{f_{q,g}}$which are used in this paper for the proof of stability and mathematical calculations and they were not used in the simulation process.

$$\theta^*_{f_{q\,v}} = \arg\text{Min}\,\{\sup\,(\hat{f}_{q,v}(x,\theta_{f_{q\,v}}) - f_{q,v}(x,t)\}$$
$$\theta^*_{g_{q\,v}} = \arg\text{Min}\,\{\sup\,(\hat{g}_{q,v}(x,\theta_{g_q}) - g_{q,v}(x,t)\} \quad (3.12)$$

Where, $f_{q.v}(x.t)$ and $g_{q.v}(x.t)$ are the unknown nonlinear functions, approximated by T1FLS expressed by $\hat{f}_{q.v}(x.\theta_{f_{q,v}})$ and $\hat{g}_{q.v}(x.\theta_{g_{q,v}})$. The subscripts q and v express the pitch rate and speed, respectively.

Then, the parameter estimation errors can be defined as $\varphi_f = \theta_f^* - \theta_f$ and $\varphi_g = \theta_g^* - \theta_g$. Therefore, the approximated functions become $\phi_{f_q}^T \psi_{f_q}(x) = \hat{f}_q(x.\theta_{f_q}^*) - \hat{f}_q(x.\theta_{f_q})$ and $\phi_{g_q}^T \psi_{g_q}(x) = \hat{g}_q(x.\theta_{g_q}^*) - \hat{g}_q(x.\theta_{g_q})$ (Labiod, Boucherit, & Guerra, 2005). Thus, the expressions $\hat{f}_q(x, \theta_{f_q}^*)$ and $\hat{g}_q(x, \theta_{g_q}^*)$ in Eq. (3.11) can be replaced as follows (Yoo & Ham, 1998a):

$$\dot{S}_q(t) = w + \phi_{f_q}^T \psi_{f_q}(x) + \hat{f}_q(x, \theta_{f_q}) + \phi_{g_q}^T \psi_{g_q}(x)\eta + \hat{g}_q(x, \theta_{g_q})\eta - \ddot{q}_d(t) + C\dot{e}_q(t) + d(t) \tag{3.13}$$

In the equivalent control term η_{eq1} given in Eq. (3.10), $f_q(x,t)$ and $g_q(x,t)$ are unknown and the disturbance $d(t)$ is unmeasurable. Thus, They were substituted by the bounded approximated functions $\hat{f}_q(x, \theta_{f_q})$ and $\hat{g}_q(x, \theta_{g_q})$ as calculated in Eq. (3.3) (L.-X. Wang, 1997). The boundedness of these functions is discussed in Assumptions 1 and 2. With this respect, the control law η_1 was chosen as presented in Eq. (3.14), inspired by (Roopaei et al., 2009), where η_{eq1} is the equivalent control input $\eta_{sw1} = Lsat(S_q)$ known as switching (reaching) control input.

$$\eta_1 = \underbrace{\left(\frac{1}{\hat{g}_q(x, \theta_{g_q})}\right)\left[-\hat{f}_q(x, \theta_{f_q}) + \ddot{q}_d(t) - C\dot{e}_q(t)\right]}_{\eta_{eq1}} + \underbrace{Lsat(S_q)}_{\eta_{sw1}} \quad L > 0 \tag{3.14}$$

Here, to avoid the chattering phenomenon in the reaching control law η_{sw1} in Eq. (3.14), a saturation function $\mathrm{sat}(S_q)$ was used instead of the $\mathrm{sgn}(S_q)$(Suleiman et al., 2018). Replacing η in Eq. (3.13) with the designed control law $\eta_1 = \eta_{eq1} + \eta_{sw1}$ as described in Eq. (3.14) (Roopaei et al., 2009), yields

$$\dot{S}_q(t) = w + \phi_{f_q}^T \psi_{f_q}(x) + \hat{f}_q(x, \theta_{f_q}) + \phi_{g_q}^T \psi_{g_q}(x)\eta_1 + \hat{g}_q(x, \theta_{g_q})[\eta_{eq1} + \eta_{sw1}] - \ddot{q}_d(t) + C\dot{e}_q(t) + d(t) = w + \hat{g}_q(x, \theta_{g_q})\eta_{sw1} + \tag{3.15}$$

$$\phi_{f_q}^T \psi_{f_q}(x) + \phi_{g_q}^T \psi_{g_q}(x)\eta_1 + d(t)$$

Stability Proof. The following Lyapunov candidate in Eq. (3.16) is adopted to prove the convergence of the tracking error to zero $S(t) = 0$ and $S\dot{S} \leq 0$ (Yoo & Ham, 1998a), (Khalil, 2001).

$$V_1 = \frac{1}{2} S_q^2 + \frac{1}{2\gamma_{f_q}} \phi_{f_q}^T \phi_{f_q} + \frac{1}{2\gamma_{g_q}} \phi_{g_q}^T \phi_{g_q} \tag{3.16}$$

Where γ_{f_q} and γ_{g_q} are the gains used in the adaptation laws in Eq. (3.19). Therefore, the time derivative of the selected candidate V_1 is:

$$\dot{V}_1 = S_q \dot{S}_q + \frac{1}{\gamma_{f_q}} \phi_{f_q}^T \dot{\phi}_{f_q} + \frac{1}{\gamma_{g_q}} \phi_{g_q}^T \dot{\phi}_{g_q} \tag{3.17}$$

Replacing $\dot{S}_q(t)$ by its final expression in Eq. (3.15), then Eq. (3.17) becomes:

$$\begin{aligned} \dot{V}_1 = {} & S_q w + S_q \hat{g}_q(x, \theta_{g_q})\eta_{sw1} + S_q d(t) + \left[S_q \phi_{f_q}^T \psi_{f_q}(x) + \frac{1}{\gamma_{f_q}} \phi_{f_q}^T \dot{\phi}_{f_q} \right] + \\ & \left[S \phi_{g_q}^T \psi_{g_q}(x)\eta_1 + \frac{1}{\gamma_{g_q}} \phi_{g_q}^T \dot{\phi}_{g_q} \right] = S_q w + S_q \hat{g}_q(x, \theta_{g_q})\eta_{sw1} + S_q d(t) + \\ & \frac{1}{\gamma_{f_q}} \phi_{f_q}^T \left(\dot{\phi}_{f_q} + S_q \gamma_{f_q} \psi_{f_q}(x) \right) + \frac{1}{\gamma_{g_q}} \phi_{g_q}^T \left(\dot{\phi}_{g_q} + S_q \gamma_{g_q} \psi_{g_q}(x)\eta_1 \right) \end{aligned} \tag{3.18}$$

Referring to Eq. (3.17), the following adaptation laws were employed as shown in Eq. (3.19) to consistently update the approximated functions during the simulation iteration. Based on the performance of the controller during the simulation, the terms $-\sigma_{f,g}\gamma_{f,g}\theta_{f,g}$ were added to the adaptation laws to enhance the adaptation process. In the adaptation laws defined in Eq. (3.19), $\psi_{f_q}(x)$ and $\psi_{g_q}(x)$ denote Fuzzy Basis Functions (FBFs), that were calculated in Eq. (3.7).

$$\dot{\theta}_{f_q} = -\sigma_{f_q}\gamma_{f_q}\theta_{f_q} + S_q\gamma_{f_q}\psi_{f_q}(x)$$
$$\dot{\theta}_{g_q} = -\sigma_{g_q}\gamma_{g_q}\theta_{g_q} + S_q\gamma_{g_q}\psi_{g_q}(x)\eta_1 \tag{3.19}$$

knowing $\dot{\phi} = -\dot{\theta}$ (Yoo & Ham, 1998a), it can be written as follows:

$$\dot{\phi}_{f_q} = \sigma_{f_q}\gamma_{f_q}\phi_{f_q} - S_q\gamma_{f_q}\psi_{f_q}(x)$$
$$\dot{\phi}_{g_q} = \sigma_{g_q}\gamma_{g_q}\phi_{g_q} - S_q\gamma_{g_q}\psi_{g_q}(x)\eta_1 \tag{3.20}$$

Therefore, by substituting the adaptation laws $\dot{\phi}_{f_q}$, and $\dot{\phi}_{g_q}$ from Eq. (3.20) into Eq. (3.18), and knowing $\eta_{sw1} = Lsat(S_q)$, it can be written in the following form:

$$\dot{V}_1 = S_q w + S_q\hat{g}\left(x\middle|\theta_{g_q}\right)Lsat(S_q) + S_q d(t) - \frac{1}{\gamma_f}\theta_{f_q}^T\left(\sigma_{f_q}\gamma_{f_q}\theta_{f_q}\right) -$$
$$\frac{1}{\gamma_g}\theta_{g_q}^T\left(\sigma_{g_q}\gamma_{g_q}\theta_{g_q}\right) = S_q w + L\,S_q\hat{g}_q(x.\theta_{g_q})\text{sat}(S_q) + S_q d(t) - \sigma_{f_q}\theta_{f_q}^T\theta_{f_q} -$$
$$\sigma_{g_q}\theta_{g_q}^T\theta_{g_q} \tag{3.21}$$

Hence, the expression in Eq. (3.21) can be written in the next inequality form shown in Eq. (3.22) (Roopaei et al., 2009). It should be noted $\theta_{f,g_q}^T\theta_{f,g_q} = \left|\theta_{f_q,g_q}\right|^2$ in this equation.

$$\dot{V}_1 \le |S_q||w| + L|S_q|\left|\hat{g}_q(x.\theta_{g_q})\right| + |S_q||d(t)| - \sigma_{f_q}\left|\theta_{f_q}\right|^2 - \sigma_{g_q}\left|\theta_{g_q}\right|^2 \le$$
$$|S_q||w| + L|S_q|\left|\hat{g}_q(x.\theta_{g_q})\right| + |S_q||d(t)| - \sigma_{f_q}\left|\theta_{f_q}\right|^2 - \sigma_{g_q}\left|\theta_{g_q}\right|^2 \tag{3.22}$$

Using the minimum approximation error in Eq. (3.11), $w = f_q(x,t) - \hat{f}_q(x.\theta_{f_q}^*) + \left(g_q(x,t) - \hat{g}_q(x.\theta_{g_q}^*)\right)\eta$, If the criteria in the Assumptions 1 and 2 are satisfied, we can conclude that w never goes to infinity and it is essentially bounded to certain small value (ε_1). Respectively, with these assumptions, Eq. (3.23) can be developed using the Triangular inequality as follows (Roopaei et al., 2009):

$$
\begin{aligned}
|w| &= \left|f_q(x\ t) - \hat{f}_q(x,\theta^*_{f_q})\right| + \left|g_q(x,t) - \hat{g}_q(x,\theta^*_{g_q})\right||\eta_1| \\
&\leq |f_q(x\ t)| + \left|\hat{f}_q(x,\theta^*_{f_q})\right| + \left\{|g_q(x\ t)| + \left|\hat{g}_q(x,\theta^*_{g_q})\right|\right\}|\eta_1| \\
&\leq \left\|\theta^{*\,T}_{f_q}\right\|\left\|\psi_{f_q}(x)\right\| + |f_q(x,t)| + \left\|\theta^{*\,T}_{g_q}\right\|\left\|\psi_{g_q}(x)\right\||\eta_1| \\
&+ |g_q(x\ t)||\eta_1| \leq P_{f_q} + F_q + (P_{g_q} + g_{q_{max}})(\sup(|\eta_1|)) < \varepsilon_1
\end{aligned}
\tag{3.23}
$$

As obtained in the Eq. (3.23), $|w| < \varepsilon_1$,and with respect to the boundedness of $|d(t)| \leq T$ and $g_{q_{min}} < \hat{g}_q(x.\theta_{g_q}) < g_{q_{max}}$, Eq. (3.22) can be reformulated as shown in Eq. (3.24) (Yau & Chen, 2006):

$$
\begin{aligned}
\dot{V}_1 \leq |\,S_q|\varepsilon_1 - L|\,S_q|g_{q_{max}} + T|\,S_q| - \sigma_{f_q}\left|\theta_{f_q}\right|^2 - \sigma_{g_q}\left|\theta_{g_q}\right|^2 \leq -\Big(Lg_{q_{max}} - \\
\varepsilon_1 - T\Big)|\,S_q| - \sigma_{f_q}\left|\theta_{f_q}\right|^2 - \sigma_{g_q}\left|\theta_{g_q}\right|^2
\end{aligned}
\tag{3.24}
$$

Where, σ_{f_q} and σ_{g_q} are considered as positive constants. Observing the variations of $\hat{g}_q(x.\theta_{g_q})$ during simulations which were in the interval]0,1] for all flight conditions, the value of L used in Eq. (14) was chosen such that $L > \frac{\varepsilon_1 + T}{|g_{q_{max}}|}$ to ensure that the expression $-\Big(Lg_{q_{max}} - \varepsilon_1 - T\Big)|\,S_q|$ remains negative. Thus, it can be concluded that $\dot{V}_1 = S_q\dot{S}_q < 0$, and if only S_q equals to zero, then $\dot{V}_1$ will be zero (Yoo & Ham, 1998a) Moreover, according to the Barbalat's lemma, for two bounded functions as S_q and $\dot{S}_q$, if $\lim_{t\to\infty} S_q = 0$, then the asymptotical stability of the aircraft can be achieved as the tracking error will be zero over the time (Khalil, 2001 ; Slotine & Li, 1991 ; Yau & Chen, 2006).

To compensate for the steady state error, we decided to apply an integral control term into the primary control law η_1 in Eq. (3.14), which yields the following final control input η_T:

$$\eta_T = \left[\frac{1}{\hat{g}_q(x,\theta_{g_q})}\right]\left[-\hat{f}_q(x,\theta_{f_q}) + \ddot{q}_d(t) - C\dot{e}_q(t)\right] + Lsat(S_q) + k\int e_q(t)dt \tag{3.25}$$

Based on the Heine-Cantor Theorem (Gillespie, 1955), if the tracking error is bounded within an interval $[a, b]$, then it is uniformly continuous. According to the properties of the Riemann integral, $\int e_q(t)dt$ will be also bounded, and it ensures that the suggested integral term in Eq. (3.25) does not induce instability in the system.

3.2.3 Aircraft Speed Control System

Developing a reliable control system for aircraft speed is crucial for aircraft stability and safety requirements, particularly when encountering turbulence. This article employed another T1AFSMC to rectify this challenge. With this regard, tracking error was defined as $e_v = V(t) - V_d(t)$, where V_d is desired speed and V is the actual aircraft speed. Using e_v and its derivative $\dot{e}_v = \dot{V}(t) - \dot{V}_d(t)$, we selected the sliding surface S_v as shown in Eq. (3.26) (Londhe & Patre, 2019):

$$S_v = e_v + D\dot{e}_v \tag{3.26}$$

where $D > 0$.

The equivalent control law η_{eq2} in Eq. (3.27) can be calculated by $\dot{S}_v(t) = 0$,. Knowing that functions $f_v(x.t)$ and $g_v(x.t)$ are unknown, the same T1FLS is used to obtain each approximated $\hat{f}_v(x.\theta_{f_v})$ and $\hat{g}_v(x.\theta_{g_v})$ in Eq. (3.27). Therefore, the aircraft speed control law η_2 becomes (Bessa, 2022):

$$\eta_2 = \underbrace{\left(\frac{1}{\hat{g}_v(x,\theta_{g_v})}\right)\left[-\hat{f}_v(x,\theta_{f_v}) + \dot{V}_d(t) - D\ddot{e}_v\right]}_{\eta_{eq2}} - \underbrace{H\text{sat}(S_v)}_{\eta_{sw2}}, \quad D\ H > 0 \tag{3.27}$$

Where $\text{sat}(S_v)$ refers to the saturation function.

Considering the speed control law $\eta_2 = \eta_{eq2} + \eta_{sw2}$ designed in Eq. (3.27), the proof of stability is presented in the Appendix I using the Lyapunov theorem and Barbalat's lemma to ensure the error converges asymptotically to zero ($S\dot{S} \leq 0$) (Khalil, 2001 ; Yoo & Ham, 1998a). The adaptation laws denoted by θ_{f_v} and θ_{g_v} were calculated in Eq. (3.28) to update the approximated functions $\hat{f}_v(x.\theta_{f_v})$ and $\hat{g}_v(x.\theta_{g_v})$(Yoo & Ham, 1998a).

$$\begin{aligned} \dot{\theta}_{f_v} &= -\sigma_{f_v}\gamma_{f_v}\theta_{f_v} + S_v\gamma_{f_v}\psi_{f_v}(x) \\ \dot{\theta}_{g_v} &= -\sigma_{g_v}\gamma_{g_v}\theta_{g_v} + S_v\gamma_{g_v}\psi_{g_v}(x)\eta_2 \end{aligned} \tag{3.28}$$

3.2.4 Dryden Turbulence Model

Mainly, there are two common turbulence models in the flight mechanics, known as Von Karman and the Dryden turbulence models as described in (Yeager, 1998) and (Hakim & Arifianto, 2018). In this article, it has been decided to use the Dryden turbulence model using the wind profile shown in Fig. 3.4. This turbulence model is a continuous mathematical model that can describe the turbulence an aircraft may face during flight, which has been verified by the United States Department of Defense to be used in the aircraft design and simulation purposes. In comparison with the Von Karman model, the Dryden model is easier to implement while the same results can be obtained by both of these methods. Moreover, this model has been formulated in terms of the appropriate scale lengths and the turbulence components intensities defined in MIL-F-8785C (Moorhouse & Woodcock, 1982). The employed turbulence profile was generated using the continuous Dryden model existing in the Simulink Aerospace Blockset with a moderate probability for exceedance of high-altitude intensity (10^{-3}) as follows:

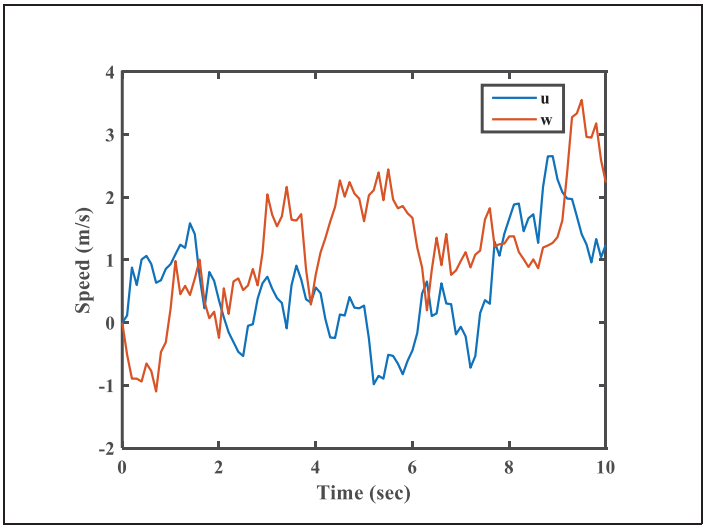

Figure 3.4 Turbulence Profile for the Longitudinal Motion

3.3 Simulations Results

The developed control systems for the pitch rate and speed of Cessna Citation X aircraft were simulated under different flight conditions during the cruise with and without turbulence using a nonlinear simulation platform which was initialized by the values given in Table 4 specified for the Weight, Center of Gravity (X_{cg}), Altitude, and Calibration AirSpeed (CAS) to select each 925 flight conditions within the flight envelope limits. In addition, the T1FLS approximator used the pitch rate and its reference in the pitch rate control system and the TAS and AOA in the aircraft speed control system to generate the membership functions configured by the parameter values expressed in Table 3.1. Moreover, Table 3.5 shows the corresponding design parameters used in each control system.

Table 3.4 Values of the Altitude, CAS, Weight, Xcg in the 925 flight conditions

	Units	Flight Conditions								
Altitude	ft	8000	10000	15000	20000	25000	30000	35000	40000	45000
CAS	knots	170	200	230	250	300	330			
Weight	lbs	26000	27000	28000	29000	30000				
Xcg	%	24	26	28	30	32				

Table 3.5 Design Parameters Values

	Parameters	Values
Pitch Rate Controller	Sliding Surface Coefficient (C)	15
	Adaptation Law Parameter (σ_f)	10^{-4}
	Adaptation Law Parameter (σ_g)	10^{-4}
	Adaptation Law Parameter (γ_f)	10^{2}
	Adaptation Law Parameter (γ_g)	10^{2}
	Switching Control Gain (L)	140
	Integral Control Gain (k)	4000
TAS Controller	Switching Control Gain (H)	800
	Sliding Surface Coefficient (D)	500
	Adaptation Gain (γ_{f_v})	1
	Adaptation Gain (γ_{g_v})	1
	Adaptation Design Parameter (σ_{f_v})	10^{-5}
	Adaptation Design Parameter (σ_{g_v})	10^{-5}

Furthermore, a model-based reference signal was considered for the aircraft pitch rate, as given in Eq. (3.29):

$$\frac{q_d(s)}{r(s)} = \frac{\omega_n^2}{s^2 + 2\xi\omega_n s + \omega_n^2} \tag{3.29}$$

Where $r(s)$: reference signal, $\xi = 0.7$, and $\omega_n = 3$.

In the first step, a comparison is provided between the designed T1AFSMC in this paper and a Model Referenced Adaptive Recurrent Neural Network (ARNN) control system proposed by us in (S. Hosseini, Inga, et al., 2023) for the pitch rate of Cessna Citation X aircraft. Both methodologies were developed for the same 12 flight conditions detailed in Table 3.4:

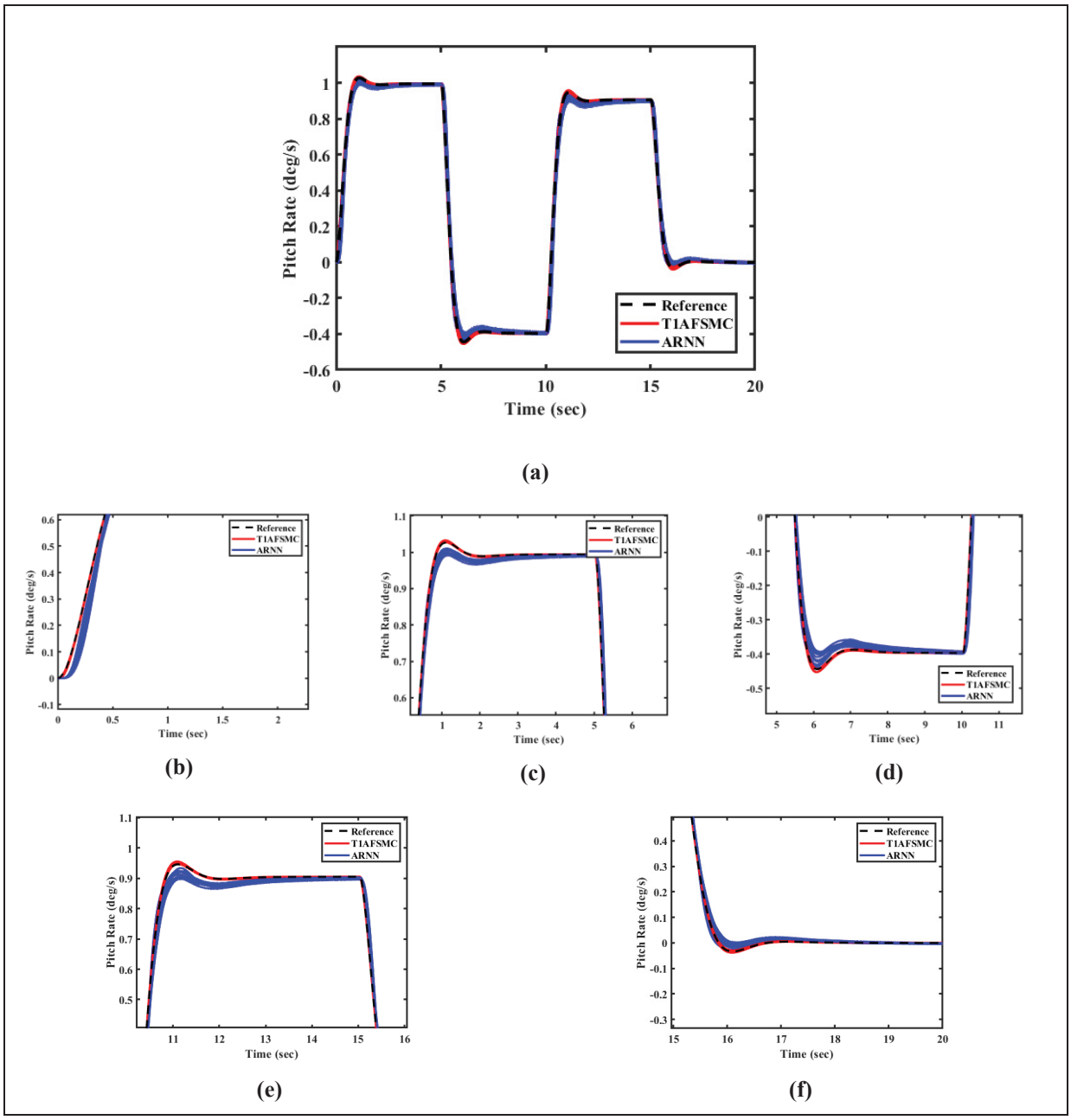

Figure 3.5 Comparison Between T1AFSMC and ARNN Control Systems

Fig. 3.5(a) shows the efficiency of both methods, and they satisfied the pitch rate tracking performance for all 12 flight conditions. However, Figs. 3.5(b)-3.5(f), showing close-up views of Fig. 3.5(a), show a steady state error between the pitch rate and its reference signal for the ARNN Control System, while the pitch rate got aligned perfectly with the reference

signal using the T1ASMC. Moreover, the obtained elevator deflections shown in Figs. 3.6(a) and 3.6(b) indicate that the T1AFSMC generated a smoother command rather than the ARNN.

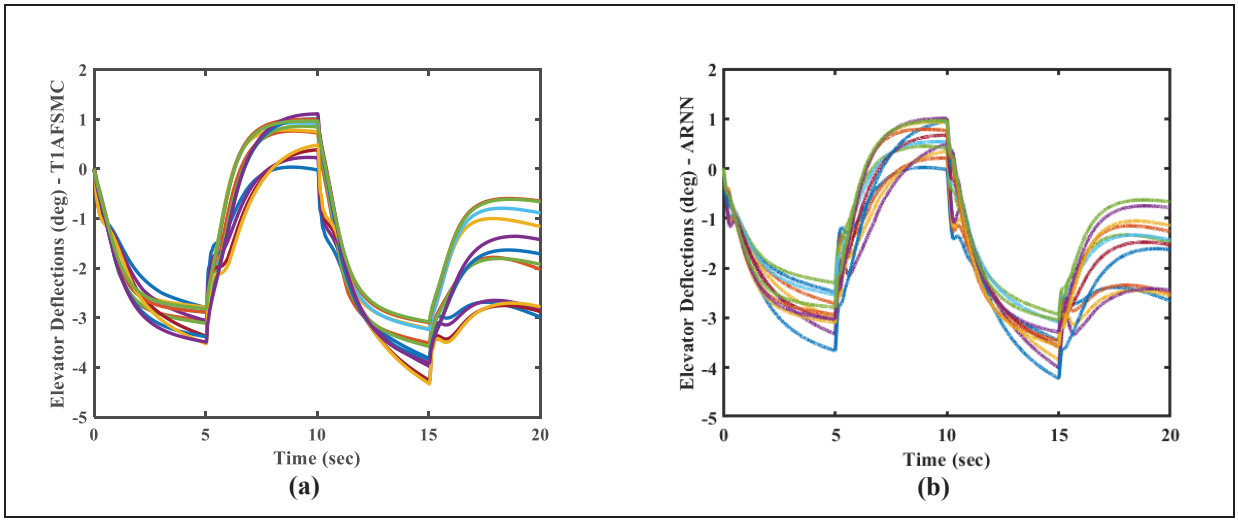

Figure 3.6 Time Variations of the Elevator Deflections for T1AFSMC (a) and ARNN (b) control Systems

This comparison shows the superiority of the T1AFSMC versus the ARNN control system. To ensure the performance of the proposed control system in this study, further simulation results are presented and discussed below:

Using the reference signal generated by the filter in Eq. (3.29), Figures 3.7 and 3.8 represent excellent signal performance as the pitch rate and pitch angle of the Cessna Citation X aircraft could consistently and steadily track their references. Thus, the controller could satisfy the expected tracking performance for all 925 flight conditions.

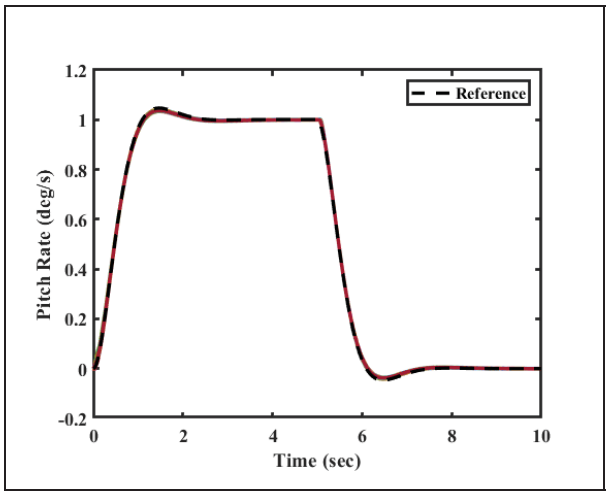

Figure 3.7 Pitch Rate Time Variations for All 925 Flight Conditions

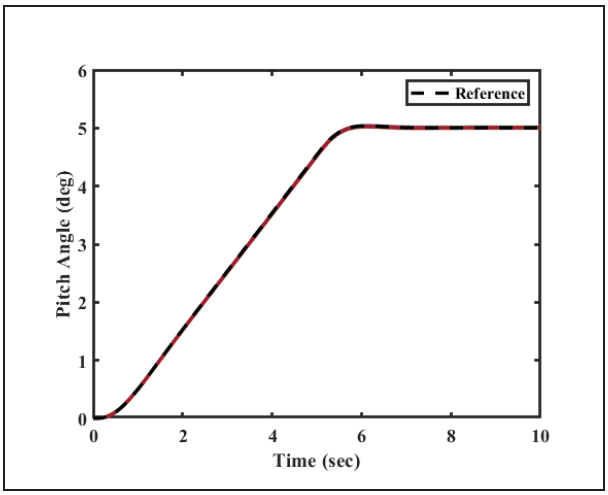

Figure 3.8 Pitch Angle Time Variations for All 925 Flight Conditions

Similar to the previous comparison between the T1AFSMC and the ARNN control, the smoothness of the control input signal is essential since high-frequency oscillations in the elevator control input can mechanically damage the actuators. Such mechanical damages must be avoided, as they can negatively affect the overall performance and safety of aircraft. Hence, it is imperative to ensure that elevator deflections are smooth and free of high-frequency oscillations.

The validation provided in Fig. 3.9 for elevator deflections, indicates that the controller satisfied this important criterion. For the TAS controller, we assumed that the aircraft pitch rate is constant to its trimmed value and the aircraft is accelerating based on the given speed reference signal. Therefore, the performance of the speed controller was assessed based on the time variations of the True AirSpeed (TAS), and the best results were obtained for 100 out of the 925 selected flight conditions, as shown in Fig. 3.10.

A more detailed representation of the results is provided in Fig. 3.11, illustrating the aircraft tracking performance for the TAS across all altitudes (from 8000 ft to 45000 ft) separately, considering all 925 flight conditions.

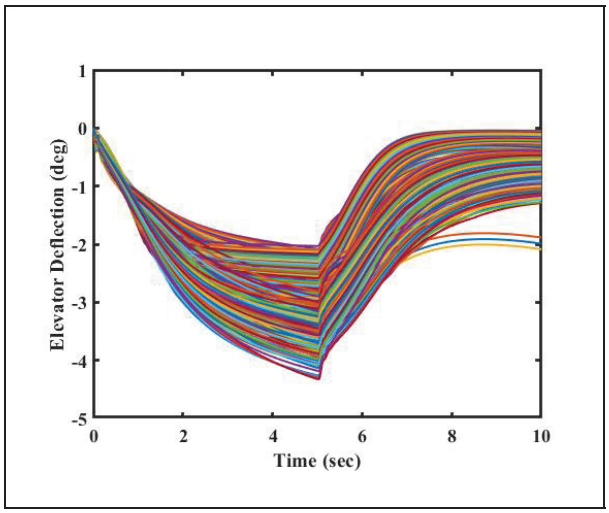

Figure 3.9 Elevator Deflection Time Variations for All 925 Flight Conditions

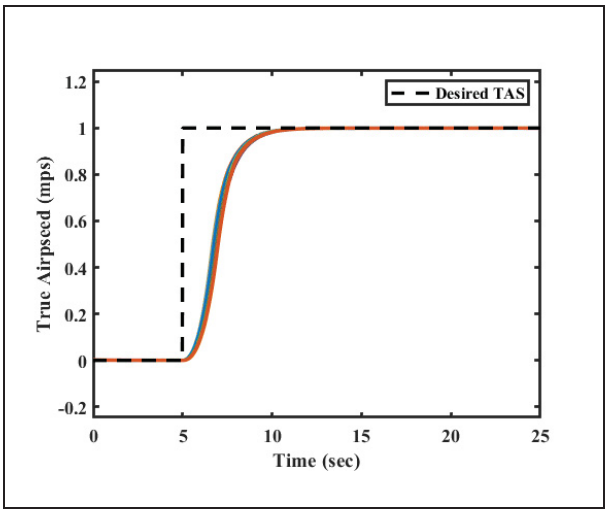

Figure 3.10 Normalized True Airspeed Tracking Performance for 100 Flight Conditions

The results presented in Figures 3.10 and 3.11 were normalized between 0 and 1 due to the variations in the trim values of the True Airspeed. This normalization was carried out to clarify of the aircraft performance evaluation and to compare its performance across all the chosen flight conditions.

According to the results shown in Fig. 3.11, the TAS controller could help the aircraft to accelerate with the given reference speed. However, the rise time (t_r) is longer at high altitudes due to the low air density, that reduces the engine performance compared to the air density at low altitudes. Therefore, the results obtained for the True Airspeed tracking performance are very well within the acceptable range.

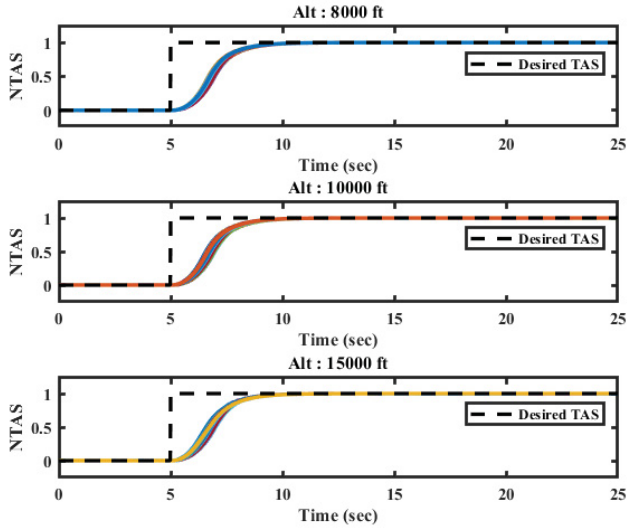

(a)

Figure 3.11 Normalized True Airspeed (NTAS) Variations across 925 Flight Conditions (a) at Altitudes = 8000 ft, 10,000 ft, and 15,000 ft (b) for Altitudes = 20,000 ft, 25,000 ft, and 30,000 ft, (c) for Altitudes = 35,000 ft, 40,000 ft, and 45,000 ft

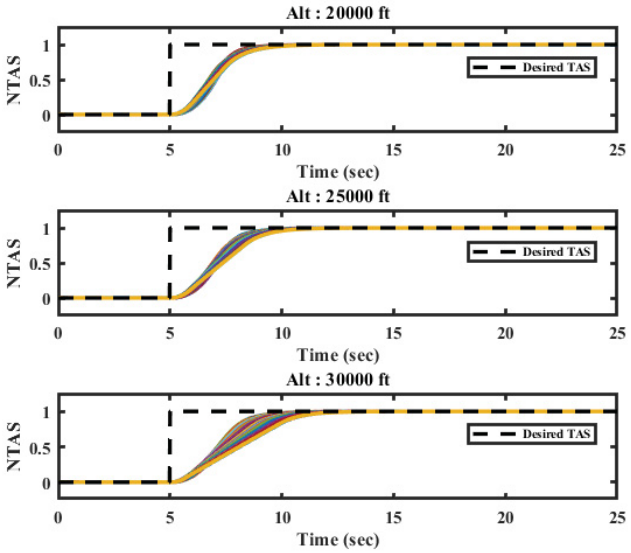

(b)

Figure 3.11 Normalized True Airspeed (NTAS) Variations across 925 Flight Conditions (b) for Altitudes = 20,000 ft, 25,000 ft, and 30,000 ft

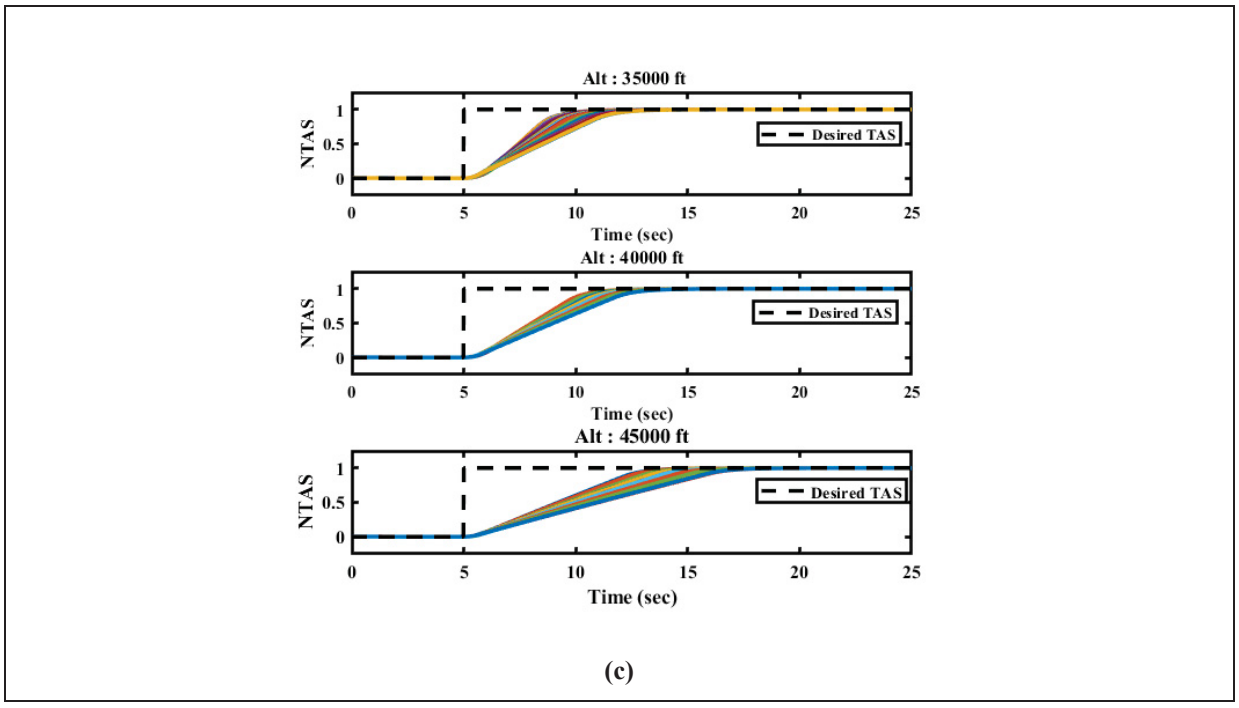

Figure 3.11 Normalized True Airspeed (NTAS) Variations across 925 Flight Conditions (c) for Altitudes = 35,000 ft, 40,000 ft, and 45,000 ft

To provide more details about the performance of the proposed control techniques, the distributions of the Average Mean Squared Error (AMSE) are given in Figures 3.12 and 3.13.

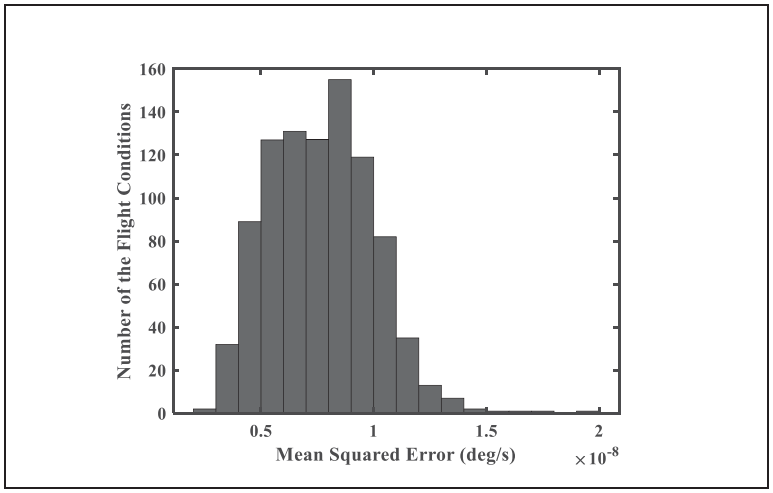

Figure 3.12 Distributions of the AMSE for the Pitch Rate

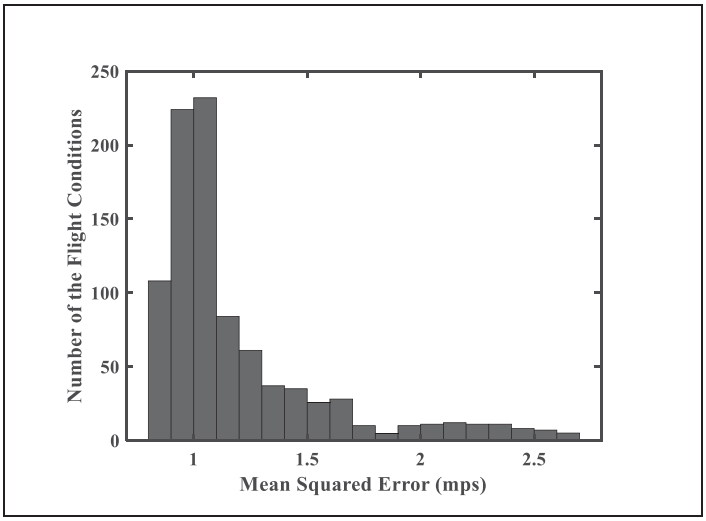

Figure 3.13 Distributions of the AMSE for the TAS

The distributions of the AMSE for the pitch rate and TAS are presented in Figures 3.12 and 3.13 for all 925 flight conditions without turbulence with respect to the results shown in Figures 3.7 and 3.11. These errors results prove that the controllers operate efficiently, as their error values are accepted in this research.

In addition, the performance of the aircraft equipped with these two controllers was evaluated in the presence of turbulence, a critical environmental condition. For the simulation, it was assumed that the aircraft flies at constant speed with an increase in the pitch rate or pitch angle, as shown in Figures 3.14 and 3.15.

It is extremely challenging to control aircraft dynamics under the effects of turbulence. Despite these difficulties, the proposed controllers can stabilize the aircraft and maintain it within the equilibrium and balanced operating region during the simulation iterations by minimizing the model dynamics variations.

The results shown in Fig. 3.14 indicate that by using the proposed methodology, the pitch rate can be adapted to the determined reference signal with the least possible oscillations. These signal characteristics have also been met for the pitch angle, as shown in Fig.3.15. In addition, the variation of the aircraft speed in the presence of turbulence is represented in

Fig.3.16, revealing that the controller could reduce the speed oscillations induced by the turbulence and thus keep the TAS variations within the ±2.57 m/s (±5 kts) range by aiming to keep the aircraft speed at its trimmed value for each flight condition. It must be noted that these variations are acceptable and negligible for the objectives of this research.

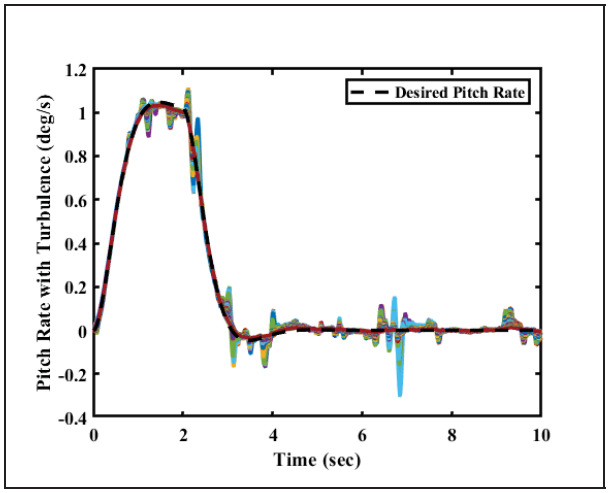

Figure 3.14 Pitch Rate Time Variations with Turbulence

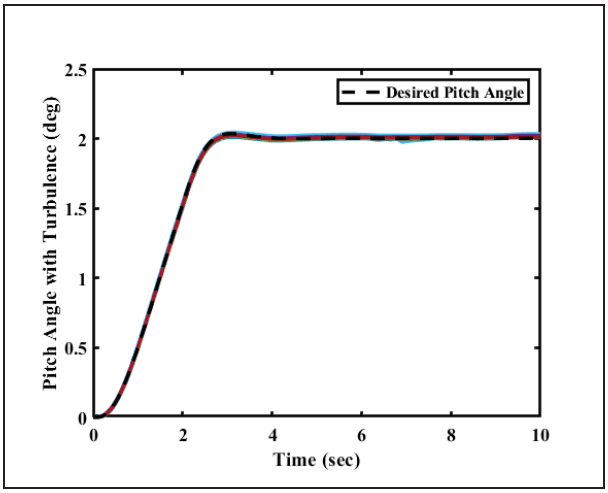

Figure 3.15 Pitch Angle Time Variations with Turbulence

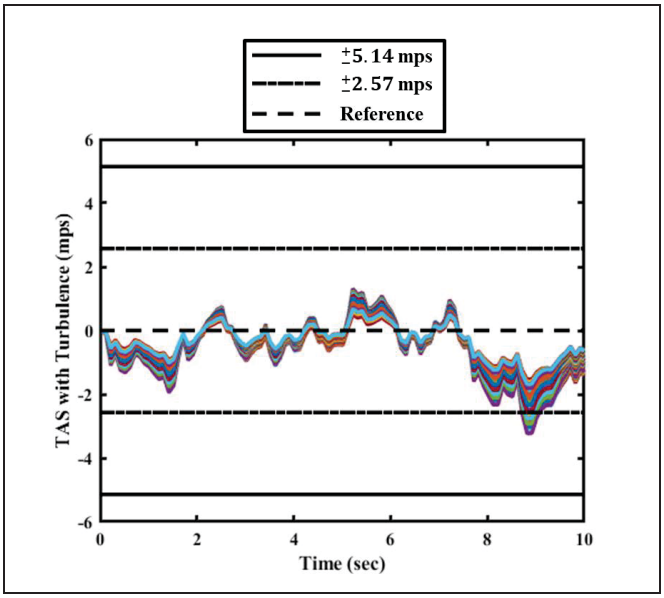

Figure 3.16 True Airspeed Time Variations with Turbulence

To clarify the TAS variations with turbulence, all TAS signals were overlaid in Fig. 3.16 (trimmed values were subtracted from all signals to let them start from zero).

In the Tables 3.6 and 3.7, the performances of the suggested controllers are evaluated at 9 different altitudes while the values of the weight, center of gravity (Xcg), and CAS change at each flight condition. This evaluation describes the ability and the reliability of the designed controllers at different altitudes for the Cessna Citation X aircraft. The tracking errors were calculated using the Average Mean Squared error (AMSE), the Average Root Mean Squared Error (ARMSE), the Average Mean Absolute Error (AMAE) and the Average Integral Squared Error (AISE).

Table 3.6 Pitch Rate Errors at Different Altitudes without Turbulence

Altitude (ft)	Without Turbulence			
	AMSE	ARMSE	AMAE	AISE
	(deg/s)	(deg/s)	(deg/s)	(deg/s)
8000	5.76×10^{-9}	3.32×10^{-6}	5.38×10^{-5}	0.0021
10,000	6.93×10^{-9}	4.87×10^{-6}	5.79×10^{-5}	0.0022
15,000	7.42×10^{-9}	6.23×10^{-6}	6.01×10^{-5}	0.0023
20,000	7.41×10^{-9}	6.20×10^{-6}	6.10×10^{-5}	0.0023
25,000	7.54×10^{-9}	6.18×10^{-6}	6.25×10^{-5}	0.0024
30,000	8.01×10^{-9}	6.88×10^{-6}	6.53×10^{-5}	0.0025
35,000	8.18×10^{-9}	5.80×10^{-6}	6.84×10^{-5}	0.0027
40,000	8.86×10^{-9}	4.30×10^{-6}	7.38×10^{-5}	0.0030
45,000	8.89×10^{-9}	3.35×10^{-6}	7.65×10^{-5}	0.0032

Table 3.7 Pitch Rate Errors at Different Altitudes with Turbulence

Altitude (ft)	With Turbulence			
	AMSE	ARMSE	AMAE	AISE
	(deg/s)	(deg/s)	(deg/s)	(deg/s)
8000	1.55×10^{-7}	1.91×10^{-5}	2.51×10^{-4}	0.0125
10,000	2.05×10^{-7}	1.72×10^{-5}	2.78×10^{-4}	0.0134
15,000	9.02×10^{-8}	1.83×10^{-5}	2.06×10^{-4}	0.0101
20,000	5.79×10^{-8}	1.96×10^{-5}	1.72×10^{-4}	0.0084
25,000	4.20×10^{-8}	2.10×10^{-5}	1.49×10^{-4}	0.0071
30,000	3.10×10^{-8}	2.09×10^{-5}	1.29×10^{-4}	0.0060
35,000	2.43×10^{-8}	2.27×10^{-5}	1.14×10^{-4}	0.0051
40,000	2.19×10^{-8}	2.26×10^{-5}	1.09×10^{-4}	0.0048
45,000	1.99×10^{-8}	3.03×10^{-5}	1.04×10^{-4}	0.0044

Since Tables 3.6 and 3.7 show negligible error values, it can be said that the designed controllers (one for aircraft pitch rate and the other for aircraft True Air Speed) are valid for both ideal and turbulence conditions.

To summarize, the proposed control methodologies are highly efficient and accurate in achieving adequate performance. These controllers were validated via an analysis of the calculated errors for each individual flight condition under both ideal conditions and in the presence of turbulence. The error values remained consistently low across all flight conditions, indicated the proper performance of the Cessna Citation aircraft in terms of its stability, robustness and reliability using the suggested Type One Adaptive Fuzzy Sliding Mode Control system. Furthermore, controllers equipped with the approximated functions by the proposed type-one fuzzy logic system could handle dynamic variations caused by turbulence or changes in flight conditions. The adaptive characteristics of this control methodology enable real-time parameter adjustments, which cannot be obtained in non-

adaptive or classical approximation methods. Moreover, traditional sliding mode control may induce chattering, whereas combining the type one fuzzy logic system and sliding mode control could smooth out the control input given to the actuation system. Moreover, this control system is also flexible, meaning that it can be applied to various aircraft types. The main challenge in this research lies in its heavy reliance on the designer's knowledge about an aircraft operational limits to select appropriate membership functions. Generally, it can be challenging to define appropriate fuzzy rules for approximating aircraft dynamics. The designed adaptation laws could update the approximated functions during the simulation, considering the dynamic variations and the presence of turbulence.

3.4 Conclusions

This paper presented a novel control law for the longitudinal motion of the Cessna Citation X aircraft. This methodology is developed based on a combination of a Type one fuzzy logic-based model, an adaptive control approach and a Sliding Mode control technique to control the aircraft pitch rate. The importance of this research may be summarized with respect to the effects of uncertainties, nonlinearities, parameter variations and perturbations on aircraft performance. Based on the presented results, the approximation of aircraft nonlinearities by the proposed Type one fuzzy-logic methodology can be a potential solution, as it can be updated by the adaptation laws suggested in this research. In addition, the Sliding Mode Control system increases the system's stability and robustness. As a benefit, this control system does not require any explicit knowledge regarding the mathematical aspects of the aircraft model, and it uses qualifications of the measured variables instead of their crisp values. In contrast to conventional control systems, the same structure and constant gains can be used for all flight conditions, regardless of dynamic variations. Based on the obtained results the two controllers, for aircraft pitch and for aircraft speed, can efficiently satisfy the tracking performance for the pitch rate while stabilizing the aircraft speed in the presence of turbulence. Also, the validation results for all flight conditions uniformly distributed over the aircraft flight envelope proved the validity of the proposed control systems for the longitudinal motion of the Cessna Citation X during the cruise phase.

CHAPTER 4

NEW TYPE-II FUZZY LOGIC BASED CONTROL SYSTEM FOR THE CESSNA CITATION X

S.M. Hosseini, G. Ghazi, and R.M. Botez

Research Laboratory in Active Controls, Avionics and AeroServoElasticity (LARCASE),
Department of Systems Engineering, École de Technologie Supérieure,
1100 Notre-Dame West, Montreal, Quebec, Canada H3C 1K3

Paper published in *Journal of Aerospace Information Systems*, September 2024

Resumé: Cet article présente une nouvelle loi de contrôle basée sur un système de logique floue de type 2 (T2FLS) pour l'avion Cessna Citation X en croisière. Cette méthodologie combine trois systèmes de contrôle : un T2FLS, un système de contrôle par mode glissant (SMC) et un système de contrôle adaptatif. Contrairement aux contrôleurs conventionnels, ce système de contrôle peut gérer les incertitudes et les variations de la dynamique de l'avion à l'aide de l'approximateur T2FLS. Les fonctions approximées ont été mises à jour pendant les itérations de simulation à l'aide de lois d'adaptation dérivées du théorème de Lyapounov. La caractéristique d'adaptabilité de ce contrôleur permet de mettre à jour les fonctions approximées alors que les autres paramètres de conception restent inchangés. Ce fait simplifie le processus de conception du contrôleur et élimine la nécessité d'utiliser un groupe de contrôleurs conventionnels avec différents gains pour contrôler l'avion dans diverses conditions de vol. En outre, le système de commande par mode glissant contribue à garantir la stabilité et la robustesse de l'avion, ainsi que deux autres méthodologies en présence et en l'absence de turbulences. La performance de cette méthodologie de contrôle a été validée avec une plateforme de simulation non linéaire développée pour l'avion d'affaires Cessna CitationX en utilisant des données de vol précises dérivées d'un simulateur de vol Level D au Laboratoire de recherche sur les commandes actives, l'avionique et l'aéro-servoélasticité (LARCASE).

Abstract: This paper presents a newcontrol lawbased on type-2 fuzzy logic system(T2FLS) for the Cessna Citation X aircraft during cruise. This methodology combines three control systems: a T2FLS, a sliding mode control (SMC) system, and an adaptive control system. Differing from conventional controllers, this control system can deal with uncertainties and aircraft dynamics variations using the T2FLS approximator. The approximated functions were updated during the simulation iterations using adaptation laws derived from the Lyapunov theorem. The adaptability characteristic of this controller allows updating the approximated functions while the other design parameters remain unchanged. This fact simplifies the controller design process and eliminates the need to use a group of conventional controllers with different gains to control the aircraft in various flight conditions. In addition, the sliding mode control system helps to guarantee the aircraft's stability and robustness, along with two other methodologies in the presence and absence of turbulence. The performance of this control methodology was validated with a nonlinear simulation platform developed for the Cessna CitationXbusiness aircraft using accurate flight data derived from a LevelDflight simulator at the Research Laboratory in Active Controls, Avionics and AeroServoElasticity (LARCASE).

4.1 Introduction

Nowadays, aircraft have become highly complex due to the constant drive to improve flight performance, which may increase the pilot's workload during flight, especially under critical conditions such as turbulence. This complexity and the inherent uncertainties in controlling business aircraft are the main motivations for our research, which explores the integration of a type-2 fuzzy logic system, sliding mode control, and adaptive control systems. Conventional control methodologies often struggle to maintain robust performance when dealing with dynamics variations, uncertainties, and changes in flight conditions, potentially leading to unsatisfactory performance or stability.

Type-2 fuzzy logic systems provide the capability to handle higher levels of uncertainties compared to Type-1 systems, making them particularly suitable for approximating the aircraft dynamics and managing uncertainties. However, despite their ability to handle uncertainties, Type 2 fuzzy systems can be improved by enhancing their adaptability and response to sudden changes in aircraft dynamics. This enhancement can be achieved through the application of sliding mode control and adaptive control systems. Sliding mode control is well-known for its robustness and ability to ensure system stability under various operating conditions, including system uncertainties and external disturbances. Meanwhile, adaptive control systems adjust the parameters in the control system in real-time, enabling these systems to adapt to changes in the system dynamics or due to the external environment. By combining Type Two Fuzzy Logic System (T2FLS), Sliding Mode Control (SMC) system and Adaptive Control methodologies, our research aims to develop a comprehensive control system for business aircraft that leverages the strengths of each approach. The integration seeks to offer a novel solution that is not only capable of handling high levels of uncertainties, but also would be adaptive and robust against turbulence and dynamic variations.

In addition to the operational benefits of the Type Two Adaptive Fuzzy Sliding Mode Control system, the proposed fuzzy logic-based methodology in this paper may reduce the pilot's workload by considering the challenge stated earlier and we believe that our findings in this applied research contribute valuable insights to the aviation and aerospace industry, showcasing excellent results for Cessna Citation X (CCX) aircraft business jet aircraft with and without moderate intensity turbulence.

A brief overview of relevant studies on the design of various conventional and AI-based control methodologies is presented and applied to different aircraft and UAVs.

To ensure the safety of low-altitude flights, a robust LQG control system was designed in (Xiong & Liu, 2023) to mitigate the effects of disturbances. This methodology included a specific barrier function that helped to maintain the aircraft altitude within a safe margin. Also, a combination of an L1-adaptive control system, a linear control methodology, and a

dynamic inversion method was implemented in both inner and outer loops to reduce the effects of turbulence and actuator failures in UAVs (Moncayo et al., 2013).

To optimize the gains of conventional control methods, such as Proportional-Integral (PI) control system and Non-Linear Dynamic Inversion (NLDI) methods, an enhanced Genetic Algorithm (GA) was presented in (K. Wilburn et al., 2014). Throughout this methodology, the tracking performance can be guaranteed for various types of UAVs. In addition, to guarantee the stability of a group of quadrotors, a hierarchical control system was developed in (Qian & Liu, 2022). In this research, the controller features an outer loop with an Uncertainty and Disturbance Estimator (UDE) based robust controller for pathway tracking and an inner loop for attitude control.

For the design of the flight control system, two Proportional-Derivative (PD) control systems were combined with an Adaptive Fuzzy Terminal Sliding Mode Control system to stabilize the position and attitude of a quadrotor (Nekoukar & Mahdian Dehkordi, 2021). This controller was designed to enable the quadrotor to track a designated flight path in different flight scenarios.

A fault-tolerant nonlinear dynamic inversion method was applied in (Dhadekar & Talole, 2018) to estimate uncertainties and disturbances, ensuring the robustness of the controller. The results obtained in this study demonstrated that the controller could handle any possible faults or failures in the actuator. Similarly, Liu *et al.* in (J. Liu, Sun, Chen, & Sun, 2019) used a new fixed-time extended state observer to determine model disturbances and uncertainties. The observer was then combined with fixed-time output feedback control methodology for high angle of attack maneuvers with the thrust vector of a fighter aircraft.

Stability is one of the most crucial criteria to consider when operating an aircraft (Susanto et al., 2021). Therefore, different conventional control methodologies were implemented to achieve a stable flight procedure. In (Qi et al., 2021), a modified uncertainty and disturbance estimator were used in conjunction with a Proportional Integral Derivative (PID) controller

with the aim to effectively reject actuator disturbances. This methodology significantly improved the attitude tracking performance of quadrotors by reducing both the disturbance estimation and tracking errors. In another study, the efficiency of a PID controller was evaluated with a focus on enhancing the stability of a Boeing commercial aircraft, aiming to reduce overshoots and rise time (Rehman et al., 2021). In comparison to conventional PID controllers, the fuzzy logic-based PID control system proposed in (J. Dong & He, 2019) has been identified as a better method for reducing tracking error in quadrotor UAVs. On the other hand, the adaptive control methodology and Sliding Mode Control system were combined to guarantee the stability of an F-16 unknown external disturbance and aerodynamical uncertainties (Ijaz et al., 2021).

Several studies have also been focused on the application of Fuzzy Logic-based control systems. The research in (Zeghlache et al., 2017) assessed the performance of a hybrid control system that combined an interval type-2 fuzzy system with a PID based sliding mode control system. Their results indicated that the proposed controller was able to satisfy the needs of both robustness and asymptotic stability of an Octo-rotor aircraft with minimum chattering (unwanted oscillations with finite frequency and amplitude). Another compound control system, consisting of two subsystems, was developed for a quadrotor (X. Zhang et al., 2021). First, an adaptive fuzzy quantized control strategy was designed to remove the nonlinearities caused by a quantizer in the quadrotor, and then an adaptive fuzzy dynamic surface control system was developed for under-actuated quadcopters. Experimental results demonstrated that this control system provided very good performance for the Quanser QBall-X4 quadrotor.

Controlling an aircraft becomes particularly important when dealing with system failure and external disturbances. For instance, the stability of a quadrotor was maintained using an interval type-2 fuzzy sliding mode control, even in the case of a failure in its actuator system (Saggai, Zeghlache, Benyettou, & Djerioui, 2021). The asymptotical stability of the quadrotor was guaranteed by the Lyapunov theorem. The Type-2 Fuzzy Logic System was used to minimize the chattering effects. By addressing faults and collision avoidance for a

group of fixed-wing UAVs in (Ziquan Yu, Xu, Zhang, Jiang, & Su, 2023), a hybrid control system was employed using fractional order-based sliding mode surfaces, disturbance observers, and an interval type-2 fuzzy neural network system. This article demonstrated that this combination guaranteed error convergence in all follower UAVs. The tracking performance of these UAVs can be also achieved using the methodology developed in (Ziquan Yu, Zhang, Liu, Qu, & Su, 2019). This distributed fault-tolerant cooperative control system, which is based on fuzzy neural networks, estimates the nonlinearities that arise from actuator faults and model uncertainties. A combination of type two adaptive fuzzy system with the Backstepping (BP) method was applied to compensate for the failures in actuation system in the vertical flight (Zeghlache et al., 2019).

A combination of Sliding Mode Control system and a general Type-2 fuzzy neural network system was suggested for the longitudinal motion of a Boeing 747 aircraft to address the challenges arising from parameter uncertainty, actuators, and noise that could cause passenger discomfort (Tavoosi, 2020). Yu *et al.* in (X. Yu, Fu, Li, & Zhang, 2018) introduced a combination of multivariable sliding mode control and self-constructing fuzzy neural networks to ensure the finite-time stability of the Boeing 747 aircraft longitudinal motion, even when actuator failures were considered. This control system also guaranteed good tracking performance. Furthermore, an artificial immune system was integrated into the design of a model reference based PID controller for generating angular rate commands. Respectively, a Non-Linear Dynamic Inversion (NLDI) technique was employed within this architecture to mitigate its nonlinearities effects under abnormal conditions (Perez et al., 2015). In addition, a coaxial tri-rotor helicopter was controlled in (Zeghlache et al., 2015) using interval type-2 fuzzy logic control and sliding mode control methodologies to resolve the chattering and satisfy its robustness and stability encountering the failures.

In addition, a Direct Adaptive Fuzzy Control system was designed with One Adaptive Parameter (OAP) adaptation laws. This design aimed to reduce the tracking errors in the presence of uncertainties, such as external disturbances and nonlinearities in the aircraft wing rock phenomenon (Lai et al., 2022). Moreover, the work in (Jie, Xiaozhou, & Jinhuan, 2017)

suggested the use of a fuzzy-based adaptive sliding mode control to address uncertainties and disturbances in real-time attitude control for a quadrotor aircraft. An interval type-2 fuzzy adaptive sliding mode control proposed in (X. Jiao, Fidan, Jiang, & Kamel, 2019) to guarantee the tracking performance of a generic hypersonic aircraft dealing with aerodynamic uncertainties.

This study focusses on the design of a controller for the longitudinal motion of the Cessna Citation X aircraft. Many studies have focused on this popular type of business jet, some of which are discussed next.

Satisfying the handling qualities of an aircraft has been the main question of several studies. As suggested in (Ghazi & Botez, 2015b), this aspect is more difficult in the presence of uncertainties. One approach to address this challenge is to design a controller using specific techniques, and subsequently to use a suitable method to assess its robustness. For instance, Ghazi *et al.* in (Ghazi & Botez, 2015b) adopted this approach to design a controller for the lateral motion of the Cessna Citation X, that was found to be robust to uncertainties. The authors applied the well-known Linear Quadratic regulator (LQR) theory to design the controller and used the Guardian Maps theory to evaluate its robustness. The parameters of the controller were optimized using a Genetic Algorithm. A similar approach was considered in (Ghazi & Botez, 2014) to design a flight controller for the Lynx helicopter, aiming to achieve optimal handling qualities.

In another study (Yamina Boughari, Botez, et al., 2017), an H_∞ robust control system was designed with genetic and differential evolution algorithms to optimize the weighting functions. The results showed that very good handling qualities were achieved for both the longitudinal and lateral dynamics stability of the Cessna Citation X aircraft.

An optimal control system was employed in (Yamina Boughari, Georges Ghazi, et al., 2017) while using a meta-heuristic algorithm to reduce the design complexity caused by trial and error determination of the controller parameters. According to (Yamina, Georges, Ruxandra

Mihaela, & Florian, 2017b), the performance of the control methodology designed in previous articles was valid for the whole flight envelope of the Cessna Citation X aircraft in terms of its linear and nonlinear dynamics stability, eigenvalues, and handling qualities criteria for the Cessna Citation X control clearance. The authors concentrated in (Ghazi et al., 2016) on the design of a controller for the Control and Stability Augmentation Systems (CAS + SAS). For the CAS, it has been shown that the Proportional-Integral (PI) controller can adequately control the variations of the Cessna Citation X pitch rate using the Guardian Maps theory.

The articles mentioned above highlighted the effectiveness and accuracy of classical and robust control systems for both longitudinal and lateral motions of the CCX aircraft. However, despite their abilities to obtain very good results, these controllers are highly sensitive to dynamic variations and unforeseen flight conditions. Leveraging Artificial Intelligence (AI)-based control methods might provide a solution to these limitations.
In this article, a Type-2 Adaptive Fuzzy Sliding Mode Control System was designed for the longitudinal motion of the Cessna Citation X aircraft. Two controllers were developed, one for controlling the aircraft pitch rate and another for stabilizing aircraft speed, and their performance was evaluated for both turbulent and non-turbulent conditions. The main contribution of this article lies in the following cases:

1) Apart from theoretical aspects, the novelty of this research lies on the application of this AI-based control methodology for the Cessna Citation X aircraft as a business aircraft. Referring to the literature review and the comparison presented in Table 4.1, this combination of control methodologies was commonly applied to hypersonic aircraft, Unmanned Air Vehicles (UAVs), and Quadcopters, and it was hardly designed for business aircraft. The developed controllers in this paper were designed using a nonlinear simulation platform designed validated with the flight data obtained from the highest (Level-D) certified Research Aircraft Flight Simulator (RAFS) for Cessna Citation X aircraft all over the flight envelope. This platform provides valuable insights and a highly realistic assessment of the performance of our control

system to ensure that the proposed control methodology meets the highest safety and performance standards.

2) According to Table 4.1, Fuzzy logic-based methods were mainly employed for the design of the switching control law in Aerospace and Aviation applications; however, this article uses the Type Two Fuzzy Logic system (T2FLS) for the approximation of the unknown aircraft dynamics and nonlinearities (this research considered the aircraft model as a black box and there is no need to have insights on its details e.g. on the equations of the motions). The Cessna Citation X aircraft deals with two main uncertainties: in aircraft model and in turbulence generated by the Dryden turbulence model configured by the specifications provided in the MIL-F-8785C for moderate-intensity turbulence (Moorhouse & Woodcock, 1982). The Type Two fuzzy logic system-based control system can offer improved system performance, reliability, and adaptability, outweighing the costs associated with its complexity. Unlike the T1FLS, whose membership function defines a precise value of its degree for each element that may limit its ability to handle uncertainties, or it may not adequately represent real-world complexities where uncertainties are dynamic and not precisely defined, in the T2FLS, the membership degree is itself fuzzy. In contrast with the previous studies in the literature, we considered obtaining a smooth control input as the elevator deflections. Moreover, the combination of the T2FLS as an approximator, Adaptive control system, and sliding mode control system could efficiently eliminate the chattering imposed on the deflections of the elevator.

3) The T2FLS in this article is equipped with adaptation laws to adjust the approximated functions in real-time, responding to the variations of aircraft dynamics, turbulence, and uncertainties, particularly in this article that considered unknown the aircraft dynamics. These adaptation laws enhance the stability of the aircraft in comparison with the static control systems while reducing human intervention in the design process. This approach eliminates the need for a training process used by the Neural Network (NN) based methodologies.

4) According to the provided literature review, the Center Of Sets (COS) type reduction method was commonly employed in all previous papers, whereas this article proposed to apply a non-iterative type reduction method, known as Nagar-Bardini (NB) algorithm that was first introduced in (Chen, 2019 ; El-Nagar & El-Bardini, 2014). The previous studies in (Zeghlache et al., 2019, 2017, 2015) suggested the use of Karnik-Mendel (KM) algorithms that increase the computational cost. As a solution for this issue, it was claimed in (El-Nagar & El-Bardini, 2014) that the NB algorithm could reduce the computational cost compared with the KM algorithms while improving the performance of Type Two Fuzzy Logic System (T2FLS) in real-time applications. With this algorithm, the endpoints of the centroid interval include two linear type one fuzzy logic systems using Upper and Lower Membership Functions LMFs and UMFs (Chen, 2019 ; El-Nagar & El-Bardini, 2014).

5) In our research, based on the controller performance, we opted to choose the switching control term U_q^{sw} in Eq. (4.15) for the design of a new pitch rate control law, denoted by U_q^{Final} in Eq. (4.26). Furthermore, the Lyapunov theorem was used with an adapted candidate to prove the aircraft stability and the convergence of tracking errors for both control laws. This theorem also simplifies the formulation of the adaptation laws, updating the approximated functions for each flight conditions during simulation. Due to the extreme effects of the turbulence on the aircraft speed and pitch rate, we decided to employ the same control methodology to stabilize the aircraft True Airspeed around its trimmed value at each flight condition.

Table 4.1 Analyzing the Applications of Fuzzy Logic Methodology in Aerospace and Aviation Industry

Authors	Date	A/C Model	SMC	T1FLS	T2FLS	Adaptive	Other	Advantages	Notes	Refs
Ijaz *et al*	2021	F-16	*			*		Robustness against the Perturbation	1. No Approximated Dynamics	(Ijaz et al., 2021)
Nekoukar and Dehkordi	2021	Quadrotor	*	*		*	PID	Stability in Presence of the Frame Vibrations, Blade Instability and Imbalance Mass	1. No Test on Long Flights	(Nekoukar & Mahdian Dehkordi, 2021)
Zeghlache *et al*	2019	Quadrotor			*	*	BP	Optimal Performance with Actuator Faults	1. IKM Method with Averaging for Type Reduction	(Zeghlache et al., 2019)
Zeghlache *et al*	2015	Tri-rotor helicopter	*		*			Attenuating the Chattering Effects and Improved Performance in Presence of Benign Faults	1. No Approximated Dynamics 2. IKM Method with Averaging for Type Reduction	(Zeghlache et al., 2015)
Zeghlache *et al*	2017	6 DOF Octo-rotor Aircraft	*		*	*		Satisfied Tracking Performance and Robustness	1. No Approximated Dynamics 2. IKM Method with Averaging for Type Reduction	(Zeghlache et al., 2017)
Jiao et al	2017	Hypersonic aircraft	*		*	*		Satisfied Tracking Performance and Robustness	1. No Approximated Dynamics 2. Center Of Set Type Reducer	(X. Jiao et al., 2019)
Saggai et al	2021	Quadrotor	*		*			Stabilized with Actuator Fault	1. No Approximated Dynamics 2. Type Reducer not Specified.	(Saggai et al., 2021)

Referring the problem statement and research motivation described earlier, the main content of this paper is developed as follows:

In Section 4.2, the nonlinear state-space model of aircraft will be presented whose unknown functions are approximated by the proposed Type-2 fuzzy logic system whose architecture is discussed in detail in this section. Then, the applied Dryden turbulence model is explained in last subsection as an unknown eternal disturbance and uncertainty. Next, Section 4.3 summarizes the design of the control laws for each aircraft pitch rate and speed control system. This section explains how three methodologies interact: Sliding Mode Control System, Type Two Fuzzy Logic System, and Adaptive Control System. The Lyapunov theorem was also incorporated to prove the stability of the pitch rate control system in this section and the aircraft speed control system in the Appendix. The simulation results are then presented in Section 4.4, followed by a discussion. Section 4.5 concludes with remarks on the proposed methodology for the Type-2 Adaptive Fuzzy Sliding Mode Control Systems based on simulation results.

4.2 Aircraft Dynamics Approximation and Turbulence

According to the problem statement, research motivations, and contributions described in the previous section, the applied methodology of this article is explained that was used for the development of two controllers for the longitudinal motion of the Cessna Citation X aircraft, one for the aircraft pitch rate and the other for an aircraft speed control system. These controllers are designed based on three control methodologies: Sliding Mode Control (SMC), a Fuzzy Logic system, and an Adaptive control system. Initially, the state-space representation of the aircraft system will be discussed with the existing unknown functions and the architecture of the Type Two Fuzzy Logic System to approximate them. In addition, the employed turbulence model will be summarized as a critical environmental condition.

4.2.1. Nonlinear State Space Representation and Aircraft Simulation Platform

Generally, the nonlinear dynamics of an aircraft can be represented by differential equations, called Equations of Motion (EoM). Basically, these equations are expressed in terms of the force, kinematic, moment and navigation equations (Stevens, Lewis, & Johnson, 2015). As stated in (Wayne Durham, 2013), the dynamics and the parameter variations intensify the importance of an appropriate aircraft control system to maintain an equilibrium and stable flight within the safety margins.

These state-space representation of the aircraft dynamics can be written in the following form:

$$x^{(n)}(t) = F(x) + G(x)u(t) + D(t) \tag{4.1}$$

where $F(x)$ and $G(x)$ are the unknown nonlinear functions that are approximated by the Type Two Adaptive Fuzzy System proposed in this article. and $x = [\, q \,, v \,]^{\mathrm{T}}$ is the measured state vector, composed of the aircraft pitch rate q, and the aircraft airspeed v. Moreover, $u(t) = \left[U_q, U_{sp}\right]^T$ refers to the control vector, including the elevator deflection U_q, and the engine fan speed U_{sp} which are typically used to control the pitch rate and speed of the aircraft, respectively. Stabilizing the aircraft speed, besides controlling the pitch rate, was essential in this study to avoid induced instability in the pitch rate tracking performance caused by the effects of turbulence on the aircraft speed.

An in-house platform in MATLAB/Simulink, developed at the LARCASE, was used to simulate the dynamics and to generate the nonlinear longitudinal model of the Cessna Citation X business jet aircraft. This simulation platform was designed using data from a Level-D Research Aircraft Flight Simulator (RAFS) of the Cessna Citation X, shown in Fig. 4.1 (Ghazi & Botez, 2015a). It should be noted that the Level-D is the highest level of certification issued by the Federal Aviation Administration (FAA) for aircraft flight simulators.

Figure 4.1 Level-D Flight Simulator for the Cessna Citation X Business Jet Aircraft at LARCASE

For the purposes of this research, two assumptions were made to prove the stability of the Cessna Citation X aircraft. These assumptions were considered to reduce the complexity of the aircraft dynamics and facilitate subsequent stability analysis within this paper.

Assumption 1 ((Slotine & Li, 1991 ; C.-H. Wang et al., 2002 ; L.-X. Wang, 1997)) In the aircraft model represented by Eq. (4.1), $F(x)$ and $G(x)$ are considered as two unknown nonlinear functions containing the aircraft dynamics, and $D(t)$ is the unknown external disturbance (e.g., wind turbulences). For these functions, the following assumptions are considered:

$$|F(x)| \leq \mathcal{F} < \infty \tag{4.2}$$
$$0 < G_{min} < G(x) < G_{max} \text{ and } |D(t)| \leq L_D$$

In Eq. (4.2), $\mathcal{F}$, $G_{min} \neq 0$, G_{max} , and L_D are considered to have positive constant values.

The two inequalities in Eq. (4.2) indicate that $F(x)$ is a bounded function with a smaller value less than a specified positive constant represented by $\mathcal{F}$. In most control systems, it is important to consider that the system dynamics remains within a defined range and bounds to

ensure the controllability of the system. Moreover, the other unknown function denoted by $G(x)$ is limited by its minimum and maximum positive constants, denoted by G_{min} and G_{max}, respectively. This constraint implies that $G(x)$ can vary within these two values without being equal to zero. Similarly, it was assumed that the function $D(t)$ reflecting the effects of the turbulence is bounded by a value denoted by L_D.

Assumption 2 ((C.-H. Wang et al., 2002)). This assumption considers that Θ_F and Θ_G are two fuzzy adjustable parameters existing in the following sets $\Omega_F = \{\Theta_F \in R^Q, \|\Theta_F\| \leq C_f\}$, $\Omega_G = \{\Theta_G \in R^Q, \|\Theta_G\| \leq C_g\}$, where C_f and C_g are two finite and positive constants to ensure the boundedness of Θ_F and Θ_G.
In the following section, the main structure of the Type-2 Fuzzy Logic System is presented, along with its mathematical characteristics, according to the aircraft model described in this section and the two assumptions mentioned above.

4.2.2. Turbulence Model

To ensure the stability of the aircraft in a critical condition, it was considered to evaluate the performance of the proposed control methodologies in this article in presence of turbulence denoted by $D(t)$ as an unpredictable phenomena and uncertainty. For this purpose, the Dryden Turbulence model was selected in this study as the means with which the aircraft is deviated from its trimmed conditions. Under these turbulent conditions, the controllers must ensure the aircraft stability and safety, while mitigating the adverse effects of turbulence on its maneuvers and dynamics.

As described in (Hakim & Arifianto, 2018), turbulence can be defined as air motion resulting from variations in atmospheric pressure and temperature. To simulate the motion of the aircraft and evaluate the performance of flight control systems in presence of atmospheric and external disturbances, researchers commonly use Dryden and Von Karman turbulence models. To obtain a better understanding of the difference between the Dryden and Von Karman turbulence models, they should be compared in terms of the model accuracy and

complexity. The turbulence profile used in this study was generated with the continuous Dryden model from the Simulink Aerospace Blockset, with a moderate probability for exceedance of high-altitude intensity (10^{-3}) conform to the MIL-F-8785C specifications (Moorhouse & Woodcock, 1982).

4.2.3. Description of Type-2 Fuzzy Logic System (T2FLS) Approximator

The objective of this section is to provide a brief explanation of the Type-2 Fuzzy Logic System (FLS) utilized to approximate the unknown nonlinear functions existing in Eq. (4.1). Generally, a Type-2 Fuzzy Logic System is considered as an extended version of a Type-1 Fuzzy Logic System. The architecture of a Type-2 Fuzzy Logic system can be illustrated as shown in Fig. 4.2 (Mohammadzadeh et al., 2023).

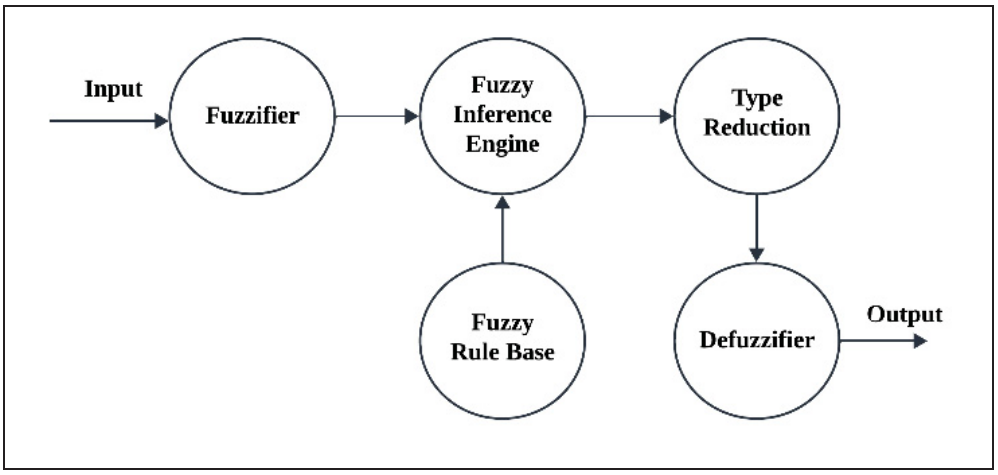

Figure 4.2 Simple Architecture of the Type-2 Fuzzy Logic System

A type two fuzzy logic system contains an Upper Membership Function (UMF) and a Lower Membership Function (LMF). Each of these membership functions represents the highest and lowest possible membership degrees. In other words, the type two membership function can be designed by the UMF and LMF as two type one membership functions. The margin between the UMF and LMF is known as the Footprint of Uncertainties (FOU) shown by the shaded area in Fig. 4.3. The approximation of the unknown functions denoted by F(x) and G(x) in Eq. (4.1) using the Type Two Fuzzy Logic System begins with the use of the

Fuzzifier component converting the crisp inputs to fuzzy inputs representing their degrees of membership values with respect to fuzzy sets through the upper and lower membership functions. For our application, five fuzzy sets were used for the pitch rate signal values such as {Slightly Down, Moderately Up, Gently Up, Steeply Up, and Rapid Up}, as presented in Table 4.2. By considering the {Moderately Up} fuzzy set in a T1FLS, each fuzzy set would assign a single membership value to the input (e.g., the pitch rate value of -0.5 deg/s has a single membership degree of 0.48 shown by the red line (LMF) in Fig. 4.3). However, in a T2FLS, each fuzzy set assigns a range of membership values to the input, reflecting the uncertainty or ambiguity (e.g., the pitch rate value equals -0.5 deg/s gets a range of memberships from 0.48 to 0.69 shown by the colored region located between the red line (Lower Membership Functions - LMF) and the black line (Upper Membership Functions - UMF) in Fig. 4.3).

As in the Type One Fuzzy Logic System case, the fuzzy rules define the relationship between the inputs and the outputs of a fuzzy logic system by IF-THEN statements. In these rules, the antecedent (IF-part) describes the "conditions" under which these rules apply, and the consequent (THEN-part) represents the "output" of the fuzzy rules under these conditions, as shown in Eq. (4.3). Then, the Inference Engine combines the defined fuzzy rules and maps the input T2 fuzzy set to the output T2 fuzzy set. Finally, the type reduction component aggregates the output of fuzzy rules (T2 fuzzy sets) into a single type one fuzzy set. After this type reduction, the defuzzifer converts the obtained fuzzy set to a crisp value (Mohammadzadeh et al., 2023).

The selected methodology for the Type-2 FLS for this research is explained as follows: For m inputs $x_{1:m}$, and one output y, this Type-2 fuzzy system has n rules, where the nth rule can be defined as follows:

$$\text{Fuzzy Rules } (R^n)\text{: } If\ x_1\ is\ \tilde{I}_1^n\ and\ x_2\ is\ \tilde{I}_2^n \ldots and\ x_m\ is\ \tilde{I}_m^n\ then\ y\ is\ \tilde{Y}^n \tag{4.3}$$

In the fuzzy rule given in Eq. (4.3), the measured inputs $x_1, \ldots, x_m$ are mapped into the fuzzy sets denoted by $\tilde{I}_{1:m}^n$ using an appropriate membership function and where $\tilde{Y}^n$ denotes the

output fuzzy set. In this study, Gaussian membership functions were considered using Eq. (4.4), in which the mean value was denoted by a, and the standard deviation parameter by b.

$$\mu_g(x; a\ b) = \exp\left[-0{,}5\left(\frac{x-a}{b}\right)^2\right] \tag{4.4}$$

The selected membership functions (including the UMF and LMF) for the pitch rate, reference pitch rate, Angle of Attack (AOA) and TAS are shown in Fig. 4.3. These membership functions were assumed to be uniformly distributed over the determined ranges of each of the measured inputs.

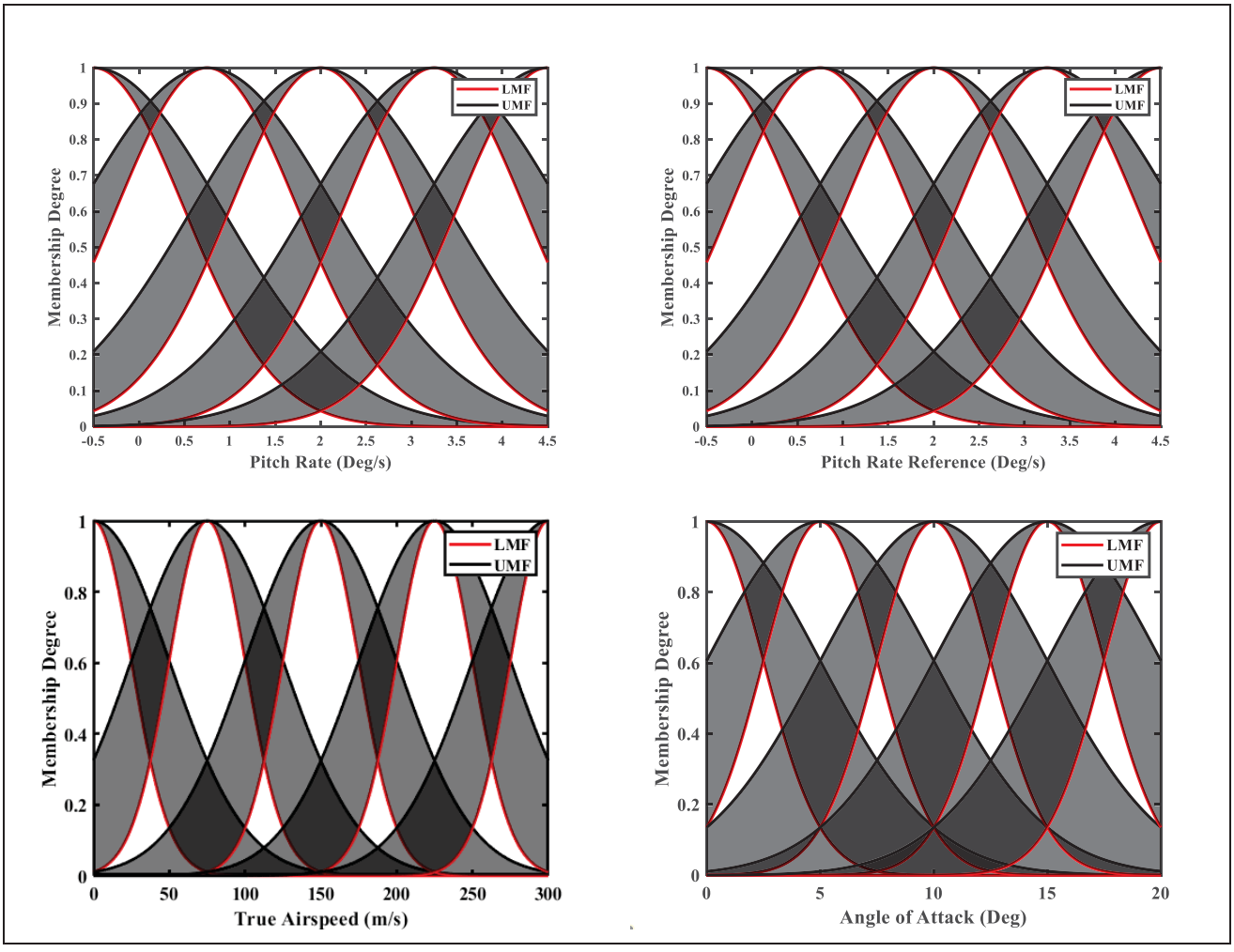

Figure 4.3 Selected Membership Functions for q, q_{ref}, the AoA, and the TAS

The membership functions represented in Fig. 4.3 were designed using Eq. (4.4), with the values of a and b^2 and their related linguistic variables are shown in Table 4.2:

Table 4.2 Linguistic variables and the related values of their membership functions parameters

Crisp inputs	Linguistic Variables	Value of a	Value of b^2		Crisp inputs	Linguistic Variables	Values of a	Value of b^2	
Pitch Rate (deg/s)	Slightly Down	-0.5	UMF	2	Pitch Rate Reference (deg/s)	Slight Nose Down	-0.5	UMF	2
			LMF	1				LMF	1
	Moderately Up	0.75	UMF	2		Gentle Nose Up	0.75	UMF	2
			LMF	1				LMF	1
	Gently Up	2	UMF	2		Moderate Nose Up	2	UMF	2
			LMF	1				LMF	1
	Steeply Up	3.25	UMF	2		Steep Nose Up	3.25	UMF	2
			LMF	1				LMF	1
	Rapid Up	4.5	UMF	2		Very Steep Nose Up	4.5	UMF	2
			LMF	1				LMF	1
TAS (m/s)	Too Slow	0	UMF	2500	AOA (deg)	Level Flight	0	UMF	25
			LMF	625				LMF	6.25
	Slow	75	UMF	2500		Slight Lift	5	UMF	25
			LMF	625				LMF	6.25
	Moderate	150	UMF	2500		Moderate Lift	10	UMF	25
			LMF	625				LMF	6.25
	Fast	225	UMF	2500		High Lift	15	UMF	25
			LMF	625				LMF	6.25
	Too Fast	300	UMF	2500		Near Stall	20	UMF	25
			LMF	625				LMF	6.25

Using the linguistic variables defined in Table 4.2 in terms of pitch rate, reference pitch rate, TAS and AOA, the following inference rules in Tables 4.3 and 4.4 were employed for approximating the unknown functions such as $A(x)$ and $B(x)$ in the pitch rate control, and $M(x)$ and $N(x)$ in the aircraft speed control systems.

Table 4.3 Inference Rules used for the Pitch Rate Control System

		Linguistic Variables for the Pitch Rate				
		Slightly Down	Moderately Up	Gently Up	Steeply Up	Rapid Up
Linguistic Variables for the Pitch Rate Reference	Slight Nose Down	$\Theta_{A,B}^{n=1}$	$\Theta_{A,B}^{n=2}$	$\Theta_{A,B}^{n=3}$	$\Theta_{A,B}^{n=4}$	$\Theta_{A,B}^{n=5}$
	Gentle Nose Up	$\Theta_{A,B}^{n=6}$	$\Theta_{A,B}^{n=7}$	$\Theta_{A,B}^{n=8}$	$\Theta_{A,B}^{n=9}$	$\Theta_{A,B}^{n=10}$
	Moderate Nose Up	$\Theta_{A,B}^{n=11}$	$\Theta_{A,B}^{n=12}$	$\Theta_{A,B}^{n=13}$	$\Theta_{A,B}^{n=14}$	$\Theta_{A,B}^{n=15}$
	Steep Nose Up	$\Theta_{A,B}^{n=16}$	$\Theta_{A,B}^{n=17}$	$\Theta_{A,B}^{n=18}$	$\Theta_{A,B}^{n=19}$	$\Theta_{A,B}^{n=20}$
	Very Steep Nose Up	$\Theta_{A,B}^{n=21}$	$\Theta_{A,B}^{n=22}$	$\Theta_{A,B}^{n=23}$	$\Theta_{A,B}^{n=24}$	$\Theta_{A,B}^{n=25}$

Table 4.4 Inference Rules used for the Aircraft Speed Control System

		Linguistic Variables for the AOA				
		Slightly Down	Slight Lift	Moderate Lift	High Lift	Near Stall
Linguistic Variables for the TAS	Too Slow	$\Theta_{M,N}^{n=1}$	$\Theta_{M,N}^{n=2}$	$\Theta_{M,N}^{n=3}$	$\Theta_{M,N}^{n=4}$	$\Theta_{M,N}^{n=5}$
	Low	$\Theta_{M,N}^{n=6}$	$\Theta_{M,N}^{n=7}$	$\Theta_{M,N}^{n=8}$	$\Theta_{M,N}^{n=9}$	$\Theta_{M,N}^{n=10}$
	Slow	$\Theta_{M,N}^{n=11}$	$\Theta_{M,N}^{n=12}$	$\Theta_{M,N}^{n=13}$	$\Theta_{M,N}^{n=14}$	$\Theta_{M,N}^{n=15}$
	High	$\Theta_{M,N}^{n=16}$	$\Theta_{M,N}^{n=17}$	$\Theta_{M,N}^{n=18}$	$\Theta_{M,N}^{n=19}$	$\Theta_{M,N}^{n=20}$
	Moderate	$\Theta_{M,N}^{n=21}$	$\Theta_{M,N}^{n=22}$	$\Theta_{A,B}^{n=23}$	$\Theta_{M,N}^{n=24}$	$\Theta_{M,N}^{n=25}$

To calculate the output of the Type-2 Fuzzy Logic System (T2FLS) in this methodology, the singleton Fuzzifier, Product (t-norm) Inference Engine, and the non-iterative Nagar-Bardini

(NB) Type Reduction (TR) algorithm were used (Chen, 2019 ; El-Nagar & El-Bardini, 2014). This special type of TR algorithm can perform both type reduction and defuzzification operations.

In this type two fuzzy logic system, it should be noted that $P^n = \left[\underline{P}^n, \overline{P}^n\right]$ where $\underline{P}^n = \underline{\mu}_{I_1^n} \times \underline{\mu}_{I_2^n} \times ... \times \underline{\mu}_{I_m^n}$ and $\overline{P}^n = \overline{\mu}_{\tilde{I}_1^n} \times \overline{\mu}_{\tilde{I}_2^n} \times ... \times \overline{\mu}_{\tilde{I}_m^n}$, as $\times$ denotes the Product (t-norm) operation and the adjustable parameters can be defined as $\Theta^T = [\underline{\Theta}_m^n, \overline{\Theta}_m^n]$. In addition, the Fuzzy Basis Functions (FBFs) can be calculated separately for the lower and upper fuzzy sets denoted by $\underline{\psi}(X)$ and $\overline{\psi}(X)$, as shown in Eq. (4.7). These terms were used in the calculated outputs in Eq. (4.5), and they play a key role in the adaptation laws design shown in Eq. (4.23) in the next section and Eq. (4.10) in the appendix. In the Nagar-Bardini (NB) algorithm (Chen, 2019 ; El-Nagar & El-Bardini, 2014), as the $\overline{P}^n(x_m)$ and $\underline{P}^n(x_m)$ were obtained by the product inference engine, and the $\overline{\Theta}_m^n$ and $\underline{\Theta}_m^n$ were discretized equally into M points to meet $\overline{\Theta}_1^n < \overline{\Theta}_2^n < \cdots < \overline{\Theta}_M^n$ and $\underline{\Theta}_1^n < \underline{\Theta}_2^n < \cdots < \underline{\Theta}_M^n$, then, the upper and lower endpoints of the centroid interval can be calculated individually by Eq. (4.5). Therefore, the defuzzified output can be obtained as shown in Eq. (4.7):

$$\overline{y} = \frac{\sum_{m=1}^{M} \overline{\Theta}_m^n \overline{P}^n(x_m)}{\sum_{m=1}^{M} [\overline{P}^n(x_m)]} \text{ and } \underline{y} = \frac{\sum_{m=1}^{M} \underline{\Theta}_m^n \underline{P}^n(x_m)}{\sum_{m=1}^{M} [\underline{P}^n(x_m)]} \tag{4.5}$$

$$\overline{\psi}(X) = \frac{\overline{P}^n}{\sum_{m=1}^{M} [\overline{P}^n]} \text{ and } \underline{\psi}(X) = \frac{\underline{P}^n}{\sum_{m=1}^{M} [\underline{P}^n]} \tag{4.6}$$

$$\psi^T(X) = [\underline{\psi}(X)\ \overline{\psi}(X)]$$

$$y(X) = \frac{1}{2}(\overline{y} + \underline{y}) = \frac{1}{2}\Theta^T \psi(X) \tag{4.7}$$

The terms $\overline{\psi}(X)$ and $\underline{\psi}(X)$ are the upper and lower Fuzzy Basis Functions as shown in Eq. (4.6). The main benefit of the Nagar-Bardini (NB) algorithm as a non-iterative algorithm is its simplicity, as $\overline{y}$ and $\underline{y}$ are two Type One (T1) fuzzy logic systems, which makes it

different from other conventional methods, such as Iterative Karnik-Mendel (IKM) algorithms (Chen, 2019 ; El-Nagar & El-Bardini, 2014).

In this methodology, it is assumed that there is always at least one active rule in the calculated Fuzzy Basis Functions (FBFs) (L.-X. Wang, 1994). The type two fuzzy logic system presented here was used to approximate the unknown nonlinear functions $F(x)$and $G(x)$ in Eq. (4.1) (These unknown functions were denoted respectively by $A(x)$ and $B(x)$ in the pitch rate control system and by $M(X)$ and $N(X)$ in the aircraft speed control system). Furthermore, using the designed adaptation laws that will be presented later for the adjustable parameters $\Theta^T = [\underline{\Theta}_m^n, \overline{\Theta}_m^n]$, these approximated functions can be updated at each simulation iteration.

The architecture presented in this section for the Type-2 Fuzzy Logic System (T2FLS) will be employed for approximating the nonlinear functions in both the aircraft pitch rate control and speed control systems in the next sections.

4.3 Type-2 Adaptive Fuzzy Sliding Mode Controllers

A detailed description of the design of Type-2 Adaptive Fuzzy Sliding Mode control systems is presented here for the aircraft pitch rate and speed.

4.3.1. Pitch Rate Control System

The aim of this study is to control the aircraft pitch rate by developing a suitable control input fed into the elevator actuation system. This controller should be designed to satisfy both maneuverability and aircraft stabilization. The command signal generated for the deflections of the elevator should be smooth, as any rapid and drastic (high frequency) changes in the position of a control surface will not be possible in real world applications since these aspects could potentially damage the actuators mechanical parts.

For this reason, a combination of three control systems is proposed in this section, comprising a Type-2 Fuzzy Logic System as an approximator complemented by adaptation laws and a Sliding Mode Controller (SMC). The T2FLS approximates the unknown aircraft dynamics $A(x)$ and $B(x)$ while using the characteristic of the adaptive control approach to update the adjustable parameters Θ existing in the approximated functions by T2FLS through the adaptation laws obtained by the Lyapunov theorem that will be presented later in this section. These combined control methodologies also guarantee the robustness and stability of the aircraft using the Sliding Mode Control (SMC) system, especially in presence of turbulence.

To develop the structure of the proposed Type Two Adaptive Fuzzy Sliding Mode Control (T2AFSMC) system, it is necessary to define the tracking error using the measured pitch rate q and its reference signal q_{ref} as $E(t) = q(t) - q_{ref}(t)$. Based on the calculated error for the pitch rate E and its time derivative $\dot{E}$, the sliding surface σ can be defined as follows (Londhe & Patre, 2019):

$$\sigma(t) = \dot{E}(t) + mE(t) = \dot{q}(t) - \dot{q}_{ref}(t) + mE(t) \tag{4.8}$$

where m is a positive constant ($m > 0$).

Calculating the time derivative of the sliding manifold in Eq. (4.8), and replacing $\ddot{q}(t)$ using a nonlinear state-space representation as shown in Eq. (4.1) and such that $\ddot{q}(t) = A(x) + B(x)U_q + D(t)$ as shown in Eq. (4.1), while $U_q = U_q^{eq} + U_q^{sw}$,yield:

$$\dot{\sigma}(t) = \ddot{q}(t) - \ddot{q}_{ref}(t) + m\dot{E}(t) + D(t) = A(x) + B(x)U_q - \ddot{q}_{ref}(t) + m\dot{E}(t) + D(t) \tag{4.9}$$

The equivalent control law U_q^{eq} can be calculated by imposing $\dot{\sigma}(t) = 0$, which leads to:

$$U_q^{eq} = \frac{1}{B(x)}[-A(x) + \ddot{q}_{ref}(t) - m\dot{E}(t) - D(t)] \tag{4.10}$$

The minimum approximation error R can then be written as shown in Eq. (4.11.a) using Θ^* as the optimal fuzzy parameter (this parameter is not a real variable) (Yoo & Ham, 1998b). Subsequently, by considering that R is a function in a bounded space ($R \in L^{\infty}$) and referring to both assumptions 1 and 2, it can be written that (Roopaei et al., 2009):

$$R = \left[A(x) - \hat{A}(x|\Theta^*)\right] + \left[B(x) - \hat{B}(x|\Theta^*)\right]U_q \tag{4.11.a}$$

$$\begin{aligned} |R| \le \left|A(x) - \hat{A}(x|\Theta^*)\right| + \left|B(x) - \hat{B}(x|\Theta^*)\right|\left|U_q\right| \le |A(x)| + \left|\hat{A}(x|\Theta^*)\right| + \\ \left[|B(x)| + \left|\hat{B}(x|\Theta^*)\right|\right]\left|U_q\right| \le |A(x)| + \|\Theta_A^*\|\|\psi_A(x)\| + [|B(x)| + \\ \|\Theta_B^*\|\|\psi_B(x)\|]\left|U_q\right| \le C_A + F_A + [C_B + G_{Bmax}]\left(\max\left|U_q\right|\right) \le \delta \\ \text{Therefore, } |R| \le \delta \text{ as } \delta = C_A + F_A + [C_B + G_{Bmax}]\left(\max\left|U_q\right|\right) \end{aligned} \tag{4.11.b}$$

Referring to the assumptions 1 and 2, in Eq. (4.11.b), it was assumed that the nonlinear functions $A(x)$ and $B(x)$ are bounded to F_A and G_{Bmax} as two positive constants. Also, $\|\Theta_A^*\|$ and $\|\Theta_B^*\|$ were bounded to C_A, and C_B as two finite positive constants. it is worth reminding that $0 \le G_{Bmin} \le B(x) \le G_{Bmax}$.

In this paper, the control input U_q is a bounded signal, then R must be a bounded function. Given the definition of the minimum approximation error in Eq. (4.11.a), $R = \left[A(x) - \hat{A}(x|\Theta_A^*)\right] + \left[B(x) - \hat{B}(x|\Theta_B^*)\right]U_q$, therefore Eq. (4.9) becomes:

$$\begin{aligned} \dot{\sigma}(t) = A(x) - \hat{A}(x|\Theta_A^*) + \hat{A}(x|\Theta_A^*) + \left(B(x) - \hat{B}(X|\Theta_B^*)\right)U_q + \hat{B}(X|\Theta_B^*)U_q - \\ \ddot{q}_{ref}(t) + m\dot{E}(t) + D(t) = \left[A(x) - \hat{A}(x|\Theta_A^*)\right] + \left[B(x) - \hat{B}(x|\Theta_B^*)\right]U_q + \\ \hat{A}(x|\Theta_A^*) + \hat{B}(x|\Theta_B^*)U_q - \ddot{q}_{ref}(t) + m\dot{E}(t) = R + \hat{A}(x|\Theta_A^*) + \hat{B}(x|\Theta_B^*)U_q - \\ \ddot{q}_{ref}(t) + m\dot{E}(t) + D(t) \end{aligned} \tag{4.12}$$

Referring to (« Adaptive fuzzy control of a class of MIMO nonlinear systems », 2005), if $\phi = \Theta - \Theta^*$, therefore, $\phi_A^T \psi_A(X)$ and $\phi_B^T \psi_B(X)$ can be formulated as given in Eq. (4.13.a). Then, by introducing these expressions into Eq. (4.12), we can reformulate $\dot{\sigma}(t)$ with Eq. (4.13.b):

$$\phi_A^T \psi_A(x) = \hat{A}(x|\Theta_A) - \hat{A}(x|\Theta_A^*) \tag{4.13.a}$$

$$\phi_B^T \psi_B(x) = \left(\hat{B}(x|\Theta_B) - \hat{B}(x|\Theta_B^*)\right)$$

$$\dot{\sigma}(t) = R + \left(\hat{A}(x|\Theta_A^*) - \hat{A}(x|\Theta_A) + \hat{A}(x|\Theta_A) + \hat{B}(x|\Theta_B^*)U_q - \hat{B}(x|\Theta_B)U_q + \right. \tag{4.13.b}$$

$$\left. \hat{B}(x|\Theta_B)U_q - \ddot{q}_{ref}(t) + m\dot{E}(t) + D(t)\right) = R + \left(-\phi_A^T \psi_A(x) + \hat{A}(x|\Theta_A) - \right.$$

$$\left. \phi_B^T \psi_B(x)U_q + \hat{B}(x|\Theta_B)U_q - \ddot{q}_{ref}(t) + m\dot{E}(t) + D(t)\right)$$

In the sliding mode control system, the general form of the sliding mode control law is $U_q = U_q^{eq} + U_q^{sw}$. In general, the switching (reaching) control law can be selected as $U_q^{sw} = [-Tsign(\sigma)]/B(x)$ with $T > 0$. In this article, it was decided to design the switching control law as $U_q^{sw} = [Tsat(\sigma)]/B(x)$. This design yielded better simulation results compared to those obtained with conventional approach, which caused instability in the aircraft motion. The function $sat(\sigma)$, illustrated in Fig. 4.4, represents the saturation function, and is defined as follows (Cheng, Guan, Wang, & Han, 2011):

$$sat\left(\frac{\sigma}{\emptyset}\right) = \begin{cases} \frac{\sigma}{\emptyset} & if \ \left|\frac{\sigma}{\emptyset}\right| \leq 1 \\ sgn\left(\frac{\sigma}{\emptyset}\right) & if \ \left|\frac{\sigma}{\emptyset}\right| > 1 \end{cases} \tag{4.14}$$

where $\emptyset = 1$ is the thickness of the boundary layer. This function was used in order to decrease the effects of chattering phenomenon in the control system.

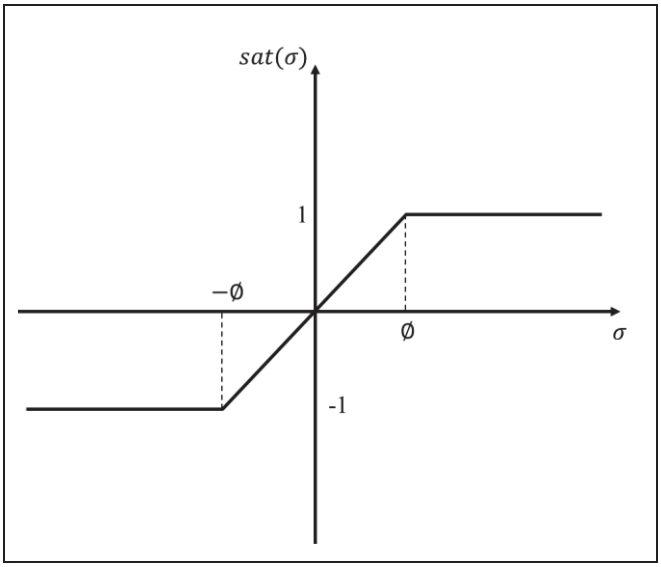

Figure 4.4 Diagram of the Saturation Function

It should be noted that in Eq. (4.10) the dynamics of the aircraft $A(x)$ and $B(x)$ are unknown and the turbulence denoted by $D(t)$ is practically unmeasurable. Consequently, the functions $A(x)$ and $B(x)$ must be replaced by their approximations $\hat{A}(x|\Theta_A)$ and $\hat{B}(x|\Theta_B)$, respectively, in Eq. (4.10). Taking this change into account, the control law $U_q = U_q^{eq} + U_q^{sw}$ can be rewritten as follows:

$$U_q = \underbrace{\frac{1}{\hat{B}(x|\Theta_B)}\left[-\hat{A}(x|\Theta_A) + \ddot{q}_{ref}(t) - m\dot{E}(t)\right]}_{U_q^{eq}} + \underbrace{\frac{1}{\hat{B}(x|\Theta_B)}Tsat(\sigma)}_{U_q^{sw}} \tag{4.15}$$

According to the Lyapunov theorem, the aircraft state variables will approach the sliding manifold if the first derivative of the Lyapunov candidate satisfies $\dot{L}(x) \leq -\eta|\sigma|$ (Roopaei, Zolghadri Jahromi, Ranjbar-Sahraei, & Lin, 2011). Here, η is the positive switching gain. Therefore, substituting U_q with the designed control law in Eq. (4.13.b), $\dot{\sigma}(t)$ can be written as:

$$\dot{\sigma}(t) = R + \Bigg(-\phi_A^T\psi_A(x) + \hat{A}(x|\Theta_A) - \phi_B^T\psi_B(x)U_q + \hat{B}(x|\Theta_B)\left(\frac{1}{\hat{B}(x|\Theta_B)}\left[-\hat{A}(x|\Theta_A) + \ddot{q}_{ref}(t) - m\dot{E}(t) + Tsat(\sigma)\right]\right) - \ddot{q}_{ref}(t) + m\dot{E}(t) + D(t)\Bigg) \tag{4.16}$$

Rearranging the previous expressions, Eq. (4.17) can be derived as:

$$\dot{\sigma}(t) = R + \left(-\phi_A^T \psi_A(x) - \phi_B^T \psi_B(x) U_q + Tsat(\sigma) + D(t)\right) \tag{4.17}$$

Proof of Stability. The Lyapunov theorem is commonly used to prove the stability of a system. Throughout this analysis, the boundedness of the applied methodology will be verified, even if there are no equilibrium points in the system (Khalil, 2001).

Theorem 1. Having $x = 0$ as the equilibrium point of the system and $Q \subset R^n$ as a domain including $x = 0$, if we select a continuous differentiable Lyapunov candidate as $L: Q \to R^n$, L must satisfy the following conditions (Khalil, 2001):

$$L(0) = 0 \text{ and } L(x) > 0 \text{ in } Q - \{0\}, \text{ therefore } \dot{L}(x) \leq 0 \text{ in } Q \tag{4.18}$$

then it can be concluded that $x = 0$ is stable.

To begin with the proof of the boundedness and stability of the methodology, the Lyapunov candidate L_q expressed in Eq. (4.19) can be selected as inspired from (S. M. Hosseini & Manthouri, 2022 ; Yoo & Ham, 1998a):

$$L_q = \frac{1}{2}\sigma^2 + \frac{1}{2\overline{g}_A}\overline{\phi}_A^T\overline{\phi}_A + \frac{1}{2\underline{g}_A}\underline{\phi}_A^T\underline{\phi}_A + \frac{1}{2\overline{g}_B}\overline{\phi}_B^T\overline{\phi}_B + \frac{1}{2\underline{g}_B}\underline{\phi}_B^T\underline{\phi}_B \tag{4.19}$$

To continue, it is necessary to calculate the time derivative of theLyapunov candidate L_q as follows:

$$\dot{L}_q = \sigma\dot{\sigma} + \frac{1}{\overline{g}_A}\overline{\phi}_A^T\dot{\overline{\phi}}_A + \frac{1}{\underline{g}_A}\underline{\phi}_A^T\dot{\underline{\phi}}_A + \frac{1}{\overline{g}_B}\overline{\phi}_B^T\dot{\overline{\phi}}_B + \frac{1}{\underline{g}_B}\underline{\phi}_B^T\dot{\underline{\phi}}_B \tag{4.20}$$

By replacing the obtained expression for $\dot{\sigma}$ in Eq. (4.17) into Eq. (4.20), it becomes:

$$\dot{L}_q = \sigma R + \sigma\{-\phi_A^T\psi_A(x) - \phi_B^T\psi_B(x)U_q + Tsat(\sigma)\} + \sigma D(t) + \frac{1}{\overline{g}_A}\overline{\phi}_A^T\dot{\overline{\phi}}_A + \frac{1}{\underline{g}_A}\underline{\phi}_A^T\dot{\underline{\phi}}_A + \frac{1}{\overline{g}_B}\overline{\phi}_B^T\dot{\overline{\phi}}_B + \frac{1}{\underline{g}_B}\underline{\phi}_B^T\dot{\underline{\phi}}_B \quad (4.21)$$

where $\phi_A^T\psi_A(x) = 0.5\left[\underline{\phi}_A^T\ \overline{\phi}_A^T\right]\begin{bmatrix}\underline{\psi}_A(x)\\ \overline{\psi}_A(x)\end{bmatrix}$ and $\phi_B^T\psi_B(x) = 0.5\left[\underline{\phi}_B^T\ \overline{\phi}_B^T\right]\begin{bmatrix}\underline{\psi}_B(x)\\ \overline{\psi}_B(x)\end{bmatrix}$ using NB Type Reduction algorithm and Center of Sets defuzzification method (Chen, 2019 ; El-Nagar & El-Bardini, 2014). Moreover, since $\phi = \Theta - \Theta^*$, then $\dot{\phi} = \dot{\Theta}_{A,B}$ since Θ^* is not a real value (Wu, Liu, Jing, Li, & Wu, 2017). As a result, Eq. (4.21) can be rewritten as:

$$\begin{aligned}\dot{L}_q = {} & \sigma R - \sigma\left\{0.5\sigma\underline{\phi}_A^T\underline{\psi}_A(x) + 0.5\sigma\overline{\phi}_A^T\overline{\psi}_A(x) + 0.5\sigma\underline{\phi}_B^T\underline{\psi}_B(x)U_q + 0.5\sigma\overline{\phi}_B^T\overline{\psi}_B(x)U_q - Tsat(\sigma)\right\} + \sigma D(t) + \frac{1}{\overline{g}_A}\overline{\phi}_A^T\dot{\overline{\phi}}_A + \frac{1}{\underline{g}_A}\underline{\phi}_A^T\dot{\underline{\phi}}_A + \\ & \frac{1}{\overline{g}_B}\overline{\phi}_B^T\dot{\overline{\phi}}_B + \frac{1}{\underline{g}_B}\underline{\phi}_B^T\dot{\underline{\phi}}_B = \sigma R + \sigma Tsat(\sigma) + \sigma D(t) + \\ & \frac{1}{\underline{g}_A}\underline{\phi}_A^T\left[-0.5\sigma\underline{g}_A\underline{\psi}_A(x) + \dot{\underline{\Theta}}_A\right] + \frac{1}{\overline{g}_A}\overline{\phi}_A^T\left[-0.5\sigma\overline{g}_A\overline{\psi}_A(x) + \dot{\overline{\Theta}}_A\right] + \\ & \frac{1}{\overline{g}_B}\overline{\phi}_B^T[-0.5\sigma\overline{g}_B\overline{\psi}_B(x)U_q + \dot{\overline{\Theta}}_B] + \frac{1}{\underline{g}_B}\underline{\phi}_B^T[-0.5\sigma\underline{g}_B\underline{\psi}_B(x)U_q + \dot{\underline{\Theta}}_B]\end{aligned} \quad (4.22)$$

The adaptation laws for each $\dot{\underline{\Theta}}_A$, $\dot{\overline{\Theta}}_A$, $\dot{\overline{\Theta}}_B$, and $\dot{\underline{\Theta}}_B$ can be calculated based on the final expression of Eq. (4.22), as shown in Eq. (4.23).

$$\begin{aligned}\dot{\underline{\Theta}}_A &= 0{,}5\sigma\underline{g}_A\underline{\psi}_A(x)\\ \dot{\overline{\Theta}}_A &= 0{,}5\sigma\overline{g}_A\overline{\psi}_A(x)\\ \dot{\overline{\Theta}}_B &= 0{,}5\sigma\overline{g}_B\overline{\psi}_B(x)U_q\\ \dot{\underline{\Theta}}_B &= 0{,}5\sigma\underline{g}_B\underline{\psi}_B(x)U_q\end{aligned} \quad (4.23)$$

These adaptation laws in Eq. (4.23) enhance the performance and functionality of the fuzzy logic system in the presence of parameter variations and uncertainties existing in the aircraft

nonlinear model. In addition, they update the approximated functions $\hat{A}(x|\Theta_A)$ and $\hat{B}(x|\Theta_B)$ for each flight condition, and during the simulation. Therefore, substituting the adaptation laws from Eq. (4.23) into Eq. (4.22) yields:

$$\dot{L}_q = \sigma R + \sigma T sat(\sigma) + \sigma D(t) \tag{4.24}$$

As discussed earlier in Equations (4.11.a) and (4.11.b), we have shown that $|R| \leq \delta$ is a bounded signal with $\delta = C_A + F_A + [C_B + G_{Bmax}]\big(\max|U_q|\big)$. Therefore, Eq. (4.24) can be reformulated as Eq. (4.25), where it has been considered that the turbulence was bounded such that $|D(t)| \leq L_D$. Based on these considerations, the following inequality can be written:

$$\dot{L}_q = \sigma(R + T + L_D) \leq \ \delta|\sigma| + L_D|\sigma| - T|\sigma| = -[T - (\delta + L_D)]|\sigma| \tag{4.25}$$

Hence, if T is chosen such that $T > \delta + L_D$, one can deduce that the condition $\sigma\dot{\sigma} \leq 0$ is consistently met and the proof of stability is established as the error trajectory approaches the sliding surface where $\sigma = 0$ (Yau & Chen, 2006).

It was shown previously that the proposed control system for the pitch rate guaranteed the aircraft stability while proving the boundedness of the error using the control law suggested in Eq. (4.15). However, this control law still requires an integral control term to reduce the steady state error on the pitch rate. Therefore, the final control law for the pitch rate can be written as shown in Eq. (4.26):

$$\begin{aligned} U_q^{Final} = \left(\frac{1}{\hat{B}(x|\Theta_B)}\right)\left[-\hat{A}(x|\Theta_A) + \ddot{q}_{ref}(t) - m\dot{E}(t) + Tsat(\sigma)\right] \\ + \rho_i \int E(t)d(t) \end{aligned} \tag{4.26}$$

where ρ_i denotes a positive gain for the integral control term.

According to the Heine-Cantor theorem, when the tracking error varies in an interval $(E_{min}. E_{max})$, it exhibits uniform continuity. In line with the characteristics of the Riemann integral, the integral of the tracking error $\int E(t)dt$ will also remain bounded, which confirms that the integral component in Eq. (4.26) will not render the system unstable.

4.3.2. Aircraft Speed Control System

This section presents the architecture selected for the aircraft speed controller. This controller is based on a combination of three approaches: a Sliding Mode Control system, a Type-2 Fuzzy Logic System, and an Adaptive Control methodology, as on the control of the pitch rate shown in the previous section. The main purpose of this controller is to stabilize the aircraft speed at its trimmed value for each flight condition.

As shown with the system developed for pitch rate control, it is essential to calculate the tracking error $E_{sp} = v(t) - v_{ref}(t)$, using the actual True AirSpeed (TAS) v, and its reference value v_{ref}. The sliding surface can be defined as follows with $I > 0$:

$$\sigma_{sp} = E_{sp} + I\dot{E}_{sp} \tag{4.27}$$

The suggested control law in this article is presented in Eq. (4.28). In this control law, U_{sp}^{eq} can be found by imposing the condition $\dot{\sigma}_{sp} = 0$. In addition, U_{sp}^{sw} denotes the reaching (switching) control law which keeps the state variables of the aircraft on the sliding surface to reach their equilibrium points. In Eq. (4.28), $\widehat{M}(x|\Theta_M)$ and $\widehat{N}(x|\Theta_N)$ are the approximated functions by the Type Two Fuzzy Logic System for unknown functions existing in the aircraft state-space representation as described earlier in Eq. (4.1).

$$U_{sp} = \underbrace{\left(\frac{1}{\widehat{N}(x|\Theta_N)}\right)\left[-\widehat{M}(x|\Theta_M) + \dot{v}_{ref}(t) - I\ddot{E}_{sp}\right]}_{U_{sp}^{eq}} - \underbrace{Wsat(\sigma_{sp})}_{U_{sp}^{sw}} \tag{4.28}$$

As described in the pitch rate control section, the stability and boundedness of the speed control system should be evaluated by proposing an appropriate Lyapunov candidate. For this purpose, inspired from (S. M. Hosseini & Manthouri, 2022 ; Yoo & Ham, 1998a), the following Lyapunov candidate was used:

$$L_{sp} = \frac{1}{2}\sigma_{sp}^2 + \frac{1}{2\overline{g}_M}\overline{\phi}_M^T\overline{\phi}_M + \frac{1}{2\underline{g}_M}\underline{\phi}_M^T\underline{\phi}_M + \frac{1}{2\overline{g}_N}\overline{\phi}_N^T\overline{\phi}_N + \frac{1}{2\underline{g}_N}\underline{\phi}_N^T\underline{\phi}_N \tag{4.29}$$

And then, it was possible to calculate the following adaptation laws given in Eq. (4.30) using the Lyapunov candidate L_{sp} in Eq. (4.29):

$$\begin{aligned}
\dot{\underline{\Theta}}_M &= -\underline{\Delta}_M\underline{g}_M\underline{\Theta}_M + 0{,}5\sigma_{sp}\underline{g}_M\underline{\psi}_M(x) \\
\dot{\overline{\Theta}}_M &= -\overline{\Delta}_M\overline{g}_M\overline{\Theta}_M + 0{,}5\sigma_{sp}\overline{g}_M\overline{\psi}_M(x) \\
\dot{\underline{\Theta}}_N &= -\underline{\Delta}_M\underline{g}_N\underline{\Theta}_N + 0{,}5\sigma_{sp}\underline{g}_N\underline{\psi}_N(x)U_{sp} \\
\dot{\overline{\Theta}}_N &= -\overline{\Delta}_M\overline{g}_N\overline{\Theta}_N + 0{,}5\sigma_{sp}\overline{g}_N\overline{\psi}_N(x)U_{sp}
\end{aligned} \tag{4.30}$$

Stability Proof. To analyze the stability of the aircraft using the controller proposed in Eq. (4.28), the Lyapunov theorem was applied on the candidate given in Eq. (4.29). With this theorem we can conclude that $\dot{L}_{sp} \leq -\hbar L_{sp} + \Omega$, which guarantees the convergence of the tracking error using the proposed aircraft speed control system (Bounar, Labdai, Boulkroune, Farza, & M'Saad, 2020). The details of stability proof are provided in the Appendix II.

Throughout this methodology, it has been shown that the tracking error defined for the aircraft speed was stabilized and uniformly ultimate bounded (UUB) (Khalil, 2001). Moreover, the determined adaptation laws provided bounded adjustable parameters in this controller by using its appropriate values for each design parameter. The following scheme in Fig. 4.5 presents the block diagram of all applied control systems in this article:

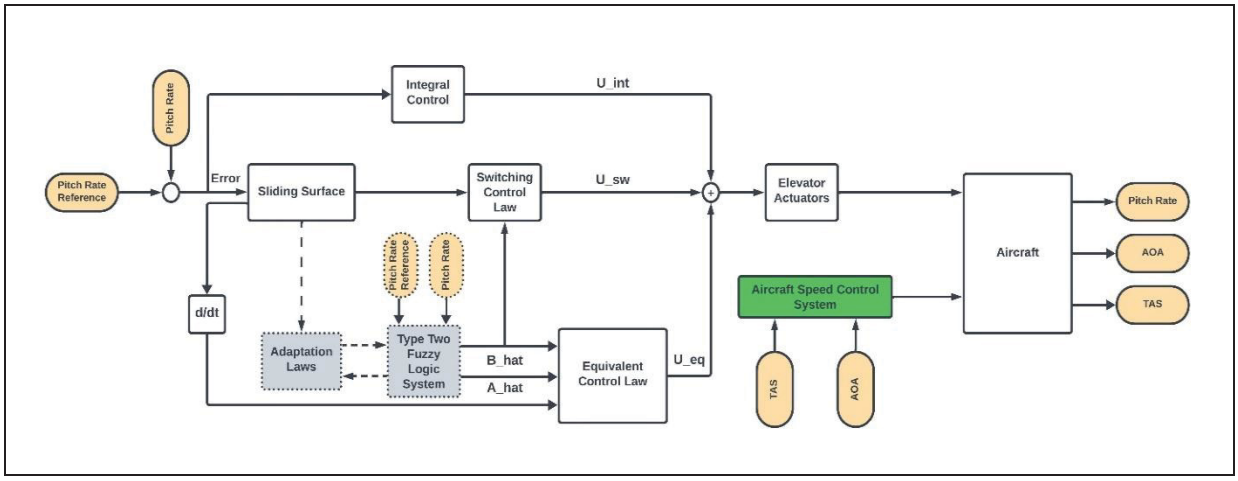

Figure 4.5 Basic Scheme of Control Systems designed for the Aicraft Pitch Rate and its Speed

4.4 Simulations Results

In this study, two distinct flight control systems were developed for the longitudinal motion of the Cessna Citation X to control the pitch rate and speed during cruise. This section presents the results for the validation of two flight control systems. For this purpose, several analyses carried out. First, the performances of the pitch rate and True AirSpeed (TAS) controllers were evaluated separately under ideal flight conditions. Subsequently, the results for both controllers in presence of turbulence are shown, considering that the speed controller was designed to stabilize the aircraft speed and mitigate the effects of turbulence. To demonstrate the efficiency of the methodology described in this paper, both controllers were tested and validated over a wide range of cruise flight conditions, varying altitude, true airspeed, aircraft weight, and center of gravity location, according to their values given in Table 4.5. The combination of all these conditions resulted in a total of 925 scenarios, covering most of the aircraft operational envelope.

Table 4.5 Flight conditions for the cruise phase of the Cessna Citation X

Parameters	Units	Flight Conditions								
Altitude	ft	8000	10000	15000	20000	25000	30000	35000	40000	45000
CAS	kts	170	200	230	250	300	330			
Weight	lbs	26000	27000	28000	29000	30000				
Center of Gravity	%	24	26	28	30	32				

As explained in Section 4.2.3, to approximate the unknown functions in the nonlinear model of the Cessna Citation X aircraft, it is necessary to define two variables and establish suitable membership functions for them. In this study, the inputs of the proposed type-2 fuzzy logic system in the pitch rate control system are the aircraft pitch rate (q) and its reference signal denoted by (q_{ref}), while for the aircraft speed controller, the aircraft True AirSpeed (v) and the angle of attack (α) were selected as inputs.

For each of these inputs, five uniformly distributed Gaussian membership functions represented in Eq. (4.5), were used within the intervals given in Table 4.6.

Table 4.6 Determined intervals for the inputs

Variables	Units	Min	Max
q	deg/s	-0.5	4.5
q_{ref}	deg/s	-0.5	4.5
v	m/s	0	300
α	deg	0	20

It should be noted that to minimize variations in the reference signal and thus to avoid numerical derivative problems due to too abrupt changes in the reference signal, a reference model based on the following second-order filter has been imposed:

$$T(s) = \frac{\omega_n^2}{s^2 + 2\xi\omega_n s + \omega_n^2} \tag{4.31}$$

where $\xi = 0.7$ is the damping ratio, and $\omega_n = 3$ rad/s is the natural pulsation.

As mentioned before, the Type Two Fuzzy Logic System (T2FLS) is an improved version of the Type One Fuzzy Logic System (T1FLS), and it was combined with Sliding Mode Control (SMC) and Adaptive Control (AC) methodologies. This enhanced methodology showed its superiority in controlling nonlinear and complex systems in the literature. In comparison with the T1FLS, the proposed T2FLS effectively handled a wider range of uncertainties, highlighting the benefits of integrating such a methodology for improved control system performance.

To demonstrate the greater performance of the proposed control strategy, a comparison is provided in Figures 4.6-4.9 between the Type Two Adaptive Fuzzy Sliding Mode Control (T2AFSMC) system developed in this paper and the Type One Adaptive Fuzzy Sliding Mode Control (T1AFSMC) system previously designed in (S. Hosseini, Ghazi, et al., 2023a) for the Cessna Citation X aircraft. The comparison is based on the same 15 flight conditions, selected with different combinations of Altitude = {8000,15000,25000,35000,45000} fts, CAS = {170,200,230,250,300,330} knots, Weight = {26000} lbs and Center of Gravity = {24} % of the chord, and by assuming zero-wind speed. These conditions were chosen to ensure a complete evaluation of both systems in identical flight scenarios, while covering the aircraft operating flight envelope.

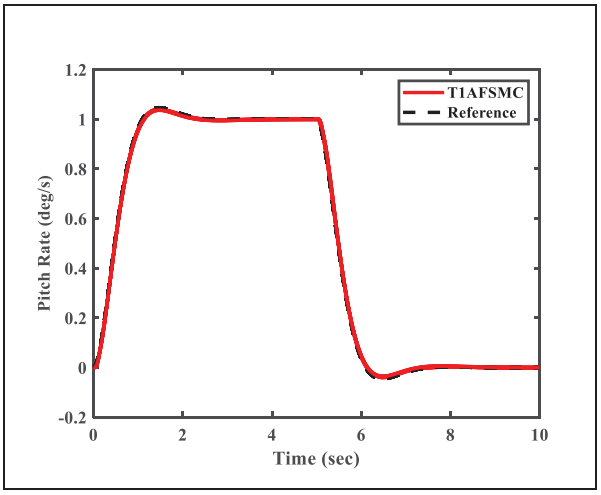

Figure 4.6 Pitch Rate Time Variations for 15 Flight Conditions (T1AFSMC)

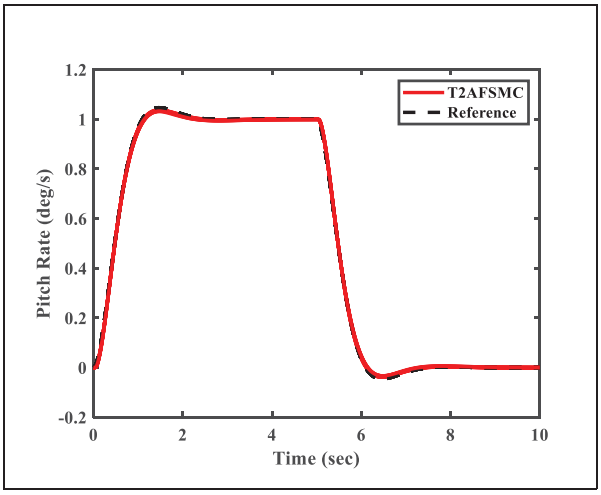

Figure 4.7 Pitch Rate Time Variations for 15 Flight Conditions (T2AFSMC)

Figures 4.6 and 4.7 show that both methods gave good results under ideal flight conditions as they achieved appropriate tracking performance of the reference pitch rate. As these results of these methodologies seem to be close in these figures, a comparison is provided in Fig. 4.8 for the Mean Absolute Errors obtained for both T2AFSMC and T1AFSMC.

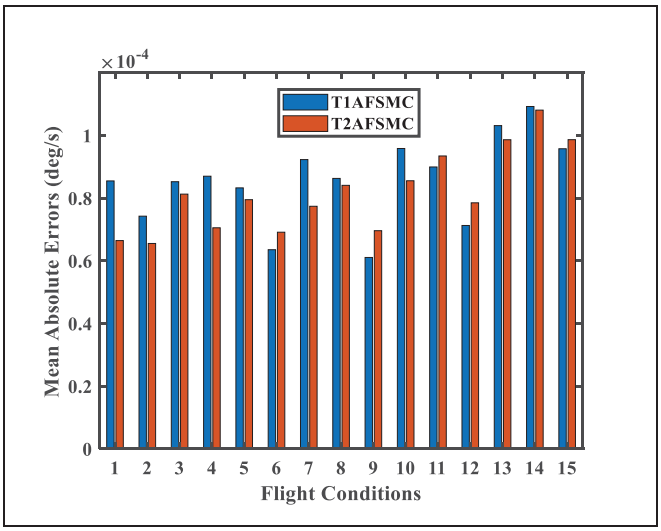

Figure 4.8 Pitch Rate Mean Absolute Error (MAE) for each of the 15 Selected Flight Conditions

In Fig. 4.8, it is shown that the T2AFSMC performed better than the T1AFSMC in controlling the aircraft pitch rate under same flight conditions. While there are some flight conditions in which the values of the MAE obtained for the T2AFSMC were higher than those for the T1AFSMC (in the flight conditions 6,9,11,12 and 15), these differences were not significant (in the worst scenario, in the flight condition 9, the difference was 8.6×10^{-6} deg/s). In addition, the T2FLS ability to handle a wider range of uncertainties contributes to generate smoother control inputs, reducing the effects of noise and disturbance, and improving aircraft robustness. This improvement is further enhanced by the adaptability features introduced by the adaptation laws proposed in our controller. For this purpose, the obtained results for the time variations of elevator deflections are represented in Fig. 4.9. These results demonstrate the smoothness of the control commands produced on the

elevators of the CCX. Based on these evaluations, we can conclude that the T2AFSMC performed better than the T1AFSMC for the scope of this research. Therefore, in the rest of this article, the performance of the T2AFSMC will be validated for all flight conditions across the flight envelope of the CCX aircraft using the parameters shown in Table 4.5.

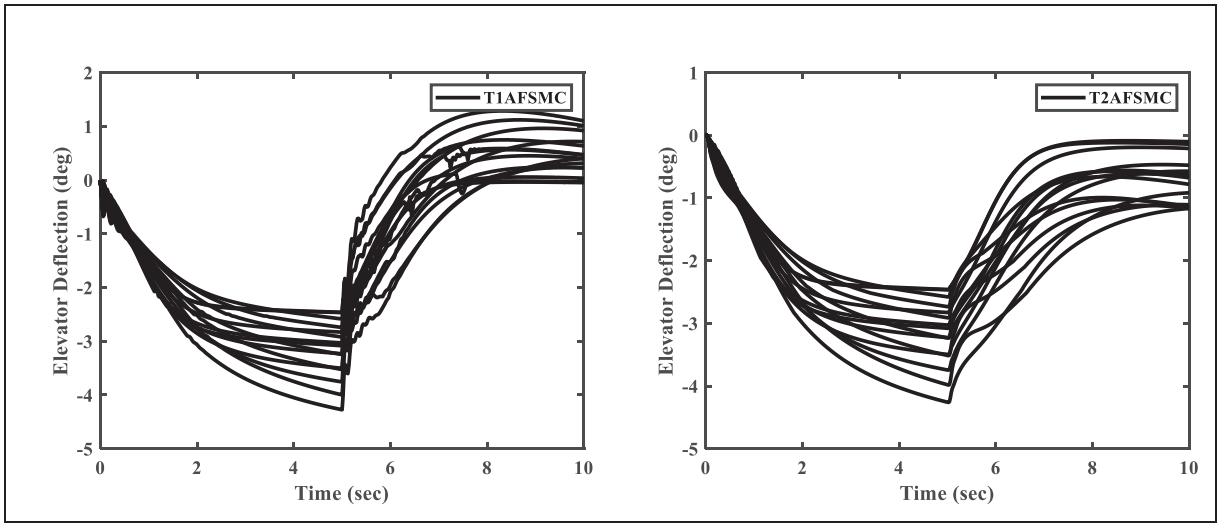

Figure 4.9 Time Variations of Elevator Deflections for the T1AFSMC and T2AFSMC Systems

After comparing the controllers in previous figures, the performance of the pitch rate control system by T2ASMC was validated for all 925 flight conditions distributed across the Cessna Citation X aircraft flight envelope, as shown in Fig. 4.10. This figure shows that the pitch rate controller performed adequately under ideal flight environment (without turbulence) for all 925 flight conditions. In addition, the pitch rate not only tracked the reference signal accurately, but no unwanted signal behavior has been seen, such that the pitch rate in Fig. 4.10.a varies with the desired overshoot generated by the transfer function in Eq. (4.31). Furthermore, the pitch angle increases with no oscillations and follows its reference as shown in Fig. 4.10.b.

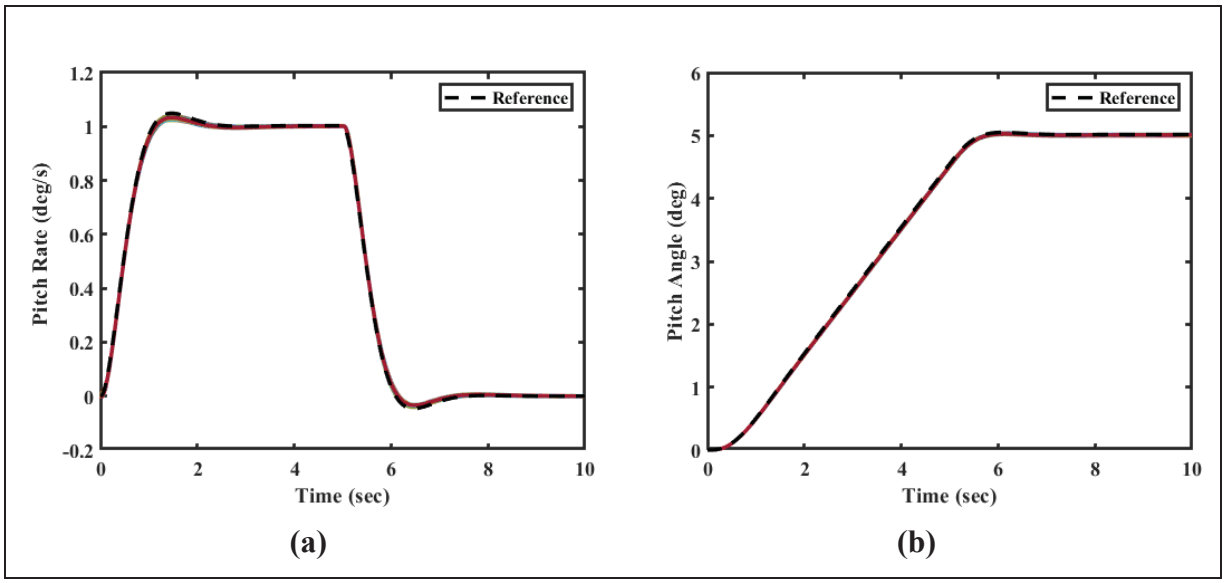

Figure 4.10 Pitch Rate (a) and Pitch Angle (b) Time-Variations for all 925 Flight Conditions

Another important issue is to design the pitch rate controller with respect to some actuation aspects. In real-life flights, high-frequency control inputs are not acceptable due to the mechanical damages that would be caused to the actuators of the elevator. So, the obtained signal showing the deflections of the elevator angle using the designed controller must be smooth. In this regard, no undesirable signal characteristics including sudden variations and highly frequency oscillations were found for the signal of the elevator deflection, as shown in Fig. 4.11.

To analyze the performance of the aircraft speed control system described in Section 4.3.2, the simulation results are shown in Fig. 4.12 and discussed below.

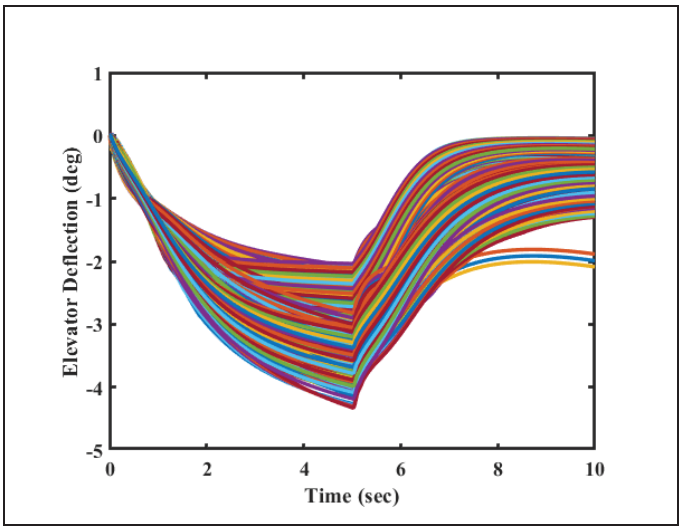

Figure 4.11 Time Variations of the Elevator Deflections for 925 Flight Conditions

Fig. 4.12 shows the TAS control results for all 925 flight scenarios for various altitudes. It worth noting that instead of showing the actual value of true airspeed, which changes gradually through the scenarios, Fig. 4.12 shows the airspeed variations with respect to its initial value for each flight scenario.

From a general point of view, for all flight scenarios, the controller was able to control the aircraft airspeed, and reach the given reference value. In addition, the results obtained varying altitudes suggest that as the aircraft flies to higher altitudes, the engine efficiency decreases due to the reduced air density. Consequently, it took a minimum of 3 seconds at 8000 ft and a maximum of 13 seconds at 45000 ft for the TAS to track the reference signal. Nevertheless, the results were considered as being within the acceptable range for the scope of this research and the aircraft tracking performance was successfully achieved with respect to the desired characteristics determined for the pitch rate reference signal in the longitudinal motion of the Cessna Citation X aircraft using this control methodology.

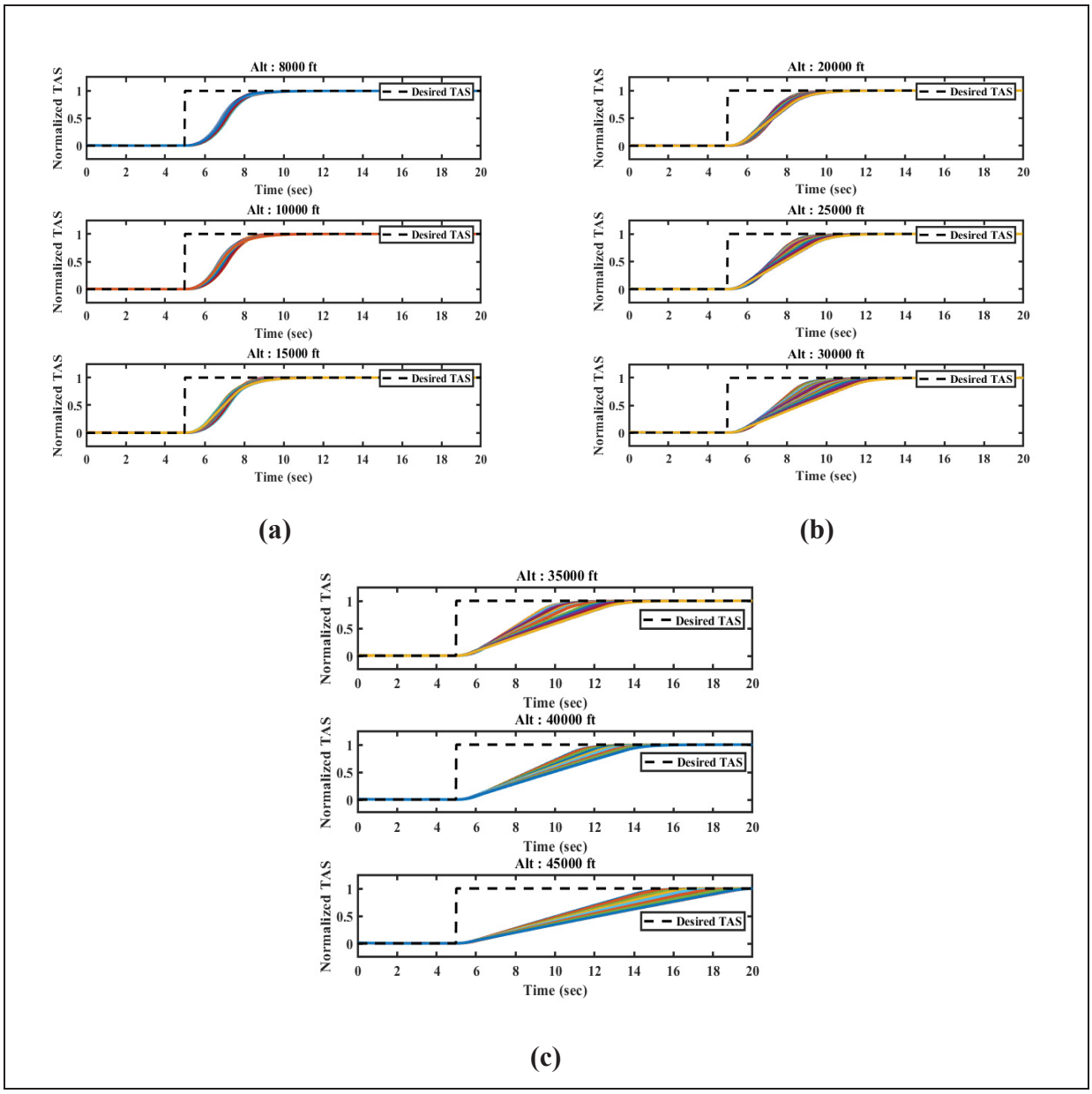

Figure 4.12 Normalized Variations of the True AirSpeed (TAS) versus Time at different altitudes (925 Flight Conditions)

To further demonstrate the efficiency of the designed controllers, their performance was evaluated in the presence of turbulence in Fig. 4.13 for the pitch rate, in Fig. 4.14 for the pitch angle, and in Fig. 4.15 for the aircraft airspeed. From these figures, T2AFSMC controllers could effectively reduce the effects of turbulence for both the aircraft's pitch rate and speed, ensuring stability in the aircraft longitudinal motion even under perturbed flight conditions. Moreover, we defined two variation limits, $\pm$2.5 m/s (i.e., $\pm$5 kts) and $\pm$5.14 m/s

(i.e., ±10 kts) for the aircraft True AirSpeed, according to the objectives of this research. The results shown in Fig. 4.15 indicate that the oscillations induced by the turbulence are too small and can be considered negligible, as the aircraft speed remains at its trimmed value (the reference signal) under different flight conditions.

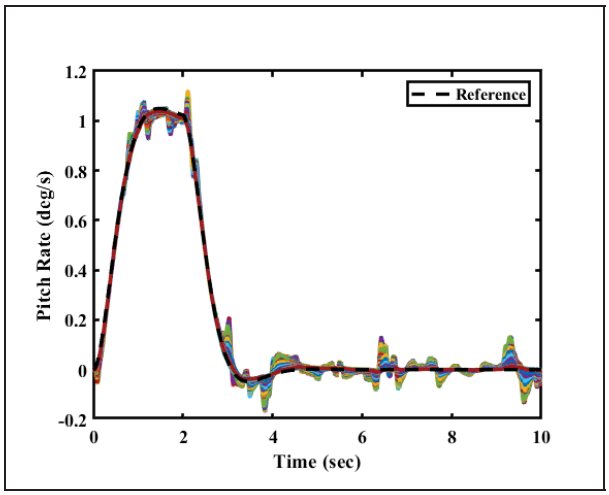

Figure 4.13 Pitch Rate Time Variations with Turbulence

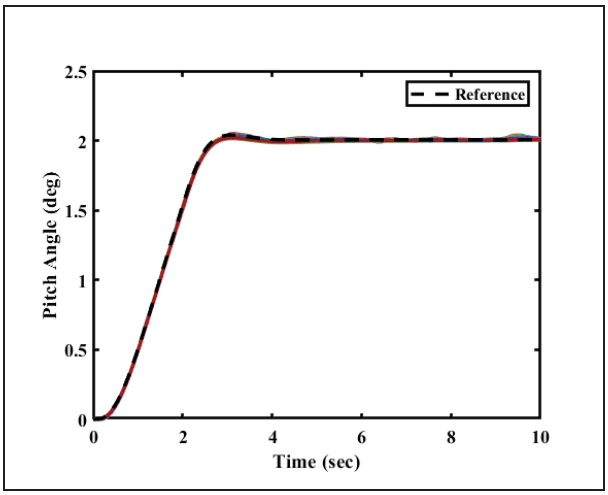

Figure 4.14 Pitch Angle Time Variations with Turbulence

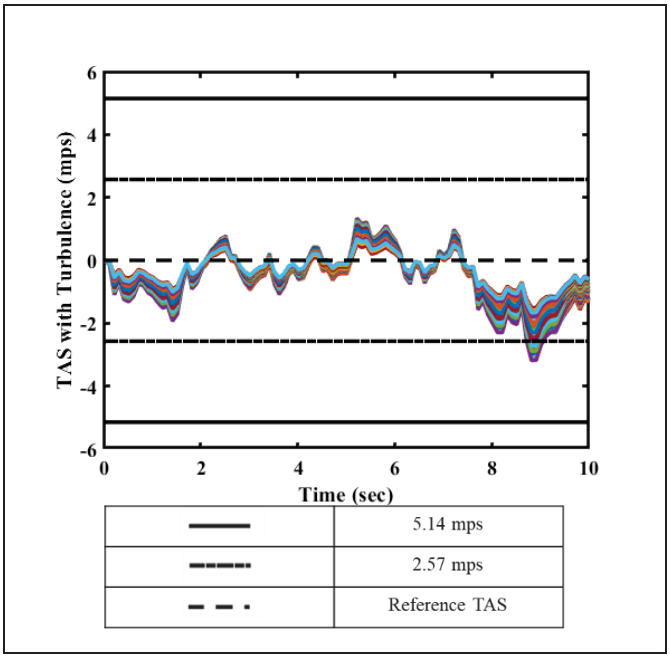

Figure 4.15 True AirSpeed Time Variations in Presence of Turbulence

In Figures 4.13-4.15, the results for all 925 flight conditions were shown. Furthermore, a comprehensive analysis is presented here for the performance of the pitch rate control system in terms of two different error metrics, the Mean Squared Error (ERR_{MSE}) and the Mean Absolute Error (ERR_{MAE}), whose mathematical equations are given as follows:

$$ERR_{MSE} = \frac{1}{n}\sum_{r=1}^{n}(Y_r - Y_{d_r})^2 \tag{4.32}$$

$$ERR_{MAE} = \frac{1}{n}\sum_{r=1}^{n}\left|Y_r - Y_{d_r}\right| \tag{4.33}$$

Where Y is the actual output, Y_d is the desired output, and n is the number of sampled data for a given simulation.

The results show that the tracking error values are consistently small across all flight conditions. Further details on the obtained results, using both Mean Squared Error (MSE) and Mean Absolute Error (MAE) as error metrics, will be provided later in this section. As shown in Eq. (4.32) and Eq. (4.33), MSE, unlike MAE, gives more weight to outliers (error values at each moment that significantly deviate from other values during the simulation). In contrast, MAE is less sensitive to large error values, as it calculates the tracking error.

In Fig. 4.16, the results under both ideal conditions and turbulence align with the research objectives. Under ideal conditions, the Type-2 Adaptive Fuzzy Sliding Mode Control system successfully met the tracking performance. It is interesting to notice that at low altitude values (from 8000 ft to 10000 ft) turbulence effects lead to larger Average Mean Absolute Error (AMAE) values compared to those at high altitude values. This observation is also reflected in the error values measured by the Mean Squared Error (MSE).

Considering the issue explained previously regarding the nature of the MAE metrics, it would also be useful to calculate the error by means of the MSE, as it gives a more intuitive analysis because it penalizes the large error values. Accordingly, a detailed chart is provided in Fig. 4.17 showing the error value for the simulated flight conditions at each altitude evaluated, from 8000 ft to 45000 ft.

where Y is the actual output, Y_d is the desired output, and n is the number of sampled data for a given simulation.

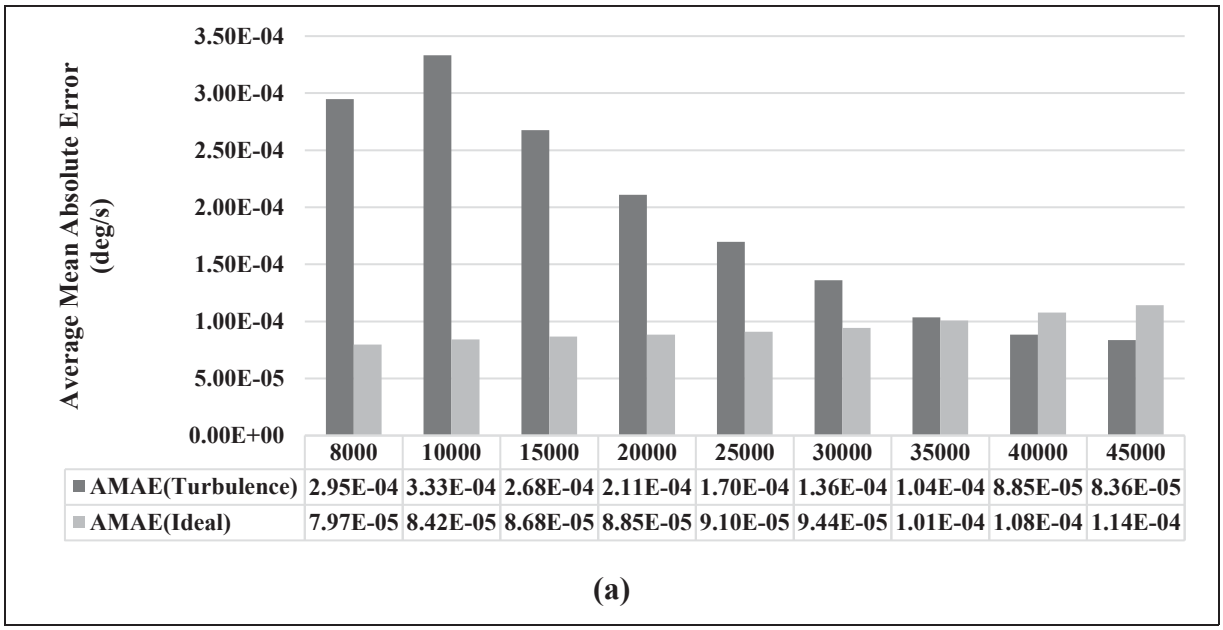

Figure 4.16 a) Average b) Maximum c) Minimum MAEs for the Pitch Rate Controller with and without Turbulence at Different Altitudes over 925 Flight Conditions

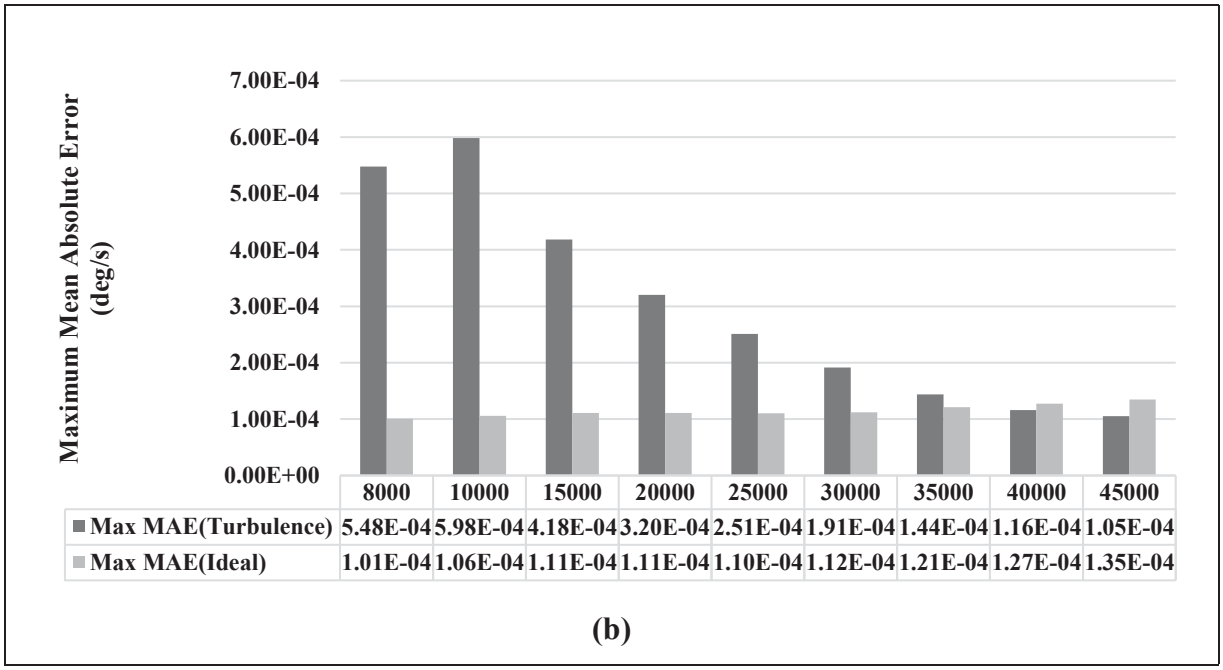

Figure 4.16 b) Maximum MAEs for the Pitch Rate Controller with and without Turbulence at Different Altitudes over 925 Flight Conditions

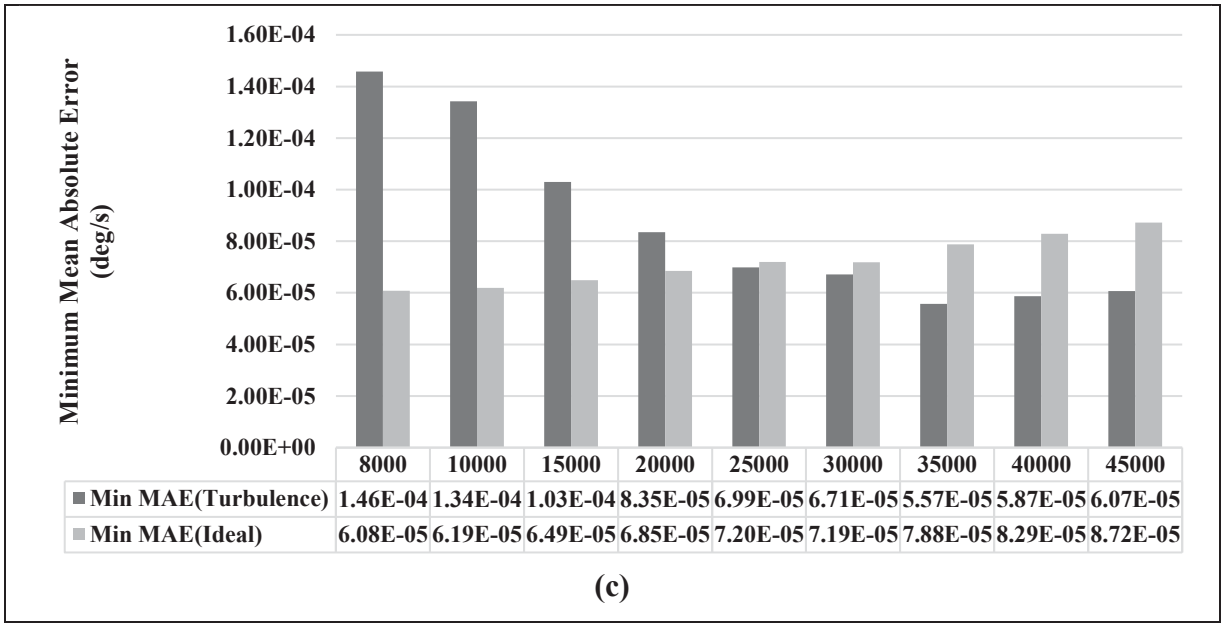

Figure 4.16 c) Minimum MAEs for the Pitch Rate Controller with and without Turbulence at Different Altitudes over 925 Flight Conditions

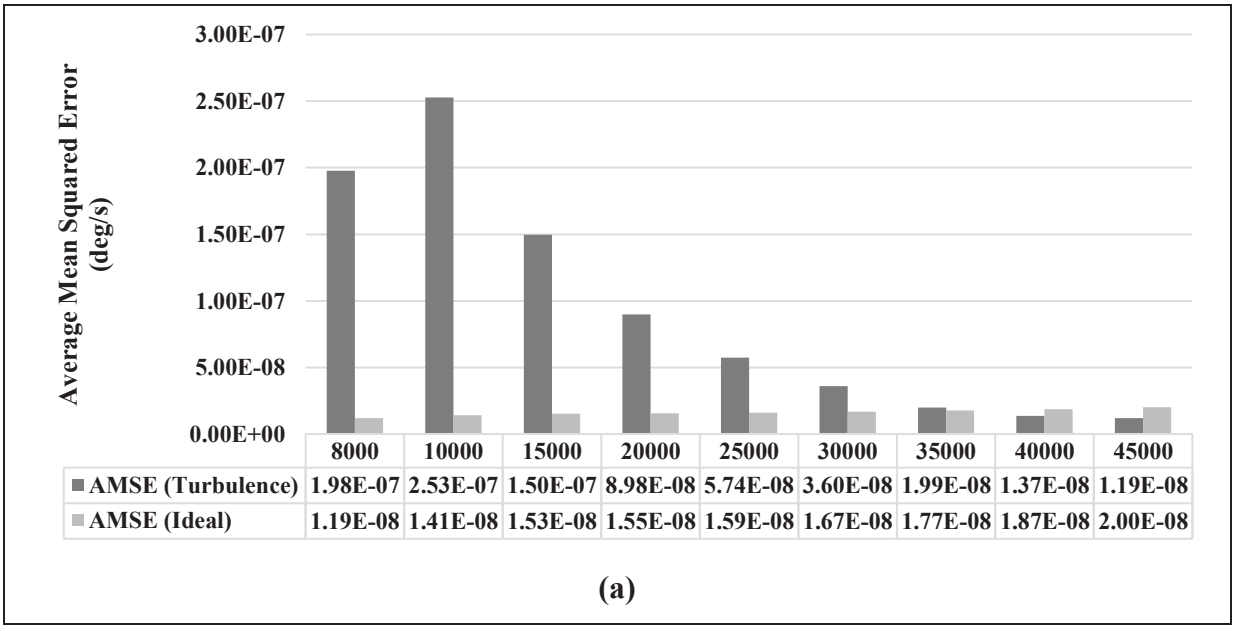

Figure 4.17 a) Average b) Maximum c) Minimum MSEs for the Pitch Rate Controller with and without Turbulence at Different Altitudes over 925 Flight Conditions

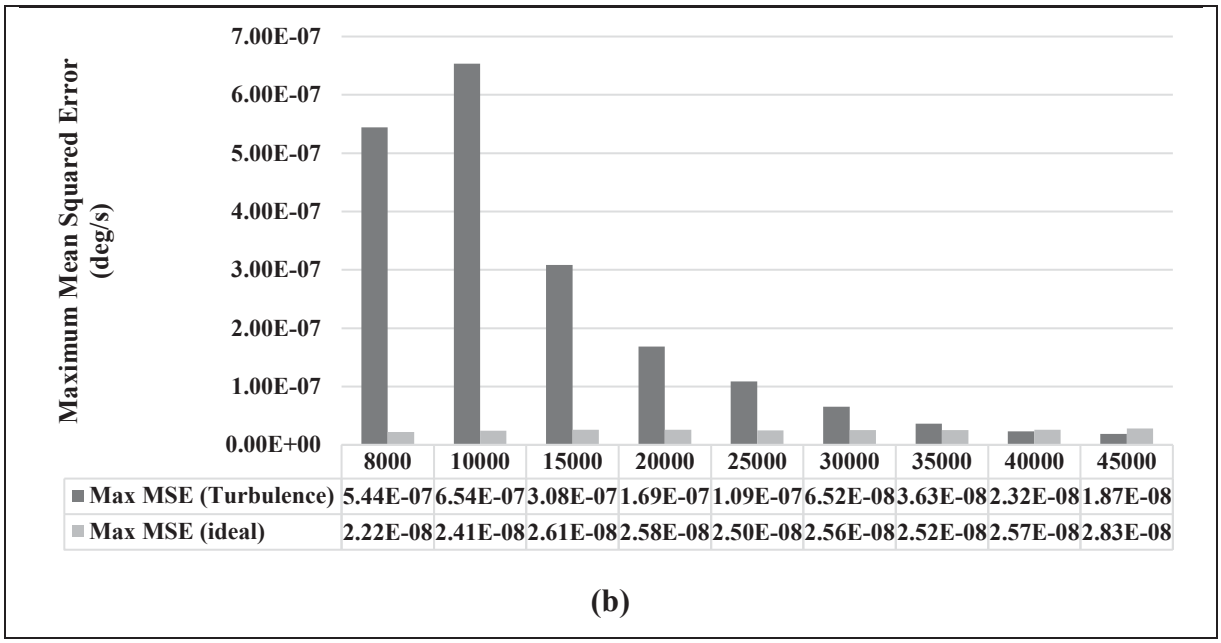

Figure 4.17 b) Maximum MSEs for the Pitch Rate Controller with and without Turbulence at Different Altitudes over 925 Flight Conditions

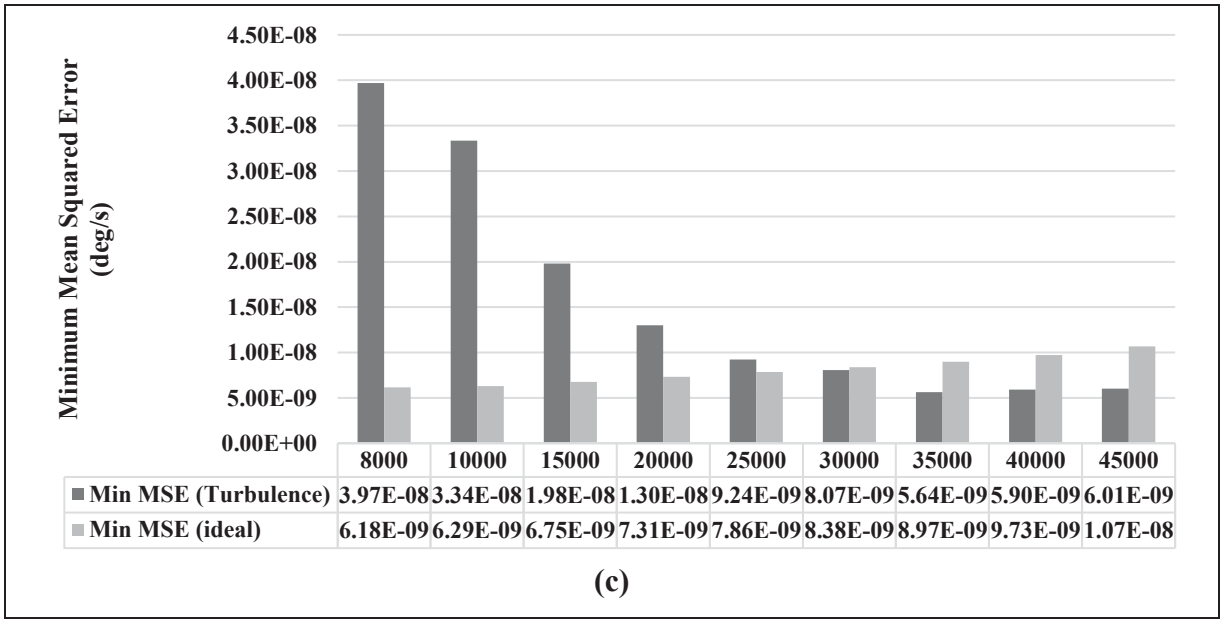

Figure 4.17 c) Minimum MSEs for the Pitch Rate Controller with and without Turbulence at Different Altitudes over 925 Flight Conditions

The minimum and maximum error values for both the MAE and MSE metrics provide additional information about the performance of the pitch rate control system in the best and

worst cases across all flight conditions. Furthermore, according to the objectives of this research, while applying the turbulence to the aircraft model, it was necessary to stabilize the aircraft airspeed at its trimmed value for each flight condition. Therefore, the performance of the aircraft speed control system, designed by a Type-2 Adaptive Fuzzy Sliding Mode control methodology, was evaluated in the presence of turbulence, as shown in Fig. 4.18.

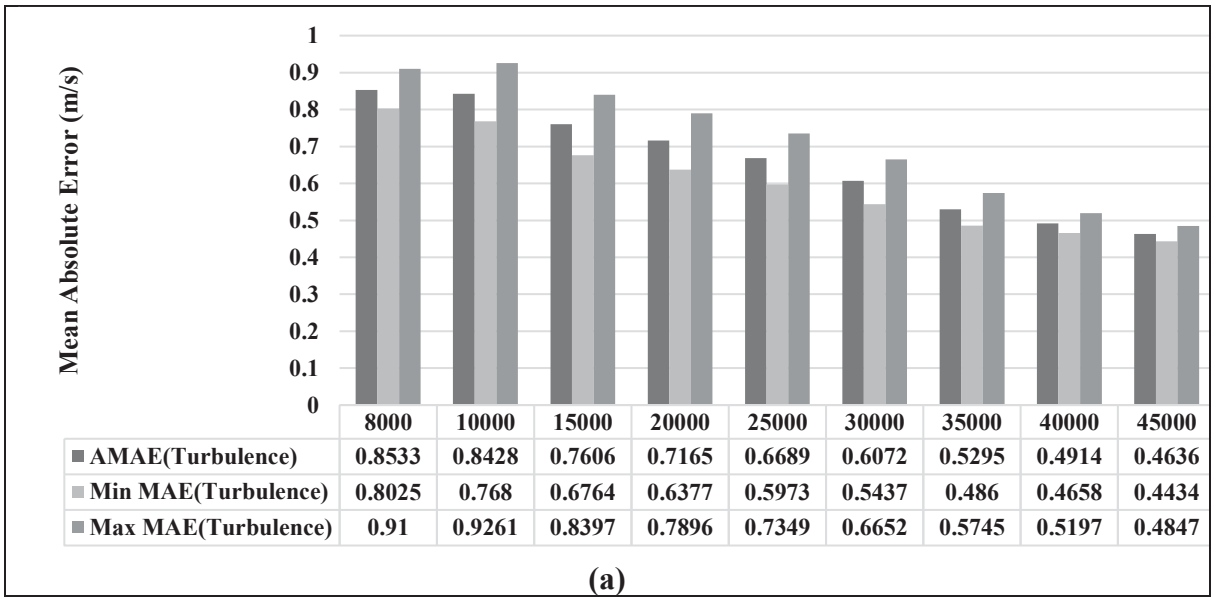

Figure 4.18 a) Average Mean Absolute Error b) Average Mean Squared Error for the True AirSpeed Controller with Turbulence at Different Altitudes over 925 Flight Conditions

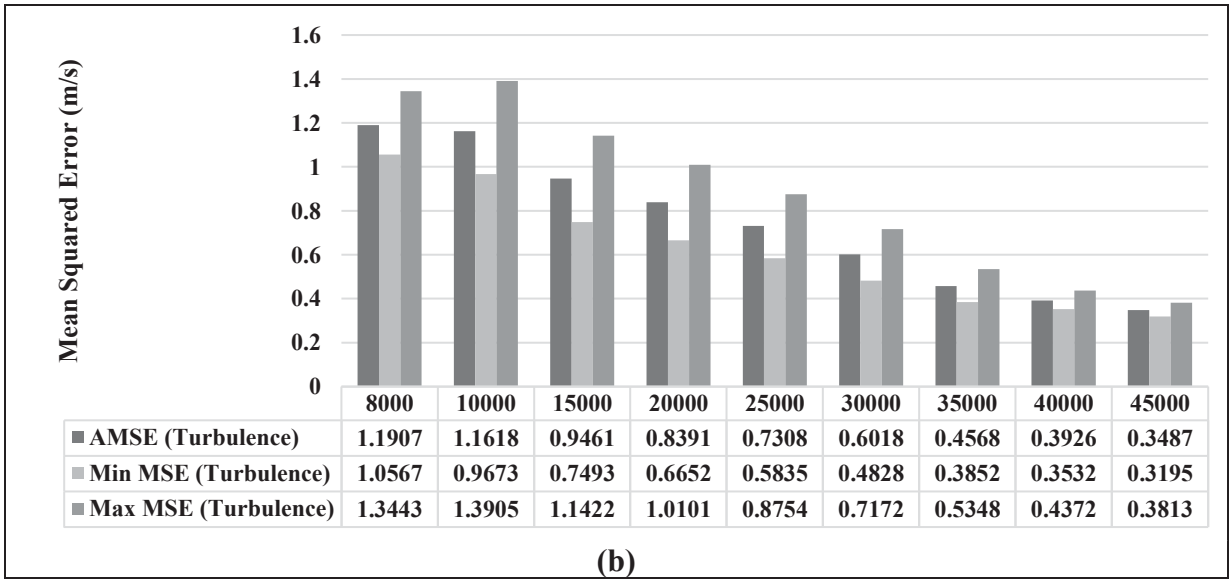

Figure 4.18 b) Average Mean Squared Error for the True AirSpeed Controller with Turbulence at Different Altitudes over 925 Flight Conditions

The metrics given in Equations. (4.32) and (4.33) were used to calculate the error values under turbulent flight conditions. The results are shown in Fig. 4.18. As in case of results obtained for the pitch rate, it can be seen from Fig. 4.18(a) that turbulence significantly affects aircraft performance at lower altitudes when compared to error values at higher altitudes. Nevertheless, all these values are very good with respect to the objectives of this study, in accordance with the average values of the MAE and MSE and their minimum and maximum values obtained for all of the flight conditions at each altitude evaluated.

In conclusion, the simulation results have shown the performance capabilities and advantages of the proposed control systems under a wide range of flight conditions for both aircraft pitch rate and speed using the parameter values given in Table 4.7. These outcomes provide empirical evidence supporting their use in terms of aircraft safety, as well as their robustness, given their good tracking performance and small error values, proving the controllers' efficiency, especially under critical flight conditions induced by turbulence.

Table 4.7 Design Parameters for the Pitch Rate and TAS Control Systems

	Parameters	Values
Pitch Rate Control	Sliding Surface Constant (m)	10.5
	Adaptation gain ($\underline{g}_A$)	10^2
	Adaptation gain ($\overline{g}_A$)	10^2
	Adaptation gain ($\overline{g}_B$)	3×10^3
	Adaptation gain ($\underline{g}_B$)	3×10^3
	Switching Control Coefficient (T)	131
	Integral Control Gain (ρ_i)	5700
True Airspeed Control	Switching Control Coefficient (I)	70
	Sliding Surface Constant (W)	3000
	Adaptation gain ($\underline{g}_M$)	10^4
	Adaptation gain ($\overline{g}_M$)	10^4
	Adaptation gain ($\underline{g}_N$)	200
	Adaptation gain ($\overline{g}_N$)	200
	Adaptation gain ($\underline{\Delta}_M$)	10^{-6}
	Adaptation gain ($\overline{\Delta}_M$)	10^{-6}
	Adaptation gain ($\underline{\Delta}_N$)	10^{-6}
	Adaptation gain ($\overline{\Delta}_N$)	10^{-6}

4.5 Conclusion

This article describes the development of two Type-2 Adaptive Fuzzy Sliding Mode Control systems to control the pitch rate and to stabilize the speed of the Cessna Citation X business aircraft under critical environmental conditions such as turbulence with a moderate intensity. In both these control systems, Type-2 Fuzzy Logic System (T2FLS) was designed to approximate the unknown nonlinear functions in the related aircraft dynamics equation separately for the pitch rate and aircraft True AirSpeed. The main advantage of this method over the Type-1 Fuzzy Logic system is its ability to handle the uncertainties in the aircraft model and to deal with dynamic variations, especially when an aircraft flies through various flight conditions. This methodology considered with two other control techniques, a Sliding Mode control to allow the aircraft dynamics to reach their balanced points, and an Adaptive control system to update the functions approximated by the T2FLS to control an aircraft containing numerous complex systems. The adaptation laws, designed based on the Lyapunov theorem, were integrated into the approximated function by the T2FLS. As a result, the approximate functions could be updated during the simulation iterations, while the Sliding Mode Control system forced the aircraft dynamics to reach their equilibriums as well as maintain the aircraft stability and satisfy the robustness of the aircraft, both under ideal conditions and in the presence of the turbulence that deviates the aircraft from its balanced condition. It is also worth mentioning that this controller does not need any prior knowledge regarding the aircraft model, and it can be developed by qualifying the variations of the measured variables, and by decreasing their tracking error, rather than using their crisp values. The performance of the proposed controller was simulated and validated using the simulation platform created by researchers at the LARCASE. This platform was designed based on real flight data in a Level-D flight simulator for the Cessna Citation X business aircraft. The results show a very good performance of the Type-2 Adaptive Fuzzy Sliding Mode Control System with its negligible tracking error, and in preserving aircraft stability under both ideal and perturbed conditions over the 925 flight conditions evaluated, from low to high altitudes. Furthermore, the stability of the aircraft was validated by the Lyapunov theorem for both the pitch rate and speed control systems.

CHAPTER 5

ENHANCED FUZZY-BASED SUPER-TWISTING SLIDING-MODE CONTROL SYSTEM FOR THE CESSNA CITATION X LATERAL MOTION

S.M. Hosseini, I. Bematol, G. Ghazi and R.M. Botez

Research Laboratory in Active Controls, Avionics and AeroServoElasticity (LARCASE),
Department of Systems Engineering, École de Technologie Supérieure,
1100 Notre-Dame West, Montreal, Quebec, Canada H3C 1K3

Paper published in *Aerospace* journal, July 2024

Resumé: Cet article présente une nouvelle combinaison de trois systèmes de contrôle : un système de contrôle adaptatif, un système de logique floue de type deux et un système de contrôle par mode glissant super-torsion (STSMC). Cette combinaison a été mise au point au Laboratoire de recherche appliquée aux commandes actives, à l'avionique et à l'aéro-servoélasticité (LARCASE). Ce contrôleur incorpore deux méthodes pour calculer les gains du terme de commutation dans le STSMC à l'aide de l'algorithme d'optimisation par essaim particulaire : (1) gains adaptatifs et (2) gains optimisés. Cette méthodologie a été appliquée à un modèle non linéaire de l'avion d'affaires Cessna Citation X généré par la plateforme de simulation développée au LARCASE dans Simulink/MATLAB (R2022b) pour le mouvement latéral de l'avion. La plateforme a été validée avec des données de vol obtenues à partir d'un simulateur de vol d'avion de recherche de niveau D fabriqué par CAE (Montréal, Canada). Le niveau D correspond à la qualification la plus élevée délivrée par la FAA pour les simulateurs de vol de recherche. Les performances des contrôleurs ont été évaluées en utilisant les turbulences générées par le modèle Dryden. Les résultats de la simulation montrent que ce contrôleur peut gérer à la fois les turbulences et les incertitudes existantes. Enfin, le contrôleur a été validé pour 925 conditions de vol sur l'ensemble de l'enveloppe de vol pour une configuration unique en utilisant des gains adaptatifs et optimisés en termes de commutation du STSMC.

Abstract: A novel combination of three control systems is presented in this paper: an adaptive control system, a type-two fuzzy logic system, and a super-twisting sliding mode control (STSMC) system. This combination was developed at the Laboratory of Applied Research in Active Controls, Avionics and AeroServoElasticity (LARCASE). This controller incor-porates two methods to calculate the gains of the switching term in the STSMC utilizing the particle swarm optimization algorithm: (1) adaptive gains and (2) optimized gains. This methodology was applied to a nonlinear model of the Cessna Citation X business jet aircraft generated by the simu-lation platform developed at the LARCASE in Simulink/MATLAB (R2022b) for aircraft lateral motion. The platform was validated with flight data obtained from a Level-D research aircraft flight simulator manufactured by the CAE (Montreal, Canada). Level D denotes the highest qualification that the FAA issues for research flight simulators. The performances of controllers were evaluated using the turbulence generated by the Dryden model. The simulation results show that this controller can address both turbulence and existing uncertainties. Finally, the controller was validated for 925 flight conditions over the whole flight envelope for a single configuration using both adaptive and optimized gains in switching terms of the STSMC.

Keywords: type-two fuzzy system; super-twisting sliding-mode control; adaptive control; particle swarm optimization; Cessna Citation X; lateral motion; flight control system; fuzzy logic system; Dryden turbulence

5.1 Introduction

Artificial intelligence-based control systems have become the main topic of much research. The recent developments in aircraft systems have increased pilots' workload; our primary motivation in this paper is to reduce that workload and ease flight procedures for pilots, especially in critical conditions such as atmospheric turbulence. This objective could help to reduce aircraft accidents. As claimed in (William Rankin, Ph.D., 2007), 80% of aircraft accidents are caused by human errors rather than system failures. The novel methodology proposed here benefits from the advantages of the approximation capability of the Type-Two

Fuzzy Logic System (T2FLS) while facing existing uncertainties, the robustness of super-twisting sliding-mode control (STSMC), and the characteristics given by adaptation laws to update approximated functions by a T2FLS during the lateral motion simulation of the Cessna Citation X aircraft in cruise. The gains in the switching control term designed in the STSMC were determined by two different methodologies: one uses adaptation laws, and the other uses the Particle Swarm Optimization method, both of which are discussed in more detail later in this paper.

Concerning the selected methodologies in this article, a brief discussion of the previous studies is presented in this section to provide some essential background. These methodologies have been used for different applications in aerospace and aeronautics.

Satisfying the stability and maneuverability of an aircraft with a control system is essential to guarantee flight safety and passengers' comfort. These problems have been addressed by a wide range of control techniques and methodologies, as detailed next.

Previously, conventional methodologies showed their compatibility and precision for various types of air vehicles. Idir et al. (Idir, Bensafia, Khettab, & Canale, 2023) introduced a novel methodology using a combination of an optimal reduced-order fractional proportional–integral–derivative (PID) controller with the Harris Hawks Optimization Algorithm to control the pitch angle of an aircraft using the Matsuda and the Oustaloup approximation methods. Although these control methodologies have shown superior performance in terms of transient response analysis and the signal characteristics of the pitch angle compared to other controllers, it is necessary to add a robust controller to guarantee the boundedness of the control system, especially in the presence of a load disturbance. To control the pitch of a general aviation aircraft, Deepa and Sudha (Deepa & Sudha, 2016) suggested using tuning methods such as the Zeigler–Nichols, modified Zeigler–Nichols, Tyreus–Luyben, and Astrom–Hagglund methods to find the gains of a PID controller. Based on the presented performance analysis, the Zeigler–Nichols method found more appropriate gain values to remove drastic oscillations, which can be used for both linearized and nonlinear aircraft

models. Wilburn et al. (K. et al., 2014) developed a new Genetic Algorithm (GA) to optimize the performance of several controllers, including a PID, a Nonlinear Dynamic Inverse (NLDI), and an adaptive PID. The enhanced GA used in this paper benefits from excessive normalization, proposing a mutation operator matrix, varying parameter bounds, and initializing the GA population with predefined values. This study demonstrated that this novel GA algorithm can be used with other controllers, such as artificial immune system-based PID control systems, with the aim of improving the robustness and trajectory tracking performance of an Unmanned Aerial Vehicle (UAV). Moreover, the efficiency of an optimized bio-inspired adaptive control approach with a GA was evaluated in (Perez et al., 2015) to compensate for aircraft failures. In addition to addressing these failures, that study highlighted the ability of the proposed method to significantly improve aircraft handling qualities. The proposed adaptive immunity-based controllers acted as model-referenced baseline control systems to generate control inputs for the angular rates. This baseline control system and a nonlinear dynamic inversion (NLDI) approach were developed to deal with nonlinearities. Compared with an adaptive neural network system, the combination of the adaptive immunity-based controllers and NLDI provided better results in nominal and abnormal pilot-in-the-loop simulations.

In (Ingabire & Sklyarov, 2019b), extensive studies were conducted to evaluate the performance of Linear Quadratic Regulator (LQR), Linear Quadratic Gaussian (LQG), and nonlinear methods for controlling the pitch angle of a UAV. Among these control methods, the LQG successfully attenuated the disturbance, and the LQR performed better under ideal flight conditions. In contrast, the nonlinear control system outperformed both the LQR and LQG methods in terms of smoothness of the response, robustness, and speed of convergence to the reference signal. Further exploration by Vishal and Ohri (Vishal & Ohri, 2014b) showed that a Genetic Algorithm (GA) can effectively adjust the parameters of LQR and PID controllers, offering better results in terms of pitch angle control of an aircraft compared to its parameters manual adjustments. Between the GA-based PID controller and the GA-LQR combination, the GA-LQR offered better signal characteristics, such as rise time, settling time, and peak overshoot. In addition, the steady-state error obtained for the GA-LQR was

smaller than that of the GA-based PID method. Qi et al. (Qi et al., 2021) developed a Modified Uncertainty and Disturbance Estimator (MUDE) for achieving accurate attitude-tracking performance in quadcopters using a precise actuation model. This method was compared with cascaded PID and conventional uncertainty and disturbance estimator-based controllers. This comparison revealed that the MUDE-based controller performs better in reducing both tracking and disturbance estimation errors. Furthermore, to solve the path-following problem and attain asymptotic stability for a minimum of three quadrotors, a Robust Load Priority (RLP) control system was proposed in (Qian & Liu, 2022). In this article, a nonlinear control system was developed by leveraging Kane's method with the direct Lyapunov method to convert the position and attitude errors into a virtual lift control input. This control input helps the quadrotors to rotate and manipulate their loads. On the other hand, a UDE-based robust controller was proposed for a single quadrotor to achieve path-tracking control performance while lifting a suspended payload under disturbances. A two-loop control system was implemented to address external disturbances, such as turbulence, on fixed-wing UAVs flying at low altitudes (Xiong & Liu, 2023). It included an LQR and $H^{\infty}$and a Luenberger observer serving as a full-state estimator. In addition to mitigating the effects of disturbances, this control method ensured the safety margin of the UAVs with respect to the ground by tuning the reference altitude. The L1 adaptive control system is another methodology, which was applied in (Moncayo et al., 2013) as a fault-tolerant control system to address the challenges caused by actuation failures and turbulence. This control mechanism enhanced the functionalities of a linear controller, and an extended NLDI control system was developed to reduce the distance error with respect to the desired flight path of the West Virginia University Unmanned Aerial Vehicle (UAV). To deal with parameters uncertainties, disturbance, and coupled dynamics in quadrotors, Labbadi et al. (Labbadi et al., 2020) have developed super-twisting proportional–integral–derivative sliding-mode control (STPIDSMC) methodologies based on the fractional-order control methodology for each of the position and attitude control systems. This combination offered a highly robust and accurate tracking performance under various scenarios in comparison with fractional-order backstepping sliding-mode control and nonlinear internal control systems by considering their Integral Absolute Error (IAE) values. In addition, to satisfy the

3D trajectory tracking performance of quadcopters, a group of six second-order sliding-mode control (SMC) systems using the super-twisting algorithm within two separate controller mechanisms, one for attitude and altitude of the quadcopters and the other one for the position of the quadcopters, was proposed by Matouk et al. (Matouk et al., 2020). Compared to a conventional SMC and a fuzzy sliding-mode control system, this control methodology provided improved model robustness to parametric variations, uncertainties, and disturbances and gave more accurate tracking performance without undesired chattering.

In recent years, the evolution of control methodologies has seen a significant shift from conventional approaches to AI-based techniques, demonstrating a broad spectrum of very good adaptability and precision. As an AI-based control system, Deep Recurrent Neural Networks (DRNNs) were used to control highly nonlinear hypersonic vehicles (Nivison & Khargonekar, 2017b), offering very high adaptability to time-varying trajectories and robust performance in the presence of aerodynamic uncertainties. The DRNNs were equipped with gated recurrent units at the hidden neurons to enhance long-term learning and avoid the gradient decay problem. This paper showed that the proposed DRNN-based controller could perform better than the gain-scheduled LQR control approach. This study, among many others, highlights a significant shift from traditional control methods toward exploiting the adaptive capabilities of neural networks. An Aggregated Multiple Reinforcement Learning System (AMRLS) with multiple Reinforcement Learning (RL) algorithms and Cerebellar Model Articulation Controller (CMAC) techniques was proposed in (Jiang & Kamel, 2007) to solve the problem of the exponential increase of dimensionality due to the excessive size of continuous state space equation form used for the pitch control of a B747 aircraft. This control algorithm accelerated the convergence rate and reduced the steady-state pitch error. Furthermore, Andrianantara et al. in (Rojo P. Andrianantara et al., 2024 ; Rojo Princy Andrianantara et al., 2023) explored advanced control strategies for the pitch rate control of the Cessna Citation X (CCX) business jet. In (Rojo Princy Andrianantara et al., 2023), a linear PID control system was combined with an adaptive neural network (ANN) and dynamic inversion (DI) methodology to achieve tracking performance and to ensure aircraft stability without prior knowledge of aircraft dynamics. This control methodology gave better

results than single PID, PID-DI, and PID-NN control systems. With the same objectives, Andrianantara et al. (Rojo P. Andrianantara et al., 2024) integrated an adaptive neural network system with an online Recursive Least Square (RLS)-based Model Predictive Controller (MPC) to control the CCX pitch rate under different flight conditions.

According to (Khalid et al., 2019), different controllers, such as PID, fuzzy PID, and sliding-mode control systems, might be chosen for controlling the pitch rate of an aircraft in the presence of unpredicted conditions such as external disturbances. In this article, although the fuzzy PID control system showed the best signal characteristics in terms of tracking performance, besides its ability to update the control parameters during the simulation, the SMC systems worked perfectly in terms of both rise and settling times among all the presented methods. Nair et al. (Vishnu G. Nair, Dileep M. V, & V. I. George, 2012) studied the performance of a Linear Quadratic Controller (LQR) system and a Fuzzy Logic Controller (FLC) based on their time response characteristics in controlling the aircraft yaw rate. This study revealed that both methods have specific steady-state errors and overshoots; however, the LQR controller converges to the given desired signals faster than the FLC system. With the aim of achieving a robust automatic landing system in the presence of coupling effects and uncertainties, a proportional–derivative fuzzy logic control system was developed for the nonlinear six-degree-of-freedom models of a medium-sized aircraft. The performance analysis illustrated that this control methodology was appropriate in terms of the stability and steady-state error criteria (Nho & Agarwal, 2000). Jiao et al. (R. Jiao, Chou, Rong, & Dong, 2020) focused on the stability of quadrotor Unmanned Aerial Vehicles (UAVs) equipped with a 2-degree-of-freedom robotic arm and a combination of Sliding-Mode Extended State Observer (SMESO) and a Fuzzy Adaptive Saturation Super-Twisting Extended State Observer (FASTESO) that updated observer gains for the accurate attitude control in the presence of disturbances. In addition, an adaptive super-twisting sliding-mode methodology was developed by Humaidi and Hasan in (Humaidi & Hasan, 2019) to control a two-axes helicopter with uncertainties in its model to achieve tracking performance while reducing the chattering on the control input. This control model was equipped with the

Particle Swarm Optimization (PSO) algorithm to find the best values for the design parameters.

Dealing with uncertainties is another challenging issue for aircraft control. Hashemi and Botez (S. M. Hashemi & Botez, 2022) suggested using a robust adaptive T-S fuzzy logic control system for the Hydra Technologies UAS-S4 Ehécatl to handle various uncertainties, such as unknown parameters in the control system, modelling errors, and disturbances. To minimize energy consumption, improve tracking performance, and maintain stability in a chaotic environment in a Click Mechanism Flapping Wing (CMFW) of an insect-inspired Nano Air Vehicle (NAV), which was defined by T-S fuzzy rules, the authors in (Seyed Mohammad Hashemi et al., 2020) proposed using a fuzzy controller integrated with a state feedback control system. In this methodology, the gains of the fuzzy logic-based control system were updated using several adaptive control laws derived from the Lyapunov theorem.

Yu et al. (Ziquan Yu et al., 2019) validated the performance of a fault-tolerant control method for UAVs to maintain their attitude with the occurrence of failures in the actuation system while dealing with the existing model uncertainties. This control system employed a fractional-order-based control system based on an adaptive fuzzy neural network system to approximate the uncertainties due to the failures in the follower UAV actuation systems. In addition, distributed sliding-mode systems were designed to estimate the attitudes of the leader UAVs to ensure attitude-tracking performance and to achieve a safe formation. As another fault-tolerant control system for UAVs, a new event-triggered methodology was included using fractional-order calculus and interval type-2 fuzzy neural network systems to satisfy attitude-tracking performance and stability (Ziquan Yu, Yang, et al., 2023). The stability of the UAVs was demonstrated by analyzing their performance at different attitudes while tracking the issued reference signals. These control systems have reduced the communication load while improving the fault tolerance properties in this application. Moreover, it was suggested in (Ziquan Yu et al., 2022) to apply a combination of fixed-time performance functions, fractional calculus, and sliding-mode surfaces, enhanced by recurrent

fuzzy neural networks, to keep the tracking errors within certain bounds and improve fault tolerance characteristics of the UAVs in the presence of actuators faults.

Continuing the investigations outlined for the longitudinal motion of a Cessna Citation X using fuzzy logic-based control systems in (S. Hosseini, Ghazi, et al., 2023a, 2023b)and a model reference adaptive recurrent neural network control system in (S. Hosseini, Inga, et al., 2023), this study aims to explore their compatibility with the lateral motion of the aircraft, which is more complex than the longitudinal motion due to the coupling between the roll and yaw motions. Therefore, this paper mainly contributes to the application of an artificial intelligence methodology with the Type-Two Adaptive Fuzzy Logic System (T2AFLS) combined with a nonlinear super-twisting sliding-mode control (STSMC) system for the lateral motion of aircraft, as detailed below:

- Previously, most studies were devoted to designing an AI-based controller for the longitudinal motion of aircraft. However, this article presents a new combination of control systems comprising T2AFLS and STSMC methodologies for the lateral motion of the Cessna Citation X aircraft. This methodology addresses two main challenges in the control of an aircraft: (1) the issues that arise with structured uncertainties, such as variations of flight conditions, and unstructured uncertainties, such as unmodeled parameters, and (2) aircraft stabilization in the presence of turbulence. We used the Dryden turbulence model to generate a moderate-intensity turbulence profile, which has not been used before with the considered methodology in the paper. This controller benefits from an improved uncertainty handling offered by the T2FLS, while the adaptation laws determined based on the Lyapunov theorem help to continuously update the approximated function by the fuzzy logic system. Enhanced robustness and stability were achieved using a nonlinear super-twisting sliding-mode control (STSMC). Two methodologies were employed to fine-tune the gains in the STSMC term: (1) adaptive control laws (calculated by the Lyapunov theorem) presented later in this paper (Shtessel et al., 2012 ; Yan et al., 2019), and (2) the Particle Swarm

Optimization (PSO) algorithm. Although the adaptation laws used for the switching control term in this paper were designed based on the methodology proposed in (Yan et al., 2019), our new method suggests combining the T2AFLS-based approximator with the adaptive super-twisting sliding-mode control, a considerable contribution to the theory. The performances of these approaches are compared to each other to help the reader understand the advantages of each method in this particular application. The validation process was conducted across the entire flight envelope (over 925 flight conditions covering the whole flight envelope) to ensure its reliability and effectiveness with and without turbulence.

- The super-twisting sliding-mode control system (STSMC) has been studied for different aircraft types alone and with other control systems (Humaidi & Hasan, 2019 ; R. Jiao et al., 2020). The methodology proposed here is novel according to several features; for example, in (R. Jiao et al., 2020), the authors combined the Type-One Adaptive Fuzzy Logic System (T1AFLS) with the STSMC, where the T1AFLS was employed to approximate the gain in the switching control term, whereas the proposed Type-Two Adaptive Fuzzy Logic System (T2AFLS) in our paper was used to approximate the unknown dynamics of the aircraft. Furthermore, our controller employs two methodologies to find the gains in the switching control term formulated based on the super-twisting algorithm, the adaptive switching term, and the optimized switching term by using the PSO algorithm. Although the authors in (Humaidi & Hasan, 2019) applied the PSO algorithm to optimize those gains, our methodology offers some improvement. Our paper proposes a different cost function to optimize three parameters, which could reduce the computational burden regarding the number of iterations and the swarm population compared with the one used in (Humaidi & Hasan, 2019) for optimizing eight parameters.

- We validated our new methodologies using a highly accurate nonlinear simulation platform designed with actual flight data derived from a Level-D Research

Aircraft Flight Simulator (RAFS) for Cessna Citation X business aircraft. We believe this simulation platform can precisely represent the dynamics of Cessna Citation X aircraft at each flight phase. This paper is thus among the pioneer articles that applied this methodology to a business aircraft containing much more nonlinearities and complexity than the Unmanned Air Vehicles (UAVs) (R. Jiao et al., 2020), helicopter models (Humaidi & Hasan, 2019), Teledyne Ryan BQM-34 (Firebee) aircraft used in (Yan et al., 2019), quadrotors (Labbadi et al., 2020 ; Matouk et al., 2020), and hypersonic aircraft (Nho & Agarwal, 2000).

The rest of this article is organized as follows: Section 5.2 begins with a description of the lateral aircraft model, followed by a detailed explanation of the applied control methodology in Section 5.2.2. Next, Section 5.3 discusses the simulation results for each control approach, including a comparison of their performances. This paper will be concluded in Section 5.4.

5.2 Methodology

This section explains the methodology for developing a Super-Twisting Adaptive Type-Two Fuzzy Sliding-Mode Control (STAT2FSMC) system. This control system integrates the robustness of a super-twisting control system with the adaptive approximation capability of a Type-Two Adaptive Fuzzy Logic System (T2AFLS). The super-twisting sliding-mode control system (STSMC) is an enhanced type of sliding-mode control system commonly used for mitigating chattering (unwanted oscillations with finite frequency and amplitude) (Utkin & Lee, 2006).

The nonlinear aircraft model is described in Section 5.2.1. This model contains unknown dynamics that can be approximated by an Adaptive Type-Two Fuzzy Logic System (AT2FLS). The adaptive characteristic of this approximator is that it fine-tunes the adjustable parameters in real time in order to acquire optimal performance under various flight conditions. A Particle Swarm Optimization (PSO) method was utilized to find the appropriate values for the design parameters of this controller.

5.2.1. Aircraft Mathematical Model

This article uses a nonlinear model of the Cessna Citation X business jet aircraft. The aircraft is represented by a state-space model to provide adequate understanding and prediction abilities for its response of an aircraft to control inputs and external disturbances. For this purpose, a simulation platform was employed to reproduce the nonlinear lateral dynamics of the Cessna Citation X. This simulation platform was developed at the LARCASE laboratory and validated with flight data obtained from a Level-D Research Aircraft Flight Simulator (RAFS), as shown in Fig. 5.1. Level D is the highest degree of qualification issued by the Federal Aviation Administration (FAA) for research flight simulators (Ghazi, Botez, & Messi Achigui, 2015).

Figure 5.1 The Level-D RAFS for the Cessna Citation X business jet aircraft

The state vector for the aircraft lateral model typically includes variables such as sideslip angle β, roll rate p, roll angle φ, and yaw rate r. These state variables are the most pertinent for describing the variations of the aircraft dynamics in lateral motion. The main objective of this research is to control the roll rate p and to stabilize the yaw rate r indirectly by controlling the sideslip angle β. Therefore, the state-space representation can be written in a standard form with its n^{th} order of time derivative, as given in (Rama K Yedavalli, 2020).

$$x^{(n)} = h(x) + g(x)u + d(t) \tag{5.1}$$

where $x = [\beta, p, \varphi, r]^T$ is the state vector, $h(x)$ and $g(x)$ are the unknown nonlinear functions to be approximated for the purpose of this research, $d(t)$ represents the unknown disturbance, and u denotes the control inputs, such as the ailerons u_{ail} and rudder u_{rud} command signals.

Practically, $g(x)$ represents the control effectiveness. This function exhibits minimal variations in business jets such as the Cessna Citation X during cruise, in which stable and smooth maneuvers are crucial. This aspect was observed during simulation. Thus, to reduce the complexity of the control system design and to focus on the aircraft's dominant nonlinearities in the presence of uncertainties and turbulence, in this methodology, $g(x)$ was approximated to be equal to 1, ($g(x) \approx 1$), and $h(x)$ was approximated by the Type-Two Adaptive Fuzzy Logic System (T2AFLS) using the methodology presented in Section 5.2.2.1.

5.2.2. Control System Design

Two control systems are designed here, one for the roll rate and the other one for the yaw rate. The roll rate control system that produced the aileron command signal was designed using a Type-Two Adaptive Fuzzy Super-Twisting Sliding-Mode Control (T2AFSTSMC). In addition, an integral (I) controller was employed to stabilize the yaw rate using the sideslip angle error (the rudder command).

The first step to designing the roll rate control system is to provide the details of the applied Type-Two Fuzzy Logic System, presented next in Section 5.2.2.1.

5.2.2.1.Type-Two Fuzzy Logic System as an Approximator

Fuzzy logic systems have emerged as a practical approach to control nonlinear systems in many studies. Unlike conventional control systems, which are designed for crisp input and outputs valus, a fuzzy logic system relies on the linguistic qualification of the input and output values, thus akin to human reasoning, which operates on a spectrum of possibilities.
For the methodology proposed here, the Type-Two Fuzzy Logic system was selected due to its ability to handle uncertainties and variations in aircraft dynamics. The Type-Two Fuzzy Logic System consists of the following 5 components (L.-X. Wang, 1997): (1) Fuzzifier, (2) Inference Engine, (3) Fuzzy Rule Base, (4) Type Reducer, and (5) Defuzzifier. A simplified architecture of a Type-Two Fuzzy Logic System is illustrated in Fig. 5.2.

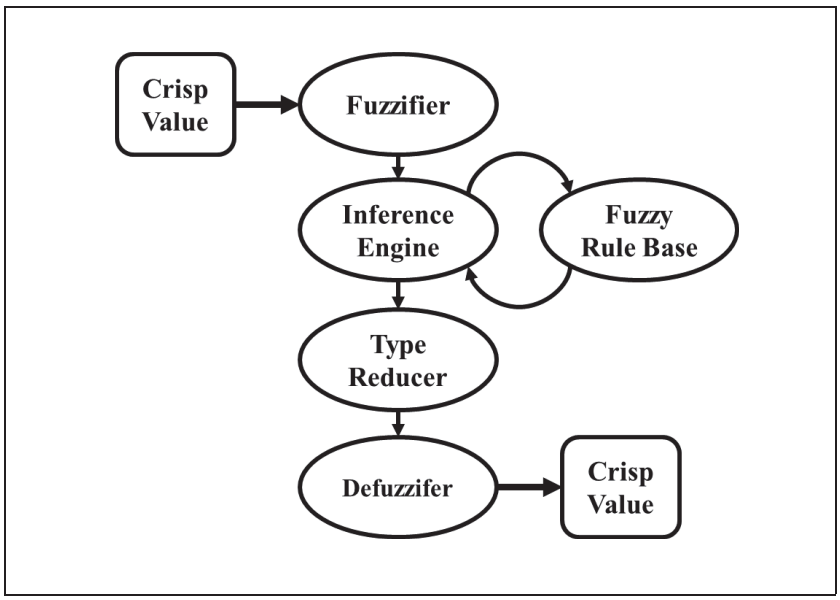

Figure 5.2 A simple Type-2 Fuzzy Logic System architecture

Initially, the inputs must be fuzzified by a membership function showing the membership degree of an input value to a fuzzy set. In this Type-Two Fuzzy Logic System, for each input

variable, such as the roll rate p and its reference signal p_{ref}, lower $\underline{\mu}$ and upper $\bar{\mu}$ membership functions were defined to compose a region called a "Footprint of Uncertainty (FOU)", as shown in cyan and red colours in Fig. 5.3. The definition of these membership functions improves the handling of uncertainties compared to the single membership function used in Type-One Fuzzy Logic Systems (Hagras & Wagner, 2012).

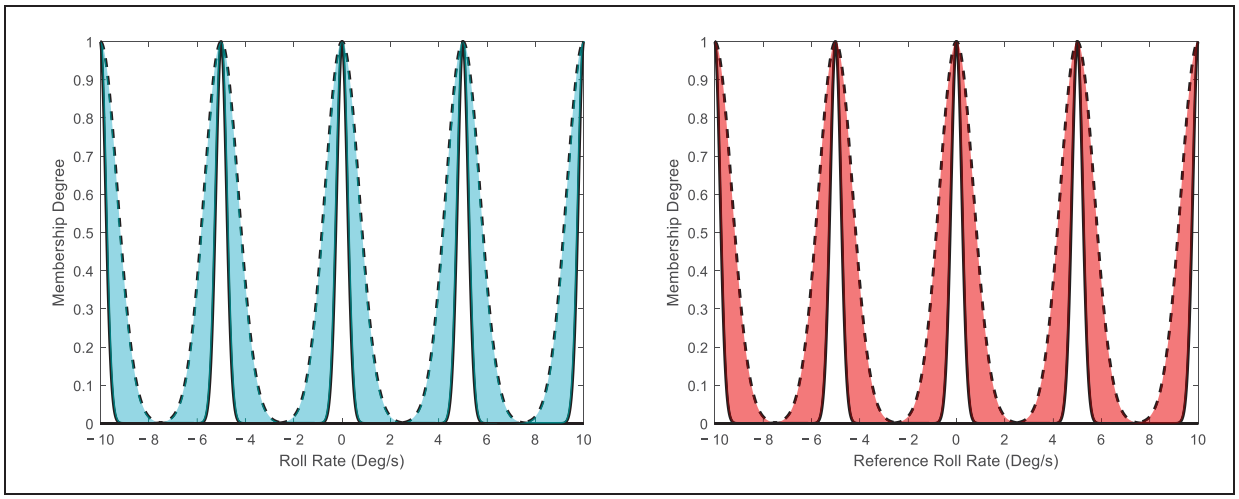

Figure 5.3 Upper (dashed line) and lower (solid line) membership functions and the FOU for the roll rate (in cyan) and its reference (in red)

In normal flight conditions, the roll rate varies between −1 and 1 degree per second. However, moderate-intensity turbulence can cause significant fluctuations, resulting in much higher roll rates. To handle this wide range of uncertainties and to ensure smoother maneuvers while maintaining passenger comfort and flight safety, the roll rate linguistic variables were defined between −10 and 10 degrees per second. This range was selected based on standard operational specifications of the CCX aircraft.

The membership functions shown in Fig. 5.3 were selected using five Gaussian membership functions formulated in Eq. (5.2). The parameters of these membership functions are presented in Table 5.1 with the linguistic terms for each constructed fuzzy set (constructed with upper and lower membership functions). The values of the a_n and b_n given in Table 5.1 were found on a trial-and-error basis.

$$\mu_i^n(x_i) = exp\ (-\frac{(x_i - a_n)^2}{2b_n^2}) \tag{5.2}$$

Table 5.1 Linguistic terms and parameter values of the membership functions

Linguistic Terms for p	Linguistic Terms for p_{ref}	Membership Functions	a_n	b_n
High Left Roll (HLR)	Critical Left Roll (CLR)	$\bar{\mu}^1$	−10	0.5
		$\underline{\mu}^1$	−10	0.05
Small Left Roll (SLR)	Moderate Left Roll (MLR)	$\bar{\mu}^2$	−5	0.5
		$\underline{\mu}^2$	−5	0.05
Balanced (B)	Stable (S)	$\bar{\mu}^3$	0	0.5
		$\underline{\mu}^3$	0	0.05
Small Right Roll (SRR)	Moderate Right Roll (MRR)	$\bar{\mu}^4$	5	0.5
		$\underline{\mu}^4$	5	0.05
High Right Roll (HRR)	Critical Right Roll (CRR)	$\bar{\mu}^5$	10	0.5
		$\underline{\mu}^5$	10	0.05

The relationship between the membership functions can be defined using the IF–THEN rules described in Eq. (5.3):

$$Rules^{(r)}\text{: If } x_1 \text{ is } \mu_1^n(x_1) \text{ and } x_2 \text{ is } \mu_2^n(x_2) \ldots \text{and} \ldots x_i \text{ is } \mu_i^n(x_i) \text{ then } \hat{h} \text{ is } Y^{(r)} \tag{5.3}$$

where $x = [x_1, x_2, \ldots, x_i]$ are the inputs of the T2FLS, $\mu_{1:i}^n$ are the membership functions defined for each input, $\hat{h}$ is the output of the T2FLS, and $Y^{(r)}$ is a singleton fuzzy set for the r^{th} rule. In this equation, i is the number of the inputs, r is the number of fuzzy rules, and n is the number of membership functions defined for each input variable (L.-X. Wang, 1994).

To approximate the aircraft dynamics for its lateral motion, two variables were selected as the inputs of the fuzzy logic system: the roll rate p and its reference signal p_{ref}. For each value of roll rate signal p and its reference signal p_{ref}, five Gaussian membership functions ($n = 5$), calculated with Eq. (5.2), were uniformly distributed between [−10,10] degrees (this

range was determined through a process of trial and error based on the obtained results). The fuzzy rules were defined in Table 5.2 using the linguistic terms explained in Table 5.1.

Table 5.2 Selected fuzzy rules using the linguistic variables of the roll rate p and the roll rate reference p_{ref}

	p: HLR	p: SLR	p: B	p: SRR	p: HRR
p_{ref}: CLR	$Y_{up,lo}^{(1)}$	$Y_{up,lo}^{(2)}$	$Y_{up,lo}^{(3)}$	$Y_{up,lo}^{(4)}$	$Y_{up,lo}^{(5)}$
p_{ref}: MLR	$Y_{up,lo}^{(6)}$	$Y_{up,lo}^{(7)}$	$Y_{up,lo}^{(8)}$	$Y_{up,lo}^{(9)}$	$Y_{up,lo}^{(10)}$
p_{ref}: S	$Y_{up,lo}^{(11)}$	$Y_{up,lo}^{(12)}$	$Y_{up,lo}^{(13)}$	$Y_{up,lo}^{(14)}$	$Y_{up,lo}^{(15)}$
p_{ref}: MRR	$Y_{up,lo}^{(16)}$	$Y_{up,lo}^{(17)}$	$Y_{up,lo}^{(18)}$	$Y_{up,lo}^{(19)}$	$Y_{up,lo}^{(20)}$
p_{ref}: CRR	$Y_{up,lo}^{(21)}$	$Y_{up,lo}^{(22)}$	$Y_{up,lo}^{(23)}$	$Y_{up,lo}^{(24)}$	$Y_{up,lo}^{(25)}$

The singleton fuzzy outputs denoted by $Y_{up,lo}^{(r=1:25)}$ in Table 5.2 create the adjustable parameters vectors shown by θ_{up} and θ_{lo} in Eq. (5.4). It should be noted that these vectors were initialized with random numbers between [0,1]. Therefore, the output of the T2FLS can be calculated as follows:

$$\hat{h}^{up} = \theta_{up}^{T}\Psi_{up}(x) \text{ ,and } \hat{h}^{lo} = \theta_{lo}^{T}\Psi_{lo}(x) \tag{5.4}$$

In Eq. (5.4), $\theta_{up} = \left[Y_{up}^{(1)}, \dots, Y_{up}^{(r)}\right]^{T}$ and $\theta_{lo} = \left[Y_{lo}^{(1)}, \dots, Y_{lo}^{(r)}\right]^{T}$ contain the singleton fuzzy outputs named as adjustable parameters which are updated during the simulation using the adaptation laws given in Eq. (5.12). In addition, $\Psi_{up}(x) = [\Psi_{up}^{1}, \dots, \Psi_{up}^{r}]^{T}$ and $\Psi_{lo}(x) = [\Psi_{lo}^{1}, \dots, \Psi_{lo}^{r}]^{T}$ are the Fuzzy Basis Functions calculated with Eq. (5.5). Having five membership functions for the roll rate p and five membership functions for the roll rate reference p_{ref}, and using the product inference engine, there will be 25 fuzzy rules, as $(\prod_{1}^{i}\mu_{p}^{n=1:5} \times \mu_{p_{ref}}^{n=1:5} \in R^{5\times5})$; therefore, $r = 25$.

$$\Psi_{up}(x) = \frac{(\prod_1^i \mu_{i,up}^n)}{\sum_1^r (\prod_1^i \mu_{i,up}^n)}$$
$$\Psi_{lo}(x) = \frac{(\prod_1^i \mu_{i,lo}^n)}{\sum_1^r (\prod_1^i \mu_{i,lo}^n)} \quad (5.5)$$

To obtain the output of the T2FLS, the Nagar–Bardini (NB) algorithm was selected, as it combined the operations of the type reduction with the Defuzzifier components (Chen, 2019 ; El-Nagar & El-Bardini, 2014). Thus, the output can be calculated as follows Eq. (5.6). In this fuzzy logic system, at each time, there is at least one active fuzzy rule during simulation, as shown above in Eq. (5.4) (L.-X. Wang, 1994).

$$\hat{h}(x,\theta) = \frac{(\hat{h}^{up} + \hat{h}^{lo})}{2} = \theta^T \Psi(x) \quad (5.6)$$

The approximated function $\hat{h}(x,\theta)$ obtained in Eq. (6) will be used in the developed Adaptive Type-Two Fuzzy Super-Twisting Sliding-Mode Control System, which is explained in Section 5.2.2.2.

5.2.2.2. Adaptive Type-Two Fuzzy Super-Twisting Sliding Mode Control System

Based on the contributions explained before in Section 5.1, we selected the sliding-mode control (SMC) system as a nonlinear control methodology to meet the robustness criteria and lead the aircraft dynamics to reach its equilibrium. Super-twisting sliding-mode control is an improved version of the conventional SMC that can compensate for the turbulence and may more effectively improve control system robustness. The sliding surface S_l can be defined as a function of the tracking error, and its first-time derivative is expressed as follows (Fei & Feng, 2019):

$$e_p = p - p_{ref} \quad (5.7)$$
$$S_l = C e_p + \dot{e}_p \quad (5.8)$$

Where $C > 0$ is a design parameter.

Taking the first-time derivative of the sliding surface in Eq. (5.8), and then replacing $\ddot{p} = h(x) + u + d(t)$, written based on Eq. (5.1) with $x = p$ as the selected state variable and $n = 2$ as the time-derivative order, yields the following:

$$\dot{S}_l = C\dot{e}_p + \ddot{e}_p = C\dot{e}_p + \ddot{p} - \ddot{p}_{ref} = C\dot{e}_p + h(x) + u - \ddot{p}_{ref} + d(t) \tag{5.9}$$

By setting $\dot{S}_l = 0$ in Eq. (5.9), the equivalent control law u_{eq} can be formulated as shown in Eq. (5.10). In this equation, the unknown function $h(x)$ was replaced with its approximation $\hat{h}(x.\theta)$, calculated by the T2AFLS in Eq. (5.6).

$$u_{eq} = -C\dot{e}_p - h(x) + \ddot{p}_{ref} + d(t) = -C\dot{e}_p - \hat{h}(x,\theta) + \ddot{p}_{ref} + d(t) \tag{5.10}$$

The switching control term u_{sw} in Eq. (5.11a) was selected as proposed in (Shtessel et al., 2012), where $h(x)$ is an unknown function. Therefore, the aileron control law can be written as given in Eq. (5.11b):

$$u_{sw} = -L_1\sqrt{|S_l|}sat(S_l) - \int \frac{L_2}{2} sat(S_l)d\tau \tag{5.11a}$$

$$u = u_{ail} = u_{eq} + u_{sw} \tag{5.11b}$$

Where $sat(.)$ denotes the saturation function. In contrast with the control input presented in (LEVANT, 1993) that used $sign(.)$, in Eq. (5.11a), we opted to use the saturation function because of its potential to reduce chattering.

In Eq. (5.11a), L_1 and L_2 are two positive constants whose values were determined using two different approaches. Initially, we employed an adaptive control methodology to continuously adjust its parameters during the simulation. In this approach, the two parameters were increased until the aircraft state variables reached the sliding surface, and then they decreased over time (Shtessel et al., 2012). The second approach is to employ the Particle

Swarm Optimization (PSO) algorithm to find optimal values for L_1 and L_2, as well as C in Equations (5.10) and (5.11a).

In the equivalent control law u_{eq} proposed in Eq. (5.10), the term $h(x)$ is unknown, while $d(t)$ is not measurable in practice. Therefore, the unknown function ($h(x)$) can be replaced with the approximated function as in Eq. (5.6) with the expression $\hat{h} = \theta^T \Psi(x)$. As described earlier, $\theta^T = [\theta_{lo}^T, \theta_{up}^T]$ can be computed using the adaptation law in Eq. (5.12):

$$\begin{aligned} \dot{\theta}_{up} &= \frac{1}{2} S_l N_{up} \Psi_{up} \\ \dot{\theta}_{lo} &= \frac{1}{2} S_l N_{lo} \Psi_{lo} \end{aligned} \tag{5.12}$$

where $N_{up} = 0.0001$ and $\mathrm{N}_{lo} = 0.0001$.

To ensure the stability and the boundedness of the proposed control law, the Lyapunov theorem was used, as explained below:

Proof of Stability. As follows, a comprehensive proof of the stability and boundedness of this control system is presented using the well-known Lyapunov theorem. We propose a Lyapunov candidate V_t as a combination of two terms denoted by V_{fuzzy} for the Type-Two Adaptive Fuzzy Sliding-Mode Control (L.-X. Wang, 1997) and V_{sw} for the super-twisting switching control (Shtessel et al., 2012). Therefore, the Lyapunov candidate V_t can be written as follows:

$$V_t = V_{fuzzy} + V_{sw} \tag{5.13}$$

where

$$V_{fuzzy} = \frac{1}{2} {S_l}^2 + \frac{1}{2\mathrm{N}_{lo}} \varphi_{lo}^T \varphi_{lo} + \frac{1}{2\mathrm{N}_{up}} \varphi_{up}^T \varphi_{up} \tag{5.14}$$

In Eq. (5.14), $\mathrm{N}_{lo}.\mathrm{N}_{up} > 0$ are two positive constants. Moreover, to prove the stability of the presented supertwisting control law, using the Lyapunov candidate denoted by V_{sw} in Eq. (5.15), it was suggested in (Shtessel et al., 2012) to use new state vectors $T = [T_1 \quad T_2]^T$ as expressed later in Eq. (5.25).

As demonstrated in (Shtessel et al., 2012), if $\lambda > 0$, the matrix $P = \begin{bmatrix} \lambda + 4\xi^2 & -2\xi \\ -2\xi & 1 \end{bmatrix}$ will be positive definite. On the other hand, Λ_1 and Λ_2 are also two positive constants. Thus, the Lyapunov candidate for the switching control law will be (Shtessel et al., 2012) :

$$V_{sw}(T_1, T_2, L_1, L_2) = V_0(T) + \frac{1}{2\Lambda_1}(L_1 - {L_1}^*)^2 + \frac{1}{2\Lambda_2}(L_2 - {L_2}^*)^2$$
$$V_0(T) = (\lambda + 4\xi^2){T_1}^2 + {T_2}^2 - 4\xi T_1 T_2 = T^T P T \tag{5.15}$$

where ξ is a real number, and ${L_1}^*$ and ${L_2}^*$ are two positive constants. In the developed control law given in Eq. (5.10), we know that $h(x)$ is unknown, and it was approximated by $\hat{h} = \theta^T \Psi(x)$. For each of the elements in the vector of the adjustable parameter θ, there is an optimal value, which can be defined as follows:

$$\theta^* = \arg\min_{x \in \mathbb{R}^n} \left[sup \left| \hat{h}(x, \theta^*) - h(x) \right| \right] \tag{5.16}$$

According to (Slotine & Li, 1991 ; C.-H. Wang et al., 2002 ; L.-X. Wang, 1997), the unknown functions $h(x)$ and $d(t)$ are assumed to be bound to positive constants, such as X_h and F_d, respectively, ($|h(x)| \leq X_h$ and $|d(t)| \leq F_d$). As presented in (C.-H. Wang et al., 2002), for the adjustable parameterθ, there will be $U = \{\theta \in R^n : \|\theta\| \leq F_h\}$, which means that θ is bound to a finite positive constant, such as F_h. In Eq. (5.16), θ^* is not a real parameter; it is only used to demonstrate the Lyapunov proof. Using the minimum approximation error given by $\epsilon = h(x) - \hat{h}(x, \theta^*)$ (Yoo & Ham, 1998b), and the triangular inequality, we obtain (Roopaei et al., 2009)

$$|\epsilon| \leq \left| h(x) - \hat{h}(x.\theta^*) \right| \leq |h(x)| + \left| \hat{h}(x.\theta^*) \right| \leq |h(x)| + \|\theta^*\| \|\Psi(x)\| \leq X_h + F_h \leq \tau$$
$$|\epsilon| \leq \tau \tag{5.17}$$

The time derivative of the sliding surface was calculated in Eq. (5.9). Therefore, it can be rewritten such that

$$\begin{aligned}\dot{S}_l &= h(x) - \hat{h}(x,\theta^*) + \hat{h}(x,\theta^*) + u - \ddot{p}_{ref} + C\dot{e}_p + d(t)\\ &= \epsilon + \hat{h}(x,\theta^*) + u - \ddot{p}_{ref} + C\dot{e}_p + d(t)\\ &= \epsilon + \hat{h}(x,\theta^*) + \hat{h}(x,\theta) - \hat{h}(x,\theta) + u - \ddot{p}_{ref} + C\dot{e}_p + d(t)\end{aligned} \tag{5.18}$$

Furthermore, it can be assumed that $\varphi = \theta - \theta^*$ and then $\dot{\varphi} = \dot{\theta}$, so that $\varphi^T\Psi(x) = \hat{h}(x,\theta) - \hat{h}(x,\theta^*)$ from (Labiod et al., 2005). By substituting $\hat{h}(x,\theta^*) = \hat{h}(x,\theta) - \varphi^T\Psi(x)$ and $u = u_{eq} + u_{sw} = -C\dot{e}_p - \hat{h}(x.\theta) + \ddot{p}_{ref} + u_{sw}$ in Eq. (5.18) (in Eq. (5.10) $h(x)$ and $d(t)$ are unknown, so $h(x)$ was then replaced with its approximation denoted by $\hat{h}(x,\theta)$ in the expression of the equivalent control law (u_{eq})), the following relationship can be obtained:

$$\dot{S}_l(t) = \epsilon - \varphi^T\Psi(x) + d(t) + u_{sw} \tag{5.19}$$

Proving the stability and boundedness of the system requires calculation of the time derivative of the Lyapunov candidate denoted by V_{fuzzy} in Eq. (5.14) and V_{sw} in Eq. (5.15). It must be noted that to explain the demonstrations more clearly for $\dot{V}_{fuzzy}$, we considered that $\dot{S}_l(t) = \epsilon - \varphi^T\Psi(x) + d(t)$ in Eq. (5.20) and the stability of the u_{sw} will be separately proved by the related Lyapunov candidate V_{sw} later in this section using Eq. (5.15):

$$\begin{aligned}\dot{V}_{fuzzy} &= S_l\dot{S}_l + \tfrac{1}{\mathrm{N}_{lo}}\varphi_{lo}^T\dot{\varphi}_{lo} + \tfrac{1}{\mathrm{N}_{up}}\varphi_{up}^T\dot{\varphi}_{up} = S_l\epsilon - S_l\varphi^T\Psi(x) + S_l d(t) +\\ &\tfrac{1}{\mathrm{N}_{lo}}\varphi_{lo}^T\dot{\varphi}_{lo} + \tfrac{1}{\mathrm{N}_{up}}\varphi_{up}^T\dot{\varphi}_{up} = S_l\epsilon - \tfrac{1}{2}S_l\varphi_{up}^T\Psi_{up} - \tfrac{1}{2}S_l\varphi_{lo}^T\Psi_{lo} + S_l d(t) +\\ &\tfrac{1}{\mathrm{N}_{lo}}\varphi_{lo}^T\dot{\varphi}_{lo} + \tfrac{1}{\mathrm{N}_{up}}\varphi_{up}^T\dot{\varphi}_{up} = S_l\epsilon + S_l d(t) + \tfrac{1}{\mathrm{N}_{lo}}\varphi_{lo}^T\left[\dot{\varphi}_{lo} - \tfrac{1}{2}S_l\mathrm{N}_{lo}\Psi_{lo}\right] +\\ &\tfrac{1}{\mathrm{N}_{up}}\varphi_{up}^T\left[\dot{\varphi}_{up} - \tfrac{1}{2}S_l\mathrm{N}_{up}\Psi_{up}\right]\end{aligned} \tag{5.20}$$

Since $\dot{\varphi} = \dot{\theta}$, we can adopt the adaptation laws designed for θ_{up} and θ_{lo} in Eq. (5.12) into the final expression of $\dot{V}_{fuzzy}$ in Eq. (5.20). Moreover, as indicated in Eq. (5.17), $|\epsilon| \leq \tau$, and the turbulence was assumed to be bound such that $|d(t)| \leq F_d$. Therefore, Eq. (5.20) can be reformulated as follows:

$$\dot{V}_{fuzzy} = S_l\epsilon + S_l d(t) \leq |S_l||\epsilon| + |S_l||d(t)| \leq \tau|S_l| + F_d|S_l| \tag{5.21}$$

The expression $\dot{V}_{fuzzy}$ in Eq. (5.21) was calculated based on the selected Lyapunov candidate for the equivalent control law in the designed Type-Two Adaptive Fuzzy Sliding-Mode System denoted by V_{fuzzy} in Eq. (5.13) ($V_t = V_{fuzzy} + V_{sw}$). In addition, to verify the stability of the proposed control methodology, the stability of the switching control term must also be proved by the related Lyapunov candidate introduced by the term $V_{sw}(T_1, T_2, L_1, L_2)$ in Eq. (5.15) (LEVANT, 1993 ; Shtessel et al., 2012). In the super-twisting adaptive sliding-mode control system, it must be considered that $(S_l, \dot{S}_l) \to 0$ in a specific time limit in the presence of bounded perturbation. Within this consideration, The finite-time convergence and stability of the adaptive switching control law u_{sw} were discussed in detail in (Shtessel et al., 2012 ; Yan et al., 2019). According to (Shtessel et al., 2012 ; Yan et al., 2019), it was explained that $\dot{S}_l = \frac{\partial S_l}{\partial t} + \frac{\partial S_l}{\partial x}h(x) + \frac{\partial S_l}{\partial x}g(x)u = L_1(x.t) + n(x.t)u$ with the following expressions for the $L_1(x,t)$ and $n(x,t)$:

$$L_1(x.t) = \frac{\partial S_l}{\partial t} + \frac{\partial S_l}{\partial x}h(x) = m_1(x.t) + m_2(x.t) \tag{5.22a}$$

where

$$|m_1(x.t)| \leq |S_l|^{\frac{1}{2}}\delta_1$$
$$|\dot{m}_2(x.t)| \leq \delta_2$$
$$n(x.t) = \frac{\partial S_l}{\partial x}g(x) = n_0(x.t) + \Delta n(x.t) \tag{5.22b}$$

where δ_1 and δ_2 are arbitrary positive finite boundaries and $n(x.t) \in \mathbb{R}$ is an uncertain function. As proposed in (LEVANT, 1993 ; Shtessel et al., 2012), it was assumed that $n_1(x,t) = 1 + \frac{\Delta n(x.t)}{n_0(x.t)}$ using the expression given for $n(x,t)$ in Eq. (5.22b), where $n_0(x,t)$ is positive function and $\Delta n(x,t)$ shows a bounded perturbation with unknown boundaries

(Shtessel et al., 2012 ; Yan et al., 2019). With these expressions, and considering $Z = n_0(x.t)u$, $\dot{S}_l$ becomes (Shtessel et al., 2012 ; Yan et al., 2019)

$$\dot{S}_l = L_1(x.t) + n_1(x.t)Z \tag{5.23}$$

Now, it is possible to rearrange u_{sw} in Eq. (5.11a) as follows (LEVANT, 1993):

$$\begin{aligned} Z &= -L_1\sqrt{|S_l|}sat(S_l) + o \\ \dot{o} &= -\frac{L_2}{2}sat(S_l) \end{aligned} \tag{5.24}$$

where L_1 and L_2 are the adaptive gains of switching control law. For the proof of stability, we should define new state vectors, as shown below regarding the methodology presented in (Shtessel et al., 2012):

$$T = \begin{bmatrix} T_1 \\ T_2 \end{bmatrix} = \begin{bmatrix} |S_l|^{\frac{1}{2}}sat(S_l) \\ \mathrm{Z}^* \end{bmatrix} \tag{5.25}$$

$$\dot{Z}^* = -\frac{L_2}{2}n_1(x,t)sat(S_l) + \dot{m}_2(x,t) + \dot{n}_1(x,t)o$$

Calculating the time derivative of Eq. (5.25), we can write the following:

$$\dot{T} = \begin{bmatrix} \dot{T}_1 \\ \dot{T}_2 \end{bmatrix} = \frac{1}{2|T_1|}\begin{bmatrix} -L_1n_1 & 1 \\ L_2n_1 & 0 \end{bmatrix}\begin{bmatrix} T_1 \\ T_2 \end{bmatrix} + \frac{1}{2|T_1|}\begin{bmatrix} 1 & 0 \\ 0 & 2|T_1| \end{bmatrix}\begin{bmatrix} m_1(x,t) \\ \dot{\mathcal{B}}(x,t) \end{bmatrix} \tag{5.26}$$

In Eq. (5.22a), we stated that $|m_1(x,t)| \leq |S_l|^{\frac{1}{2}}\delta_1$ and $|\dot{m}_2(x,t)| \leq \delta_2$; as stated earlier, δ_1 and δ_2 are positive finite boundaries. In addition, it was assumed in (Shtessel et al., 2012) that $\left|\dot{\mathcal{B}}(x.t)\right| \leq \delta_4$. Therefore, $L_1(x,t) = \sigma_1(x,t)|S_l|^{\frac{1}{2}}sat(S_l) = \sigma_1(x,t)T_1$, and $\dot{\mathcal{B}}(x.t) = \dot{m}_2(x,t) + \dot{n}_1(x,t)o$. Accordingly, Eq. (5.26) can be reformulated as follows (Shtessel et al., 2012):

$$\begin{bmatrix}\dot{T}_1\\ \dot{T}_2\end{bmatrix}=\frac{1}{2|T_1|}\begin{bmatrix}-(L_1n_1-\kappa_1(x,t)) & 1\\ -(L_2n_1-\kappa_2(x,t)) & 0\end{bmatrix}\begin{bmatrix}T_1\\ T_2\end{bmatrix}$$
$$\kappa_1(x,t)=\frac{m_1}{T_1}\ \text{as}\ \ 0<\kappa_1<\delta_1 \tag{5.27}$$
$$\kappa_2(x,t)=\frac{2\dot{B}(x.t)}{|T_1|}T_1\ \ \text{as}\ \ 0<\kappa_2<2\delta_4$$

where δ_4 are unknown bounds (LEVANT, 1993 ; Shtessel et al., 2012). Then, the time derivatives of V_0 and V_{sw} given in Eq. (5.15) become (Shtessel et al., 2012)

$$\dot{V}_0(T)=\dot{T}^TPT+T^TP\dot{T}\le-\frac{1}{T_1}T^TQT \tag{5.28a}$$

$$\dot{V}_{sw}(T_1\ T_2\ L_1\ L_2)=\dot{T}^TPT+T^TP\dot{T}+\frac{1}{\Lambda_1}\xi_{L_1}\dot{L}_1+\frac{1}{\Lambda_2}\xi_{L_2}\dot{L}_2\le-\frac{1}{T_1}T^TQT+\frac{1}{\Lambda_1}\xi_{L_1}\dot{L}_1+\frac{1}{\Lambda_2}\xi_{L_2}\dot{L}_2 \tag{5.28b}$$

Where $Q=\begin{bmatrix}Q_{11} & Q_{12}\\ Q_{21} & 4\xi\end{bmatrix}$, as $Q_{11}=2\lambda L_1n_1+4\xi n_1(2\xi L_1-L_2)-2(\lambda+4\xi^2)\kappa_1+4\xi\kappa_2$, $Q_{12}=Q_{21}=(L_2n_1-2\xi L_1n_1-\lambda-4\xi^2)$, and $\lambda,\xi>0$. Thus, in (Shtessel et al., 2012), it was concluded that $\dot{V}_{sw}$ becomes

$$\dot{V}_{sw}(T_1,T_2,L_1,L_2)\le-DV_0^{\frac{1}{2}}+\frac{1}{\Lambda_1}\xi_{L_1}\dot{L}_1+\frac{1}{\Lambda_2}\xi_{L_2}\dot{L}_2=-DV_0^{\frac{1}{2}}+\frac{1}{\Lambda_1}\xi_{L_1}\dot{L}_1+\frac{1}{\Lambda_2}\xi_{L_2}\dot{L}_2-\frac{r_1}{\sqrt{2\Lambda_1}}|\xi_{L_1}|-\frac{r_2}{\sqrt{2\Lambda_2}}|\xi_{L_2}|+\frac{r_1}{\sqrt{2\Lambda_1}}|\xi_{L_1}|+\frac{r_2}{\sqrt{2\Lambda_2}}|\xi_{L_2}|\le -\chi\sqrt{V_{sw}(T_1,T_2,L_1,L_2)}+\eta \tag{5.29}$$

where

$$\chi=\min(D,r_1,r_2)$$
$$\eta=-|\xi_{L_1}|\left(\frac{1}{\Lambda_1}\dot{L}_1-\frac{r_1}{\sqrt{2\Lambda_1}}\right)-|\xi_{L_2}|\left(\frac{1}{\Lambda_2}\dot{L}_2-\frac{r_2}{\sqrt{2\Lambda_2}}\right)$$

where $D=\frac{\xi\lambda_{min}^{\frac{1}{2}}(P)}{\lambda_{max}(P)}$, and $r_1,r_2>0$. In (Shtessel et al., 2012), it was suggested to use the following adaptation laws to update the gains of the switching control law, as shown in Eq. (5.30), as follows:

$$\dot{L}_1 = \begin{cases} r_1\sqrt{\frac{\Lambda_1}{2}}\,sat(|S_l| - H) & \text{if } L_1 > L_m \\ N & \text{if } L_1 \le L_m \end{cases} \qquad (5.30)$$

$$L_2 = 2\xi L_1$$

For the stability proof and to achieve the finite time convergence, it was explained in (Shtessel et al., 2012) that for obtaining $\eta = 0$ in Eq. (5.29), $\dot{L}_1 = r_1\sqrt{\frac{\Lambda_1}{2}}$. Moreover, in Eq. (5.30), it was shown that $L_2 = 2\xi L_1$; therefore, by differentiating L_2 and choosing $\xi = \frac{r_2}{2r_1}\sqrt{\frac{\Lambda_2}{\Lambda_1}}$, it yields:

$$\dot{L}_2 = 2\xi\dot{L}_1 = 2\left(\frac{r_2}{2r_1}\sqrt{\frac{\Lambda_2}{\Lambda_1}}\right)\left(r_1\sqrt{\frac{\Lambda_1}{2}}\right) = r_2\sqrt{\frac{\Lambda_2}{2}} \qquad (5.31)$$

Having Eq. (5.31) for $\dot{L}_2$, and with $\dot{L}_1 = r_1\sqrt{\frac{\Lambda_1}{2}}$, then η in Eq. (5.29) becomes zero and $\dot{V}_{sw}(T_1.T_2.L_1.L_2) \le -\chi\sqrt{V_{sw}(T_1.T_2.L_1.L_2)}$, proving that the sliding surface S_l and its derivative $\dot{S}_l$ converge to zero in finite time.

In addition, as shown in the expression of $\dot{L}_1$ in Eq. (5.30), there is a term $sat(|S_l| - H)$ that acts as a detector. This term ensures that when $|S_l|$ exceeds the threshold H, the gains L_1 and L_2 dynamically increase to correct the system trajectory (Shtessel et al., 2012). Conversely, if $|S_l|$ remains below the threshold H, then L_1 and L_2 start decreasing. This technique also helps reduce the chattering phenomena. In Eq. (5.30), N was used to prevent L_1 from becoming zero. More details regarding the stability proof and finite time convergence for the adaptation laws introduced in Eq. (5.30) are discussed in (Shtessel et al., 2012 ; Yan et al., 2019).

Consequently, in (Shtessel et al., 2012), it was proven that the following adaptation laws are bound and that the aircraft dynamics are driven to the sliding surface in a finite time $t \le \frac{2\sqrt{V_{sw}(t_0)}}{\chi}$. Hence, using the proposed Lyapunov candidate $V_t = V_{fuzzy} + V_{sw}$ and its expression given in Equations (5.21) and (5.29), the following equation can be obtained:

$$\dot{V}_t \leq \tau|S_l| + F_d|S_l| - \chi\sqrt{V_{sw}(T_1, T_2, L_1, L_2)} + \eta \leq -\chi\sqrt{V_{sw}(T_1, T_2, L_1, L_2)} + \eta_T$$
$$\eta_T = (\tau + F_d)|S_l| + \eta \tag{5.32}$$

Therefore, it can be concluded that using the final control law shown in Eq. (5.33), S_l approaches zero in finite time, which means that the aircraft is stable, and the error tends to zero while remaining bound within a certain region around the equilibrium.

With this respect, using the control laws expressed in Equations (5.10) and (5.11a) and its adaptive gains L_1 and L_2 calculated by Eq. (5.30), the final form of the aileron control law u_{ail} becomes

$$u_{ail} = -C\dot{e}_p - \hat{h}(x, \theta) + \ddot{p}_{ref} - L_1\sqrt{|S_l|}sat(S_l) - \int \frac{L_2}{2} sat(S_l)d\tau \tag{5.33}$$

However, as another approach, we also used the PSO algorithm instead of these adaptation laws to find the optimum values of L_1, L_2, and C in Eq. (5.33), as explained in Section 5.2.2.3.

□

5.2.2.3. A Particle Swarm Optimization (PSO) Algorithm

Here, we explain our application of a PSO optimization algorithm to find the design parameters used in the proposed control system.

a. Description of the PSO Algorithm

Particle Swarm Optimization (PSO) is a computational method that iteratively finds an optimal solution that minimizes or maximizes a given cost function. The algorithm mimics the behaviour of a set of particles moving in a swarm, each representing a potential solution. In this context, the particles move through a search space to find the optimal solution, using their individual and global experiences. In addition, each particle shares several attributes with the other particles, such as position and velocity, which are updated at each iteration.

This strategy enables progressive and efficient convergence toward the optimal solution (Gad, 2022).

The principle of the PSO algorithm can be described with Eq (5.34); in this algorithm, each particle searches for the best solution using its personal best P_{b_r} and the global best G_b (Gad, 2022) solutions:

$$\begin{aligned} {P_{b_j}}^q &= y_j^* \big| O\left(y_j^*\right) = \min_{\substack{s=1:q \\ J=1:j}} \left\{O\left(y_j^q\right)\right\} \\ {G_b}^q &= y_*^q \big| O(y_*^q) = \min_{\substack{s=1:q \\ J=1:j}} \left\{O\left(y_j^q\right)\right\} \end{aligned} \tag{5.34}$$

where $J = 1{:}\,j$ is the total number of swarm population; $s = 1{:}\,q$ is the undergoing iteration; O is the objective or cost function, which must be minimized; and y is a vector of possible solutions (positions).

Based on the definition of the personal best ${P_{b_j}}^q$ and the global best ${G_b}^q$ in Eq. (5.34), the velocity V_j and position y_j of a given particle j can be updated by applying the following rules (Gad, 2022 ; Shi & Eberhart, 1998):

$$V_j^{q+1} = w_{damp} \times V_j^q + c_1 \times r_1 \times (P_{b_j} - y_j^q) + c_2 \times r_2 \times \left(G_b - y_j^q\right) \tag{5.35a}$$

$$y_j^{q+1} = y_j^q + V_j^{q+1} \tag{5.35b}$$

Where $\left\{V_j^{q+1}.\, y_j^{q+1}\right\}$ are the new velocity and position of the particle, respectively; w_{damp} is the damping inertia; c_1 and c_2 are learning coefficients (known as acceleration coefficients); and r_1 and r_2 are random numbers between 0 and 1. The PSO algorithm is presented in Algorithm 5.1 (Gad, 2022).

Algorithm 5.1. General Particle Swarm Optimization (PSO) Algorithm.

INPUTS:
- Number of iterations (s)
- Number of particles (J)
- Lower bound for the position of the particles (y_{lo})
- Upper bound the position of the particles (y_{up})
- Damping Inertia (w_{damp})
- Personal Acceleration (c_1)
- Social Acceleration (c_2)

OUTPUT:
- Best Solution Result (G_b)

START:
1. Initialize the swarm
2. For $J = 1 \rightarrow j$
3. Initialize the position of each particle randomly (from y_{lo} to y_{up})
4. Initialize the velocity of particle:
   $V_{up} = k_s \times (y_{up} - y_{lo})$; where, $k_s = 0.2$ as the Scaling factor
   $V_{lo} = -V_{up;}$
5. Initial personal best
6. End
7. For $s = 1 \rightarrow q$
8. For J = 1→j
9. $V_J^{q+1} \leftarrow$ Apply Eq. (5.35a)
10. $y_J^{q+1} \leftarrow$ Apply Eq. (5.35b)
11. If $O(y_q^J) < O\left(P_{b_J}{}^{q-1}\right)$
12. $O\left(P_{b_J}{}^{q}\right) \leftarrow O(y_q^J)$
13. End if
14. If $O\left(P_{b_J}{}^{q}\right) < O(G_b)$
15. $O(G_b) \leftarrow O\left(P_{b_J}{}^{q}\right)$
16. End if
17. End for
18. Save G_b as global best solution.
19. End for

END

b. Definition of the Cost Function

In the PSO, the cost function plays an essential role as the objective function that the algorithm tries to optimize. Each PSO particle navigates the search space, recording its

personal experience with the aim of minimizing or maximizing the given cost function, depending on the specific problem to be solved. For the PSO algorithm designed in this article, a particular cost function has been selected to find the optimal values of the parameters of the control system (C in Eq. (5.10) and L_1 and L_2 in Eq. (5.11a)) proposed in Section 5.2.2.2. This cost function is given in the following equation:

$$O\left(y_j^q\right) = 0{,}5 \times \sum_{0}^{\tau} \left(e_p\right)^2 \tag{5.36}$$

where $e_p = p - p_{ref}$.

5.2.2.4. Integral Controller as a Yaw Rate Stabilizer

The interaction between the yaw and roll motions in an aircraft is a crucial aspect that influences the stability and maneuverability of an aircraft. This article highlights the coupling effects between roll and yaw dynamics. The yaw rate variations directly affect the roll rate. Despite the controllers being distinct and decoupled, the aircraft dynamics remain coupled due to aerodynamic interactions between roll and yaw rate dynamics. To minimize the effect of the variations of the yaw rate, we began by using a proportional–integral–derivative (PID) control technique, which has not provided a satisfactory result for the scope of this research. We determined that the integral (I) controller could perform better than the others at this task. Therefore, we focused on using the sideslip angle and its reference signal to indirectly stabilize the yaw rate signal. Specifically, the control input signal u_{rud} given in Equation (5.38) for the rudder of the Cessna Citation X aircraft (which is controlled with an electrical actuator) was generated based on the error shown in Eq. (5.37) between the actual sideslip angle β and a reference value β_{ref} (e.g., equal to zero):

$$e_\beta = \beta_{actual} - \beta_{ref} \tag{5.37}$$

$$u_{rud} = k_i \int e_\beta \, dt \tag{5.38}$$

where $k_i = -0.0002$ is a constant gain; this small gain was selected since large gain values led to instability in the aircraft.

This section presented a detailed explanation of the applied methodologies, whose block diagram is shown in Fig. 5.4. The simulation results obtained with this methodology are discussed for the Adaptive Type-Two Fuzzy Super-Twisting Sliding-Mode Control System using both PSO-based and adaptive switching control terms in the next section.

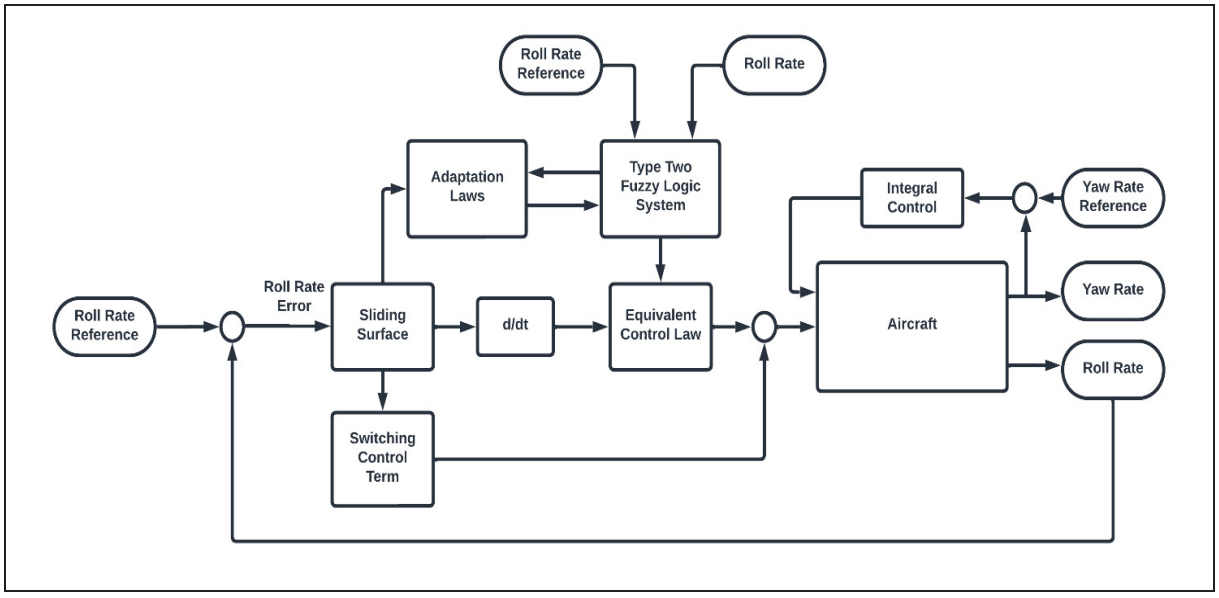

Figure 5.4 Simplified scheme of the designed control methodologies

5.3 Results

To evaluate the performance of the proposed control system, the nonlinear model of the Cessna Citation X business jet presented in Section 5.2.1 was used. For this purpose, a total of 925 different flight conditions were selected by varying aircraft weight (lbs), center of gravity position (%) of the chord, altitude (ft), and calibrated airspeed (kts), as shown in Table 5.3. These 925 flight conditions were selected to cover the entire flight envelope of the Cessna Citation X aircraft.

Table 5.3 Parameter values to generate 925 flight conditions

Altitudes (ft)	CAS (kts)	Weight (lbs)	Center of Gravity (%)
8000	150	26,000	24
10,000	200	27,000	26
15,000	230	28,000	28
20,000	250	29,000	30
25,000	300	30,000	32
30,000	330		
35,000			
40,000			
45,000			

In the first step, as they are the inputs of the fuzzy system, the roll rate and roll rate reference signals must be fuzzified by the membership function given in Equation (5.3), whose parameters are defined in Table 5.3 (these values were found on a trial-and-error basis with respect to the tracking performance of the controller). For each variable, five membership functions were distributed uniformly over the interval of [−10,10] degrees for both upper and lower membership functions for each variable, p and p_{ref}, as shown in Table 5.1.

We decided to follow two different approaches to select the best parameter values used in the sliding-mode switching control term (1) by using the adaptation laws in Equation (30) to find L_1 and L_2 (the optimal values for the other parameters were chosen by the designer, taking into account the tracking performance) and (2) by using the PSO algorithm described in Section 5.2.2.3 to find C, L_1, and L_2 in Equation (5.33), returning the values presented in Table 5.4. To find the best values for each of these parameters, we tried different numbers of iterations and population sizes, and it revealed that increasing the number of iterations did not change the results significantly; therefore, the PSO algorithm was designed using the parameters given in Table 5.4 for both ideal and turbulent flight conditions.

Table 5.4 Particle Swarm Optimization configuration

Parameters	Values
Acceleration coefficient (c_1)	2
Acceleration coefficient (c_2)	2
Inertia damping coefficient(w_{damp})	0,9
Size of the swarm (population) (N)	500
Total number of iterations (s)	2
Lowest decision variables bound (y_{lo})	0,1
Highest decision variables bound (y_{up})	500

It should be noted that the bounds y_{lo} and y_{up} were selected to optimize all three parameters, C, L_1, and L_2, at the same time. Accordingly, the design parameter values are presented in Table 5.5 for the T2AFSTSMC with both methodologies, the adaptation laws and the PSO algorithm, as follows. The PSO algorithm was used to determine the values of C, L_1, and L_2 in an offline process, and they remained fixed during the simulation across all flight conditions

Table 5.5 Parameters of the control system design

T2AFSTSMC with Adaptive Switching Term		T2AFSTSMC with PSO-Based Switching Term	
Parameters	Value	Parameters	Value
C	599.82	C	15
r_1	30.38	L_1	200
Λ_1	350.82	L_2	190
H	685.29		
N	198.29		
ξ	1		
L_m	0.01		

The parameter values of the control system design are given in Table 5.5. Based on the simulation results for 925 flight conditions, the suggested controller could perform adequately in ideal and turbulent conditions. In addition to the signal analysis provided for the obtained results in this section, a more detailed evaluation will be presented next using two tracking error metrics: the Mean Absolute Error (MAE) in Equation (5.39) and the Max Absolute Error, which is calculated for each flight condition to understand better the performance achieved by each control system. These assessments will be presented later in this section.

$$MAE = \frac{1}{2n}\sum|e_p| \tag{5.39}$$

As shown in Fig. 5.5, the controller with both types of switching terms could meet the tracking performance, as the roll rate could follow the reference signal. However, the T2AFSTSMC, equipped with an adaptive switching term, could perform slightly better than the PSO-based T2AFSTSMC in tracking the roll rate reference signal. This better performance of the adaptive switching term was achieved because the adaptation laws were able to stabilize the aircraft more effectively by updating the gain values during the simulation rather than by using the fixed parameters found by the PSO.

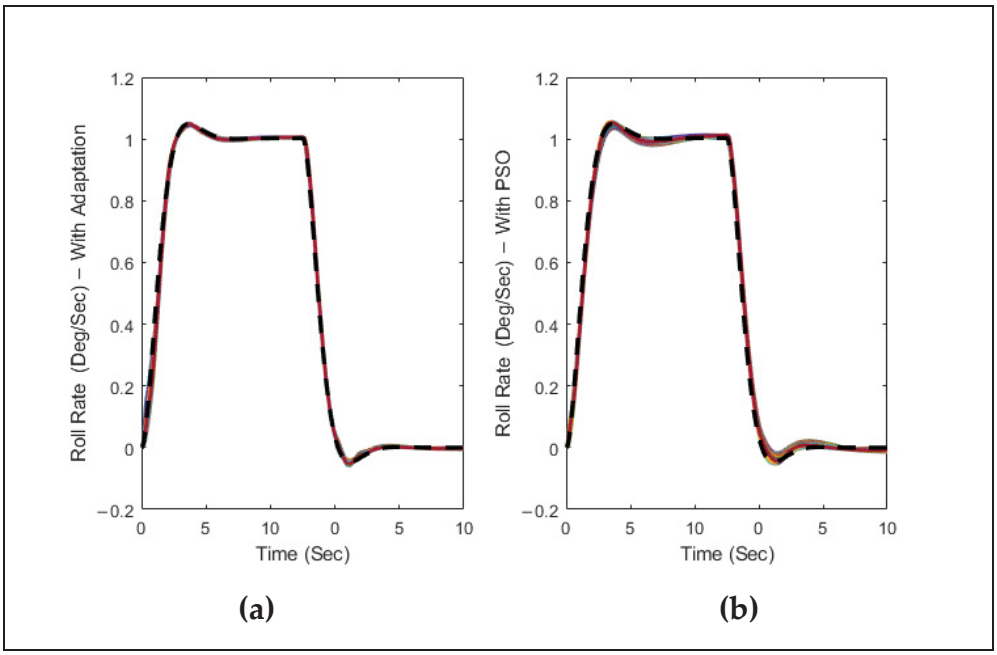

Figure 5.5 Roll rate variations for T2AFSTSMC with (a) adaptive switching control term and (b) PSO algorithm (The black dashed line represents the reference signal)

As indicated in Fig. 5.5, the results seem to be similar. Therefore, to determine which method performed better in the control of the roll rate of the Cessna Citation X aircraft, another evaluation is presented in Fig. 5.6, based on the reference signal tracking. This figure shows that the T2AFSTSMC with adaptive switching control can perform better than the PSO-based one in ideal flight conditions, as the Mean Absolute Error (MAE) values (in black) were negligible and consistently smaller than those obtained with the PSO algorithm.

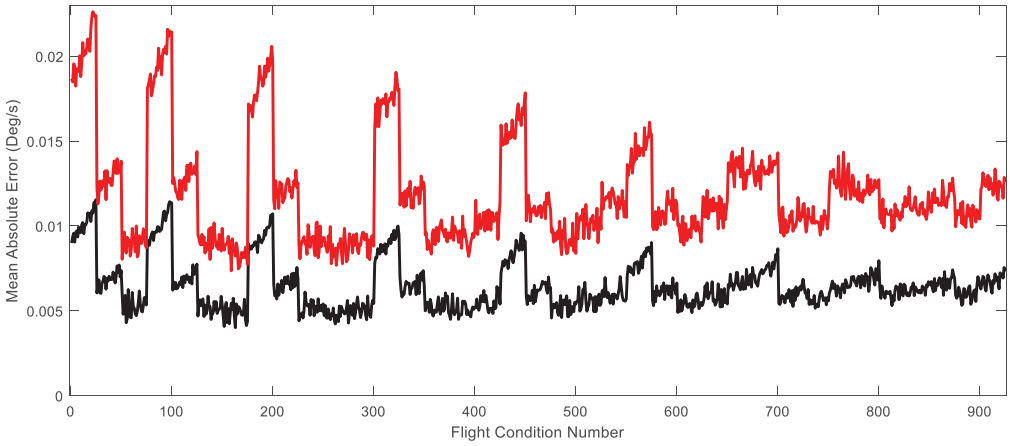

Figure 5.6 Mean absolute error for the T2AFSTSMC with adaptive switching control term (black) and the PSO algorithm (red) for each flight condition in ideal condition

In addition, the performance of the control system was assessed in terms of roll angle variations, as shown in Fig. 5.7. This figure clearly indicates that the aircraft is turning with the roll rate commanded from zero to five degrees. However, there is a discrepancy between the actual roll angle and its reference values after 6 s. Such an issue can be expected since the aircraft was experiencing some residual yaw that was induced by the motion of the aircraft. The difference between the roll angle and its reference signal in the controller with adaptive switching terms was slightly smaller than the PSO-based one. This study required a high level of roll rate tracking performance, which was successfully achieved.

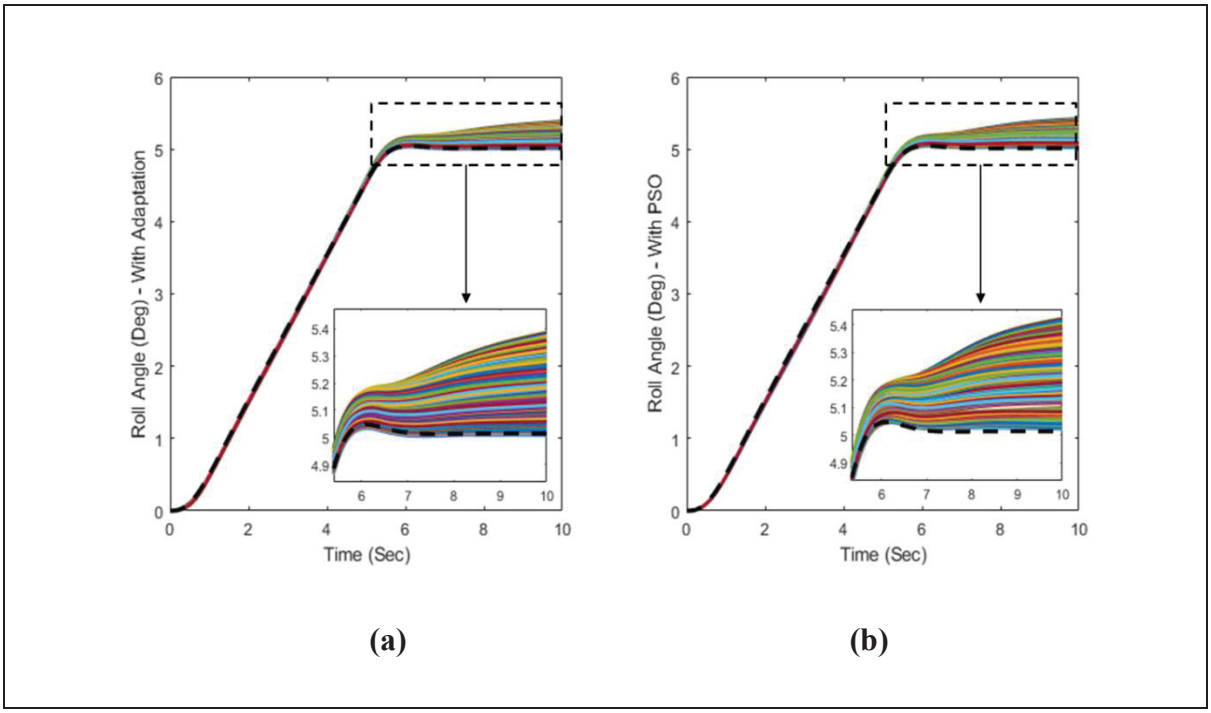

Figure 5.7 Roll angle variations for the T2AFSTSMC with (a) adaptive switching control term and (b) PSO algorithm (The black dashed line represents the reference signal)

Designing a control system to generate a smooth control input signal is crucial for several reasons, primarily in terms of passenger safety and comfort and to ensure that commands will not damage the actuation system. Sudden or abrupt maneuvers could lead to structural damage to the airframe and to accelerated wear and tear. In addition, from the flight dynamics approach, smooth commands help to maintain the stability and maneuverability of an aircraft. Our goal was to design a control system that produced a control input signal for ailerons with the most negligible high-frequency oscillations. As shown in Fig. 5.8, both control methodologies could satisfy this criterion. However, the controller with the adaptive switching control term was smoother than the one with PSO, especially during the first seconds of the simulation, as some abrupt changes (in some flight conditions) can be seen between $t = 0$ to 2 s.

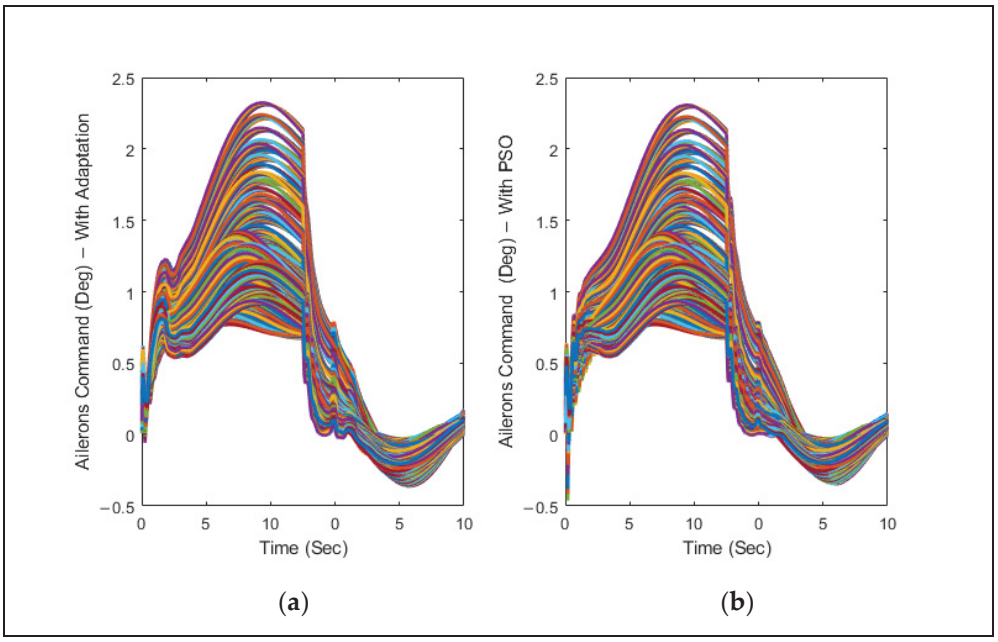

Figure 5.8 Time variations of the aileron command for T2AFSTSMC with (a) adaptive switching control term and (b) the PSO-based one

As shown in Fig. 5.9, to stabilize the yaw rate, we used an integral controller to reduce the steady-state error between the sideslip angle and its trim value (which usually equals zero-black dashed line). By maintaining the sideslip angle close to its trim value, it would be possible to ensure that the yaw rate is stable, as any variations in the sideslip angle can change the yaw rate.

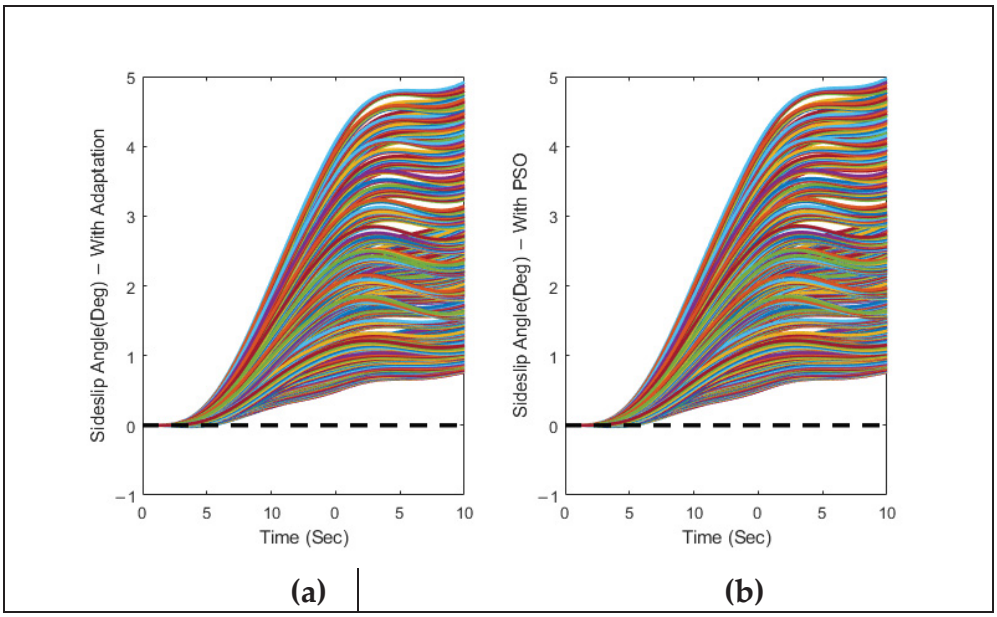

Figure 5.9 Time variations of the sideslip angle for T2AFSTSMC with (a) adaptive switching control term and (b) the PSO-based one

As illustrated in Fig. 5.10, the use of an integral feedback for the sideslip angle allowed the yaw rate variations to be maintained in a reduced range close to zero. These results validate the proposed strategy and demonstrate the effectiveness of the complete control system proposed in this paper.

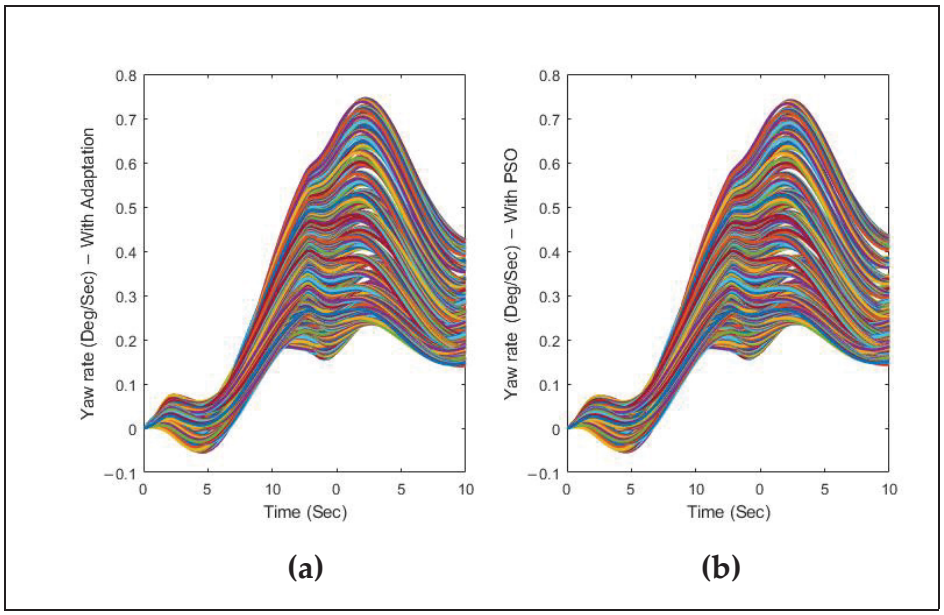

Figure 5.10 Time variations of the yaw rate for T2AFSTSMC with (a) adaptive switching control term and (b) the PSO-based one

One of the main objectives of this research was to design a control system for minimizing the effects of turbulence as a common critical condition during the cruise. To evaluate such systems, we used the Dryden turbulence model available in the Simulink Aerospace Blockset to obtain the effects of turbulence on the performance of Cessna Citation X aircraft equipped with the proposed T2AFSTSMC controllers. To achieve the objectives of this research, we selected the moderate probability for exceedance of high-altitude intensity (equal to 10^{-3}) in accordance with the specifications given in MIL-F-8785C (Moorhouse & Woodcock, 1982). Earlier in this section, we analyzed the performance of control methodologies under ideal conditions, demonstrating their efficiency and reliability. However, a test of the robustness and adaptability of an aircraft control system lies in its ability to handle real-world phenomena such as turbulence while maintaining the aircraft stability. This analysis highlights the capabilities of the designed control systems and provides precious insights to ensure optimal performance under operational conditions.

As represented in Fig. 5.11, the tracking performance was achieved with both control system methods handling the turbulence effects with a minimum amplitude variation.

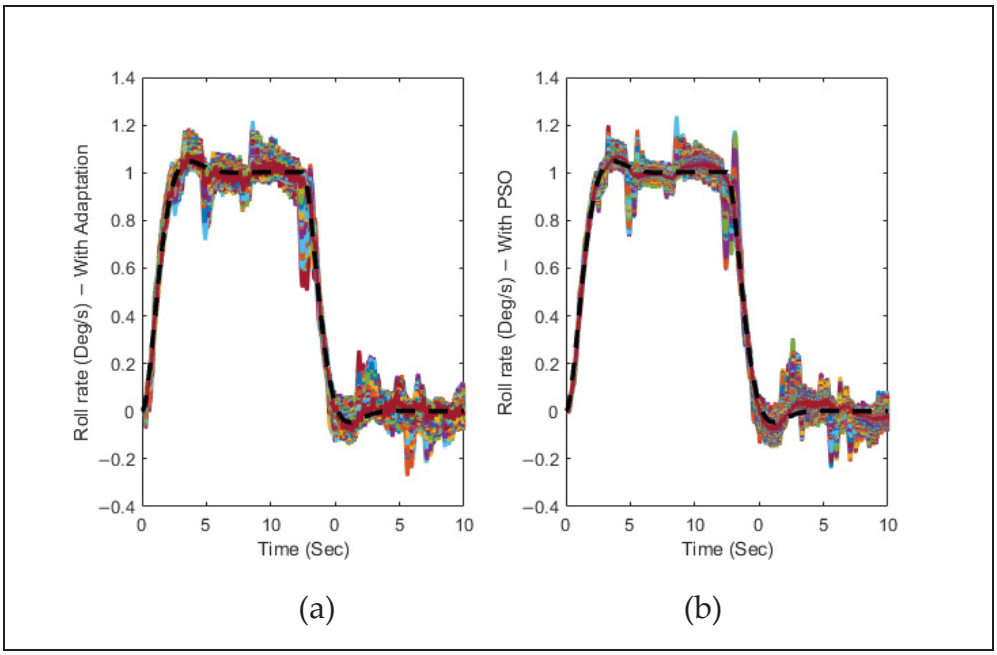

Figure 5.11 Time variations of the roll rate for T2AFSTSMC with (a) adaptive switching control term and (b) the PSO-based one (The black dashed line represents the reference signal)

The simulation results in Fig. 5.11 are numerically compared with those shown in Fig. 5.12 at each flight condition, revealing that the MAE values varied in almost the same range using the T2AFSTSMC with an adaptive switching term and with a PSO-based switching term. The trend of these variations shows that as the altitude increased, the MAE values consistently decreased (the first flight condition had the lowest altitude (8000 ft), and the 925th flight condition had the highest altitude(45,000 ft)), indicating that the controller could operate better at higher altitudes than at lower altitudes.

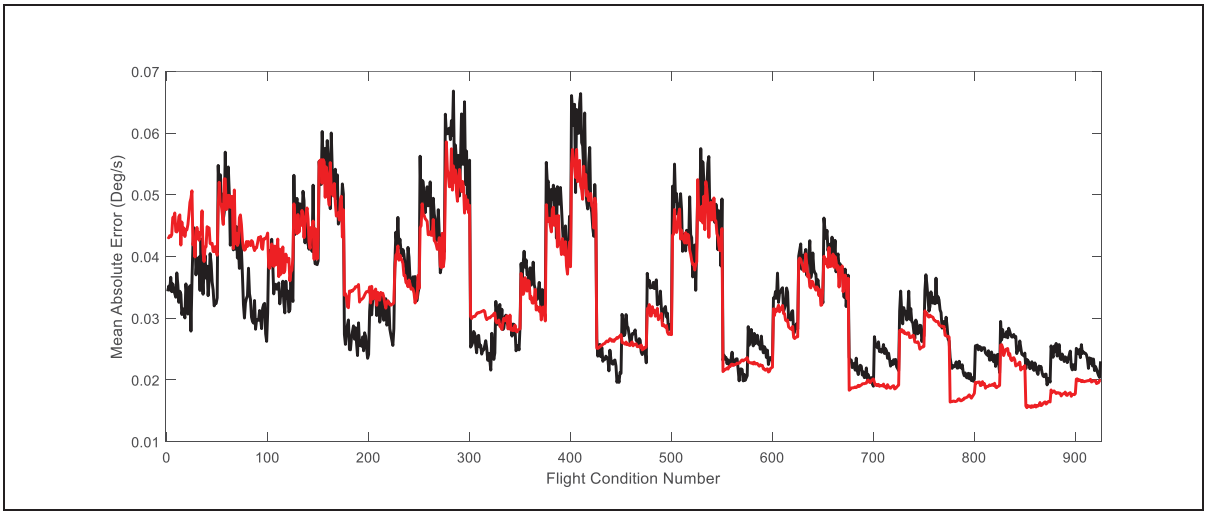

Figure 5.12 MAEs for T2AFSTSMC using an adaptive switching term (black) and a PSO-based switching term (red) for each flight condition with turbulence

While the trends of MAE variations are presented in Fig. 5.12, it was not obvious which method could operate better in the presence of turbulence. To investigate any possible differences, the distribution of the MAEs across all flight conditions was assessed, as shown by the histogram in Fig. 5.13. This evaluation showed that the controller with a PSO-based switching term operated better than the one with an adaptive term, as the MAE values for all flight conditions were less than 0.06 degrees per second. However, the maximum MAE for the controller with an adaptive switching term was very close to this value at less than 0.07 deg/s.

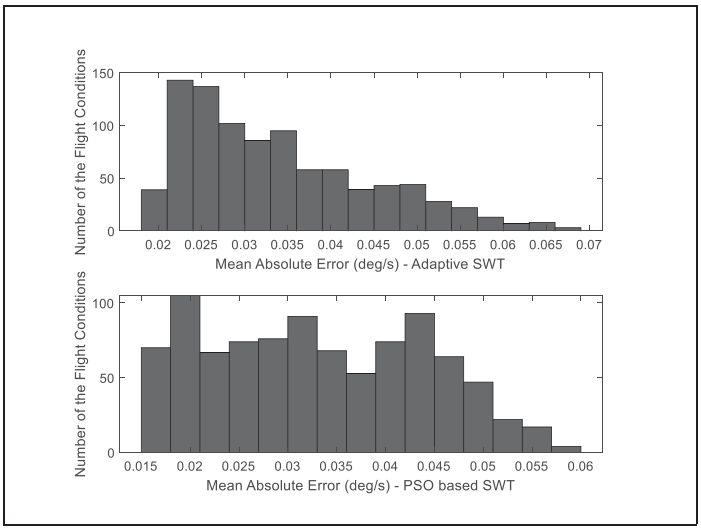

Figure 5.13 Distribution of the MAEs for T2AFSTSMC using an adaptive switching term (UP) and a PSO-based switching term (down) under turbulence in 925 flight conditions

As shown in Fig. 5.14, the aircraft equipped with both switching terms attempted to achieve the commanded roll angle of 5 degrees. However, due to the erratic effects of the turbulence, the roll angle deviated from its reference roll angle, and the aircraft could not remain stable at the targeted 5 degrees. These challenging variations imposed on the maneuverability of the aircraft have occurred in both control methodologies.

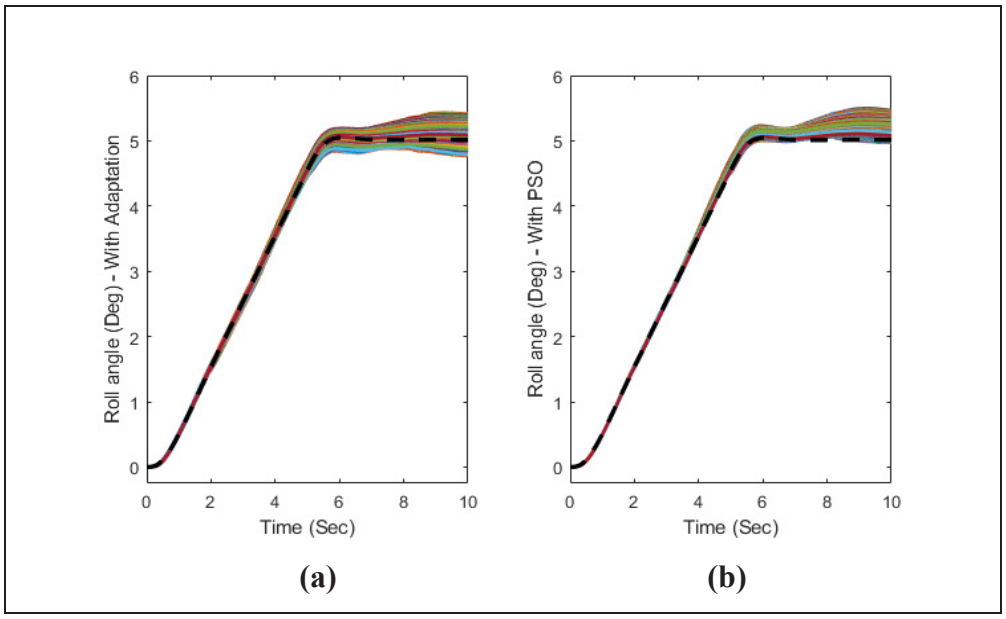

Figure 5.14 Roll angle time variations for T2AFSTSMC with turbulence using (a) an adaptive switching term and (b) a PSO-based switching term (The black dashed line represents the reference signal)

As shown in Fig. 5.15, the produced aileron control input signals had minimum abrupt oscillations (without high amplitude) in the presence of turbulence. This characteristic was successfully achieved with both methods since the imposed effects of the turbulence forced the control system to change the position of the ailerons very rapidly within a restricted deviation range.

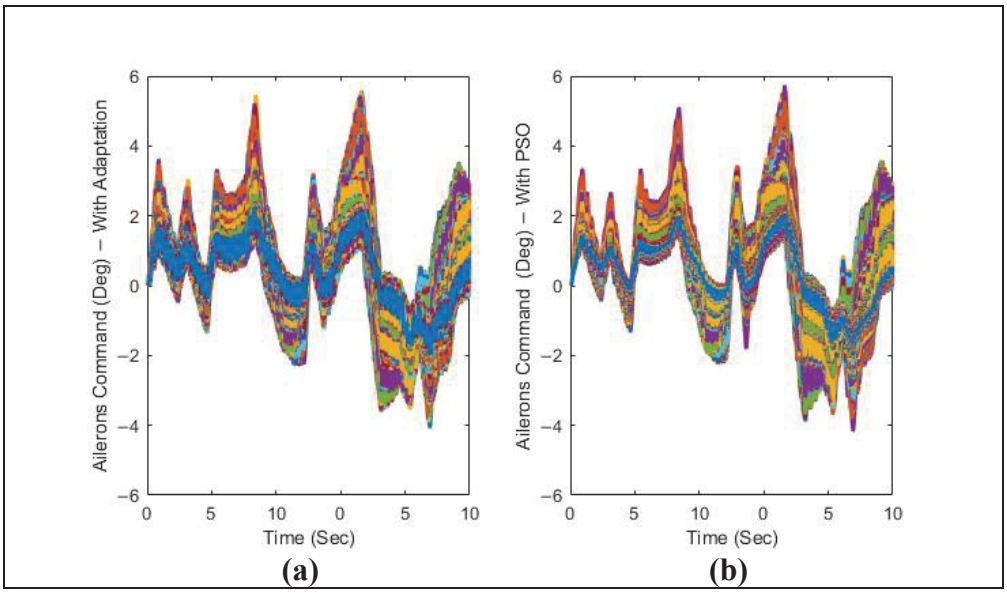

Figure 5.15 Time variations of the aileron command for T2AFSTSMC under turbulence with (a) an adaptive switching control term and (b) a PSO-based switching term

5.4 Conclusions

In this work, an enhanced Type-Two Adaptive Fuzzy Super-Twisting Sliding-Mode Control system was developed and validated with the nonlinear lateral model of the Cessna Citation X business jet aircraft. In this control system, the Type-Two Fuzzy Logic System approximated the unknown function in the state-space model of the aircraft with no prior knowledge of its parameters. This approximated function could be updated during the simulation using the adaptation laws derived from the Lyapunov theorem. This methodology helped to handle the uncertainties and parameter variations effectively. Both robustness and stability were achieved using the proposed super-twisting sliding-mode control system for the Cessna Citation X aircraft. Principally, in the sliding-mode control, the control law consisted of an equivalent control law based on the concept of the proposed Type-Two Adaptive Fuzzy System and the switching control law. Two methods were employed to choose the best gains values in the switching control law: one with the adaptation laws developed for the gains by the Lyapunov theorem and the other with the gains found by the PSO algorithm. The simulation results revealed that both control approaches were able to

guarantee the robustness and stability of the aircraft in the presence of turbulence with a moderate intensity (10^{-3}). Furthermore, the tracking performance of the roll rate was excellent while producing the aileron control input with minimum high-frequency oscillations to avoid mechanical damage to the aircraft actuation system. Regarding the tracking performance analyzed for the aircraft roll rate, it was found that the controller equipped with a PSO-based switching control term operated better than the adaptive one, with a maximum Mean Absolute Error (MAE) value equal to 0.06 degrees per second in the presence of turbulence. Finally, this controller could be applied for any aircraft model, as no knowledge regarding the aircraft model or the dynamic parameters is required, and the Adaptive Type-Two Fuzzy Logic System can update the aircraft dynamics in real time with only a measured state variable, such as the roll rate and its reference signal.

CHAPTER 6

NEW FUZZY-RNN AUTOPILOT SYSTEM FOR CESSNA CITATION X AIRCRAFT WITH A FUZZY TRANSITION ALGORITHM

S.M. Hosseini, G. Ghazi, and R.M. Botez

Research Laboratory in Active Controls, Avionics and AeroServoElasticity (LARCASE),
Department of Systems Engineering, École de Technologie Supérieure,
1100 Notre-Dame West, Montreal, Quebec, Canada H3C 1K3

Paper submitted to *the Aeronautical Journal*. October 2024.

Resumé : Cet article présente un nouveau système de commande de pilote automatique basé sur l'intelligence artificielle conçu pour le mouvement longitudinal de l'avion Cessna Citation X (CCX) pendant la croisière. Dans cette méthodologie de contrôle, la dynamique inconnue de l'avion dans les représentations de l'espace d'état de chaque mode de vitesse verticale (VS) et de maintien de l'altitude (AH) a été approximée par deux réseaux neuronaux récurrents flous (FRNN) formés en ligne à l'aide d'une nouvelle approche basée sur les algorithmes d'optimisation de l'essaim de particules et de rétropropagation. Ces MFRNN ont été utilisés avec deux contrôleurs à mode glissant pour garantir la robustesse des modes VS et AH. En outre, un nouvel algorithme de transition basé sur la logique floue a été proposé pour basculer efficacement le contrôleur entre ces modes de pilotage automatique. Les performances des contrôleurs ont été évaluées à l'aide d'une plateforme de simulation non linéaire développée pour le CCX et basée sur les données d'un simulateur de vol d'avion de recherche de niveau D certifié par la FAA. La stabilité et la robustesse du système ont été prouvées par le théorème de Lyapunov. La simulation, testée dans 925 conditions de vol, a démontré la capacité exceptionnelle de poursuite des contrôleurs dans une variété d'incertitudes, y compris des scénarios de vol turbulents et non turbulents. En outre, la conception a permis de maintenir la fluidité des signaux d'entrée de commande afin de préserver l'intégrité mécanique du système d'actionnement de la gouverne de profondeur

Abstract: This paper presents a novel artificial intelligence based autopilot control system designed for the Cessna Citation X (CCX) aircraft longitudinal motion during cruise. In this control methodology, the unknown aircraft dynamics in the state-space representations of each Vertical Speed (VS) mode and Altitude Hold (AH) mode were approximated by two Fuzzy Recurrent Neural Networks (FRNNs) trained online using a novel approach based on Particle Swarm Optimization and Backpropagation algorithms. These MFRNNs were used with two sliding mode controllers to guarantee the robustness of both VS and AH modes. In addition, a novel fuzzy logic-based transition algorithm was proposed to efficiently switch the controller between these autopilot modes. The performance of the controllers was evaluated with a nonlinear simulation platform developed for the CCX based on data from a Level D Research Aircraft Flight Simulator certified by the FAA. The system stability and robustness were proved by the Lyapunov theorem. The simulation, tested under 925 flight conditions, demonstrated the controllers exceptional tracking capability in a variety of uncertainties, including turbulent and non-turbulent flight scenarios. In addition, the design ensured that the smoothness of the control input signals was maintained in order to preserve the mechanical integrity of the elevator actuation system.

6.1 Introduction

The development of autonomous control systems has become the main topic of many articles in Aerospace and Aeronautics fields. The design of autopilot systems in aircraft is crucial for improving its safety, efficiency, and reliability. This research develops a novel autopilot system based on a Multilayer Fuzzy Recurrent Neural Network (MFRNN) with a two-mode Sliding Mode Control (SMC) to reduce the pilot's workload in various maneuvers and critical flight conditions such as turbulence. According to statistics published in (William Rankin, Ph.D., 2007), system failures have been massively reduced due to the recent technological advances in aircraft systems. On the contrary, human errors are still the leading cause of 80% of aircraft accidents and incidents.

This section presents a literature on various methods for the control of aircraft, Unmanned aerial vehicles (UAVs), and quadcopters.

(Mansoor Ahsan & Ali Hanif, 2014) presented two methods based on the Proportional Integral Derivative (PID) method to control the altitude of an Aerosonde UAV, one with a single elevator command and the other one with both throttle and elevator commands. Their work showed that the throttle and elevator control laws can give a better transient response. (Ahsan et al., 2013) compared two altitude controllers developed for an Aerosonde UAV, one with PID methods and the other method with a Lead Compensator and found that the Lead Compensator operated better than the PID.

To improve the altitude tracking performance of UAVs, (H. Liu et al., 2015) proposed to use a combination of linear Proportional (P), Derivative (D), and two Derivatives (DD) controllers and a Kalman filter to estimate the climb and descent rates. (Cárdenas et al., 2012) developed a pole-placement control methodology using linearized longitudinal and lateral-directional models of an UAV to control its altitude and heading.

(M. Liu et al., 2015) proposed PID-based airspeed, heading, and altitude controllers for an UAV equipped with a fine-tuning procedure. (Win et al., 2019) developed a pitch Attitude Hold (AH) autopilot for an YTUEC001 UAV. To achieve path-tracking performance, (Qian & Liu, 2020) used an Uncertainty and Disturbance Estimator (UDE) with a translational controller for cruising near hovering phases in the outer loop, and an attitude tracking controller in the inner loop. This methodology guaranteed the globally asymptotic stability of the quadrotor in the presence of disturbance and payload. (Qi et al., 2021) showed that a Modified UDE can guarantee the attitude control performance of a quadrotor. This estimator was developed with a cascade PID architecture, and its performance was compared with that of a real quadrotor platform, by showing its effectiveness in rejecting the disturbance and in tracking the references. To avoid the collision of UAVs around obstacles and achieve their tracking performance, (Feng & Liu, 2023) proposed a nonlinear Model Predictive Control (MPC) using a new flight scenario for two UAVs. (Zhao et al., 2021) considered controlling

the attitude of an UAV to approach a virtual tanker aircraft for an aerial fueling process. This controller was designed using a global fast terminal SMC to track the commanded attitude. As another approach for collision avoidance, (W. Zhang et al., 2023) designed an autopilot for quadrotors by using Sliding Mode Observer (SMO) to ensure the safety of the actuation system. In this methodology, an energy-saving trajectory planning strategy was considered, and the planning procedure was converted to a Quadratically Constrained Quadratic Programming (QCQP) problem. (Zareb et al., 2019) incorporated two fuzzy controllers and four PIDs to control the attitude and altitude of an AR.Drone V2 quadrotor. Genetic Algorithms (GAs) were employed to optimize the control parameters and to achieve appropriate performance. (K. Wilburn et al., 2014) developed a new GA to optimize the gains of the controllers and to guarantee the trajectory-tracking performance of the UAVs. (R. Zhou et al., 2023) developed a methodology based on finite-time SMC system and disturbance observers to track the reference signal and to decrease the communications between the UAVs, by using a developed event-triggered communication mechanism. Using this methodology an improved trajectory tracking performance was achieved.

Beside the design of autopilot controllers for UAVs and quadrotors, different methodologies were developed for hypersonic and supersonic aircraft, as discussed below.

(Sahbon et al., 2023) proposed a path-following controller for the X-15 aircraft based on the Thrust Vector Control (TVC) algorithm. This methodology used three PID controllers in the autopilot system for each roll, altitude, and yaw control system to deal with the Coriolis effects. (T. Dong et al., 2022) implemented a fractional-order PID controller whose gains were optimized using a GA algorithm to achieve active disturbance rejection performance in aircraft pitch. To achieve rapid altitude tracking performance, (H. Gao et al., 2020) studied a cascaded PID-based altitude controller for hypersonic vehicles, using a state observer to ensure the attitude stability. To compensate for the coupling and disturbance effects in hypersonic vehicles, (Fenfen et al., 2020) designed an Auto Disturbance Rejection System (ADRS) by combining a classical ADRS with a PID controller to achieve an appropriate tracking performance.

(Taha et al., 2009) concluded that a Model Reference Adaptive Control (MRAC) can be an appropriate choice for the design of the AH mode. For the speed autopilot system, the MRAC gave better results when used with an online parameter estimation method. (Perez et al., 2015) developed a new adaptive PID-based controller using a GA-based immunity feedback algorithm to ease the control of a supersonic fighter for pilots and guarantee aircraft robustness and stability under various types of failures. An artificial immunity-based algorithm was also used in (Perez, Moncayo, Moguel, Perhinschi, Al Azzawi, et al., 2014) with dynamics inversion and MRAC methods to ensure a fighter performance under actuator and structural failures. This controller handled the failures with a minimum pilot command in terms of its magnitude. (Park et al., 2023) designed an autopilot system for hypersonic vehicles based on a methodology that relies on a gain-scheduling approach to handle the model uncertainties and to control the pitch rate, and the acceleration and the flight path angle.

(Hiliuta et al., 2005b) evaluated the performance of the ANFIS methodology and of a fuzzy set theory developed based on the fuzzy subtractive clustering algorithm to approximate the aerodynamic forces in a F/A-18 aircraft aeroservoelastic model. Aiming at the analysis of the controllers effects on the aircraft structure and calculating the flutter velocities, (Hiliuta, Botez, & Brenner, 2005a) showed that the least square method is not efficient for approximating the unsteady aerodynamic forces in frequency domain. Therefore, a combination of the fuzzy logic based clustering and shape-preserving methods was proposed to approximate the intermediate frequency values of the unsteady forces of a F/A-18 SRA aircraft, modeled by finite element methods using STARS software.

In addition to the previoshowsesearch topics for UAVs, hypersonic, fighters, and supersonic aircraft, several pertinent studies of the control systems for commercial and business aircraft types are noted below.

(Theis et al., 2018) designed an autopilot system to deal with a 25-knots crosswind using two strategies: PID-based loop shaping, and an H_∞ control system for a twin-engined civil aircraft motions during landing. Meanwhile, (Qiu et al., 2017) implemented a Non-Minimum Phase cotroller based on dynamic inversion, and calculated by an U-model root solver to design an altitude-hold autopilot for a B747 aircraft to deal with right-half-plane zeros. Similarly, (Barros Dos Santos & De Oliveira, 2011) demonstrated the accurate performance of a PID control methodology using an X-plane flight simulator. This method was also applied by (Islam et al., 2016) for a general aviation civil aircraft, and by Raj and Kumar (Solomon Raj & Kumar, 2015) for a Piper PA-28-236-DAKOTA aircraft. The Root-locus design technique was used to adjust the control parameters, aiming to achieve an overshoot of less than 15% as a design requirement for each autopilot mode with turbulence.

In addition to conventional controllers, artificial intelligence (AI)-based methods have been explored for the design of autopilot systems for civil aircraft. (Nivison & Khargonekar, 2017a), for instance, proposed the application of a Deep Gated Recurrent Neural Network (DGRNN) controller for the aircraft longitudinal motion to achieve its robustness and trajectory-tracking performance. Using a combination of RNN and GA systems, (Juang & Chiou, 2006) developed an enhanced autolanding system under severe wind shear conditions. (Vandana A, Anusha Sanmathi S, Ipshita Chaturvedi, Sanjana Jaikumar, & T S Chandar, 2021) designed a two-loops autopilot system that integrated a robust control system combined with an NN and a UDE for a rigid-body aircraft.

In this article, the proposed longitudinal autopilot control system was tested and validated on a nonlinear simulation platform designed for Cessna Citation X (CCX) business aircraft. Several control systems have been proposed in the past for this aircraft, among them, a Linear Quadratic regulator (LQR) control system combined with the Guardian Maps theory was used to achieve robustness against uncertainties for its lateral motion (Ghazi & Botez, 2015b). (Yamina et al., 2017a) improved the performance of an optimal control system combined with a meta-heuristic optimization technique to ensure stability for both linear and nonlinear models of the CCX aircraft. Furthermore, (Ghazi et al., 2016) suggested using a PI

controller with Guardian Maps theory for the design of a stability and control augmentation systems to control the CCX pitch rate.

In addition to conventional controllers, several AI-based methodologies have also been proposed for the CCX aircraft. (Quintin et al., 2024) combined a Dynamic Inversion system, an adaptive neural network (ANN), and a PID controller to control the CCX roll rate control while stabilizing its yaw rate. (Rojo P. Andrianantara et al., 2024) demonstrated that a control system combining an MPC system, Recursive Least Square (RLS) algorithm, and an Adaptive Control system can efficiently control the CCX pitch rate.

Previously, the authors developed different AI-based controllers for the CCX aircraft, including Type-Two Adaptive Fuzzy SMC (T2AFSMC) (Seyed Mohammad Hosseini, Ghazi, & Botez, 2024a) and a model-referenced adaptive RNN controller (S. Hosseini, Inga, et al., 2023) for its longitudinal motion and a combination of T2AFLS, PSO-based, and adaptive Super-twisting SMC systems for its lateral motion (Seyed Mohammad Hosseini, Bematol, Ghazi, & Botez, 2024) across different flight conditions.

This article presented focuses on developing a Multilayer Fuzzy Recurrent Neural Networks (MFRNN)-based autopilot system for the CCX longitudinal motion during cruise, under both ideal and turbulent conditions with moderate-intensity value (10^{-3}). The novel methodology introduces new features to flight control systems design by using the AI. This autopilot system doesn't rely on aircraft dynamics models, and it can handle the uncertainties, highly nonlinear and unmodeled dynamics by its adaptive and real-time learning characteristics. These properties can guarantee the aircraft robustness and performance across a wide range of flight conditions without the need for constant parameters adjustment.

Therefore, the main contributions of this research are listed below.

- A Novel Dynamics Approximator: This paper introduces an online approximator for the unknown functions in the aircraft nonlinear state space representations for both Altitude Hold (AH) and Vertical Speed (VS) autopilot modes. This technique was developed based on the methodology proposed in (Fei et al., 2022) using an MFRNN. The Particle Swarm Optimization (PSO) algorithm is used to initialize the weights of the MFRNN offline, and then to update the weights of the last layer using Backpropagation (BP) via an online process. All other weights in the MFRNN remain fixed. This training approach, which differs from the strategies discussed in (Fei et al., 2022), as it introduces a novel element to this specific type of approximation methodology.

- A pioneering AI-based Autopilot System: This proposed two-loop AI-based control methodology, which integrates SMC systems with two MFRNNs, represents a novel approach for the autopilot control system of commercial aircraft such as the CCX business jet. This AI-based combination, not yet developed for different types of aircraft such as UAVs (Ahsan et al., 2013 ; Cárdenas et al., 2012 ; Darwish et al., 2021 ; Feng & Liu, 2023 ; S. Lee et al., 2022 ; H. Liu et al., 2015 ; M. Liu et al., 2015 ; Mansoor Ahsan & Ali Hanif, 2014 ; Qi et al., 2021 ; Qian & Liu, 2020 ; Santoso et al., 2008 ; Win et al., 2019 ; Zareb et al., 2019 ; W. Zhang et al., 2023 ; Zhao et al., 2021 ; R. Zhou et al., 2023), hypersonic aircraft (T. Dong et al., 2022 ; Fenfen et al., 2020 ; H. Gao et al., 2020 ; Hiliuta et al., 2005b ; Napolitano & Kincheloe, 1995 ; Park et al., 2023 ; Perez, Moncayo, Moguel, Perhinschi, Al Azzawi, et al., 2014 ; Perez et al., 2015 ; Sahbon et al., 2023 ; Taha et al., 2009) or even commercial aircraft (Barros Dos Santos & De Oliveira, 2011 ; Islam et al., 2016 ; Juang & Chiou, 2006 ; Nivison & Khargonekar, 2017a ; Qiu et al., 2017 ; Solomon Raj & Kumar, 2015 ; Theis et al., 2018 ; Vandana A et al., 2021), represents a significant advancement in Aerospace and Aeronautics fields. Moreover, this autopilot system was validated on a nonlinear simulation platform developed for the CCX aircraft (Ghazi, 2014), using highly accurate flight data obtained from a Level D (Highest level of cetification

by the FAA) Research Aircraft Flight Simulator (RAFS), available at LARCASE, which provided the possibility of performance validation under a variety of flight conditions (925 flight conditions, covering the entire CCX flight envelope in both ideal and turbulent conditions) to ensure the aircraft safety, and reliability.

- A new Fuzzy-based Transition Algorithm: A new fuzzy logic-based mode transition algorithm was developed to switch between the AH and VS modes. This algorithm was inspired by the performance of the algorithm proposed in (Ghazi, 2014). This algorithm eliminates the need for a third mode such as Altitude Capture mode, which was used in (Ghazi, 2014).

- The inner loop of our proposed autopilot to control the CCX pitch rate was developed based on our previous work on the application of a Type-One Adaptive Fuzzy Sliding Mode Control (T1AFSMC) system in (Seyed Mohammad Hosseini, Ghazi, et al., 2024b).

As explained above, this research is novel both in its application to commercial aircraft such as the CCX and in its theoretical aspects, as it proposes a new Fuzzy-based transition algorithm and a MFRNN approximation method for the aircraft dynamics, trained by a new approach. A simple scheme of the research contributions are shown in Fig. 6.1.

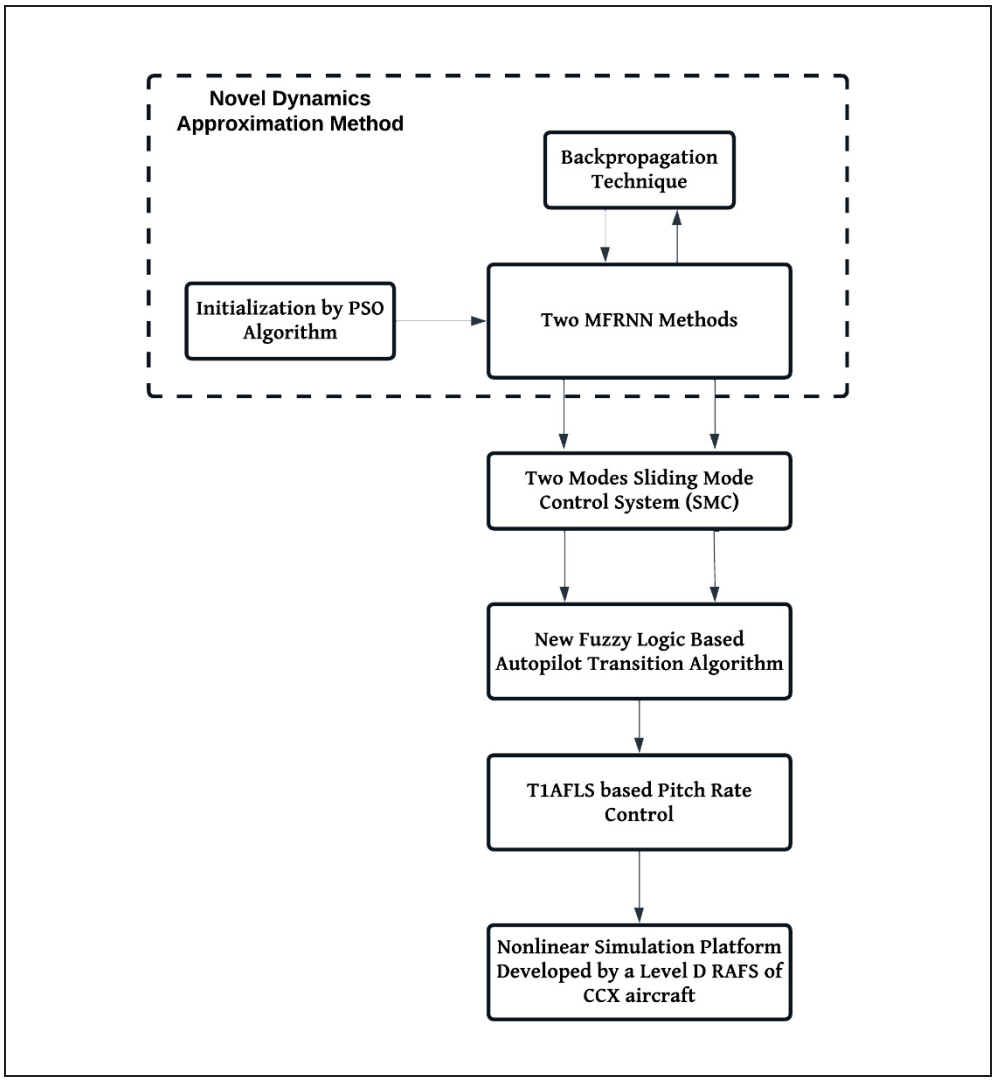

Figure 6.1 Simple Scheme of the Research Contributions

The rest of this paper is organized as follows: Section 6.2 provides an introduction to the aircraft nonlinear state-space representation, the PSO-based MFRNN approximator design, VS Mode and AH Mode controller designs, and an explanation of the Fuzzy Logic-based transition algorithm. Section 6.3 presents the results and a comprehensive analysis of the autopilot system performance. Finally, Section 6.4 concludes the paper with a summary of the findings.

6.2 Background

In this section, the three methods used in this study are discussed for designing an autopilot for the aircraft longitudinal motion during cruise.

6.2.1 Nonlinear State-Space Aircraft Representation

The state-space model is a well-known representation of the system dynamics. This representation is typically characterized by two functions, $F_{(vs,h)}$ and $G_{(vs,h)}$, which reflect the aircraft dynamics variations, as the functions existing in the vertical speed (vs) and altitude (h) control systems (R.K. Yedavalli, 2022). Generally, $G_{(vs,h)}$ in aircraft control systems shows the effectiveness of the control inputs which varies in small ranges during the cruise. Moreover, it was observed that $G_{(vs,h)}$ varied with values around 1. Therefore, to reduce the complexity of the control system design, we assumed that $G_{(vs,h)}$ is approximately equal to 1 $G_{(vs,h)} \approx 1$. Consequently, the aircraft state-space representation for the vertical speed and altitude modes can be described with a vector of state variables and the control input (i.e., command) denoted by $x^T = [VS, h]$ and $u_{(vs,h)}$, respectively:

$$x^{(n)} = F_{(vs\ h)} + G_{(vs\ h)}u_{(vs\ h)} + D = F_{(vs\ h)} + u_{(vs\ h)} + D \tag{6.1}$$

where n is the order of derivative, and D is the atmospheric turbulence.

Furthermore, we used a simulation platform developed at the LARCASE for the CCX business jet aircraft (Ghazi, 2014). This platform was validated using the flight data from a Level-D RAFS available at LARCASE for this business aircraft, as illustrated in Fig. 6.2. Level D represents the highest certification be issued by the Federal Aviation Authority (FAA) for aircraft flight simulation in terms of flight data accuracy (Ghazi, 2014).

Figure 6.2 Level D RAFS For the CCX Aircraft at LARCASE

6.2.2 PSO-Based Multilayer Fuzzy Recurrent Neural Network (MFRNN) Approximators

As discussed earlier, the nonlinear state-space representations of the CCX aircraft contain the unknown functions $F_{(vs,h)}$, which were approximated by the following MFRNN, as proposed in (Fei et al., 2022), for the design of autopilot system.

The main architecture of the MFRNN is presented in Fig. 6.3, which includes four main layers: 1) the Input layer, 2) the Membership layer, 3) the Rules layer, and 4) the Output layer. There are some feedback loops in the MFRNN, as shown in Fig. 6.3, which can provide the MFRNN with a self-learning ability to approximate the aircraft dynamics.

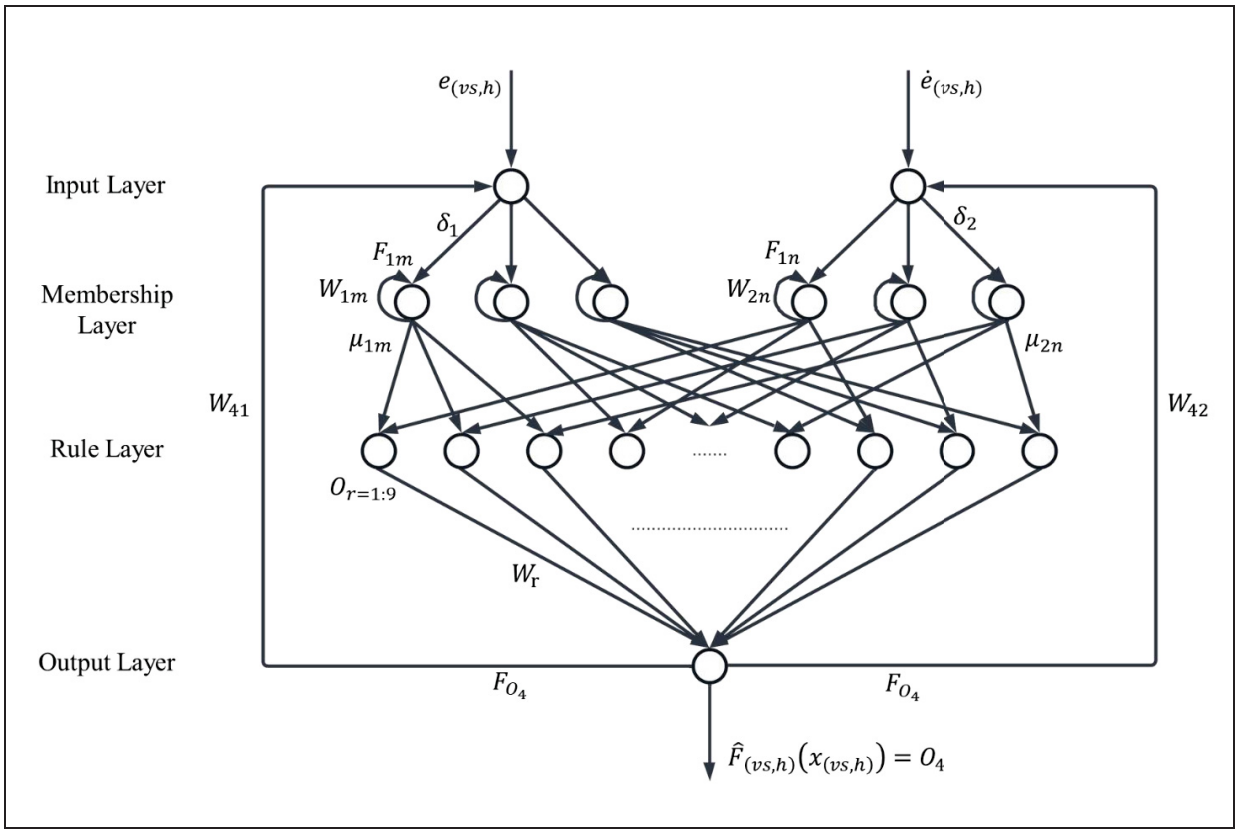

Figure 6.3 Multilayer Fuzzy Recurrent Neural Network (MFRNN) Scheme

In this autopilot system, two MFRNNs were developed, one for VS mode and the other architecture for AH mode. The main structure of the layers in these MFRNNs is explained below:

1) Input layer (2 neurons):

Initially, two signals were measured from the CCX simulation platform: the Vertical Speed VS and the aircraft altitude h. These signals were used in the definition of the tracking errors e_{vs}, and e_h as calculated in Eqs. (6.2) and (6.3):

$$e_{vs} = VS - VS_{ref} \tag{6.2}$$

$$e_h = h - h_{ref} \tag{6.3}$$

Two inputs vectors represented by I_{vs} (for the VS mode) and I_h (for the AH mode) were used in the MFRNNs, each composed of the tracking error $e_{(vs,h)}$ and its first-order derivative $\dot{e}_{(vs,h)}$, as shown in Eqs. (6.4.a) and (6.4.b), for the VS and AH modes, respectively.

$$I_{vs} = [e_{vs}; \dot{e}_{vs}] \tag{6.4.a}$$

$$I_h = [e_h; \dot{e}_h] \tag{6.4.b}$$

In these MFRNNs, shown in Fig. 6.3, there is a feedback loop from the output layer ($\hat{F}_{(vs,h)} = O_4$) to the input layer expressed by F_{O_4}. Using the elements in the inputs vectors given in Eq. (6.4.a) for the VS mode denoted by I_{vs}, and in Eq. (6.4.b) for the AH mode represented by I_h, we can write:

$$\delta_1 = e_{(vs\,h)} W_{41} F_{O_4} \tag{6.5.a}$$

$$\delta_2 = \dot{e}_{(vs\,h)} W_{42} F_{O_4} \tag{6.5.b}$$

where δ_1 is the first neuron output, and δ_2 is the second neuron output in the input layer. Moreover, W_{41} and W_{42} denote the recurrent weights acting on the connections (internal feedback loop) between the output and the input layers.

2) Membership layer (6 neurons) :

In this layer, each neuron is a Gaussian membership function denoted by μ_{1m} and μ_{2n} that processes the output of the previous layer (the input layer), denoted by δ_1 and δ_2 in Eqs. (6.5.a) and (6.5.b), and the feedback connections shown by F_{1m} and F_{2n}, multiplied by their weights W_{1m} and W_{2n}, respectively. F_{1m} and F_{2n} contains the previous output values (feedback) of the the membership functions calculated by Eqs. (6.8.a) and (6.8.b) (Fei et al., 2022).

$$\delta_{1m} = \delta_1 + W_{1m} F_{1m} \tag{6.7.a}$$

$$\delta_{2n} = \delta_2 + W_{2n}F_{2n} \tag{6.7.b}$$

$$\mu_{1m}(x) = e^{-0,5(\frac{\delta_{1m}-b_{1m}}{a_{1m}})^2} \tag{6.8.a}$$

$$\mu_{2n}(x) = e^{-0,5(\frac{\delta_{2n}-b_{2n}}{a_{2n}})^2} \tag{6.8.b}$$

In Eqs. (6.7.a) - (6.8.b), $m = \{1,2,3\}$ and $n = \{1,2,3\}$ are the neurons indices. Equations (6.7.a) and (6.7.b) show that when calculating the input layers δ_{1m} and δ_{2n}, the weights W_{1m} and W_{2n} act on the internal feedback loops (F_{1m} and F_{2n}) in the membership layers. The values of the parameters in the Gaussian Memberships are provided in Tables 6.1 and 6.2 for each VS and AH mode approximator, as follows.

Table 6.1 Configurations of the Membership Functions in the VS Mode

m,n indices	Parameters	Value	Parameters	Value
1	$a_{11}= a_{21}$	400	$b_{11} = b_{21}$	0
2	$a_{12} = a_{22}$	400	$b_{12} = b_{22}$	1825
3	$a_{13} = a_{23}$	400	$b_{13} = b_{23}$	3650

Table 6.2 Configurations of the Membership Functions in the AH Mode

m,n indices	Parameters	Value	Parameters	Value
1	$a_{11}= a_{21}$	4000	$b_{11} = b_{21}$	0
2	$a_{12} = a_{22}$	4000	$b_{12} = b_{22}$	3810
3	$a_{13} = a_{23}$	4000	$b_{13} = b_{23}$	7620

3) Rules layer (9 neurons)

Each neuron in this layer was used to calculate the product of the input signals serving as the product inference engine in the Fuzzy Logic System (FLS) architecture. The output of this layer O_r is given in Eq. (6.9):

$$O_r = \prod_{m,n=1}^{3} \mu_{1m}(x), \mu_{2n}(x) \tag{6.9}$$

where $r = \{1, \dots, 9\}$ is the total number of the rules.

4) Output Layer (1 neuron)

Using the 9 outputs O_r obtained at each neuron in the rules layer and their corresponding weights, the final output of the MFRNN based approximators can be expressed in Eq. (6.10) for both the VS and AH controllers:

$$\hat{F}_{(vs\,h)}\left(x_{(vs\,h)}\right) = \sum_{r=1}^{9} W_r O_r \tag{6.10}$$

6.2.2.1 The MFRNN Training algorithm

Each of the MFRNN based approximators explained earlier for both autopilot modes, was trained using a new approach, as follows:

i. Initially the MFRNNs receive the vector x_{vs} in the VS controller and the vector x_h in AH controller as input layers.

ii. All weights $\{W_{41}, W_{42}, W_{1m}, W_{2n}$ and $W_r\}$ were initialized using the PSO algorithm designed by the expressions in Eqs. (6.11) and (6.12) (Gad, 2022), and the cost function given in Eq. (6.13), while $W_{41} = W_{42}$ and $W_{1m} = W_{2n}$ on the feedback loops. Thus, the PSO was used to find the values of three weights, called *Decision Variables* = $\{W_{4(1,2)}, W_{(1m,2n)}, W_r\}$. Each particle X_p^i in the PSO searches in a space between its bounds $[X_{lo}, X_{up}]$, which means that all decision variables could only take a value within the defined range. In addition, in Eq. (6.11), P_{best} and G_{best} are the personal and global best results, respectively, and β_1 and β_2 denote two random values within [0,1] (Gad, 2022).

$$\sum_{i=1}^{i_{max}} \sum_{p=1}^{p_{max}} Y_p^{i+1} = \alpha_{damp} \times Y_p^i + \Omega_1 \times \beta_1 * (P_{best} - X_p^i) + \Omega_2 \times \beta_2 \left(G_{best} - X_p^i \right) \tag{6.11}$$

$$\sum_{i=1}^{i_{max}} \sum_{p=1}^{p_{max}} X_p^{i+1} = X_p^i + Y_p^{i+1} \tag{6.12}$$

$$Cost\left(Y_p^i\right) = \frac{1}{2} \times \sum_{0}^{\tau} \left(e_{(vs\,h)}\right)^2 \tag{6.13}$$

In Eqs. (6.11) to (6.13), Ω_1 and Ω_2 are the personal and social acceleration parameters, respectively, α_{damp} is the damping inertia, p_{max} is the total swarm size (population), i_{max} is the maximum number of iterations, Y_p^i is the particle velocity and X_p^i is the particle position. The selected values for each parameter in Eqs. (6.11) and (6.12) are defined in Table 6.3.

Table 6.3 PSO Algorithm Parameters

Constants	Values
Acceleration parameter (Ω_1)	2
Acceleration parameter (Ω_2)	2
Inertia damping parameter (α_{damp})	0,99
Swarm Size (Total population) (p_{max})	500
Maximum number of the iterations (i_{max})	10
Lowest bound of searching range (X_{lo})	-1
Highest bound of searching range (X_{up})	1

iii. Finally, the weights connecting the rules layer to the output layer, denoted by $W_{r_{(1\times9)}}$, were updated with the initial values founded by the PSO, using a Back Propagation (BP) algorithm, as shown below.

$$W_r(t+1) = W_r(t) - \eta_{w_r} \Delta W_r \tag{6.14}$$

$$\tilde{F}_{(vs\,h)} = F_{(vs\,h)} - \hat{F}_{(vs\,h)} \tag{6.15}$$

$$\Delta W_r = \tilde{F}_{(vs\,h)} O_r \tag{6.16}$$

where $\eta_{w_r} = 0.7$ is the learning rate which was found after trying different values, $W_r(t)$ represents the current weights and $W_r(t+1)$ denotes the future value of the weights, and $\tilde{F}_{(vs,h)}$ is the error between the predicted signal $\hat{F}_{(vs,h)}$ and the reference signal $F_{(vs,h)}$. This training algorithm helps to update the approximated function with respect to the given reference online at each iteration. The reference signal in the VS controller was $F_{vs} = \dot{VS}$, and in the AH controller $F_h = \dot{h}$ measured from the nonlinear simulation platform for the CCX aircraft.

6.2.3 Design of the VS and AH Mode Control Systems

This section describes the control methodologies designed for the VS and AH modes. These controllers were developed based on a SMC system combined with PSO-based MFRNN approximators, as explained in the previous section. Furthermore, a novel transition algorithm was implemented using the FLS to switch between autopilot modes during the flight, thus efficiently to capture the altitude.

6.2.3.1 VS Mode Control System design

In the VS mode control system, a MFRNN-based sliding mode controller was proposed to force the aircraft to track the desired vertical speed. Accordingly, the tracking error $e_{vs} = VS - VS_{ref}$ given in Eq. (6.2) and its first-order derivative $\dot{e}_{vs}$ were used to define the sliding surface, given in Eq. (6.17) (Khalil, 2001):

$$S_{vs} = \dot{e}_{vs} + L_{vs} e_{vs} \tag{6.17}$$

where $L_{vs} > 0$.

Taking the first-order derivative of the sliding surface defined in Eq. (6.17), and knowing that $\ddot{e}_{vs} = \ddot{VS} - \ddot{VS}_{ref} = F_{vs} + u_{vs} + D - \ddot{VS}_{ref}$ from the state-space representation in Eq. (6.1), it gives:

$$\dot{S}_{vs} = \ddot{e}_{vs} + L_{vs}\dot{e}_{vs} = F_{vs} + u_{vs} + D - \ddot{VS}_{ref} + L_{vs}\dot{e}_{vs} \tag{6.18}$$

Therefore, the equivalent control law $u_{eq_{vs}}$ in the SMC system can be obtained by considering $\dot{S}_{vs} = 0$ (Khalil, 2001). In addition, the turbulence D is unknown, so $u_{eq_{vs}}$ becomes:

$$u_{eq_{vs}} = -F_{vs} + \ddot{VS}_{ref} - L_{vs}\dot{e}_{vs} \tag{6.19}$$

The switching control law $u_{sw_{vs}}$ was designed in its conventional form (Khalil, 2001), where sat stands for the saturation function, and $k_{vs} > 0$:

$$u_{sw_{vs}} = -k_{vs}sat(S_{vs}) \tag{6.20}$$

In Eq. (6.19), we assumed that F_{vs} is an unknown nonlinear function; therefore, it should be replaced with its approximated function $\hat{F}_{vs}$, as calculated with Eq. (6.10). Thus, the VS mode control law u_{vs}, using both Eqs. (6.19) and (6.20), becomes:

$$u_{vs} = u_{eq_{vs}} + u_{sw_{vs}} = -\hat{F}_{vs} + \ddot{VS}_{ref} - L_{vs}\dot{e}_{vs} - k_{vs}sat(S_{vs}) \tag{6.21}$$

To prove the stability of the system, the following Lyapunov candidate V_{vs} is defined (Khalil, 2001):

$$V_{vs} = \frac{1}{2}(S_{vs})^2 \tag{6.22}$$

Then, the derivative of the V_{vs} is calculated as given in Eq. (6.23), by using the expression of $\dot{S}_{vs}$ in Eq. (6.18) and by replacing u_{vs} with its expression in Eq. (6.21), as follows:

$$\dot{V}_{vs} = S_{vs}\dot{S}_{vs} = S_{vs}\left[F_{vs} + u_{vs} + D - \ddot{VS}_{ref} + L_{vs}\dot{e}_{vs}\right] = S_{vs}[F_{vs} - \hat{F}_{vs} + D - k_{vs}sat(S_{vs})] \tag{6.23}$$

In this equation, we assumed that F_{vs} and D are two unknown bounded functions such that $|F_{vs}| \leq F_{vs_{MAX}}$ and $|D| \leq D_{MAX}$ (Slotine & Li, 1991 ; C.-H. Wang et al., 2002 ; L.-X. Wang, 1997), where $F_{vs_{MAX}}$ and D_{MAX} are two positive values. Thus, due to the following aspects, $\hat{F}_{vs}(x_{vs})$ can be considered as a bounded function:

i. As presented in the membership layer of the MFRNN, we used two Gaussian memberhsip functions denoted by $\mu_{1m}(x)$ and $\mu_{2n}(x)$ in Eqs. (6.8.a) and (6.8.b), respectively. These membership functions are smooth that are naturally bounded and whose outputs change over a finite interval, meaning that they are bounded. These outputs are propagated to the next layer (the rules layer) which calculates the product of the received inputs.Thus, mathematically, the product of some bounded inputs is also bounded (Apostol, 1974).

ii. As explained in Section 6.2.2.1, the weights between the rules layer and the output layer are updated by $W_r(t+1) = W_r(t) - \eta_{w_r}\Delta W_r$ (see Eq. (6.14)). In this equation, η_{w_r} should be selected to be small enough to ensure that weights W_r are adjusted such that the error between the approximated function and its given reference is reduced over time.

iii. According to the explanations above and by knowing the boundedness of the output of the rule layer, we can conclude that $\hat{F}_{vs}$ also varies in a bounded interval, so that $\left|\hat{F}_{vs}\right| \leq Q_{vs_{MAX}}$, where $Q_{vs_{MAX}} > 0$.

Therefore, using the Triangle Inequality (Mitrinović, Pečarić, & Fink, 1993), we can write:

$$\left|F_{vs} - \hat{F}_{vs}\right| \leq |F_{vs}| + \left|-\hat{F}_{vs}\right| \tag{6.24}$$

where $|F_{vs}| \leq F_{vs_{MAX}}$ and $\left|\hat{F}_{vs}\right| \leq Q_{vs_{MAX}}$. Thus, $\left|F_{vs} - \hat{F}_{vs}\right| \leq F_{vs_{MAX}} + Q_{MAX} = \varepsilon_{vs}$ and ε_{vs} is a too small positive constant.

According to the proof of boundedness in Eq. (6.23), we can rewrite $\dot{V}_{vs}$ as follows:

$$\dot{V}_{vs} \leq |S_{vs}|\left|F_{vs} - \hat{F}_{vs}\right| + |S_{vs}||D| - k_{vs}|S_{vs}| \leq |S_{vs}|(\varepsilon_{vs} + D_{MAX} - k_{vs}) \tag{6.25}$$

So that:

$$\dot{V}_{vs} \leq |S_{vs}|(\varepsilon_{vs} + D_{MAX} - k_{vs}) \tag{6.26}$$

The expression in Eq. (6.26) indicates that for $k_{vs} > \varepsilon_{vs} + D_{MAX}$, there will be always $\dot{V}_{vs} < 0$, and therefore the proposed control system will be asymptotically stable.

□

6.2.3.2 AH Mode Control System Design

Similarly, the AH Mode Controller can be designed using the sliding surface defined in terms of the tracking error e_h in Eq. (6.3) and its first-order derivative $\dot{e}_h$, as follows (Khalil, 2001):

$$S_h = \dot{e}_h + L_h e_h \tag{6.27}$$

where L_h is a positive constant.

Taking the derivative of the sliding surface S_h, and using the state-space representation $\ddot{h}(x) = F_h + u_h + D$ according to Eq. (6.1), and the second order time derivative of the tracking error $\ddot{e}_h = \ddot{h} - \ddot{h}_{ref}$ from Eq. (6.3), the sliding surface derivative becomes:

$$\dot{S}_h = \ddot{e}_h + L_h \dot{e}_h = F_h + u_h + D - \ddot{h}_{ref} + L_h \dot{e}_h \tag{6.28}$$

As presented for the VS mode in Section 6.2.3.1, for the AH mode, the equivalent control term $u_{eq_h}$was designed using $\dot{S}_h = 0$ (Khalil, 2001), which lead to the final form of the control law u_h:

$$u_h = u_{eq_h} + u_{sw_h} = \underbrace{-\hat{F}_h + \ddot{h}_{ref} - L_h\dot{e}_h}_{u_{eq_h}} \underbrace{-k_h sat(S_h)}_{u_{sw_h}} \tag{6.29}$$

To prove the stability of the control law in Eq. (6.29), the Lyapunov candidate in Eq. (6.30) and its derivative in Eqs. (6.31) and (6.32) become (Khalil, 2001).

$$V_h = \frac{1}{2}(S_h)^2 \tag{6.30}$$

$$\dot{V}_h = S_h\dot{S}_h = S_h\left[F_h + u_h + D - \ddot{h}_{ref} + L_h\dot{e}_h\right] \tag{6.31}$$

$$\dot{V}_h = S_h\left[F_h - \hat{F}_h + D - k_h sat(S_h)\right] \tag{6.32}$$

The same calculations were applied for the AH mode controller as for the VS mode controller. Replacing u_h in Eq. (6.31) with its expression given in Eq. (6.29) and knowing that $\left|F_h - \hat{F}_h\right| \leq F_{h_{MAX}} + Q_{h_{MAX}} = \varepsilon_h$, which was calculated from the Triangle inequality (Mitrinović et al., 1993) (with $|F_h| \leq F_{h_{MAX}}$ and $\left|\hat{F}_h\right| \leq Q_{h_{MAX}}$, where $F_{h_{MAX}}$ and $Q_{h_{MAX}}$ are positive values and $|sat(S_h)| \leq |S_h|$), the final expression of $\dot{V}_h$ is obtained as shown in Eq. (6.33):

$$\dot{V}_h \leq |S_h|(\varepsilon_h + D_{MAX} - k_h) \tag{6.33}$$

Similarly, with respect to the expression in Eq. (6.33) and with $k_h > \varepsilon_h + D_{MAX}$, it can be concluded that $\dot{V}_h < 0$, representing the asymptotical stability of the proposed control methodology for the AH mode system.

□

To ensure the appropriate transition between the VS and AH modes, a new algorithm was developed to switch between these modes and is described next in Section 6.2.4.

6.2.4 FLS-Based Autopilot Mode Transition Algorithm

This section presents a novel mode transition algorithm based on the FLS to make smooth transition between modes. Using this transition algorithm, when the aircraft climbs or descends to the pilot's commanded altitude, as soon as it reaches a specific distance (Δh) from this commanded altitude, the transition algorithm switches from the VS mode to the AH mode. Once the aircraft reaches this distance, the AH control system tries to maintain the commanded altitude, preventing the aircraft from climbing further or descending to lower altitudes.

As explained in (Ghazi, 2014) , the distance at which the AH mode becomes engaged can be calculated with in Eq. (6.34):

$$\Delta h = h_{ref} - h_{trans} = \left(\frac{{VS_{ref}}^2}{0{,}05 \times g}\right)\left(\frac{e-1}{e}\right) \tag{6.34}$$

where $g \approx 9.81$ is the gravitational acceleration.

This fuzzy logic transition algorithm is the core decision-making component in this autopilot system, which switches between its modes. As shown in Fig. 6.4, an FLS is composed of four main components: 1) Fuzzifier, 2) Fuzzy Rule Base, 3) Inference Engine, and 4) Defuzzifier. These components are explained in details in (L.-X. Wang, 1997).

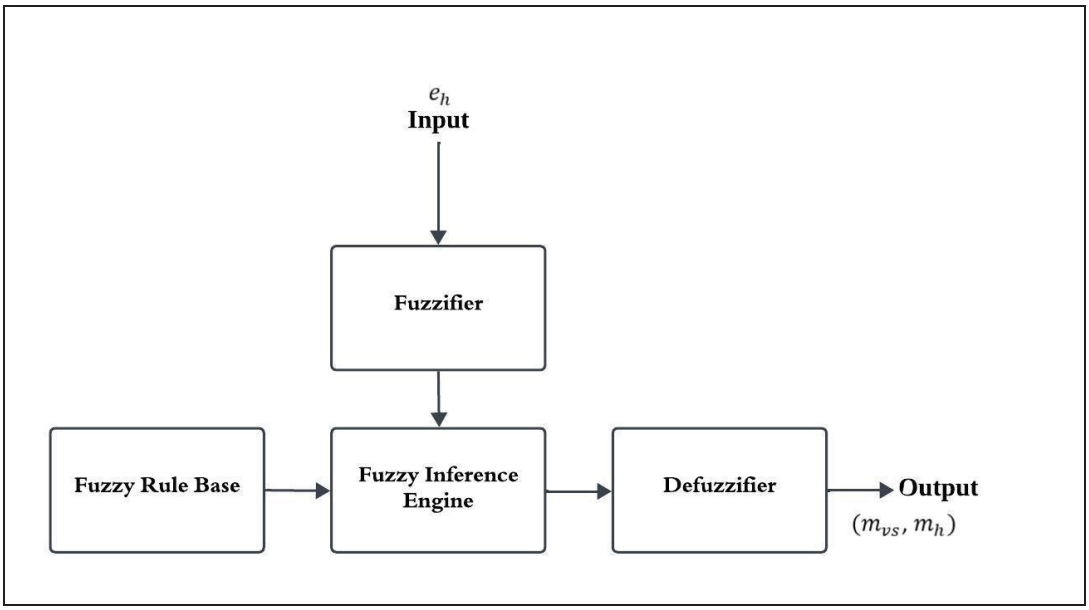

Figure 6.4 Main Components of the FLS

In this algorithm, we used the altitude tracking error e_h in Eq. (6.3) as the input that was given to the FLS. This variable was fuzzified using three different membership functions defined by some linguistic variables such as “Negative High Error (NHE)”, “Medium Error (ME)”, and “Positive High Error (PHE)”. Regarding these linguistic variables, we defined a minimum number of fuzzy rules to simplify the design of the FLS. In addition, the outputs were selected by two singleton values between 0 and 1 for each m_{vs} and m_h coefficient. The equations of each membership function are presented in Eqs. (6.35.a) to (6.35.c):

$$\mu_{\mathrm{NHE}}(e_h\ a_1\ a_2\ a_3\ a_4) = \begin{cases} 0 & if\ e_h < a_1 \\ \dfrac{e_h - a_1}{a_2 - a_1} & if\ a_1 \le e_h \le a_2 \\ 1 & if\ a_2 \le e_h \le a_3 \\ \dfrac{a_4 - e_h}{a_4 - a_3} & if\ a_3 \le e_h \le a_4 \\ 0 & if\ e_h < a_4 \end{cases} \tag{6.35.a}$$

$$\mu_{\mathrm{ME}}(e_h\ b_1\ b_2\ b_3) = \begin{cases} 0 & if\ e_h < b_1 \\ \dfrac{e_h - b_1}{b_2 - b_1} & if\ b_1 \le e_h \le b_2 \\ \dfrac{b_3 - e_h}{b_3 - b_2} & if\ b_2 \le e_h \le b_3 \\ 0 & if\ e_h > b_3 \end{cases} \tag{6.35.b}$$

$$\mu_{\mathrm{PHE}}(e_h\ c_1\ c_2\ c_3\ c_4) = \begin{cases} 0 & if\ e_h < c_1 \\ \dfrac{e_h - c_1}{c_2 - c_1} & if\ c_1 \le e_h \le c_2 \\ 1 & if\ c_2 \le e_h \le c_3 \\ \dfrac{c_4 - e_h}{c_4 - c_3} & if\ c_3 \le e_h \le c_4 \\ 0 & if\ e_h > c_4 \end{cases} \tag{6.35.c}$$

The parameters values selected for each membership function are presented in Table 6.4.

Table 6.4 Parameter Values of the Membership Functions in the Transition Algorithm

μ_{NHE}		μ_{ME}		μ_{PHE}	
Constant	Value	Constant	Value	Constant	Value
a_1	-51000	b_1	$-h_{trans}$	c_1	0
a_2	-50000	b_2	0	c_2	h_{trans}
a_3	$-h_{trans}$	b_3	h_{trans}	c_3	50000
a_4	0			c_4	51000

The values of h_{trans} were calculated in accordance with the variations of VS_{ref}, as shown in Eq. (6.34). After fuzzifying the altitude tracking error e_h using the membership functions in Eqs. (6.35.a) to (6.35.c), the fuzzy rules should be defined to specify the relationship between the input and the outputs in this FLS. These fuzzy rules were proposed using a single input e_h and multiple outputs such as m_{vs} and m_h. Applying each linguistic variables shown by "*NHE*", "*ME*" and "*PHE*", we defined two combined *IF-THEN* fuzzy rules, as follows:

- Rule 1. *IF* $\boldsymbol{e_h}$ is **NHE** *OR* $\boldsymbol{e_h}$ is **PHE** *THEN* $\boldsymbol{m_{vs}}$ is **Activated**
- Rule 2. *IF* $\boldsymbol{e_h}$ is **ME** *AND NOT* **NHE** *OR IF* $\boldsymbol{e_h}$ is $\boldsymbol{ME}$ *AND NOT* **PHE** *THEN* $\boldsymbol{m_h}$ is **Activated**

Typically, in an FLS, the operator "*AND*" is implemented by the "min" function, and "*NOT*" is a complement operator that can be expressed by "$1-\mu$". The relationship between the antecedent (*IF*-part) and the consequent (*THEN*-part) parts was aggregated using the "*OR*" operator implemented by the "max" function (L.-X. Wang, 1997). Therefore, the rules 1 and 2, given above, were defined as shown in Eqs. (6.36) and (6.37):

$$m_{vs} = max[min(\mu_{NHE}\ 1)\ \ min(\mu_{PHE}\ 1)] \tag{6.36}$$

$$m_h = max[min(\mu_{\mathrm{ME}}\ 1-\mu_{NHE})\ \ min\ (\mu_{\mathrm{ME}}\ 1-\mu_{PHE})] \tag{6.37}$$

By using this algorithm, at each time, one of the coefficients m_{vs} and m_h will be active with values between 0 and 1. Hence, the final control law u_{AT} was developed for the autopilot system with Eq. (6.38), using the values obtained from Eqs. (6.36) and (6.37) for each m_{vs} and m_h, respectively:

$$u_{AT} = m_{vs}g_{vs}u_{vs} + m_h g_h u_h \tag{6.38}$$

where $g_{vs}, g_h > 0$.

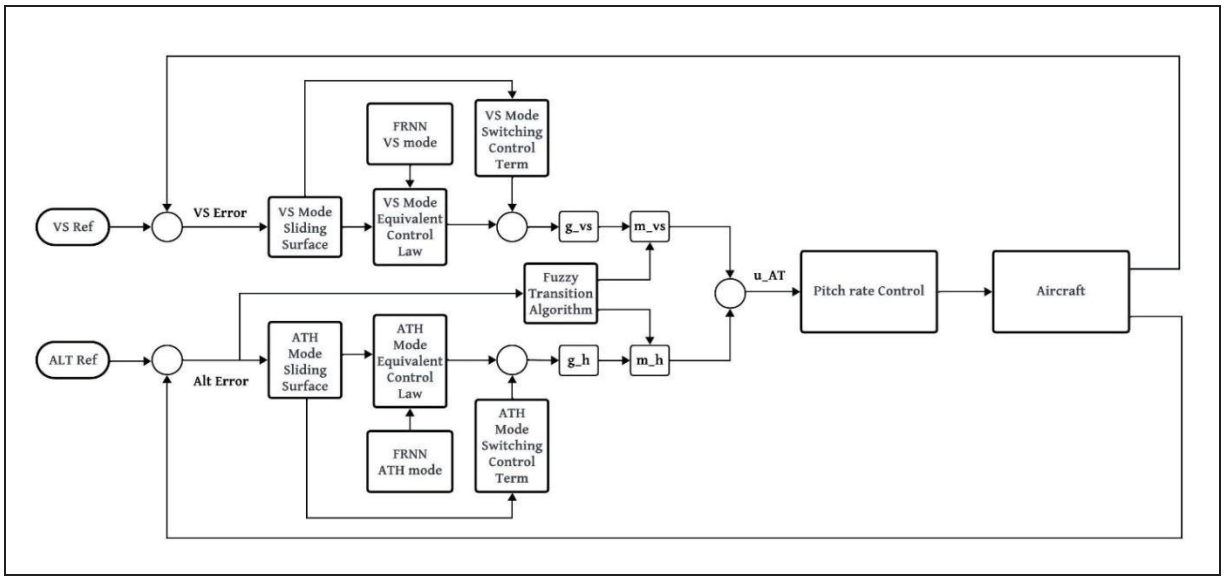

Figure 6.5 Block Diagram of the Developed Autopilot System

Fig. 6.5 illustrates the main architecture of the developed autopilot system in this article, where u_{AT} acts as the reference pitch rate signal given to the pitch rate controller in the inner loop. The pitch rate controller was designed by using a new T1AFSMC methodology, developed by researchers at LARCASE and published in (Seyed Mohammad Hosseini, Ghazi, et al., 2024b).

6.2.5 Turbulence Model

The Dryden Turbulence Model is commonly used in Aerospace and Aeronautics Engineering to simulate the atmospheric gusts and turbulence that an aircraft may encounter during flight. This realistic representation of atmospheric turbulence helps to evaluate the safety and performance of the proposed control system. We used the MATLAB/Simulink aerospace environment blockset configured according to MIL-F-8785C. In this configuration, the probability of the exceedance of high-altitude intensity was selected as moderate (10^{-3}). The turbulence intensity varies with altitude, and it is influenced by the probability of exceeding (Moorhouse & Woodcock, 1982).

6.3 Results

This section presents the experimental results obtained from a high-fidelity nonlinear simulation platform developed for the CCX aircraft, as well as comprehensive analysis using the methodologies proposed in this article for the design of the autopilot system. This platform was initialized by the parameters given in Table 6.5 to generate a total of 925 different flight conditions, covering the entire flight envelope of the CCX.

Table 6.5 Parameters for Selecting 925 Flight Conditions

Altitude (ft)	CAS (kts)	Xcg (% MAC)	Weight (lbs)
8000	180	24	26000
10000	200	26	27000
15000	230	28	28000
20000	250	30	29000
25000	300	32	30000
30000	330		
35000			
38000			
42000			

The pitch rate control system in the inner loop of this autopilot system was designed using the T1AFSMC presented in (Seyed Mohammad Hosseini, Ghazi, et al., 2024b), whose parameters are given in Table 6.6.

Table 6.6 Parameters of the Pitch Rate Control System (T1AFSMC)

Parameters	Values
Sliding Surface Coefficient (C)	1.3
Adaptation Law Parameter (σ_f)	10^{-4}
Adaptation Law Parameter (σ_g)	10^{-4}
Adaptation Law Parameter (γ_f)	100
Adaptation Law Parameter (γ_g)	100
Switching Control Gain (L)	550
Integral Control Gain (k)	5500

In addition, the other parameters values in the proposed autopilot control laws, given in Eqs. (6.21), (6.29) and (6.38) are shown in Table 6.7:

Table 6.7 Design Parameters of the Autopilot Control Laws

Mode	Parameter	Value	Mode	Parameter	Value
VS Mode	L_{vs}	5.3	AH Mode	L_h	5.5
	k_{vs}	1.3		k_h	0.8
	g_{vs}	0.085		g_h	0.085

To achieve our first control objective, which is to satisfy the tracking performance of both autopilot modes in ideal flight conditions (without turbulence), the following flight scenario was considered:

i. VS Mode Control: In this mode, the desired vertical speed was set to 9 m/s (≈1800 ft/min) to specify the Rate Of Climb (ROC).

ii. We equalized the desired altitude h_{ref} to $h_{trim} + 1000$ meters (≈3280 ft), where h_{trim} is the aircraft initial altitude in the beginning of a simulation and varies at each flight condition. In this scenario, the aircraft started climbing at the commanded vertical speed. As soon as the aircraft arrived at a specified altitude

($h_{ref} \pm h_{trans}$), the transition algorithm automatically engaged the AH mode to capture and maintain the desired altitude h_{ref}.

iii. After 500 secs, we set the desired rate of descent was set to 5 m/s (≈1000 ft/min), and then the desired altitude h_{ref} was changed to $h_{trim} + 300$ meters (≈984 ft), meaning that the aircraft descended by 700 meters (≈ 2296 ft) with respect to the previous reference altitude h_{ref} in the climb maneuver.

The obtained results for the scenario described above are shown in Figs. 6.6 to 6.11. For the VS mode, we have chosen the climbing rate at 9 m/s (≈1800 ft/min). This rate was immediately increased to reach the desired vertical speed. Once the aircraft reached the desired climbing rate, it maintained the desired vertical speed until it reached a distance h_{trans} from the desired altitude that was calculated using Eq. (6.34). At this point, the VS mode control system was desactivated (the VS signal returned to zero). During the climb, the VS mode remained engaged until $t = 106$ sec, and then it was reactivated between $t = 500$ sec and $t = 638$ sec for the descent maneuver. The AH mode was engaged outside of these periods during the simulation. As shown in Figs. 6.6 and 6.7, at $t = 500$ sec, a descent command was issued, making the AH mode inactive, and the VS started to decrease to 5 m/s (≈1000 ft/min). As the aircraft achieved the desired descent rate, it remained within an interval of $h_{ref} \pm h_{trans}$, where the AH mode was activated. Figs. 6.6 and 6.7 represent the results for the time variations of the aircraft vertical speed, and the aircraft altitude for flight conditions with altitudes a) 8000, 10000, and 15000 ft, b) 20000, 25000, and 30000 ft, and c) 35000, 38000, and 42000 ft.

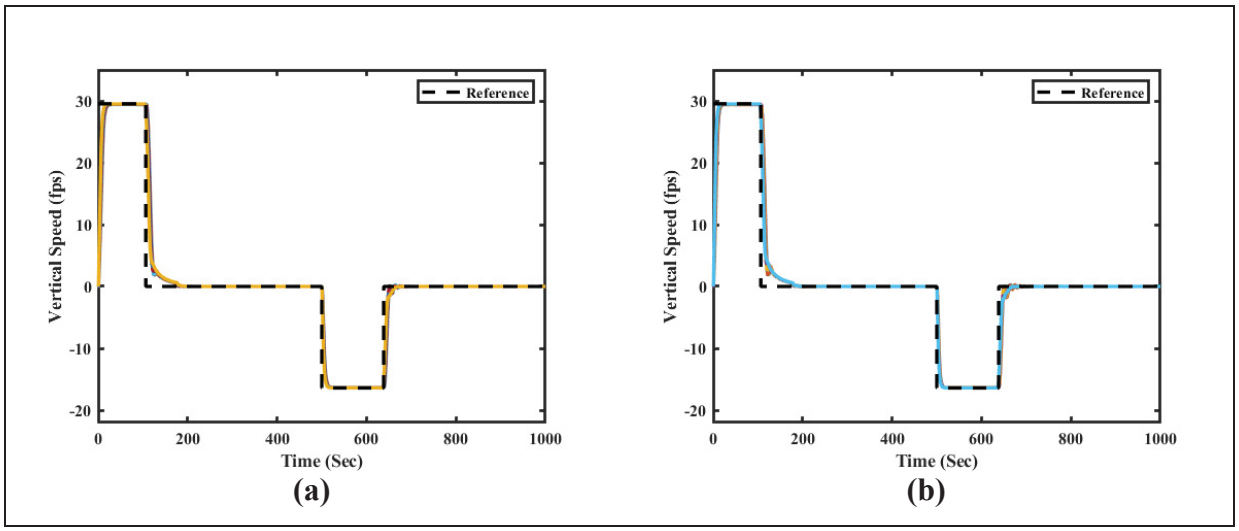

Figure 6.6 VS Time Variations at the Altitudes a) 8000 to 15000 b) 20000 to 30000 and c) 35000 to 42000 ft without Turbulence

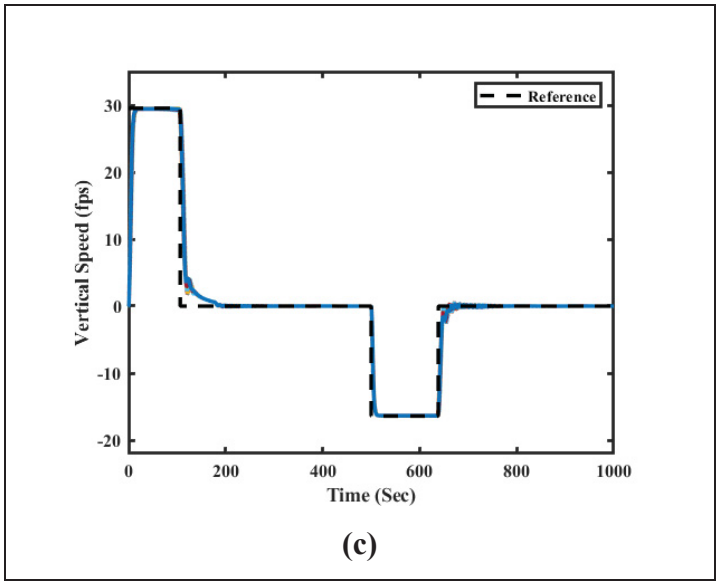

Figure 6.6 VS Time Variations at the Altitudes c) 35000 to 42000 ft without Turbulence

The initial altitude values at each flight condition were different; therefore, for the sake of clarity in the presentation of our results, we superposed all altitude signals to start from zero in Fig. 6.7. In addition, Fig. 6.7 shows the variations of aircraft altitude according to the performance of the VS mode and the AH mode controllers. The dashed blue lines in Fig. 6.7

depict the altitude range ($h_{ref} \pm h_{trans}$) where the AH mode was engaged (between the blue lines); outside of this range, the VS mode control system became engaged. Fig. 6.7 clearly shows how the width of the region varied with respect to the variations of the VS_{ref}.

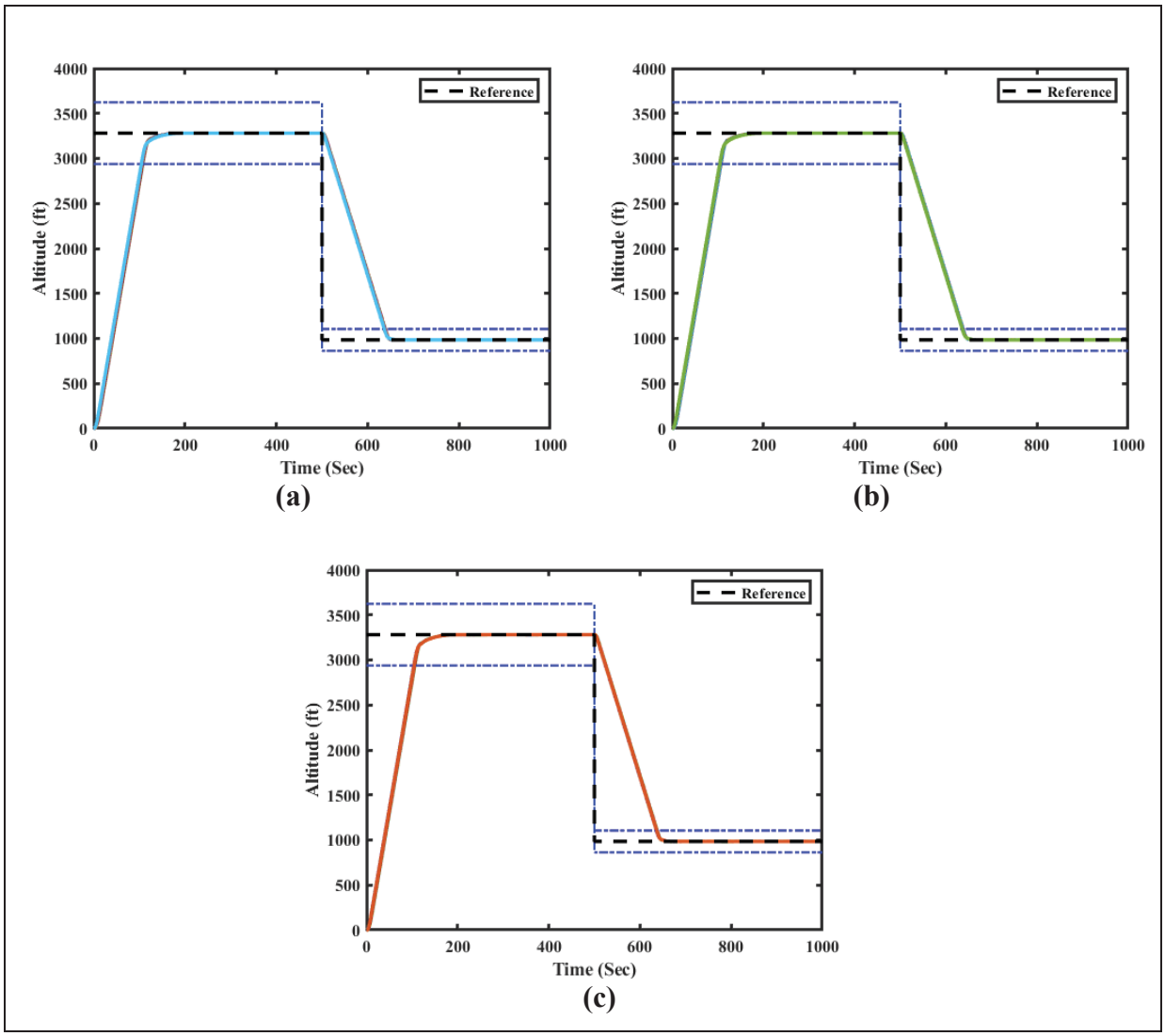

Figure 6.7 Altitude Time Variations at Altitudes a) 8000 to 15000 ft, b) 20000 to 30000 ft, and c) 35000-to 42000 ft without Turbulence

The results in Figs. 6.6 and 6.7 demonstrate the excellent performance of the proposed autopilot system under ideal flight conditions, with no oscillations or overshoots. The variations of the altitude signal also showed that the aircraft successfully captured the commanded altitude h_{ref} using the proposed controllers, and that it was adequately

stabilized at the altitude reference signal over the time. A detailed analysis of these results is presented in Fig. 6.8 to illustrate the performance of the fuzzy logic-based transition algorithm described in section 6.2.4.

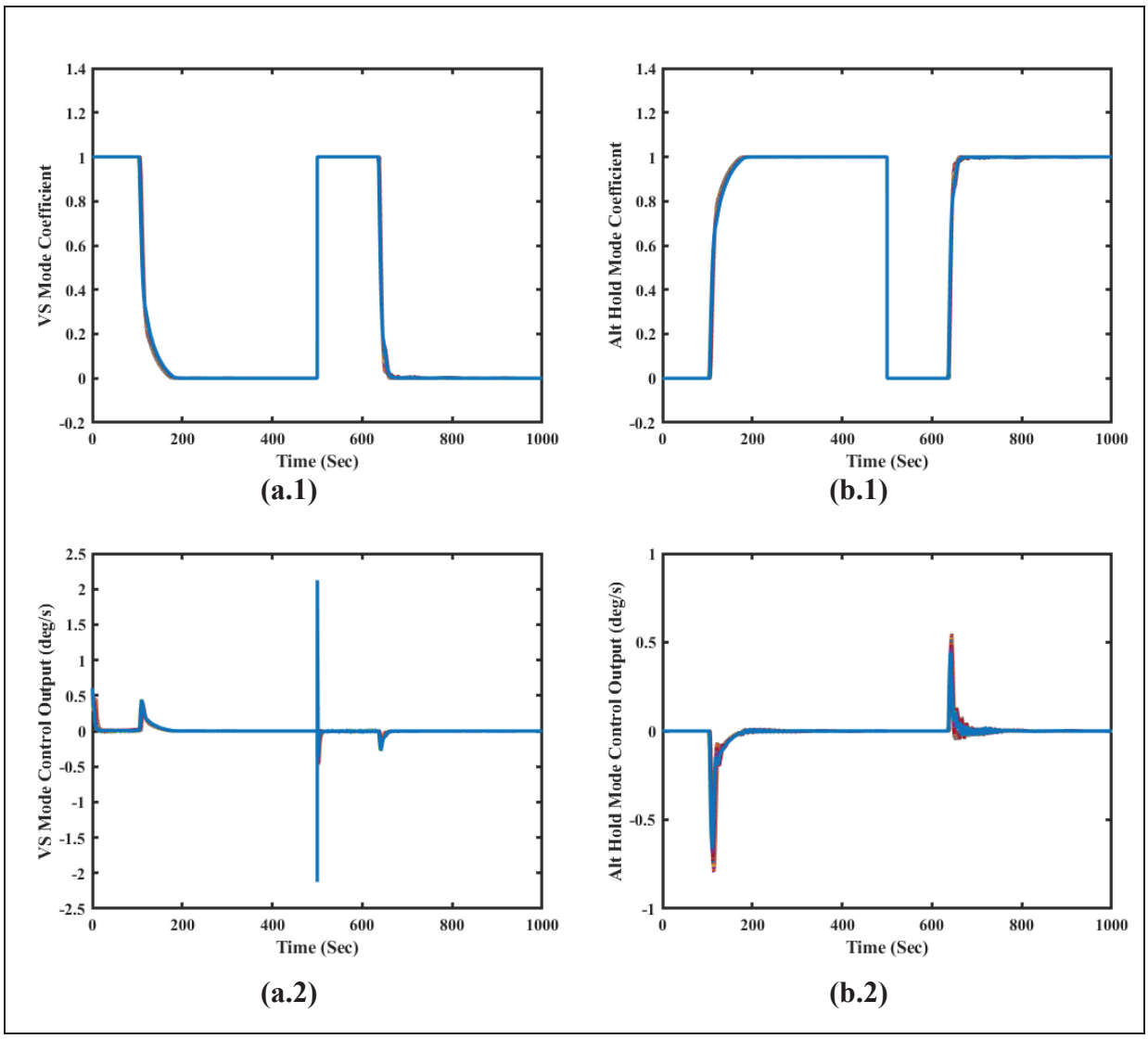

Figure 6.8 Time Variations of the Coefficients m_{vs} and m_h (in (a.1) and (b.1), respectively), and of the signals: a.2) $m_{vs}u_{vs}$ and b.2) $m_h u_h$, without Turbulence

The procedure implemented by the proposed fuzzy logic-based transition algorithm is illustrated in Fig. 8(a.1), showing the variations of the m_{vs}, while Fig. 6.8(a.2) illustrates the controller output ($m_{vs}u_{vs}$) for the VS mode control system. The variations for the AH control system are shown in Figs. 6.8(b.1) and 6.8(b.2). In these figures, when the VS mode

controller or the AH mode controller is engaged, m_{vs} and m_h , respectively, are equal to 1, and when they are not engaged, they decrease to 0. Due to the abrupt variations of m_{vs} and m_h, there are some spikes on the signals in Fig. 6.8(a.2), e.g., at $t = 500$ sec, and in Fig. 6.8(b.2) at $t = 638$ sec. To smooth out these signals, we used a filter to produce an input that could be easily handled by the pitch rate control system in the inner loop of the proposed autopilot system (see Eq. (6.39). It should be mentioned that the sum of the control signals u_{vs} and u_h generated by $u_{AT} = q_{ref}$, which was calculated in Eq. (6.38), is reference pitch rate signal (deg/s) controlled by the T1AFSMC.

$$\frac{q_{ref}}{r} = \frac{\omega_n^2}{s^2 + 2\xi\omega_n s + \omega_n^2} \tag{6.39}$$

In Eq. (6.39), $\omega_n = 3$ rad/s is the natural frequency and $\xi = 0.7$ is the damping ratio.

Thus, the obtained pitch rate signal used in the inner loop of the autopilot system is presented in Fig. 6.9, for altitudes 8000, 10000, 15000, and 20000 ft, and for altitudes 25000, 30000, 35000, 38000, and 42000 ft in Fig. 6.10.

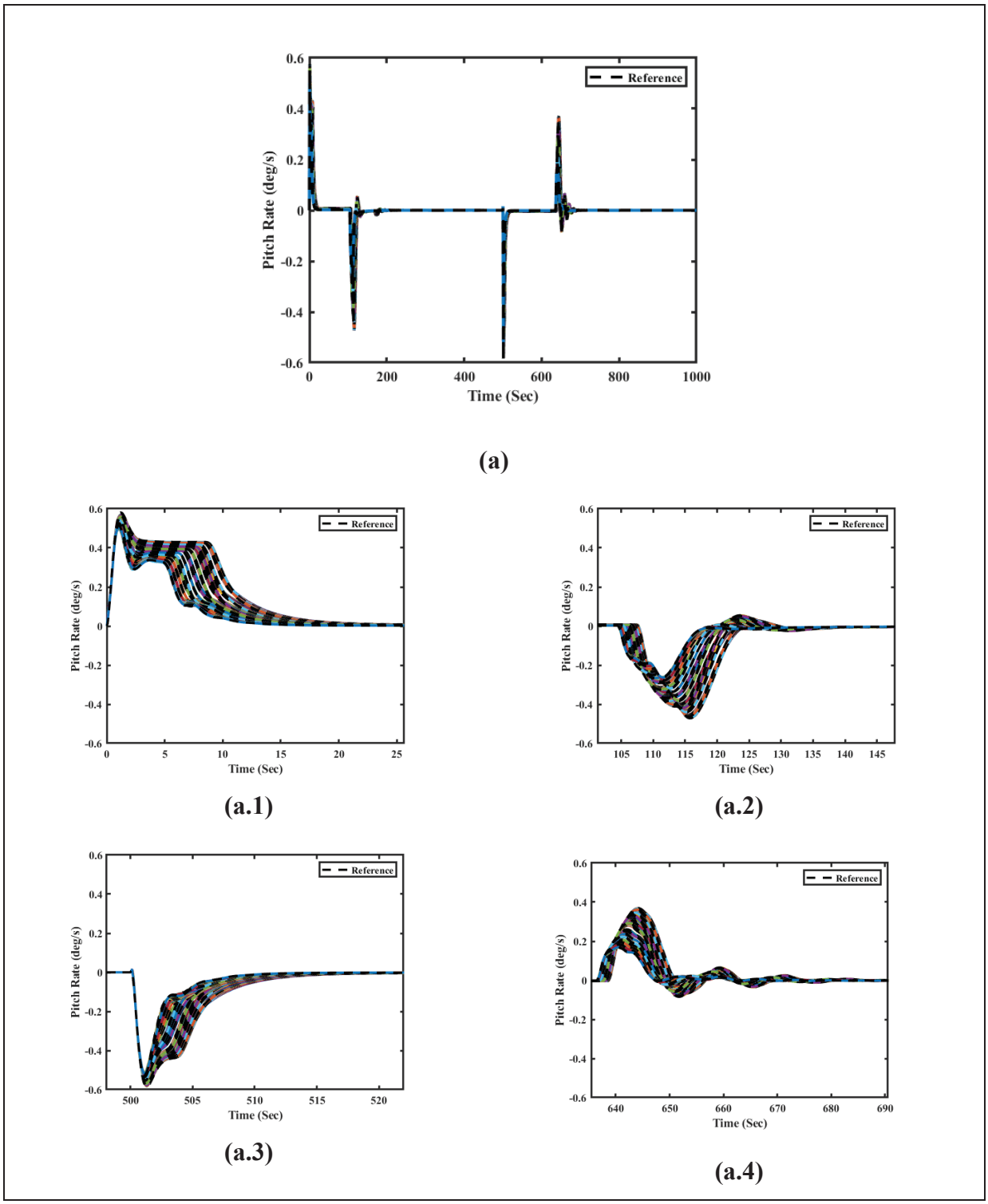

Figure 6.9 Time Variations of the Pitch Rate Reference at the altitudes of 8000, 10000, 15000, and 20000 ft without Turbulence

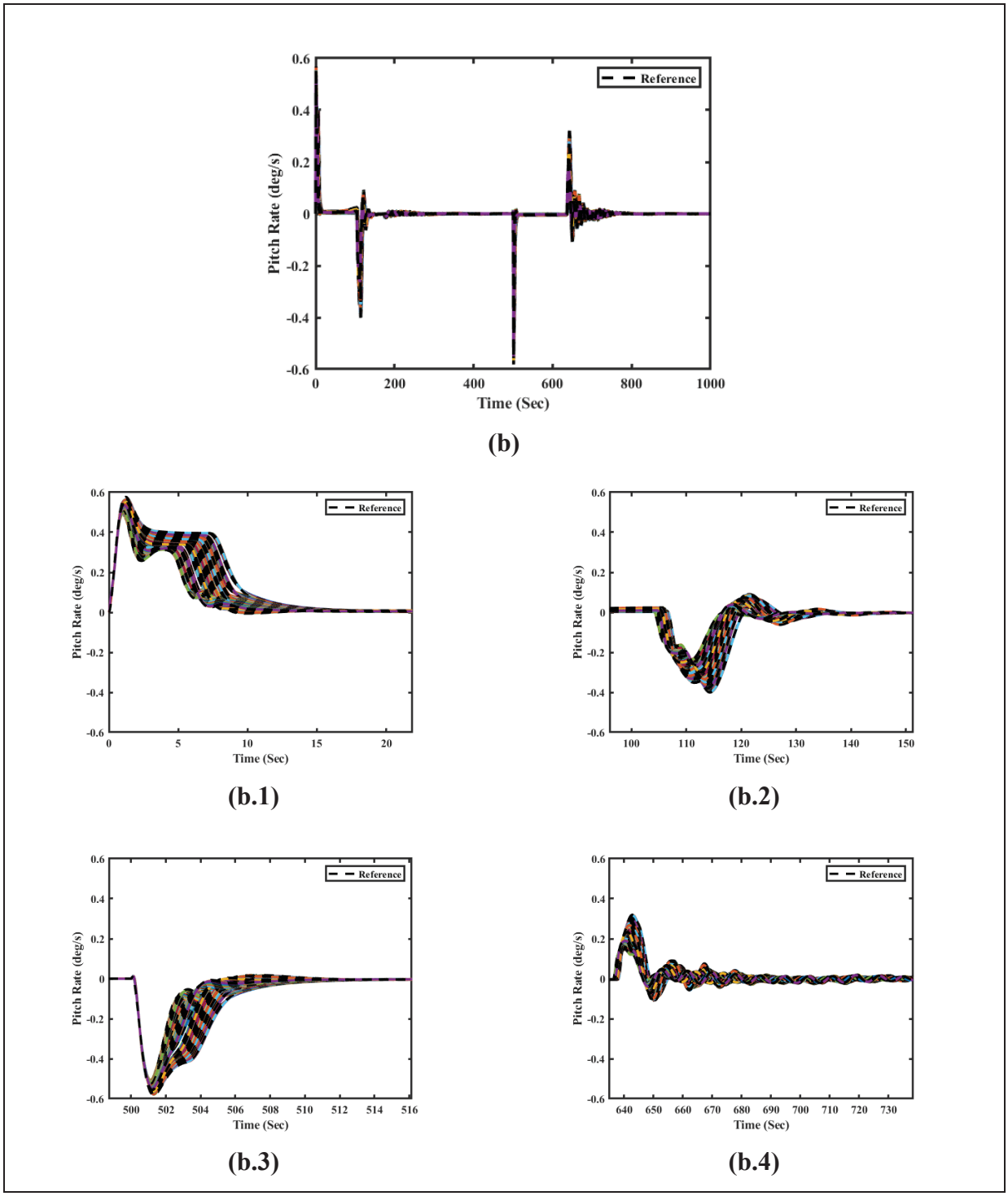

Figure 6.10 Time Variations of the Pitch Rate Reference at 25000, 30000, 35000, 38000, and 42000 ft without Turbulence

The pitch rate reference signals shown in Figs. 6.9 and 6.10 for all 925 flight conditions were zoomed out in Figs. 6.9(a.1) to 6.9(a.4) and Figs. 6.10(b.1) to 6.10(b.4) to represent the smoothness of the pitch rate reference signal produced by the filter in Eq. (6.39).

Another goal considered in the design of the autopilot control system was to generate elevator control signals without high-frequency oscillations to avoid mechanical damages to the elevator actuators. This characteristic can be clearly seen in Fig. 6.11 for the elevator deflections across all 925 flight conditions.

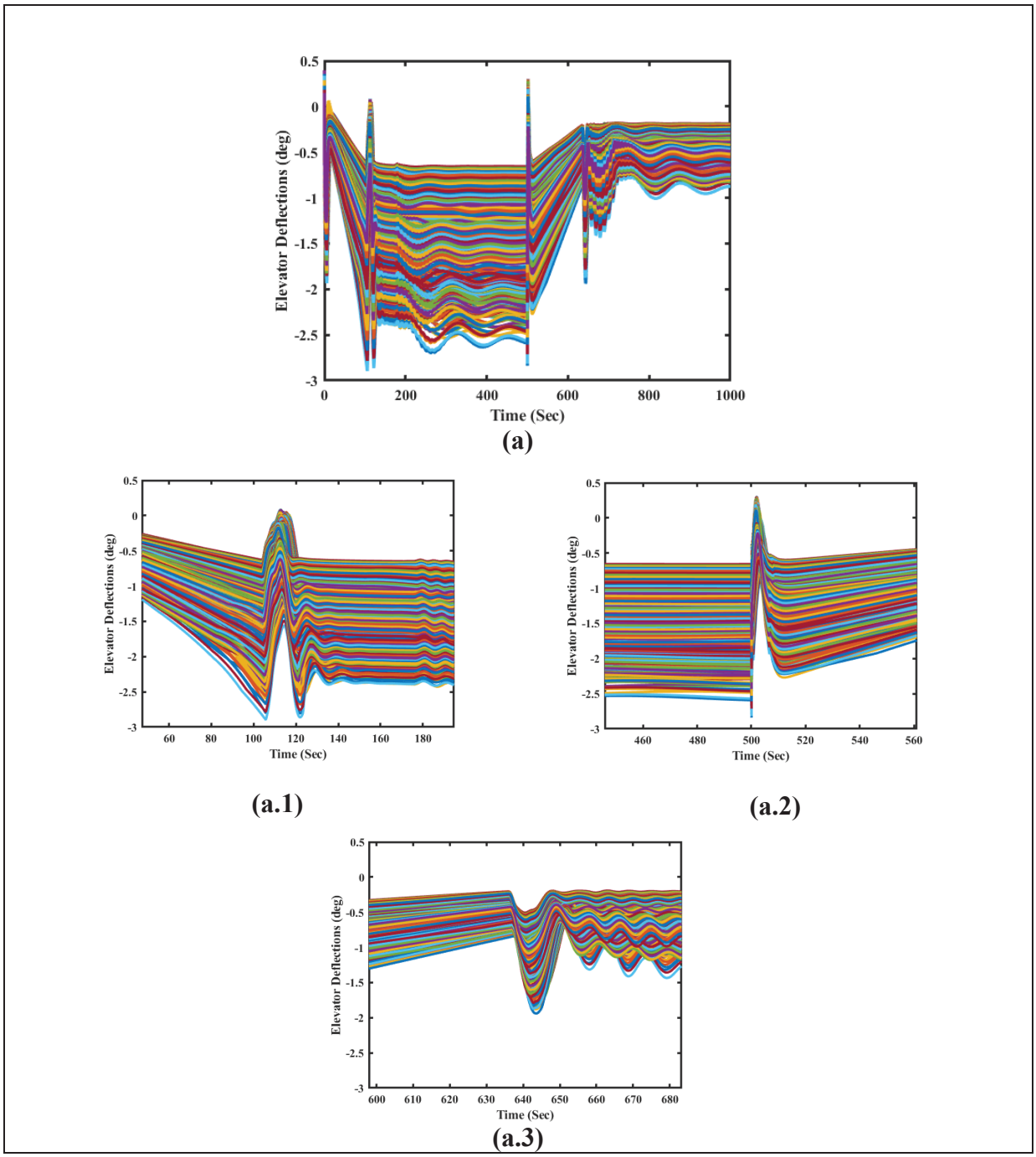

Figure 6.11 Time Variations of the Elevator Deflections without Turbulence

To evaluate the performance of our autopilot system in critical flight conditions and to provide evidence of the validity of our proposed methodologies, further simulations were performed in the presence of the moderate-intensity turbulence (10^{-3}) during flight.

For this purpose, another flight scenario was defined in which the aircraft was climbing to a specific altitude and then maintained that altitude. The results shown in Fig. 6.12 and Fig. 6.13 indicated that the VS mode controller remained activated until the aircraft reached the transition altitude h_{trans} represented by the blue line (used to calculate the distance Δh in Eq. (6.34)). At this point, the transition algorithm automatically engaged the AH mode control system to maintain the aircraft at the specified reference altitude, even in the presence of the turbulence effects.

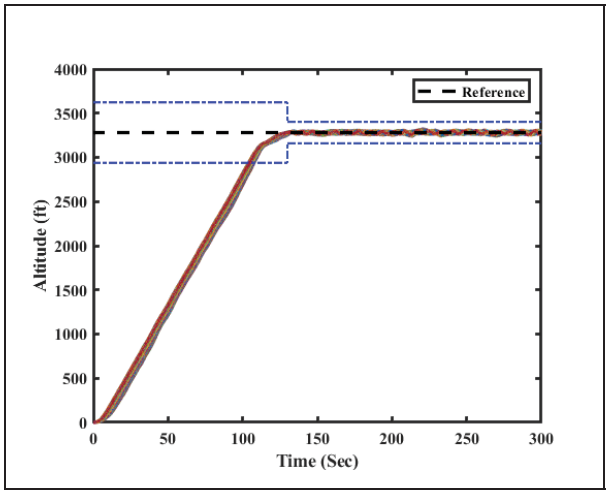

Figure 6.12 Time Variations of the Aircraft Altitude under Turbulence

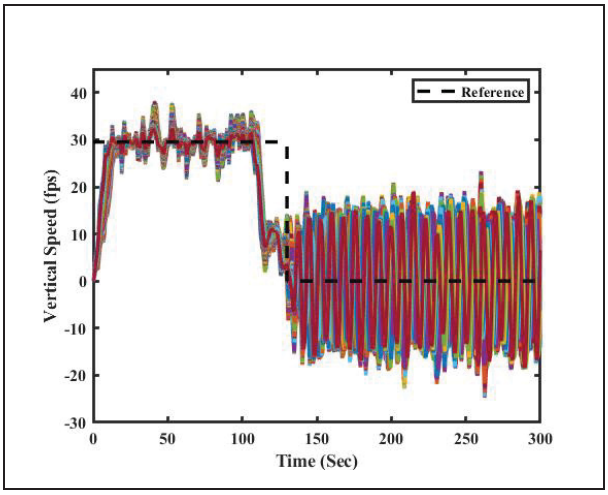

Figure 6.13 Time Variations of the Aircraft Vertical Speed under Turbulence

Fig. 6.13 also shows that the VS mode control system could track the given VS reference with a small number of oscillations with the least possible amplitudes, which are acceptable in this research (when the VS mode was engaged between $t = 0$ sec and $t = 105$ sec). It should be noted that the oscillations after the activation of the AH mode control system following to the absence of the aircraft VS control system. The oscillations from $t = 105$ sec to $t = 300$ sec on the vertical speed signal were induced by the turbulence which is natural and expected as the VS mode control system is not active to directly dampen these fluctuations. Instead in this period, the AH mode was active in the autopilot system and the aircraft altitude was stabilized and controlled with too small oscillations, as shown in Fig. 6.12.

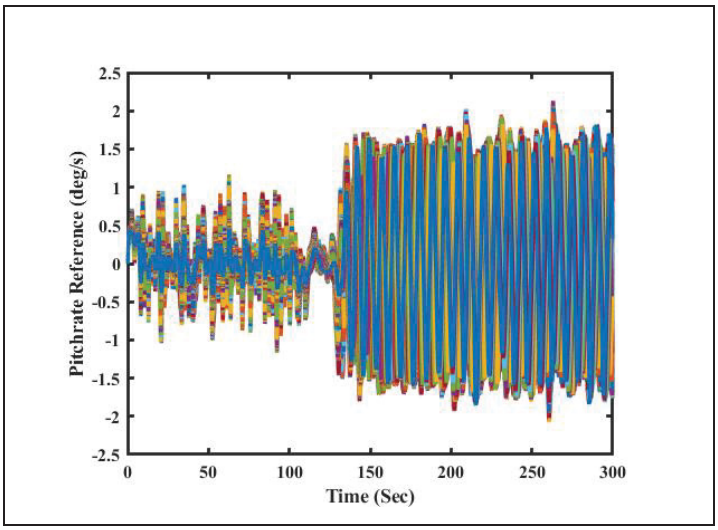

Figure 6.14 Time Variations of the Pitch Rate Reference at 925 Flight Conditions under Turbulence

Accordingly, the control signal generated by the autpilot, which is the aircraft pitch rate reference used in the inner loop, is shown in Fig. 6.14. This signal varied within a bounded interval in response to the turbulence. The observed oscillations are expected to result from the turbulence-induced effects on the aircraft vertical speed and altitude.

Previously, we analyzed the performance of the aircraft autopilot control systems under both turbulent and non-turbulent conditions and assessed the validity of the results. Furthermore, the performances of the VS and AH controllers were also validated in terms of tracking error values, calculated by Mean Absolute Error (MAE) metric with and without turbulence. Table 8 shows the flight condition numbers related to each altitude range at all 925 Flight Conditions (F.C) that were used in Figures. 15 and 16, to examine the precision and the accuracy of the tracking performance of the autopilot system at different altitudes.

Table 6.8 Distributions of the Flight Conditions in Terms of Alttiudes Authorized in the CCX Flight Envelope

F.C No	1-75	76-175	176-300	301-425	426-550	551-675	696-775	776-850	851-925
Altitudes	8000	10000	15000	20000	25000	30000	35000	38000	42000

Fig. 6.15(a) presents the MAE values for the VS mode calculated with respect to the time variations of the VS signals in Fig. 6.6. Similarly, Fig. 6.15(b) presents the MAE values for the AH mode calculated with respect to the time variations of the altitude signals in Fig. 6.7. In both figures, the black lines depict the MAE values during the climb maneuver, and the red lines show the MAE values for each flight condition range during the descent.

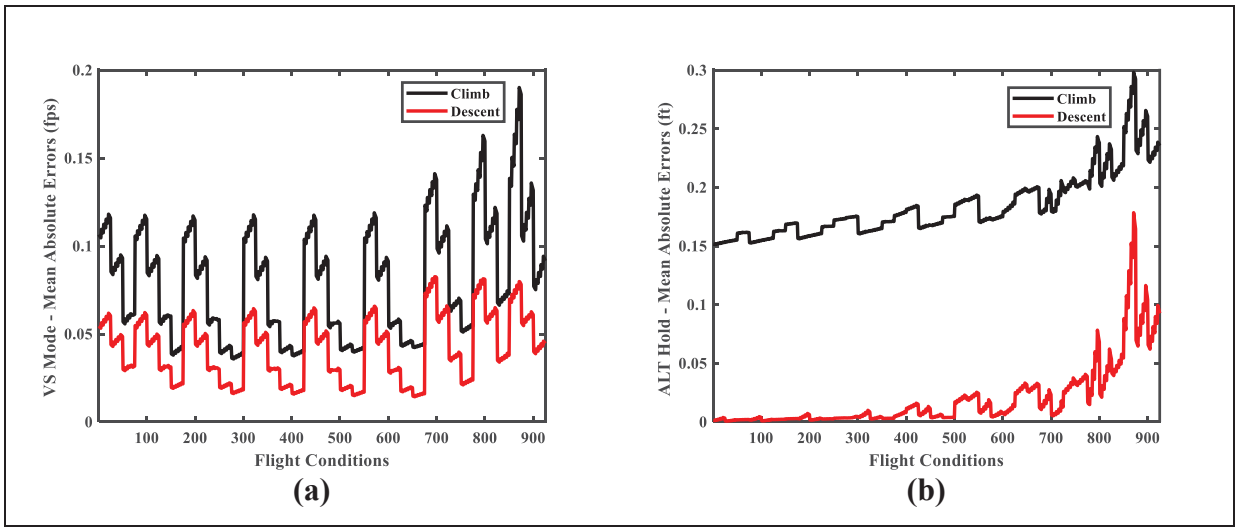

Figure 6.15 MAE Values at Each Flight Condition for (a) VS Mode and (b) AH Mode without Turbulence

The MAE values shown in Figs. 6.15(a) and 6.15(b) demonstrated that the proposed controllers for both autopilot modes have negligible error values under all flight conditions without turbulence, indicating that the aircraft VS and AH controllers could track very well their commanded reference values.

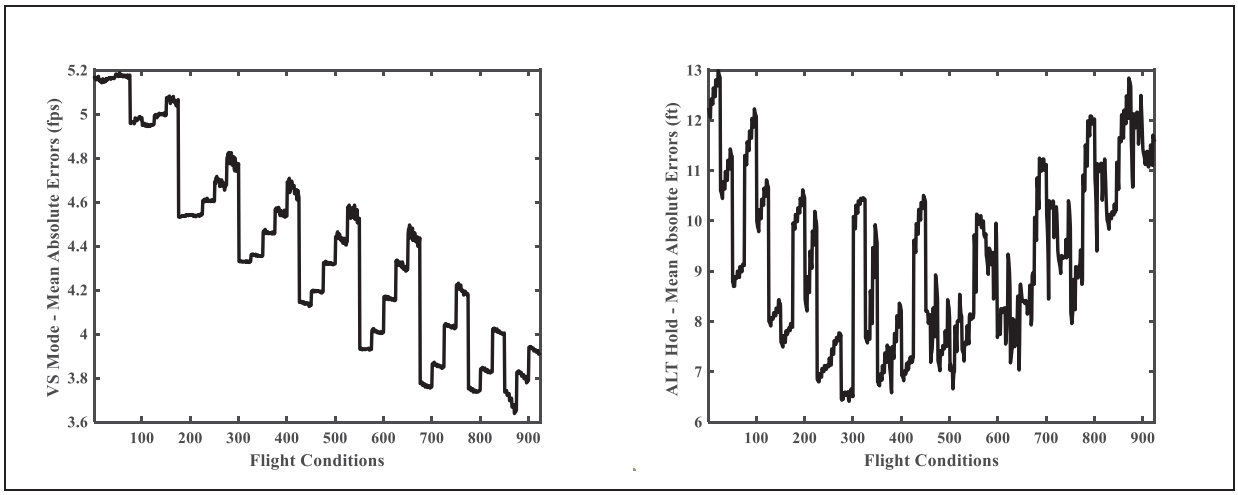

Figure 6.16 MAE Values at Each Flight Condition for (a) VS Mode and (b) AH Mode under Turbulence

The MAE values presented in Figs. 6.16(a) and 6.16(b) provide more details about the results presented in Figs. 6.12 and 6.13. The ranges of the MAE values shown in Fig. 6.16 for both VS and AH modes are acceptable in the presence of moderate-intensity (10^{-3}) turbulence for the scope of this research. In addition, for the VS mode, Fig. 6.16(a) shows that the developed controller could perform better at higher altitudes than at lower ones, as MAE values decreased as the altitude increased from the first flight condition to the 925th, referring to Table 6.8.

6.4 Conclusion

This article proposed applying a hybrid control system constructed by use of Multilayer Fuzzy Recurrent Neural Networks (MFRNNs) as approximators for the aircraft dynamics, and a multi-modal Sliding Mode Control system in which each mode was activated using two distinct coefficients. These coefficients values were calculated by a new mode transition algorithm developed based on a Fuzzy Logic System. This algorithm operated so that when the Vertical Speed (VS) mode was engaged, the Altitude Hold (AH) mode became inactive, and vice versa based on the variations of the altitude tracking error without using a conventional altitude capture mode. As stated earlier, two MFRNNs were developed separately, for approximating the aircraft dynamics in the state-space representations of the

VS an AH modes. These approximations were successfully obtained only by using the measured altitude and vertical speed tracking errors and their first-order derivatives even under turbulent flight condition. These MFRNNs were trained by initializing all weights with the PSO algorithm. Only the weights between the rules layer and the output layer were updated online, using the backpropagation method, while the other weights were fixed at their initialized values. The approximations were obtained without knowledge of the aircraft dynamics mathematics in the state-space representations. The Lyapunov theorem was used to prove the stability and boundedness of each controller. In addition, the results showed that the control systems developed for each autopilot mode could meet the desired tracking performance with negligible tracking errors with and without turbulence. In addition, control systems attenuated the drastic effects of moderate-intensity turbulence across the whole flight envelope of the CCX aircraft.

CHAPTER 7

DISCUSSION OF RESULTS

This thesis primarily focused on developing Artificial Intelligence (AI)-based control laws for aircraft. The methodologies developed in this thesis can be further applied on various types of business aircraft. Flight Control Systems (FCSs) have experienced significant developments lately to enhance aircraft performance, safety, and efficiency. Although these developments increased the reliability and precision of flight control systems, and improved the maneuverability and performance of aircraft, there is still opportunity to improve them, especially with the introduction of Artificial Intelligence (AI) systems. AI-based systems can make aircraft control easier for pilots and help reduce potential errors during flight, particularly in critical flight conditions where pilot decisions are crucial. To reduce pilot workload and address challenges such as dealing with uncertainties, environmental variations, and system dynamics, three novel control methodologies were employed for the Cessna Citation X (CCX) aircraft.

According to the literature review, these AI-based controllers were not previously developed for aircraft flight control systems. The AI-based control systems presented in this thesis, were developed to achieve the main objectives of this research which are to reduce the pilot's workload and also to handle the uncertainties in both ideal and turbulent flight conditions. For these purposes, different flight control systems were developed for: 1) Longitudinal motion control, 2) Lateral motion control, and 3) Autopilot system. The performance of the control methodologies developed in this thesis was evaluated using a nonlinear simulation platform designed for the Cessna Citation X (CCX) aircraft, developed by real flight data derived from a level-D research aircraft flight simulator at the LARCASE.

First, two different Fuzzy logic-based control methodologies were developed to control the longitudinal motion of an aircraft following the first sub-objective: 1) Type One Adaptive

Fuzzy Sliding Mode Control System (T1AFSMC) and 2) Type Two Adaptive Fuzzy Sliding Mode Control System (T2AFSMC).

These methodologies were developed with a focus on controlling the pitch rate and stabilizing the True AirSpeed (TAS) during the cruise phase. Respectively, the Type One Adaptive Fuzzy Logic System (T1FLS) served as a dynamic approximator for the functions present in the aircraft state-space representation. These approximations were integrated into the Sliding Mode Control (SMC) system. The simulation results showed that the T1AFSMC achieved better tracking performance than a Model Reference Recurrent Neural Network, which was designed to control the CCX pitch rate for 12 flight conditions distributed over the entire CCX flight envelope. This superior performance was demonstrated in terms of their controllers tracking performance in ideal flight condition and the elevator control inputs smoothness.

To ensure the overall performance of the T1AFSMC, it was simulated across all 925 flight conditions within the CCX flight envelope in ideal flight conditions and in moderate intensity (10^{-3}) turbulence. The Average Mean Squared Error (AMSE) was calculated for each flight condition in the absence of turbulence, showing that the highest value of the pitch rate AMSE was 2×10^{-8} deg/s, while the True AirSpeed AMSE values were less than 9.72 km/h. Moreover, tracking errors were calculated for the TAS at different altitudes in ideal and turbulent flight conditions to evaluate the performance of the TAS controller at various flight level across the aircraft flight envelope. All these simulation results confirmed that the pitch rate and TAS control systems developed in this thesis were validated.

In the second thesis study, the performances of the T1AFSMC were compared to those of a new T2AFSMC control system in a second methodology developed for both pitch rate control and TAS stabilization. For the design of the T2FLS, a new non-iterative Type Reduction (TR) algorithm, known as Nagar-Bardini (NB), was employed. This TR algorithm combines both type reduction and defuzzification operations, thereby reducing the mathematical burden in the design of the Type 2 Fuzzy Logic System. Compared with the

T1FLS, the T2FLS can deal with more uncertainties and input variations since its membership functions contain an upper and a lower bound, which increases the system robustness in the presence of uncertainties, input variations, and disturbances. The results obtained by these two methodologies were compared for 15 flight conditions, showing that the T2AFSMC produced better results than the T1AFSMC in terms of the mean absolute tracking errors for each flight condition.

Moreover, the T2AFSMC produced smoother elevator commands than those of the T1AFSMC. Consequently, to ensure the performance of the proposed T2AFSMC, simulation results were presented for all 925 flight conditions for each pair of the pitch rate and TAS control systems, separately for each flight altitude. These results showed that the T2AFSMC operated adequately to control the pitch rate, and to stabilize the TAS across the entire CCX flight envelope. The Average Mean Absolute Error (AMAE) was used to analyze the aircraft pitch rate tracking performance. The pitch rate (deg/s) results were presented for each flight altitude, which varied between 7.97×10^{-5} deg/s to 1.14×10^{-4} deg/s for the CCX in ideal flight conditions and between 8.36×10^{-5} deg/s and 3.33×10^{-4} deg/s with turbulence. The pitch rate maximum and minimum AMAEs were also represented for each altitude. This analysis was expanded by calculating the AMSE values to illustrate the effectiveness of this methodology as the AMSE penalizes the significant deviations from the reference signal and it helps to detect significant inaccuracies in the obtained results. The AMAE tracking errors of the TAS control system at each altitude varied between 1.67 km/h and 3.07 km/h and the AMSE varied between 1.25 km/h and 4.28 km/h in turbulent flight conditions.

Due to the better results obtained with the T2AFSMC in the control of the longitudinal motion, it was decided to combine the T2AFLS with a Super-Twisting Sliding Mode Control (STSMC) system for the lateral motion of the CCX aircraft. This methodology used two approaches to design the super twisting switching term: 1) an adaptive-based super twisting sliding mode control and 2) a PSO-based super twisting sliding mode control. The results obtained for 925 flight conditions showed that the T2AFLS and Adaptive STSMC combination performed better than those of the PSO-based control system in ideal flight

conditions. However, a detailed comparison of the results obtained in turbulent flight conditions showed that the PSO-based STSMC performed “slightly” better than the Adaptive STSMC based on the AMAE errors obtained for the roll rate tracking performance of the CCX aircraft. These results demonstrated that both methodologies are very good with no explicit knowledge about the aircraft model was required to design these control systems.

The last research sub-objective focused on designing a novel autopilot system using Fuzzy Logic Systems (FLSs), which demonstrated very good performances in both longitudinal and lateral control systems. This autopilot system was developed using a novel approximation method based on a combination of a Fuzzy Logic System (FLS) with a Recurrent Neural Network (RNN). This combination leverages the strengths of both fuzzy logic and recurrent neural networks systems, particularly their ability to handle uncertainties and time-series data, and to improve the control system robustness.

Moreover, a new training method was applied to find the weights of the FRNNs developed for both the Vertical Speed and Altitude Hold modes. This training process used the PSO algorithm to initialize the weights, and then updated the last layer weights using the online backpropagation algorithm. These approximators were integrated into the two Sliding Mode Controllers developed for the AH and VS modes to enhance the stability of the autopilot system.

Furthermore, a novel fuzzy-based autopilot mode transition algorithm was developed to ensure a smooth transition between the AH and VS modes. Two scenarios; one in the absence of turbulence, and the other with moderate-intensity turbulence, were selected to validate the stability and robustness of the controllers designed for the autopilot. These simulations were conducted for all 925 flight conditions, covering the entire CCX flight envelope.

In the ideal flight condition, both autopilot modes performed better during the descent than in the climbing maneuver, referring to the calculated AMAEs for each flight condition.

On the other hand, another maneuver in which the aircraft climbed to a specific altitude was simulated to evaluate the controllers performances under turbulent flight conditions. This simulation showed that the FRNN-based proposed controllers can guarantee the aircraft stability and robustness in all flight conditions with respect to the Mean Absolute Errors which were found to be small, and therefore acceptable for the scope of this research. In this FRNN-based autopilot methodology, the T1AFSMC control system, developed in the first sub-objective one, was employed in the inner loop to control the aircraft pitch rate.

In this thesis, the Lyapunov theorem was used to theoretically prove the stability and boundedness of the proposed methodologies for each sub-objective. This analysis was important to ensure that the tracking error consistently remained within a bounded interval, thereby avoiding any possible instabilities during flight.

CONCLUSION

This research was dedicated to developing AI-based control laws for different aircraft longitudinal and lateral motions in cruise. As discussed in many research topics, Flight Control Systems (FCS) are essential to guarantee aircraft stability and robustness in various maneuvers to track the given commands, that is important for satisfied for the passengers' safety and comfort. Previously, conventional control techniques were successfully implemented on aircraft systems, offering precise and reliable performance.

Meanwhile, AI-based control systems can introduce new features and characteristics to current FCS, such as adaptability, learning ability, handling uncertainties and dynamics variations, and dealing with critical flight conditions by reducing the pilot's workload and intervention. The controller methodologies were validated using a nonlinear simulation platform previously developed at LARCASE for the Cessna Citation X aircraft. This platform was developed using the real flight data obtained from a Level D research aircraft flight simulator available at the LARCASE. The Level D is the highest certification degree that can be issued by the FAA for flight simulators.

In the first study of this thesis, a new combination of adaptive control systems, Type One Fuzzy Logic System and Sliding Mode Control (SMC) systems was analyzed for both, for the pitch rate and TAS controls of the CCX longitudinal motion. In this new controller, the aircraft dynamics were approximated without explicit knowledge of the aircraft model, while these approximations were updated online using Lyapunov-based adaptation laws. Integrating these approximations within the SMC system improved the robustness, stability, and tracking performances of the CCX in the absence and presence of turbulence.

On the other hand, in the second study of this thesis, the T1AFLS was enhanced using a Type Two Adaptive Fuzzy Logic System equipped with a Nagar-Bardini Type Reduction method. This system was able to handle more uncertainties and parametric variations than the T1AFSMC. Integrating this approximation into the SMC led to better results than the

T1AFSMC system in terms of robustness, stability, and tracking performance for both pitch rate and TAS controllers.

In the third study of this thesis, the T2AFLS methodology was combined with the Super-twisting Sliding Mode Control (STSMC) to obtain a robust and stable roll rate tracking performance. Two approaches were employed to find the optimal parameter values of the STSMC: the adaptive and the PSO-based super-twisting SMC systems. Simulation results in both ideal and turbulent flight conditions showed that the adaptive approach performed better for the roll rate tracking performance than the PSO-based Supertwisting SMC system.

The last research topic focused on developing an autopilot system using a combination of Fuzzy Recurrent Neural Network systems, which were trained online, and SMC systems for both Altitude Hold and Vertical Speed modes. In addition, this autopilot system was designed using a novel Fuzzy Logic transition algorithm to switch between the two modes during climb and descent maneuvers during the cruise. The stability and boundedness of the controllers proposed in this thesis were analyzed using the Lyapunov theorem to ensure that the aircraft remains within its operational limits both in the presence and absence of turbulence.

RECOMMENDATIONS

This thesis presented the application of Artificial Intelligence (AI)-base control systems for the control of aircraft. While significant progress and advancements have been made in this thesis, further potential investigations and research directions can be outlined as follows the findings of this thesis.

Firstly, it will be essential to validate these methodologies with real aircraft data for the CCX and further apply them to other types of business aircraft, depending on the possible flight data obtained from the aerospace companies.

As mentioned, aircraft is a highly nonlinear system that contains different types of uncertainties. Although the methodologies proposed in this thesis, could handle the uncertainties and dynamics variations very good, this characteristic especially in the Fuzzy Logic Systems can be still enhanced using dynamic membership functions, these types of membership functions can be adapted to the variations of the aircraft dynamics.

Furthermore, the performance of these control systems can be validated for other flight phases to developed Auto Take-Off (T.O) and Auto Landing systems.

In addition, another suggestion is to expand these methodologies to fault-tolerance controllers, which can compensate for failures in aircraft systems, such as actuator faults, engine failures, etc. In addition, the application of advanced machine learning techniques such as reinforcement learning, and deep learning can be of interest. These methodologies can control different aircraft motions with one single controller and without the need for multiple controllers for each of the aircraft motions. These methods can also enhance the adaptability and robustness of flight control systems in diverse operational conditions. Moreover, such AI-based control systems can utilize various types of input data, such as navigation data, images, and more, which introduce new capabilities and features to the design of aircraft control systems.

APPENDIX I

Aircraft Speed Control System (T1AFSMC)

In this controller the tracking error e_v was calculated using desired reference speed V_d and the actual speed V, as given in Eq. (AI.1).

$$\begin{aligned} e_v &= V(t) - V_d(t) \\ \dot{e}_v &= \dot{V}(t) - \dot{V}_d(t) \end{aligned} \tag{AI.1}$$

The sliding surface for the aircraft speed control system was selected in Eq. (AI.2) (Londhe & Patre, 2019):

$$S_v = e_v + D\dot{e}_v \tag{AI.2}$$

where $D > 0$.

The derivative of the designed sliding surface in Eq. (AI.2) should then be calculated based on the state-space form introduced for the aircraft dynamics in Eq. (1) in Section 6.2.1. Thus, considering $\dot{V}(t) = f_v(x.t) + g_v(x.t)\eta$, the derivative of the sliding surface becomes:

$$\dot{S}_v = \dot{e}_v + D\ddot{e}_v = f_v(x,t) + g_v(x,t)\eta - \dot{V}_d(t) + D\ddot{e}_v + d(t) \tag{AI.3}$$

In this equation, $d(t)$ is the disturbance, f_v, and g_v are unknown functions which must be approximated by T1FLS, and η denoted the control input that will be designed later in this appendix for the aircraft speed. With respect to the Eq. (AI.3), and doing the same calculations as presented in Eqs (12) and (14) in Section 6.2.2, it can be shown that:

$$\begin{aligned} \dot{S}_v(t) = [f_v(x.t) - \hat{f}_v(x.\theta^*_{f_v})] + \hat{f}_v(x.\theta^*_{f_v}) + [g_v(x.t) - \hat{g}_v(x.\theta^*_{g_v})]\eta + \\ \hat{g}_v(x.\theta^*_{g_v})\eta - \dot{V}_d(t) + D\ddot{e}_v + d(t) \end{aligned} \tag{AI.4}$$

Therefore, by defining the minimum approximation error as $Y = f_v(x,t) - \hat{f}_v(x.\theta_{f_v}^*) + \left[g_v(x,t) - \hat{g}_v(x.\theta_{g_v}^*)\right]\eta$, Eq. (AI.4) can be rewritten as:

$$\dot{S}_v(t) = Y + \hat{f}_v(x,\theta_{f_v}^*) + \hat{g}_v(x,\theta_{g_v}^*)\eta - \dot{V}_d(t) + D\ddot{e}_v + d(t) \tag{AI.5}$$

As in Eq. (13) in Section 6.2.2 and considering that the expression of $\dot{S}_v$ in Eq. (3) equals to zero (i.e., $\dot{S}_v(t) = 0$), η_{eq2} can be obtained. Furthermore, the reaching control law is designed as $\eta_{sw2} = -H\text{sat}(S_v)$. Therefore, the proposed control law for the aircraft speed which is the form of $\eta_2 = \eta_{eq2} + \eta_{sw2}$ can be written as in Eq. (AI.6) (Bessa, 2022):

$$\eta_2 = \underbrace{\left(\frac{1}{\hat{g}_v(x,\theta_{g_v})}\right)\left[-\hat{f}_v(x,\theta_{f_v}) + \dot{V}_d(t) - D\ddot{e}_v\right]}_{\eta_{eq2}} - \underbrace{H\text{sat}(S_v)}_{\eta_{sw2}}, \quad H > 0 \tag{AI.6}$$

where $\text{sat}(S_v)$ refers to the Saturation Function, and H is a design parameter for the switching control law.

To facilitate the analysis, $\theta_{f_v}^*$ and $\theta_{g_v}^*$ are considered as the optimal parameters in $\varphi_{f_v} = \theta_{f_v}^* - \theta_{f_v}$ and $\varphi_{g_v} = \theta_{g_v}^* - \theta_{g_v}$, which yield $\phi_{f_v}^T\psi_{f_v}(x) = \hat{f}_v(x.\theta_{f_v}^*) - \hat{f}_v(x.\theta_{f_v})$, $\phi_{g_v}^T\psi_{g_v}(x) = \hat{g}_v(x.\theta_{g_v}^*) - \hat{g}_v(x.\theta_{g_v})$. Having these two equations, the terms $\hat{f}_v(x.\theta_{f_v}^*)$ and $\hat{g}_v(x.\theta_{g_v}^*)$ can be replaced in Eq. (AI.7) to obtain:

$$\dot{S}_v(t) = Y + \phi_{f_v}^T\psi_{f_v}(x) + \hat{f}_v(x,\theta_{f_v}) + \phi_{g_v}^T\psi_{g_v}(x)\eta + \hat{g}_v(x,\theta_{g_v})\eta - \dot{V}_d(t) + D\ddot{e}_v + d(t) \tag{AI.7}$$

In Eq. (AI.7), η must be substituted with the proposed control law $\eta_2 = \eta_{eq2} + \eta_{sw2}$ shown in Eq. (A.6). Consequently, $\dot{S}_v(t)$ in Eq. (AI.7) can be reformulated as follows:

$$\dot{S}_v(t) = Y - \hat{g}_v(x.\theta_{g_v})\eta_{sw2} + \phi_{f_v}^T\psi_{f_v}(x) + \phi_{g_v}^T\psi_{g_v}(x)\eta_2 + d(t) \tag{AI.8}$$

Stability Proof. To proceed with choosing the Lyapunov candidate for the speed control system, the same procedure will be followed as that of the pitch rate control system in the Section 6.2.2. The Lyapunov function candidate can be determined as V_2 with respect to the selected sliding surface S_v, and the adjustable parameters denoted by ϕ_{f_v} and ϕ_{g_v}, respectively, to ensure the performance of the suggested controller system for the aircraft speed, as follows:

$$V_2 = \frac{1}{2}S_v^2 + \frac{1}{2\gamma_{f_v}}\phi_{f_v}^T\phi_{f_v} + \frac{1}{2\gamma_{g_v}}\phi_{g_v}^T\phi_{g_v} \tag{AI.9}$$

To demonstrate the boundness and stability of this controller, it is necessary to take the time derivative of the Lyapunov candidate V_2 presented in Eq. (AI.9) as follows:

$$\dot{V}_2 = S_v\dot{S}_v + \frac{1}{\gamma_{f_v}}\phi_{f_v}^T\dot{\phi}_{f_v} + \frac{1}{\gamma_{g_v}}\phi_{g_v}^T\dot{\phi}_{g_v} \tag{AI.10}$$

Then, by replacing the expression of $\dot{S}_v$ in Eq. (AI.8) into Eq. (AI.10), it becomes:

$$\begin{aligned}\dot{V}_2 = {} & S_vY - S_v\hat{g}_v(x.\theta_{g_v})\eta_{sw2} + S_v\phi_{f_v}^T\psi_{f_v}(x) + S_v\phi_{g_v}^T\psi_{g_v}(x)\eta_2 + \\ & S_vd(t) + \frac{1}{\gamma_{f_v}}\phi_{f_v}^T\dot{\phi}_{f_v} + \frac{1}{\gamma_g}\phi_g^T\dot{\phi}_g = S_vY - S_v\hat{g}_v(x.\theta_{g_v})\eta_{sw2} + \\ & S_vd(t) + \frac{1}{\gamma_{f_v}}\phi_{f_v}^T\left(\dot{\phi}_{f_v} + S_v\gamma_{f_v}\psi_{f_v}(x)\right) + \frac{1}{\gamma_{g_v}}\phi_{g_v}^T\left(\dot{\phi}_{g_v} + \right. \\ & \left. S_v\gamma_{g_v}\psi_{g_v}(x)\eta_2\right)\end{aligned} \tag{AI.11}$$

The adaptation laws must be properly chosen to guarantee the stability and effectiveness of the control system, as shown in Eq. (AI.12b). Adaptation laws are considered as the rules governing the adjustment of the controller parameters, typically driven by the sliding surface, which consists of the tracking error of the desired and the actual system outputs and its derivative. These adaptation laws make it possible to update adjustable parameters in real-time to cope with changes in the system dynamics, uncertainties, or external disturbances. Based on the expression provided in Eq. (AI.11), $\dot{\phi}_{f_v}$ and $\dot{\phi}_{g_v}$ can be calculated as shown in

Eq. (AI.12a). Given that $\dot{\phi} = -\dot{\theta}$ (Yoo & Ham, 1998a), the adaptation laws can be derived as follows in Eq. (AI.12b):

$$\begin{aligned} \dot{\phi}_{f_v} &= -S_v \gamma_{f_v} \psi_{f_v}(x) \\ \dot{\phi}_{g_v} &= -S_v \gamma_{g_v} \psi_{g_v}(x) \eta_2 \end{aligned} \tag{AI.12a}$$

$$\begin{aligned} \dot{\theta}_{f_v} &= S_v \gamma_{f_v} \psi_{f_v}(x) \\ \dot{\theta}_{g_v} &= S_v \gamma_{g_v} \psi_{g_v}(x) \eta_2 \end{aligned} \tag{AI.12b}$$

Therefore, the final forms of the adaptation laws are presented in Eq. (AI.13), using the components $-\sigma_{f,g} \gamma_{f,g} \theta_{f,g}$ to ensure the convergence of the adjustable parameters in the adaptation laws shown in Eq. (12b):

$$\begin{aligned} \dot{\theta}_{f_v} &= -\sigma_{f_v} \gamma_{f_v} \theta_{f_v} + S_v \gamma_{f_v} \psi_{f_v}(x) \\ \dot{\theta}_{g_v} &= -\sigma_{g_v} \gamma_{g_v} \theta_{g_v} + S_v \gamma_{g_v} \psi_{g_v}(x) \eta_2 \end{aligned} \tag{AI.13}$$

According to the Assumptions 1 and 2, as $\left|\hat{f}_v(x.\theta_{f_v})\right| \leq F_v$, and $0 < g_{v_{min}} < \hat{g}_v(x.\theta_{g_v}) < g_{v_{max}}$,and the adaptation laws in Eq. (12b) are substituted into Eq. (11) which yields:

$$\begin{aligned} \dot{V}_2 = {} & S_v Y - S_v \hat{g}_v\left(x \middle| \theta_{g_v}\right) \eta_{sw2} + S_v d(t) - \frac{1}{\gamma_{f_v}} \theta_{f_v}^T \left(\sigma_{f_v} \gamma_{f_v} \theta_{f_v}\right) \\ & - \frac{1}{\gamma_{g_v}} \theta_{g_v}^T \left(\sigma_{g_v} \gamma_{g_v} \theta_{g_v}\right) \end{aligned} \tag{AI.14}$$

Referring to the Triangular inequality used to define Eq. (AI.22) in Section 6.2.2 (Roopaei et al., 2009), the calculated expression Eq.(AI.14) above can be rearranged based on the minimum approximation error $|Y| \leq P_{f_v} + F_v + (P_{g_v} + g_{v_{max}})(\sup(|\eta_2|)) < \varepsilon_2$, such that:

$$\begin{aligned} \dot{V}_2 \leq {} & |S_v||Y| - H|S_v|\left|g_{v_{max}}\right| + T|S_v| - \sigma_{f_v}\left\|\theta_{f_v}\right\|^2 - \sigma_{g_v}\left\|\theta_{g_v}\right\|^2 \leq \\ & \varepsilon_2|S_v| - H|S_v|\left|g_{v_{max}}\right| + T|S_v| - \sigma_{f_v}\left\|\theta_{f_v}\right\|^2 - \sigma_{g_v}\left\|\theta_{g_v}\right\|^2 \end{aligned} \tag{AI.15}$$

With the obtained terms in Eq. (AI.15), the derivative of the Lyapunov candidate will be negative $\dot{V}_2 \leq 0$. In this equation, σ_{f_q} and σ_{g_q} are small positive constants. Moreover, a large positive constant was selected for H to hold $H > \varepsilon_2 + T$. It can be concluded that, this control law meets the requirements of the Lyapunov and Barbalat's theorems with $S.\dot{S} \in \mathcal{L}_\infty$ ($S.\dot{S}$ are always bounded), therefore, the asymptotically stability of the aircraft has been proved and the error converges to zero asymptotically over the time.

APPENDIX II

Aircraft Speed Control System (T2ASMC)

To prove the stability of the aircraft using the speed control law proposed in Eq. (4.28) in Section 4.3, the Lyapunov Theorem was considered as follows in this appendix. Initially, the tracking error must be defined as $E_{sp} = v(t) - v_{ref}(t)$. Respectively, the sliding surface is designed as presented in Eq. (4.27) ($\sigma_{sp} = E_{sp} + I\dot{E}_{sp}$) for aircraft speed in Section 4.3 with $I > 0$ as inspired from (Eker, 2006). Taking the time derivative of σ_{sp} , and defining $\dot{v}(t) = M(X) + N(X)U_{sp} + D(t)$, it becomes:

$$\dot{\sigma}_{sp} = \dot{E}_{sp} + I\ddot{E}_{sp} = M(x) + N(x)U_{sp} + D(t) - \dot{v}_{ref}(t) + I\ddot{E}_{sp} \tag{AII.1}$$

In the previous equation $U_{sp} = U_{sp}^{eq} + U_{sp}^{sw}$. Therefore, we can define the equivalent control law U_{sp}^{eq} as follows by $\dot{\sigma}_{sp} = 0$:

$$U_{sp}^{eq} = \left(\frac{1}{N(x)}\right)\left[-M(x) + \dot{v}_{ref}(t) - I\ddot{E}_{sp} - D(t)\right] \tag{AII.2}$$

In Eq. (AII.2), $M(x)$ and $N(x)$ are unknown nonlinear functions, and $D(t)$ is not measurable. Using the minimum approximation error denoted by $Z = \left[M(x) - \widehat{M}(x|\Theta_M^*)\right] + \left[N(x) - \widehat{N}(x|\Theta_N^*)\right]U_{sp}$ (L.-X. Wang, 1994), (Yoo & Ham, 1998a) therefore Eq. (AII.1) can be reformulated as:

$$\begin{aligned}\dot{\sigma}_{sp} &= \left[M(x) - \widehat{M}(x|\Theta_M^*)\right] + \widehat{M}(x|\Theta_M^*) + \left[N(x) - \widehat{N}(x|\Theta_N^*)\right]U_{sp} + \widehat{N}(x|\Theta_N^*)U_{sp} - \\ &\dot{v}_{ref}(t) + I\ddot{E}_{sp} + D(t) = Z + \widehat{M}(x|\Theta_M^*) + \widehat{N}(x|\Theta_N^*)U_{sp} - \dot{v}_{ref}(t) + I\ddot{E}_{sp} + D(t)\end{aligned} \tag{AII.3}$$

With $\phi_M^T\psi_M(x) = \widehat{M}(x|\Theta_M^*) - \widehat{M}(x|\Theta_M)$ and $\phi_N^T\psi_N(x) = \widehat{N}(x|\Theta_N^*) - \widehat{N}(x|\Theta_N)$(C.-H. Wang et al., 2002), and therefore Eq. (AII.3) can be written as:

$$\dot{\sigma}_{sp} = Z + \phi_M^T \psi_M(x) + \widehat{M}(x|\Theta_M) + \phi_N^T \psi_N(x) U_{sp} + \widehat{N}(x|\Theta_N) U_{sp} - \dot{v}_{ref}(t) + I\ddot{E}_{sp} + D(t) \quad \text{(AII.4)}$$

Due to the fact that $M(x)$ and $N(x)$ are two unknown functions and $D(t)$ is not measurable in U_{sp}^{eq}, it is essential to approximate $M(X)$ and $N(X)$ by the Type Two Fuzzy Logic System as already described in Section 4.2.2, therefore U_{sp}^{eq} can be reformulated as given in Eq. (AII.5). Thus, by using the functions $\widehat{M}(X|\theta_M)$ and $\widehat{N}(X|\theta_N)$, the designed speed control law takes the following form as $U_{sp} = U_{sp}^{eq} + U_{sp}^{sw}$:

$$U_{sp} = \underbrace{\left(\frac{1}{\widehat{N}(x|\Theta_N)}\right)\left[-\widehat{M}(x|\Theta_M) + \dot{v}_{ref}(t) - I\ddot{E}_{sp}\right]}_{U_{sp}^{eq}} - \underbrace{Wsat(\sigma_{sp})}_{U_{sp}^{sw}} \quad \text{(AII.5)}$$

Now, the control law U_{sp} in Eq. (AII.5) can then be replaced in Eq. (AII.4), so that:

$$\dot{\sigma}_{sp} = Z + \phi_M^T \psi_M(x) + \phi_N^T \psi_N(X) U_{sp} - \widehat{N}(x|\Theta_N) Wsat(\sigma_{sp}) + D(t) \quad \text{(AII.6)}$$

Stability Proof. Using the Lyapunov candidate L_{sp} presented in Eq. (AII.7) inspired from (Chen, 2019 ; C.-H. Wang et al., 2002), it will be possible to guarantee the boundedness of the error and the stability of the aircraft.

$$L_{sp} = \frac{1}{2}\sigma_{sp}^2 + \frac{1}{2\overline{g}_M}\overline{\phi}_M^T\overline{\phi}_M + \frac{1}{2\underline{g}_M}\underline{\phi}_M^T\underline{\phi}_M + \frac{1}{2\overline{g}_N}\overline{\phi}_N^T\overline{\phi}_N + \frac{1}{2\underline{g}_N}\underline{\phi}_N^T\underline{\phi}_N \quad \text{(AII.7)}$$

Taking the time derivative of the Lyapunov candidate L_{sp} , and replacing the calculated expression for $\dot{\sigma}_{sp}$ Eq. (AII.4) in it, Eq. (AII.7) becomes:

$$\dot{L}_{sp} = \sigma_{sp}\dot{\sigma}_{sp} + \frac{1}{\overline{g}_M}\overline{\phi}_M^T\dot{\overline{\phi}}_M + \frac{1}{\underline{g}_M}\underline{\phi}_M^T\dot{\underline{\phi}}_M + \frac{1}{\overline{g}_N}\overline{\phi}_N^T\dot{\overline{\phi}}_N + \frac{1}{\underline{g}_N}\underline{\phi}_N^T\dot{\underline{\phi}}_N = \sigma_{sp}Z + \quad \text{(AII.8)}$$

$$\sigma_{sp}\phi_M^T\psi_M(x) + \sigma_{sp}\phi_N^T\psi_N(x)U_{sp} - \sigma_{sp}\widehat{N}(x|\Theta_N)Wsat(\sigma_{sp}) + \sigma_{sp}D(t) +$$

$$\frac{1}{\overline{g}_M}\overline{\phi}_M^T\dot{\overline{\phi}}_M + \frac{1}{\underline{g}_M}\underline{\phi}_M^T\dot{\underline{\phi}}_M + \frac{1}{\overline{g}_N}\overline{\phi}_N^T\dot{\overline{\phi}}_N + \frac{1}{\underline{g}_N}\underline{\phi}_N^T\dot{\underline{\phi}}_N$$

By using the NB type reduction and the Center of Sets defuzzification methods (Chen, 2019 ; El-Nagar & El-Bardini, 2014), we have $\phi_M^T\psi_M(x) = 0.5\left[\underline{\phi}_M^T\ \overline{\phi}_M^T\right]\begin{bmatrix}\underline{\psi}_M(x)\\ \overline{\psi}_M(x)\end{bmatrix}$ and $\phi_N^T\psi_N(x) = 0.5\left[\underline{\phi}_N^T\ \overline{\phi}_N^T\right]\begin{bmatrix}\underline{\psi}_N(x)\\ \overline{\psi}_N(x)\end{bmatrix}$,

$$\dot{L}_{sp} = \sigma_{sp}Z - \sigma_{sp}\widehat{N}(x|\Theta_N)Wsat(\sigma_{sp}) + \sigma_{sp}D(t) + 0.5\sigma_{sp}\left[\underline{\phi}_M^T\underline{\psi}_M(x) + \overline{\phi}_M^T\overline{\psi}_M(x)\right] + 0.5\sigma_{sp}\left[\underline{\phi}_N^T\underline{\psi}_N(x) + \overline{\phi}_N^T\overline{\psi}_N(x)\right]U_{sp} + \frac{1}{\overline{g}_M}\overline{\phi}_M^T\dot{\overline{\phi}}_M + \frac{1}{\underline{g}_M}\underline{\phi}_M^T\dot{\underline{\phi}}_M + \frac{1}{\overline{g}_N}\overline{\phi}_N^T\dot{\overline{\phi}}_N + \frac{1}{\underline{g}_N}\underline{\phi}_N^T\dot{\underline{\phi}}_N = \sigma_{sp}Z - \sigma_{sp}\widehat{N}(x|\Theta_N)Wsat(\sigma_{sp}) + \sigma_{sp}D(t) + \frac{1}{\underline{g}_M}\underline{\phi}_M^T[0.5\sigma_{sp}\underline{g}_M\underline{\psi}_M(x) + \dot{\underline{\phi}}_M] + \frac{1}{\overline{g}_M}\overline{\phi}_M^T[0.5\sigma_{sp}\overline{g}_M\overline{\psi}_M(x) + \dot{\overline{\phi}}_M] + \frac{1}{\underline{g}_N}\underline{\phi}_N^T[0.5\sigma_{sp}\underline{g}_N\underline{\psi}_N(x)U_{sp} + \dot{\underline{\phi}}_N] + \frac{1}{\overline{g}_N}\overline{\phi}_N^T[0.5\sigma_{sp}\overline{g}_N\overline{\psi}_N(x)U_{sp} + \dot{\overline{\phi}}_N] \quad \text{(AII.9)}$$

Now, it is possible to define the adaptation laws based on Eq. (AII.9) for each of the adjustable parameters denoted by $\dot{\underline{\Theta}}_M$, $\dot{\overline{\Theta}}_M$, $\dot{\underline{\Theta}}_N$,and $\dot{\overline{\Theta}}_N$,

$$\begin{aligned}\dot{\underline{\Theta}}_M &= -\underline{\Delta}_M\underline{g}_M\underline{\Theta}_M + 0.5\sigma_{sp}\underline{g}_M\underline{\psi}_M(x)\\ \dot{\overline{\Theta}}_M &= -\overline{\Delta}_M\overline{g}_M\overline{\Theta}_M + 0.5\sigma_{sp}\overline{g}_M\overline{\psi}_M(x)\\ \dot{\underline{\Theta}}_N &= -\underline{\Delta}_N\underline{g}_N\underline{\Theta}_N + 0.5\sigma_{sp}\underline{g}_N\underline{\psi}_N(x)U_{sp}\\ \dot{\overline{\Theta}}_N &= -\overline{\Delta}_N\overline{g}_N\overline{\Theta}_N + 0.5\sigma_{sp}\overline{g}_N\overline{\psi}_N(x)U_{sp}\end{aligned} \quad \text{(AII.10)}$$

and, knowing $\dot{\phi} = -\dot{\Theta}$ from (« Adaptive fuzzy control of a class of MIMO nonlinear systems », 2005) as $\phi = \Theta^* - \Theta$, the adaptive laws in Eq. (AII.10) can be written as:

$$\dot{L}_{sp} = \sigma_{sp}Z - \sigma_{sp}\widehat{N}(x|\Theta_N)Wsat(\sigma_{sp}) + \sigma_{sp}D(t) - \underline{\Delta}_M\underline{\phi}_M^T\underline{\Theta}_M - \overline{\Delta}_M\overline{\phi}_M^T\overline{\Theta}_M - \underline{\Delta}_N\underline{\phi}_N^T\underline{\Theta}_N - \overline{\Delta}_N\overline{\phi}_N^T\overline{\Theta}_N \quad \text{(AII.11)}$$

Using the definition of the Young's inequality (Sheikhhosseini, Moslehian, & Shebrawi, 2017), and also knowing that $|D(t)| \le L_D$ and $\widehat{N}(x|\Theta_N)$ is bounded as $\left|\widehat{N}(x|\Theta_N)\right| \le C_N$, Eq. (AII.11) can be written as follows while C_N and W are defined as two positive constants and $|Z| \le \varepsilon$ according to the assumptions 1 and 2 discussed earlier in this paper.

$$\dot{L}_{sp} \leq |Z|\left|\sigma_{sp}\right| - C_N W\left|\sigma_{sp}\right| + L_D\left|\sigma_{sp}\right| - \frac{1}{2}\underline{\Delta}_M \left\|\underline{\phi}_M\right\|^2 + \frac{1}{2}\underline{\Delta}_M\left\|\underline{\Theta}_M^*\right\|^2 - \frac{1}{2}\underline{\Delta}_N \left\|\underline{\phi}_N\right\|^2 + \frac{1}{2}\underline{\Delta}_N\left\|\underline{\Theta}_N^*\right\|^2 - \frac{1}{2}\overline{\Delta}_M\left\|\overline{\phi}_M\right\|^2 + \frac{1}{2}\overline{\Delta}_M \left\|\overline{\Theta}_M^*\right\|^2 - \frac{1}{2}\overline{\Delta}_N\left\|\overline{\phi}_N\right\|^2 + \frac{1}{2}\overline{\Delta}_N \left\|\overline{\Theta}_N^*\right\|^2 \tag{AII.12}$$

$$\dot{L}_{sp} \leq \varepsilon\left|\sigma_{sp}\right| - C_N W\left|\sigma_{sp}\right| + L_D\left|\sigma_{sp}\right| - \frac{1}{2}\underline{\Delta}_M \left\|\underline{\phi}_M\right\|^2 - \frac{1}{2}\underline{\Delta}_N \left\|\underline{\phi}_N\right\|^2 - \frac{1}{2}\overline{\Delta}_M\left\|\overline{\phi}_M\right\|^2 - \frac{1}{2}\overline{\Delta}_N\left\|\overline{\phi}_N\right\|^2 + \mathrm{H} \tag{AII.13}$$

where $\mathrm{H} = \frac{1}{2}\underline{\Delta}_M\left\|\underline{\Theta}_M^*\right\|^2 + \frac{1}{2}\underline{\Delta}_N\left\|\underline{\Theta}_N^*\right\|^2 + \frac{1}{2}\overline{\Delta}_M \left\|\overline{\Theta}_M^*\right\|^2 + \frac{1}{2}\overline{\Delta}_N \left\|\overline{\Theta}_N^*\right\|^2$. Also, in Eq. (AII.13), $\varepsilon\left|\sigma_{sp}\right|$ is considered to be very small and non-zero according to the minimum approximation error in the universal approximation theorem described in (L.-X. Wang, 1994), (Yoo & Ham, 1998a).Therefore, the coefficient of the $\left|\sigma_{sp}\right|$ can be replaced with $-\varrho = \varepsilon - C_N W + L_D$ as $\varrho > 0$. Thus, the following condition is met:

$$\dot{L}_{sp} \leq -\varrho\left|\sigma_{sp}\right| - \frac{1}{2}\underline{\Delta}_M \left\|\underline{\phi}_M\right\|^2 - \frac{1}{2}\underline{\Delta}_N \left\|\underline{\phi}_N\right\|^2 - \frac{1}{2}\overline{\Delta}_M\left\|\overline{\phi}_M\right\|^2 - \frac{1}{2}\overline{\Delta}_N\left\|\overline{\phi}_N\right\|^2 + \mathrm{H} \tag{AII.14}$$

Finally, Eq. (AII.14) leads to

$$\dot{L}_{sp} \leq -\hbar V + \mathrm{H} \tag{AII.15}$$

while $\hbar = \min\{2\varrho, \overline{g}_M\overline{\Delta}_M, \underline{g}_M\underline{\Delta}_M . \overline{g}_N\overline{\Delta}_N . \underline{g}_N\underline{\Delta}_N\}$. To complete the Lyapunov theorem proof, Eq. (AII.15) must be multiplied by $e^{\hbar t}$(Bounar et al., 2020), so:

$$\frac{d}{dt}\left(e^{\hbar t}L_{sp}\right) \leq \mathrm{H}e^{\hbar t} \tag{AII.16}$$

$$0 \leq L_{sp}(t) \leq \frac{\mathrm{H}}{\hbar} + \left(L_{sp}(0) - \frac{\mathrm{H}}{\hbar}\right)e^{-\hbar t}$$

LIST OF BIBLIOGRAPHICAL REFERENCES

Adaptive fuzzy control of a class of MIMO nonlinear systems. (2005). *Fuzzy Sets and Systems*, *151*(1), 59-77. https://doi.org/10.1016/j.fss.2004.10.009

Ahsan, M., Shafique, K., Mansoor, A. B., & Mushtaq, M. (2013). Performance comparison of two altitude-control algorithms for a fixed-wing UAV. *2013 3rd IEEE International Conference on Computer, Control and Communication (IC4)*, 1-5. https://doi.org/10.1109/IC4.2013.6653744

Al-Lami, H., Aslam, A., Quigley, T., Lewis, J., Mercer, R., & Shukla, P. (2015). The evolution of flight control systems. Technology development, system architecture and operation. *University of the West of England, Bristol*.

Andrianantara, Rojo P., Ghazi, G., & Botez, R. M. (2024). Model Predictive Controller with Adaptive Neural Networks and Online State Estimation for Pitch Rate Control of the Cessna Citation X. Dans *AIAA SCITECH 2024 Forum*. Orlando, FL : American Institute of Aeronautics and Astronautics. https://doi.org/10.2514/6.2024-0118

Andrianantara, Rojo Princy, Ghazi, G., & Botez, R. M. (2023). Neural network adaptive controller with approximate dynamic inversion for pitch control of the Cessna Citation X. Dans *AIAA AVIATION 2023 Forum*. San Diego, CA and Online : American Institute of Aeronautics and Astronautics. https://doi.org/10.2514/6.2023-3798

Apostol, T. M. (1974). *Mathematical Analysis: A Modern Approach to Advanced Calculus* (2nd edition). (S.l.) : Pearson.

Åström, K. J. (2000). Model uncertainty and robust control. *Lecture Notes on Iterative Identification and Control Design*, 63-100.

Atul Garg, Rezawana Islam Linda, & Tonoy Chowdhury. (2013). Evolution o f Aircraft Flight Control System and Fly By Light Flight Control System (Vol. 3, pp. 60-64). Communication présentée au The International Journal of Emerging Technology and Advanced Engineering. Repéré à www.ijetae.com

Babaei, A. R., Mortazavi, M., & Moradi, M. H. (2011). Classical and fuzzy-genetic autopilot design for unmanned aerial vehicles. *Applied Soft Computing*, *11*(1), 365-372. https://doi.org/10.1016/j.asoc.2009.11.027

Barros Dos Santos, S. R., & De Oliveira, N. M. F. (2011). Longitudinal autopilot controllers test platform hardware in the loop. Dans *2011 IEEE International Systems Conference* (pp. 379-386). Montreal, QC, Canada : IEEE. https://doi.org/10.1109/SYSCON.2011.5929071

Bessa, W. M. (2022, 23 mai). An adaptive fuzzy sliding mode controller for nonlinear systems with non-symmetric dead-zone and its application to an electro-hydraulic system. arXiv. https://doi.org/10.48550/arXiv.2205.13669

Bist, A., & Sondhi, S. (2022). Fractional order sliding mode control based on delayed output observer for unmanned aircraft system. *Aircraft Engineering and Aerospace Technology*, *94*(8), 1303-1311. https://doi.org/10.1108/AEAT-11-2020-0245

Boughari, Y., Ghazi, G., Theel, F., & Botez, R. M. (2013). Business aircraft flight control system using robust H-infinity controllers on Cessna Citation X. Communication présentée au 60th Aeronautics Conference and AGM (Aero13): Aerospace Clusters : Where are we Headed?, Toronto, ON, Canada. Repéré à https://espace2.etsmtl.ca/id/eprint/22752/

Boughari, Yamina, Botez, R. M., Ghazi, G., & Theel, F. (2017). Flight control clearance of the Cessna Citation X using evolutionary algorithms. *Proceedings of the Institution of Mechanical Engineers, Part G: Journal of Aerospace Engineering*, *231*(3), 510-532. https://doi.org/10.1177/0954410016640821

Boughari, Yamina, Georges Ghazi, Ruxandra Mihaela Botez, & Florian Theel. (2017). New Methodology for Optimal Flight Control using Differential Evolution Algorithms applied on the Cessna Citation X Business Aircraft–Part 1. Design and Optimization. *INCAS Bulletin*, *9*(2), 31-44. https://doi.org/10.13111/2066-8201.2017.9.2.3

Bounar, N., Labdai, S., Boulkroune, A., Farza, M., & M'Saad, M. (2020). Adaptive Fuzzy Control Scheme for Variable-Speed Wind Turbines Based on a Doubly-Fed Induction Generator. *Iranian Journal of Science and Technology, Transactions of Electrical Engineering*, *44*(2), 629-641. https://doi.org/10.1007/s40998-019-00276-6

Cárdenas, E., Boschetti, P., & Celi, M. (2012). *Design of Control Systems to Hold Altitude and Heading in Severe Atmospheric Disturbances for an Unmanned Airplane*. (S.l.) : (s.n.). https://doi.org/10.2514/6.2012-854

Castillo, O., & Cervantes, L. (2014). Genetic Design of Optimal Type-1 and Type-2 Fuzzy Systems for Longitudinal Control of an Airplane. *Intelligent Automation & Soft Computing*, *20*(2), 213-227. https://doi.org/10.1080/10798587.2014.902913

Cervantes, L., & Castillo, O. (2015). Type-2 fuzzy logic aggregation of multiple fuzzy controllers for airplane flight control. *Information Sciences*, *324*, 247-256. https://doi.org/10.1016/j.ins.2015.06.047

Chen, Y. (2019). Study on Centroid Type-Reduction of Interval Type-2 Fuzzy Logic Systems Based on Noniterative Algorithms. *Complexity*, *2019*. https://doi.org/10.1155/2019/7325053

Cheng, N. B., Guan, L. W., Wang, L. P., & Han, J. (2011). Chattering Reduction of Sliding Mode Control by Adopting Nonlinear Saturation Function. *Advanced Materials Research*, *143-144*, 53-61. https://doi.org/10.4028/www.scientific.net/AMR.143-144.53

Chrif, L., & Kadda, Z. M. (2014). Aircraft Control System Using LQG and LQR Controller with Optimal Estimation-Kalman Filter Design. *Procedia Engineering*, *80*, 245-257. https://doi.org/10.1016/j.proeng.2014.09.084

Chwa, D. (2015). Fuzzy Adaptive Output Feedback Tracking Control of VTOL Aircraft With Uncertain Input Coupling and Input-Dependent Disturbances. *IEEE Transactions on Fuzzy Systems*, *23*(5), 1505-1518. https://doi.org/10.1109/TFUZZ.2014.2362554

Collinson, R. P. G. (2011). Fly-by-Wire Flight Control. Dans R. P. G. Collinson, *Introduction to Avionics Systems* (pp. 179-253). Dordrecht : Springer Netherlands. https://doi.org/10.1007/978-94-007-0708-5_4

Darwish, M. H., Elgohary, A. A., Gomaa, M. M., Kaoud, A. M., Ashry, A. M., & Taha, H. (2021). A Comparative Assessment of the Performance of PID and MPC Controllers: A UAV Altitude Hold Autopilot Case Study. Dans *AIAA SCITECH 2022 Forum*. (S.l.) : American Institute of Aeronautics and Astronautics. https://doi.org/10.2514/6.2022-1519

Deepa, S. N., & Sudha, G. (2016). Longitudinal control of aircraft dynamics based on optimization of PID parameters. *Thermophysics and Aeromechanics*, *23*(2), 185-194. https://doi.org/10.1134/S0869864316020049

Deng, X., Huang, Y., Xu, B., & Tao, L. (2023). Position and Attitude Tracking Finite-Time Adaptive Control for a VTOL Aircraft Using Global Fast Terminal Sliding Mode Control. *Mathematics*, *11*(12), 2732. https://doi.org/10.3390/math11122732

Dhadekar, D., & Talole, S. E. (2018). Robust Fault Tolerant Longitudinal Aircraft Control. *IFAC-PapersOnLine*, *51*, 604-609. https://doi.org/10.1016/j.ifacol.2018.05.101

Dong, J., & He, B. (2019). Novel Fuzzy PID-Type Iterative Learning Control for Quadrotor UAV. *Sensors*, *19*(1), 24. https://doi.org/10.3390/s19010024

Dong, T., Qin, C., Song, S., Wang, X., & Lei, Y. (2022). Autopilot Design and Analysis of Hypersonic Aircraft Based on Fractional-Order $$PI^\lambda D^\mu $$Control. Dans Y. Jia, W. Zhang, Y. Fu, Z. Yu, & S. Zheng (Éds), *Proceedings of 2021 Chinese Intelligent Systems Conference* (pp. 184-192). Singapore : Springer. https://doi.org/10.1007/978-981-16-6320-8_19

Edwards, C., Lombaerts, T., & Smaili, H. (Éds). (2010). *Fault Tolerant Flight Control: A Benchmark Challenge* (Vol. 399). Berlin, Heidelberg : Springer Berlin Heidelberg. https://doi.org/10.1007/978-3-642-11690-2

Eker, İ. (2006). Sliding mode control with PID sliding surface and experimental application to an electromechanical plant. *ISA Transactions*, *45*(1), 109-118. https://doi.org/10.1016/S0019-0578(07)60070-6

El-Nagar, A. M., & El-Bardini, M. (2014). Simplified interval type-2 fuzzy logic system based on new type-reduction. *Journal of Intelligent & Fuzzy Systems*, *27*(4), 1999-2010. https://doi.org/10.3233/IFS-141166

Fan, W., Liu, H. H. T., & Kwong, R. H. S. (2017). Gain-Scheduling Control of Flexible Aircraft with Actuator Saturation and Stuck Faults. *Journal of Guidance, Control, and Dynamics*, *40*(3), 510-520. https://doi.org/10.2514/1.G002222

Federal Aviation Administration. (2016). Chapter 6: Flight Controls. Dans *Pilot's Handbook of Aeronautical Knowledge* (pp. 1-12). (S.l.) : U.S. Department of Transportation FEDERAL AVIATION ADMINISTRATION.

Fei, J., & Feng, Z. (2019). Adaptive Fuzzy Super-Twisting Sliding Mode Control for Microgyroscope. *Complexity*, *2019*, 1-13. https://doi.org/10.1155/2019/6942642

Fei, J., Wang, Z., Liang, X., Feng, Z., & Xue, Y. (2022). Fractional Sliding-Mode Control for Microgyroscope Based on Multilayer Recurrent Fuzzy Neural Network. *IEEE Transactions on Fuzzy Systems*, *30*(6), 1712-1721. https://doi.org/10.1109/TFUZZ.2021.3064704

Fenfen, W., Xubo, L., Haiming, T., & Tong, Z. (2020). An Improved Auto-Disturbance Rejection Control Method for Hypersonic vehicle control system. Dans *2020 Chinese Control And Decision Conference (CCDC)* (pp. 3410-3415). Hefei, China : IEEE. https://doi.org/10.1109/CCDC49329.2020.9164687

Feng, C., & Liu, H. H.-T. (2023). Collision-free Path Planning and Control of Coordinated UAVs with Tethered Payloads. Dans *2023 IEEE Conference on Control Technology and Applications (CCTA)* (pp. 243-248). https://doi.org/10.1109/CCTA54093.2023.10253112

Fielding, C., Varga, A., Bennani, S., & Selier, M. (Éds). (2002). *Advanced Techniques for Clearance of Flight Control Laws* (Vol. 283). Berlin, Heidelberg : Springer Berlin Heidelberg. https://doi.org/10.1007/3-540-45864-6

Gad, A. G. (2022). Particle Swarm Optimization Algorithm and Its Applications: A Systematic Review. *Archives of Computational Methods in Engineering*, *29*(5), 2531-2561. https://doi.org/10.1007/s11831-021-09694-4

Gao, H., Chen, Z., Sun, M., Huang, J., Wang, Z., & Chen, Z. (2020). An efficient fast altitude control for hypersonic vehicle. *Control Engineering Practice*, *100*, 104426. https://doi.org/10.1016/j.conengprac.2020.104426

Gao, Y., Liu, J., Wang, Z., & Wu, L. (2019). Interval Type-2 FNN-Based Quantized Tracking Control for Hypersonic Flight Vehicles With Prescribed Performance. *IEEE Transactions on Systems, Man, and Cybernetics: Systems*, 1-13. https://doi.org/10.1109/TSMC.2019.2911726

Ghazi, G. (2014). *Développement d'une plateforme de simulation et d'un pilote automatique - application aux Cessna Citation X et Hawker 800XP*. masters. École Polytechnique de Montréal. Repéré à https://publications.polymtl.ca/1535/

Ghazi, G., & Botez, R. (2014). New robust control analysis methodology for Lynx helicopter and Cessna Citation X aircraft using Guardian Maps, Genetic Algorithms and LQR theories combinations. Dans *AHS 70th Annual Forum*. Montreal, Quebec, Canada.

Ghazi, G., & Botez, R. (2015a). Development of a High-Fidelity Simulation Model for a Research Environment (pp. 2015-01-2569). Communication présentée au SAE 2015 AeroTech Congress & Exhibition, Seattle,USA. https://doi.org/10.4271/2015-01-2569

Ghazi, G., & Botez, R. M. (2015b). Lateral controller design for the Cessna citation X with handling qualities and robustness requirements. Communication présentée au 62nd CASI Aeronautics Conference and AGM, Montreal, Quebec, Canada.

Ghazi, G., Botez, R., & Messi Achigui, J. (2015). Cessna Citation X Engine Model Identification from Flight Tests. *SAE International Journal of Aerospace*, *8*(2), 203-213. https://doi.org/10.4271/2015-01-2390

Ghazi, G., Rezk, K. G., & Botez, R. M. (2016). Cessna citation X pitch rate control design using guardian maps. Communication présentée au International Conference on Air Transport INAIR : Proceedings, Amsterdam, Netherlands.

Ghosh Roy, A., & Peyada, N. K. (2017). Aircraft parameter estimation using Hybrid Neuro Fuzzy and Artificial Bee Colony optimization (HNFABC) algorithm. *Aerospace Science and Technology*, *71*, 772-782. https://doi.org/10.1016/j.ast.2017.10.030

Gillespie, R. P. (1955). Principles of Mathematical Analysis. By Walter Rudin. Pp. x, 227. 40s. 1953. (McGraw-Hill) - Theory of Functions of Real Variable. By Henry P. Thielman. Pp. xiv, 209. 35s. 1953. (Butterworth Scientific Publications, London). *The Mathematical Gazette*, *39*(329), 258-259. https://doi.org/10.2307/3608793

Guardeño, R., López, M. J., & Sánchez, V. M. (2019). MIMO PID Controller Tuning Method for Quadrotor Based on LQR/LQG Theory. *Robotics*, *8*(2), 36. https://doi.org/10.3390/robotics8020036

Hagras, H., & Wagner, C. (2012). Towards the Wide Spread Use of Type-2 Fuzzy Logic Systems in Real World Applications. *IEEE Computational Intelligence Magazine*, *Volume 7, Issue 3*, 14-24. https://doi.org/10.1109/MCI.2012.2200621

Hai-Jun Rong, Guang-Bin Huang, Sundararajan, N., & Saratchandran, P. (2006). Fuzzy Fault Tolerant Controller for Actuator Failures during Aircraft Autolanding. Dans *2006 IEEE International Conference on Fuzzy Systems* (pp. 1200-1204). Vancouver, BC, Canada : IEEE. https://doi.org/10.1109/FUZZY.2006.1681862

Hakim, T. M. I., & Arifianto, O. (2018). Implementation of Dryden Continuous Turbulence Model into Simulink for LSA-02 Flight Test Simulation. *Journal of Physics: Conference Series*, *1005*(1), 012017. https://doi.org/10.1088/1742-6596/1005/1/012017

Hashemi, S. M., & Botez, R. M. (2022). Lyapunov-based Robust Adaptive Configuration of the UAS-S4 Flight Dynamics Fuzzy Controller. *The Aeronautical Journal*, 1-23. https://doi.org/10.1017/aer.2022.2

Hashemi, Seyed Mohammad, Botez, R. M., & Grigorie, L. T. (2020). Adaptive Fuzzy Control of Chaotic Flapping relied upon Lyapunov-based Tuning Laws. Dans *AIAA AVIATION 2020 FORUM*. Virtual Event : American Institute of Aeronautics and Astronautics. https://doi.org/10.2514/6.2020-3193

Hashemi, S.M., & Botez, R. M. (2022). Lyapunov-based Robust Adaptive Configuration of the UAS-S4 Flight Dynamics Fuzzy Controller. *The Aeronautical Journal*, *126*(1301), 1187-1209. https://doi.org/10.1017/aer.2022.2

Hassani, H., Mansouri, A., & Ahaitouf, A. (2024). Design and real-time implementation of a robust backstepping non-singular integral terminal sliding mode attitude control for a quadrotor aircraft. *Journal of Vibration and Control*, 10775463241240641. https://doi.org/10.1177/10775463241240641

Herzallah, R. (2005). Uncertainty in control problems: A survey. *IFAC Proceedings Volumes*, *38*(1), 82-90.

Hiliuta, A., Botez, R., & Brenner, M. (2005a). Approximation of Unsteady Aerodynamic Forcesby use of Fuzzy Techniques. Communication présentée au IASTED Modeling, Identification and Control, Innsbruck, Austria.

Hiliuta, A., Botez, R. M., & Brenner, M. (2005b). Approximation of Unsteady Aerodynamic Forces Q(k,M) by Use of Fuzzy Techniques. *AIAA Journal*, *43*(10), 2093-2099. https://doi.org/10.2514/1.13600

Hosseini, S., Ghazi, G., & Botez, R. M. (2023a). Application of Type One Adaptive Fuzzy Sliding Mode Control System for the Longitudinal Motion of the Cessna Citation X. Dans *AIAA AVIATION 2023 Forum*. San Diego, CA and Online : American Institute of Aeronautics and Astronautics. https://doi.org/10.2514/6.2023-3801

Hosseini, S., Ghazi, G., & Botez, R. M. (2023b). Design of a Type Two Fuzzy-based system to Control the Pitch Rate of the Cessna Citation X. Dans *AIAA AVIATION 2023 Forum*. San Diego, CA and Online : American Institute of Aeronautics and Astronautics. https://doi.org/10.2514/6.2023-3802

Hosseini, S., Inga, C., Ghazi, G., & Botez, R. M. (2023). Model-referenced Adaptive Flight Controller based on Recurrent Neural Network for the Longitudinal Motion of Cessna Citation X. Dans *AIAA AVIATION 2023 Forum*. San Diego, CA and Online : American Institute of Aeronautics and Astronautics. https://doi.org/10.2514/6.2023-3797

Hosseini, S. M., & Manthouri, M. (2022). Type 2 adaptive fuzzy control approach applied to variable speed DFIG based wind turbines with MPPT algorithm. *Iranian Journal of Fuzzy Systems*, *19*(1), 31-45. https://doi.org/10.22111/ijfs.2022.6549

Hosseini, Seyed Mohammad, Bematol, I., Ghazi, G., & Botez, R. M. (2024). Enhanced Fuzzy-Based Super-Twisting Sliding-Mode Control System for the Cessna Citation X Lateral Motion. *Aerospace*, *11*(7), 549. https://doi.org/10.3390/aerospace11070549

Hosseini, Seyed Mohammad, Ghazi, G., & Botez, R. M. (2024a). New Type-2-Fuzzy-Logic-Based Control System for the Cessna Citation X. *Journal of Aerospace Information Systems*, 1-19. https://doi.org/10.2514/1.I011398

Hosseini, Seyed Mohammad, Ghazi, G., & Botez, R. M. (2024b). Novel Controller Methodology for the Cessna Citation X Under Turbulence During Cruise. *Journal of Aerospace Information Systems*, 1-14. https://doi.org/10.2514/1.I011374

Humaidi, A. J., & Hasan, A. F. (2019). Particle swarm optimization–based adaptive super-twisting sliding mode control design for 2-degree-of-freedom helicopter. *Measurement and Control*, *52*(9-10), 1403-1419. https://doi.org/10.1177/0020294019866863

Hunt, T. M., Vaughan, N. D., & Warring, R. H. (1996). *The hydraulic handbook* (9th ed). Kidlington, Oxford, UK : Elsevier Advanced Technology.

Hušek, P., & Narenathreyas, K. (2016). Aircraft longitudinal motion control based on Takagi–Sugeno fuzzy model. *Applied Soft Computing*, *49*, 269-278. https://doi.org/10.1016/j.asoc.2016.07.038

Idir, A., Bensafia, Y., Khettab, K., & Canale, L. (2023). Performance improvement of aircraft pitch angle control using a new reduced order fractionalized PID controller. *Asian Journal of Control*, *25*(4), 2588-2603. https://doi.org/10.1002/asjc.3009

Ijaz, S., Fuyang, C., Hamayun, M. T., & Anwaar, H. (2021). Adaptive integral-sliding-mode control strategy for maneuvering control of F16 aircraft subject to aerodynamic uncertainty. *Applied Mathematics and Computation*, *402*, 126053. https://doi.org/10.1016/j.amc.2021.126053

Ingabire, A., & Sklyarov, A. A. (2019a). Control of longitudinal flight dynamics of a fixedwing UAV using LQR, LQG and nonlinear control. *E3S Web of Conferences*, *104*, 02001. https://doi.org/10.1051/e3sconf/201910402001

Ingabire, A., & Sklyarov, A. A. (2019b). Control of longitudinal flight dynamics of a fixedwing UAV using LQR, LQG and nonlinear control. *E3S Web of Conferences*, *104*, 02001. https://doi.org/10.1051/e3sconf/201910402001

Iqbal, S., Teodor, L., Botez, R., & Andrei, V. (2012). Fuzzy Logic Control of a Smart Actuation System in a Morphing Wing. Dans *Fuzzy Controllers- Recent Advances in Theory and Applications*. (S.l.) : InTech. https://doi.org/10.5772/48778

Islam, Md. T., Alam, Md. S., Laskar, Md. A. R., & Garg, A. (2016). Modeling and simulation of longitudinal autopilot for general aviation aircraft. Dans *2016 5th International Conference on Informatics, Electronics and Vision (ICIEV)* (pp. 490-495). Dhaka, Bangladesh : IEEE. https://doi.org/10.1109/ICIEV.2016.7760051

Jasim, O. A., & Veres, S. M. (2020). A robust controller for multi rotor UAVs. *Aerospace Science and Technology*, *105*, 106010. https://doi.org/10.1016/j.ast.2020.106010

Jiang, J., & Kamel, M. S. (2007). Pitch Control of an Aircraft with Aggregated Reinforcement Learning Algorithms. Dans *2007 International Joint Conference on Neural Networks* (pp. 41-46). Orlando, FL, USA : IEEE. https://doi.org/10.1109/IJCNN.2007.4370928

Jiao, R., Chou, W., Rong, Y., & Dong, M. (2020). Anti-Disturbance Control for Quadrotor UAV Manipulator Attitude System Based on Fuzzy Adaptive Saturation Super-Twisting Sliding Mode Observer. *Applied Sciences*, *10*(11), 3719. https://doi.org/10.3390/app10113719

Jiao, X., Fidan, B., Jiang, J., & Kamel, M. (2019). Type-2 fuzzy adaptive sliding mode control of hypersonic flight. *Proceedings of the Institution of Mechanical Engineers, Part G: Journal of Aerospace Engineering*, *233*(8), 2731-2744. https://doi.org/10.1177/0954410017712329

Jiao, X., & Jiang, J. (2015). Design of adaptive switching control for hypersonic aircraft. *Advances in Mechanical Engineering*, *7*(10), 168781401561046. https://doi.org/10.1177/1687814015610465

Jiao, X., & Jiang, J. (2016). Design of Interval Type-2 Fuzzy Sliding Mode Controller for Hypersonic Aircraft. *Journal of Automation and Control Engineering*, *4*(2), 123-126. https://doi.org/10.12720/joace.4.2.123-126

Jie, W., Xiaozhou, W., & Jinhuan, W. (2017). Trajectory tracking controller design for a quadrotor aircraft based on fuzzy sliding-mode control. Dans *2017 36th Chinese Control Conference (CCC)* (pp. 1354-1358). Dalian, China : IEEE. https://doi.org/10.23919/ChiCC.2017.8027539

Juang, J.-G., & Chiou, H.-K. (2006). Hybrid RNN-GA Controller for ALS in Wind Shear Condition. Dans *2006 IEEE International Conference on Systems, Man and Cybernetics* (pp. 675-680). Taipei, Taiwan : IEEE. https://doi.org/10.1109/ICSMC.2006.384463

Juang, J.-G., Chiou, H.-K., & Chien, L.-H. (2008). Analysis and comparison of aircraft landing control using recurrent neural networks and genetic algorithms approaches. *Neurocomputing*, *71*(16-18), 3224-3238. https://doi.org/10.1016/j.neucom.2008.04.044

K., W. B., G., P. M., & N., W. J. (2014). A modified genetic algorithm for UAV trajectory tracking control laws optimization. *International Journal of Intelligent Unmanned Systems*, *2*(2), 58-90. https://doi.org/10.1108/IJIUS-03-2014-0002

K. Wilburn, B., G. Perhinschi, M., & N. Wilburn, J. (2014). A modified genetic algorithm for UAV trajectory tracking control laws optimization. *International Journal of Intelligent Unmanned Systems*, *2*(2), 58-90. https://doi.org/10.1108/IJIUS-03-2014-0002

Kamalasadan, S., & Ghandakly, A. A. (2011). A Neural Network Parallel Adaptive Controller for Fighter Aircraft Pitch-Rate Tracking. *IEEE Transactions on Instrumentation and Measurement*, *60*(1), 258-267. https://doi.org/10.1109/TIM.2010.2047310

Kamalasadan, Sukumar, & Ghandakly, A. A. (2007). Multiple Fuzzy Reference Model Adaptive Controller Design for Pitch-Rate Tracking. *IEEE Transactions on Instrumentation and Measurement*, *56*(5), 1797-1808. https://doi.org/10.1109/TIM.2007.904550

Kanokmedhakul, Y., Pholdee, N., Bureerat, S., & Panagant, N. (2019). LQR Aircraft pitch controller design for handling disturbance using differential evolution. *Journal of Research and Applications in Mechanical Engineering*, *7*(2), 145-153. https://doi.org/10.14456/jrame.2019.14

Khalid, A., Zeb, K., & Haider, A. (2019). Conventional PID, Adaptive PID, and Sliding Mode Controllers Design for Aircraft Pitch Control. Dans *2019 International Conference on Engineering and Emerging Technologies (ICEET)* (pp. 1-6). Lahore, Pakistan : IEEE. https://doi.org/10.1109/CEET1.2019.8711871

Khalil, H. (2001). *Nonlinear Systems* (3rd edition). Upper Saddle River, N.J : Pearson.

Khan, Grigorie, Botez, Mamou, & Mébarki. (2019a). Fuzzy Logic-Based Control for a Morphing Wing Tip Actuation System: Design, Numerical Simulation, and Wind Tunnel Experimental Testing. *Biomimetics*, *4*(4), 65. https://doi.org/10.3390/biomimetics4040065

Khan, S., Grigorie, T. L., Botez, R. M., Mamou, M., & Mébarki, Y. (2019b). Fuzzy Logic-Based Control for a Morphing Wing Tip Actuation System: Design, Numerical Simulation, and Wind Tunnel Experimental Testing. *Biomimetics*, *4*(4), 65. https://doi.org/10.3390/biomimetics4040065

Kodhanda, A., Kolhe, J. P., Zeru, T., & Talole, S. (2017). Robust aircraft control based on UDE theory. *Proceedings of the Institution of Mechanical Engineers, Part G: Journal of Aerospace Engineering*, *231*(4), 728-742. https://doi.org/10.1177/0954410016641617

Labbadi, M., Boukal, Y., & Cherkaoui, M. (2020). Path Following Control of Quadrotor UAV With Continuous Fractional-Order Super Twisting Sliding Mode. *Journal of Intelligent & Robotic Systems*, *100*(3), 1429-1451. https://doi.org/10.1007/s10846-020-01256-3

Labiod, S., Boucherit, M. S., & Guerra, T. M. (2005). Adaptive fuzzy control of a class of MIMO nonlinear systems. *Fuzzy Sets and Systems*, *151*(1), 59-77. https://doi.org/10.1016/j.fss.2004.10.009

Lai, G., Zhang, Y., Liu, Z., Wang, J., Chen, K., & Chen, C. L. P. (2022). Direct Adaptive Fuzzy Control Scheme With Guaranteed Tracking Performances for Uncertain Canonical Nonlinear Systems. *IEEE Transactions on Fuzzy Systems*, *30*(3), 818-829. https://doi.org/10.1109/TFUZZ.2021.3049902

Lee, C.-T., & Tsai, C.-C. (2010). Nonlinear adaptive aggressive control using recurrent neural networks for a small scale helicopter. *Mechatronics*, *20*(4), 474-484. https://doi.org/10.1016/j.mechatronics.2010.04.009

Lee, J., & Kim, Y. (2020). Neural network-based nonlinear dynamic inversion control of variable-span morphing aircraft. *Proceedings of the Institution of Mechanical Engineers, Part G: Journal of Aerospace Engineering*, *234*(10), 1624-1637. https://doi.org/10.1177/0954410019846713

Lee, S., Kim, B., Baik, H., & Cho, S.-J. (2022). A Novel Design and Implementation of an Autopilot Terrain-Following Airship. *IEEE Access*, *10*, 1-1. https://doi.org/10.1109/ACCESS.2022.3164737

LEVANT, A. (1993). Sliding order and sliding accuracy in sliding mode control. *International Journal of Control*, *58*(6), 1247-1263. https://doi.org/10.1080/00207179308923053

Li, H., Su, X., & Jiang, H. (2015). Asymmetric Variable Universe Adaptive Landing Fuzzy Controller for Carrier-Based Aircraft. *International Journal of Smart Home*, *9*(5), 31-40. https://doi.org/10.14257/ijsh.2015.9.5.04

Li, S., Wang, Y., & Tan, J. (2017). Adaptive and robust control of quadrotor aircrafts with input saturation. *Nonlinear Dynamics*, *89*(1), 255-265. https://doi.org/10.1007/s11071-017-3451-z

Li, Y. Q., & Lei, C. (2014). Adaptive Fuzzy Controller Design Based on Aircraft Model. *Applied Mechanics and Materials*, *556-562*, 2470-2473. https://doi.org/10.4028/www.scientific.net/AMM.556-562.2470

Lin, C.-M., & Boldbaatar, E.-A. (2015). Autolanding Control Using Recurrent Wavelet Elman Neural Network. *IEEE Transactions on Systems, Man, and Cybernetics: Systems*, *45*(9), 1281-1291. https://doi.org/10.1109/TSMC.2015.2389752

Lin, C.-M., & Hsu, C.-F. (2002). Recurrent Neural Network Adaptive Control of Wing-Rock Motion. *Journal of Guidance, Control, and Dynamics*, *25*(6), 1163-1165. https://doi.org/10.2514/2.4998

Liu, H., Liu, M., Wei, X., Song, Q. J., Ge, Y. J., & Wang, F. L. (2015). Auto altitude holding of quadrotor UAVs with Kalman filter based vertical velocity estimation. *Proceedings of the World Congress on Intelligent Control and Automation (WCICA)*, *2015*, 4765-4770. https://doi.org/10.1109/WCICA.2014.7053520

Liu, J., Sun, M., Chen, Z., & Sun, Q. (2019). Output feedback control for aircraft at high angle of attack based upon fixed-time extended state observer. *Aerospace Science and Technology*, *95*, 105468. https://doi.org/10.1016/j.ast.2019.105468

Liu, J., Sun, M., Chen, Z., & Sun, Q. (2020). Super-twisting sliding mode control for aircraft at high angle of attack based on finite-time extended state observer. *Nonlinear Dynamics*, *99*(4), 2785-2799. https://doi.org/10.1007/s11071-020-05481-1

Liu, M., Egan, G., & Santoso, F. (2015). Modeling, Autopilot Design, and Field Tuning of a UAV With Minimum Control Surfaces. *IEEE Transactions on Control Systems Technology*, *23*, 1-1. https://doi.org/10.1109/TCST.2015.2398316

Londhe, P. S., & Patre, B. M. (2019). Adaptive fuzzy sliding mode control for robust trajectory tracking control of an autonomous underwater vehicle. *Intelligent Service Robotics*, *12*(1), 87-102. https://doi.org/10.1007/s11370-018-0263-z

Lu, P., Liu, M., Zhang, X., Zhu, G., Li, Z., & Su, C.-Y. (2022). Neural Network Based Adaptive Event-Triggered Control for Quadrotor Unmanned Aircraft Robotics. *Machines*, *10*(8), 617. https://doi.org/10.3390/machines10080617

M. Rouyan, N., Varatharajoo, R., Eshghi, S., Junita Abdullah, E., & Suzuki, S. (2018). Aircraft pitch control tracking with sliding mode control. *International Journal of Engineering & Technology*, *7*(4.13), 62. https://doi.org/10.14419/ijet.v7i4.13.21330

MacKunis, W., Patre, P. M., Kaiser, M. K., & Dixon, W. E. (2010). Asymptotic Tracking for Aircraft via Robust and Adaptive Dynamic Inversion Methods. *IEEE Transactions on Control Systems Technology*, *18*(6), 1448-1456. https://doi.org/10.1109/TCST.2009.2039572

Mansoor Ahsan & Ali Hanif. (2014). A New Perspective to Altitude Acquire-and- Hold for Fixed Wing UAVs. Communication présentée au Student Research Paper Conference 2014, IST,Pakistan.

Matouk, D., Abdessemed, F., Gherouat, O., & Terchi, Y. (2020). SECOND-ORDER SLIDING MODE FOR POSITION AND ATTITUDE TRACKING CONTROL OF QUADCOPTER UAV: SUPER-TWISTING ALGORITHM. *International journal of innovative computing, information & control: IJICIC*, *16*, 29-43. https://doi.org/10.24507/ijicic.16.01.29

Maurino, D. E., & Salas, E. (2010). *Human factors in aviation* (2nd ed). Amsterdam Boston : Academic Press/Elsevier.

Melin, P., & Castillo, O. (1999). Intelligent adaptive control of aircraft dynamic systems with a new neuro-fuzzy-fractal approach. Dans *IJCNN'99. International Joint Conference on Neural Networks. Proceedings (Cat. No.99CH36339)* (Vol. 6, pp. 4208-4212). Washington, DC, USA : IEEE. https://doi.org/10.1109/IJCNN.1999.830840

Mitrinović, D. S., Pečarić, J. E., & Fink, A. M. (1993). Triangle Inequalities. Dans *Classical and New Inequalities in Analysis* (Vol. 61, pp. 473-513). (S.l.) : Springer, Dordrecht.

Mohammadzadeh, A., Sabzalian, M. H., Zhang, C., Castillo, O., Sakthivel, R., & El-Sousy, F. F. M. (2023). *Modern Adaptive Fuzzy Control Systems* (Vol. 421). Cham : Springer International Publishing. https://doi.org/10.1007/978-3-031-17393-6

Moncayo, H., Krishnamoorty, K., Wilburn, B., Wilburn, J., Perhinschi, M., & Lyons, B. (2013). Performance Analysis of Fault Tolerant UAV Baseline Control Laws with L1 Adaptive Augmentation. *Journal of Modeling, Simulation, Identification, and Control*, *1*(4), 137-163. https://doi.org/10.7726/jmsic.2013.1012-1

Moorhouse, D. J., & Woodcock, R. J. (1982). Background Information and User Guide for MIL-F-8785C, Military Specification - Flying Qualities of Piloted Airplanes. Repéré à https://apps.dtic.mil/sti/citations/ADA119421

Napolitano, M. R., & Kincheloe, M. (1995). On-line learning neural-network controllers for autopilot systems. *Journal of Guidance, Control, and Dynamics*, *18*(5), 1008-1015. https://doi.org/10.2514/3.21498

Nekoukar, V., & Mahdian Dehkordi, N. (2021). Robust path tracking of a quadrotor using adaptive fuzzy terminal sliding mode control. *Control Engineering Practice*, *110*, 104763. https://doi.org/10.1016/j.conengprac.2021.104763

Nelson, R. C. (1998). *Flight stability and automatic control* (2nd ed). Boston, Mass : WCB/McGraw Hill.

Nho, K., & Agarwal, R. K. (2000). Automatic Landing System Design Using Fuzzy Logic. *Journal of Guidance, Control, and Dynamics*, *23*(2), 298-304. https://doi.org/10.2514/2.4522

Nivison, S. A., & Khargonekar, P. P. (2017a). Development of a robust deep recurrent neural network controller for flight applications. Dans *2017 American Control Conference (ACC)* (pp. 5336-5342). Seattle, WA, USA : IEEE. https://doi.org/10.23919/ACC.2017.7963784

Nivison, S. A., & Khargonekar, P. P. (2017b). Development of a robust deep recurrent neural network controller for flight applications. Dans *2017 American Control Conference (ACC)* (pp. 5336-5342). Seattle, WA, USA : IEEE. https://doi.org/10.23919/ACC.2017.7963784

Oktay, T., & Kose, O. (2021). Hexarotor Longitudinal Flight Control with Deep Neural Network, PID Algorithm and Morphing. *European Journal of Science and Technology*. https://doi.org/10.31590/ejosat.946884

Pan, Y., Zhou, Y., Sun, T., & Er, M. J. (2013). Composite adaptive fuzzy H∞ tracking control of uncertain nonlinear systems. *Neurocomputing*, *99*, 15-24. https://doi.org/10.1016/j.neucom.2012.05.011

Park, J.-C., Roh, H., Lee, C.-H., Tahk, M.-J., Choi, H.-S., & Kim, S.-Y. (2023). Nonlinear Three-Loop Autopilot Design for Hypersonic Vehicles Considering Aerodynamic-Propulsion Dynamics Couplings. Dans *2023 14th International Conference on Mechanical and Aerospace Engineering (ICMAE)* (pp. 404-410). Porto, Portugal : IEEE. https://doi.org/10.1109/ICMAE59650.2023.10424637

Perez, A. E., Moncayo, H., Moguel, I., Perhinschi, M. G., Al Azzawi, D., & Togayev, A. (2014). Development of Immunity Based Adaptive Control Laws for Aircraft Fault Tolerance. Communication présentée au ASME 2014 Dynamic Systems and Control Conference, American Society of Mechanical Engineers Digital Collection. https://doi.org/10.1115/DSCC2014-5890

Perez, A. E., Moncayo, H., Moguel, I., Perhinschi, M. G., Azzawi, D. A., & Togayev, A. (2014). Development of Immunity Based Adaptive Control Laws for Aircraft Fault Tolerance. Dans *Proceedings of the ASME 2014 Dynamic Systems and Control Conference* (Vol. Volume 1, Aerospace Control Applications). San Antonio, Texas, USA. https://doi.org/10.1115/DSCC2014-5890

Perez, A. E., Moncayo, H., Perhinschi, M., Al Azzawi, D., & Togayev, A. (2015). A Bio-Inspired Adaptive Control Compensation System for an Aircraft Outside Bounds of Nominal Design. *Journal of Dynamic Systems, Measurement, and Control*, *137*(091012). https://doi.org/10.1115/1.4030613

Pratt, R. W. (Éd.). (2000). *Flight Control Systems: practical issues in design and implementation*. The Institution of Engineering and Technology, Michael Faraday House, Six Hills Way, Stevenage SG1 2AY, UK : IET. https://doi.org/10.1049/PBCE057E

Qi, Y., Zhu, Y., Wang, J., Shan, J., & Liu, H. H. T. (2021). MUDE-based control of quadrotor for accurate attitude tracking. *Control Engineering Practice*, *108*, 104721. https://doi.org/10.1016/j.conengprac.2020.104721

Qian, L., & Liu, H. H. T. (2020). Path-Following Control of A Quadrotor UAV With A Cable-Suspended Payload Under Wind Disturbances. *IEEE Transactions on Industrial Electronics*, *67*(3), 2021-2029. https://doi.org/10.1109/TIE.2019.2905811

Qian, L., & Liu, H. H. T. (2022). Robust Control Study for Tethered Payload Transportation Using Multiple Quadrotors. *Journal of Guidance, Control, and Dynamics*, *45*(3), 434-452. https://doi.org/10.2514/1.G006173

Qian Wang, & Stengel, R. F. (2005). Robust nonlinear flight control of a high-performance aircraft. *IEEE Transactions on Control Systems Technology*, *13*(1), 15-26. https://doi.org/10.1109/TCST.2004.833651

Qiu, J., Delshad, I. S., Zhu, Q., Nibouche, M., & Yao, Y. (2017). A U-model based controller design for non-minimum phase systems: Application to Boeing 747 altitude-hold autopilot. Dans *2017 9th International Conference on Modelling, Identification and Control (ICMIC)* (pp. 122-127). Kunming : IEEE. https://doi.org/10.1109/ICMIC.2017.8321624

Quintin, E., Andrianantara, R. P., Ghazi, G., & Botez, R. M. (2024). Neural Network Adaptive Controller with Approximate Dynamic Inversion for the Cessna Citation X Lateral Control. Dans *AIAA SCITECH 2024 Forum*. Orlando, FL : American Institute of Aeronautics and Astronautics. https://doi.org/10.2514/6.2024-0261

Raza, A., Malik, F. M., Khan, R., Mazhar, N., & Ullah, H. (2020). Robust output feedback control of fixed-wing aircraft. *Aircraft Engineering and Aerospace Technology*, *92*(8), 1263-1273. https://doi.org/10.1108/AEAT-04-2020-0067

Rehman, A. U., Khan, M. U., Ali, M. Z. H., Shah, M. S., Ullah, M. F., & Ayub, M. (2021). Stability Enhancement of Commercial Boeing Aircraft with Integration of PID Controller. Dans *2021 International Conference on Applied and Engineering Mathematics (ICAEM)* (pp. 43-48). Taxila, Pakistan : IEEE. https://doi.org/10.1109/ICAEM53552.2021.9547186

Resnick, C. S. (Carl S. (1991). *A method for robust control of systems with parametric uncertainty motivated by a benchmark example*. Thesis. Massachusetts Institute of Technology. (Accepted: 2008-09-03T15:52:41Z). Repéré à https://dspace.mit.edu/handle/1721.1/42507

Rong, H.-J., Han, S., & Zhao, G.-S. (2014). Adaptive fuzzy control of aircraft wing-rock motion. *Applied Soft Computing*, *14*, 181-193. https://doi.org/10.1016/j.asoc.2013.03.001

Roopaei, M., Zolghadri, M., & Meshksar, S. (2009). Enhanced adaptive fuzzy sliding mode control for uncertain nonlinear systems. *Communications in Nonlinear Science and Numerical Simulation*, *14*(9), 3670-3681. https://doi.org/10.1016/j.cnsns.2009.01.029

Roopaei, M., Zolghadri Jahromi, M., Ranjbar-Sahraei, B., & Lin, T.-C. (2011). Synchronization of two different chaotic systems using novel adaptive interval type-2 fuzzy sliding mode control. *Nonlinear Dynamics*, *66*(4), 667-680. https://doi.org/10.1007/s11071-010-9939-4

Sadik Aboud, W., S. Abd Al-Amir, H., A. Alhamdany, A., & M. Kadhim, F. (2023). Overcome uncertainties of vertical take-off and landing aircraft based on optimal sliding mode control. *Indonesian Journal of Electrical Engineering and Computer Science*, *29*(2), 703. https://doi.org/10.11591/ijeecs.v29.i2.pp703-714

Saggai, A., Zeghlache, S., Benyettou, L., & Djerioui, A. (2021). Fault Tolerant Control against Actuator Faults Based on Interval Type-2 Fuzzy Sliding Mode Controller for a Quadrotor Aircraft. Dans *2020 2nd International Workshop on Human-Centric Smart Environments for Health and Well-being (IHSH)* (pp. 181-186). Boumerdes, Algeria : IEEE. https://doi.org/10.1109/IHSH51661.2021.9378754

Sahbon, N., Jacewicz, M., Lichota, P., & Strzelecka, K. (2023). Path-Following Control for Thrust-Vectored Hypersonic Aircraft. *Energies*, *16*(5), 2501. https://doi.org/10.3390/en16052501

Santoso, F., Liu, M., & Egan, G. K. (2008). H2 and H∞ robust autopilot synthesis for longitudinal flight of a special unmanned aerial vehicle: a comparative study. *IET Control Theory & Applications*, *2*(7), 583-594. https://doi.org/10.1049/iet-cta:20070415

Sheikhhosseini, A., Moslehian, M. S., & Shebrawi, K. (2017). Inequalities for generalized Euclidean operator radius via Young's inequality. *Journal of Mathematical Analysis and Applications*, *445*(2), 1516-1529. https://doi.org/10.1016/j.jmaa.2016.03.079

Shen, S., & Xu, J. (2021). Adaptive neural network-based active disturbance rejection flight control of an unmanned helicopter. *Aerospace Science and Technology*, *119*, 107062. https://doi.org/10.1016/j.ast.2021.107062

Shi, Y., & Eberhart, R. (1998). A modified particle swarm optimizer. Dans *1998 IEEE International Conference on Evolutionary Computation Proceedings. IEEE World Congress on Computational Intelligence (Cat. No.98TH8360)* (pp. 69-73). https://doi.org/10.1109/ICEC.1998.699146

Shtessel, Y., Taleb, M., & Plestan, F. (2012). A novel adaptive-gain supertwisting sliding mode controller: Methodology and application. *Automatica*, *48*, 759-769. https://doi.org/10.1016/j.automatica.2012.02.024

Singh, D. J., Verma, N. K., Ghosh, A. K., & Malagaudanavar, A. (2022). An application of interval type-2 fuzzy model based control system for generic aircraft. *Applied Soft Computing*, *121*, 108721. https://doi.org/10.1016/j.asoc.2022.108721

Singh, P., Giri, D. K., & Ghosh, A. K. (2022). Robust backstepping sliding mode aircraft attitude and altitude control based on adaptive neural network using symmetric BLF. *Aerospace Science and Technology*, *126*, 107653. https://doi.org/10.1016/j.ast.2022.107653

Singh, P., Giri, D. K., & Ghosh, A. K. (2023). Robust sliding mode augmenting integral backstepping for lateral-directional control of a highly maneuverable aircraft. *Proceedings of the Institution of Mechanical Engineers, Part G: Journal of Aerospace Engineering*, *237*(10), 2428-2441. https://doi.org/10.1177/09544100231153433

Singh, P., Salahudden, Giri, D. K., & Ghosh, A. K. (2022). Attitude Control of Hansa-3 Aircraft with Perturbation Using Sliding-Mode Controller. Dans *2022 IEEE Aerospace Conference (AERO)* (pp. 1-9). Big Sky, MT, USA : IEEE. https://doi.org/10.1109/AERO53065.2022.9843547

Sir Elkhatem, A., Engin, S. N., Pasha, A. A., Rahman, M. M., & Pillai, S. N. (2021). Robust Control for Non-Minimum Phase Systems with Actuator Faults: Application to Aircraft Longitudinal Flight Control. *Applied Sciences*, *11*(24), 11705. https://doi.org/10.3390/app112411705

Slotine, J.-J. E., & Li, W. (1991). *Applied nonlinear control*. Englewood Cliffs, N.J : Prentice Hall.

Snyder, S., Zhao, P., & Hovakimyan, N. (2021). Adaptive control for linear parameter-varying systems with application to a VTOL aircraft. *Aerospace Science and Technology*, *112*, 106621. https://doi.org/10.1016/j.ast.2021.106621

Solomon Raj, K. D., & Kumar, P. R. (2015). Design and simulation of longitudinal autopilot modes for a conventional aircraft. Dans *2015 2nd International Conference on Electronics and Communication Systems (ICECS)* (pp. 1040-1046). Coimbatore, India : IEEE. https://doi.org/10.1109/ECS.2015.7124738

Stevens, B. L., Lewis, F. L., & Johnson, E. N. (2015). *Aircraft Control and Simulation: Dynamics, Controls Design, and Autonomous Systems, 3rd Edition*. (S.l.) : John Wiley & Sons. (Google-Books-ID: N4abCgAAQBAJ).

Suleiman, H. U., Mu'azu, M. B., Zarma, T. A., Salawudeen, A. T., Thomas, S., & Galadima, A. A. (2018). Methods of Chattering Reduction in Sliding Mode Control: A Case Study of Ball and Plate System. Dans *2018 IEEE 7th International Conference on Adaptive Science & Technology (ICAST)* (pp. 1-8). Acrraa Ghana. https://doi.org/10.1109/ICASTECH.2018.8506783

Sun, C., Gong, G., & Yang, H. (2020). Sliding Mode Control with Adaptive Fuzzy Immune Feedback Reaching Law. *International Journal of Control, Automation and Systems*, *18*(2), 363-373. https://doi.org/10.1007/s12555-019-0285-0

Suresh, S., Omkar, S. N., Mani, V., & Sundararajan, N. (2006). Direct Adaptive Neural Flight Controller for F-8 Fighter Aircraft. *Journal of Guidance, Control, and Dynamics*, *29*(2), 454-464. https://doi.org/10.2514/1.11954

Susanto, T., Bayu Setiawan, M., Jayadi, A., Rossi, F., Hamdhi, A., & Persada Sembiring, J. (2021). Application of Unmanned Aircraft PID Control System for Roll, Pitch and Yaw Stability on Fixed Wings (pp. 186-190). Communication présentée au 2021 International Conference on Computer Science, Information Technology, and Electrical Engineering (ICOMITEE), Banyuwangi, Indonesia : IEEE. https://doi.org/10.1109/ICOMITEE53461.2021.9650314

Swain, S., & Sarathi, P. (2017). Fuzzy Pi Adaptive Learning Controller for Controlling the Angle of Attack of an Aircraft. *International Journal of Advanced Computer Science and Applications*, *8*(5). https://doi.org/10.14569/IJACSA.2017.080518

Taha, H., Bayuomi, M., El-Bayoumi, G., & Hassan, S. (2009). Model Reference Adaptive Flight Path Stabilization for Altitude and Velocity Hold. *International Conference on Aerospace Sciences and Aviation Technology*, *13*(AEROSPACE SCIENCES), 1-15. https://doi.org/10.21608/asat.2009.23748

Tao, Y., Xie, G., Chen, Y., Xiong, H., Liu, H., Zheng, J., & Gao, J. (2016). A PID and fuzzy logic based method for Quadrotor aircraft control motion. *Journal of Intelligent & Fuzzy Systems*, *31*(6), 2975-2983. https://doi.org/10.3233/JIFS-169182

Tavoosi, J. (2020). A New Type-2 Fuzzy Sliding Mode Control for Longitudinal Aerodynamic Parameters of a Commercial Aircraft. Dans *Journal Européen des Systèmes Automatisés* (Vol. 53, pp. 479-485). https://doi.org/10.18280/jesa.530405

Theis, J., Ossmann, D., Thielecke, F., & Pfifer, H. (2018). Robust autopilot design for landing a large civil aircraft in crosswind. *Control Engineering Practice*, *76*, 54-64. https://doi.org/10.1016/j.conengprac.2018.04.010

Trifonov, M., Prochazka, K. F., & Krüger, S. (2019). Robust Control of an Input-redundant Aircraft against Atmospheric Disturbances and Actuator Faults. *International Journal of Mechanical Engineering and Robotics Research*, 905-910. https://doi.org/10.18178/ijmerr.8.6.905-910

Utkin, V., & Lee, H. (2006). CHATTERING PROBLEM IN SLIDING MODE CONTROL SYSTEMS. *IFAC Proceedings Volumes*, *39*(5), 1. https://doi.org/10.3182/20060607-3-IT-3902.00003

Utkin, V., Poznyak, A., Orlov, Y. V., & Polyakov, A. (2020). *Road Map for Sliding Mode Control Design*. Cham : Springer International Publishing. https://doi.org/10.1007/978-3-030-41709-3

Vandana A, Anusha Sanmathi S, Ipshita Chaturvedi, Sanjana Jaikumar, & T S Chandar. (2021). Neural Network based Robust Integrated Autopilot for an Aircraft. Dans *2021 IEEE 6th International Conference on Computing, Communication and Automation (ICCCA)* (pp. 231-236). Arad, Romania : IEEE. https://doi.org/10.1109/ICCCA52192.2021.9666325

Ventura, J. O., Morales, D. B., Oliver, J. P. O., & Quesada, E. S. E. (2023). Dynamic Sliding Mode Control With PID Surface for Trajectory Tracking of a Multirotor Aircraft. *IEEE Access*, *11*, 99878-99888. https://doi.org/10.1109/ACCESS.2023.3314382

Vishal, & Ohri, J. (2014a). GA tuned LQR and PID controller for aircraft pitch control. Dans *2014 IEEE 6th India International Conference on Power Electronics (IICPE)* (pp. 1-6). Kurukshetra, India : IEEE. https://doi.org/10.1109/IICPE.2014.7115839

Vishal, & Ohri, J. (2014b). GA tuned LQR and PID controller for aircraft pitch control. Dans *2014 IEEE 6th India International Conference on Power Electronics (IICPE)* (pp. 1-6). Kurukshetra, India : IEEE. https://doi.org/10.1109/IICPE.2014.7115839

Vishnu G. Nair, Dileep M. V, & V. I. George. (2012). Aircraft Yaw Control System using LQR and Fuzzy Logic Controller. *International Journal of Computer Applications*, *45*(9), 25-30. https://doi.org/10.5120/6808-9150

Wang, C.-H., Liu, H.-L., & Lin, T.-C. (2002). Direct adaptive fuzzy-neural control with state observer and supervisory controller for unknown nonlinear dynamical systems. *Fuzzy Systems, IEEE Transactions on*, *10*, 39-49. https://doi.org/10.1109/91.983277

Wang, Lixin, Sun, X., Liu, H., Ma, J., Cheng, W., Tai, S., … Yue, T. (2024). Sliding Mode Flight Control Law Design Requirements for Oblique Wing Aircraft Based on Perturbation Theory. *Aerospace*, *11*(5), 366. https://doi.org/10.3390/aerospace11050366

Wang, Lu, & Su, J. (2015). Robust Disturbance Rejection Control for Attitude Tracking of an Aircraft. *IEEE Transactions on Control Systems Technology*, *23*(6), 2361-2368. https://doi.org/10.1109/TCST.2015.2398811

Wang, L.-X. (1994). *Adaptive Fuzzy Systems and Control: Design and Stability Analysis*. (S.l.) : PTR Prentice Hall. (Google-Books-ID: spIeAQAAIAAJ).

Wang, L.-X. (1997). *A course in fuzzy systems and control*. Upper Saddle River, NJ : Prentice Hall PTR. Repéré à http://books.google.com/books?id=wbJQAAAAMAAJ

Wang, Y., Wu, Q., & Liu, X. (2017). Adaptive Fuzzy Sliding Mode Control for MIMO Nonaffine Dutch-Roll System. *Journal of Dynamic Systems, Measurement, and Control*, *139*(101010). https://doi.org/10.1115/1.4036551

Wayne Durham. (2013). *Flight Dynamics and Control of Aero and Space Vehicles*. (S.l.) : John Wiley & Sons.

William Rankin, Ph.D. (2007). MEDA Investigation Process. *aeromagazine*, *ChapterQTR_02,*(26), 15-21. www.boeing.com/commercial/ aeromagazine. Repéré à boeing.com/commercial/ aeromagazine

Win, T., Nyunt, H. T. C., & Tun, H. M. (2019). Pitch Attitude Hold Autopilot for YTU EC-001 Fixed-Wing Unmanned Aerial Vehicle. Dans *2019 First International Symposium on Instrumentation, Control, Artificial Intelligence, and Robotics (ICA-SYMP)* (pp. 78-81). https://doi.org/10.1109/ICA-SYMP.2019.8646286

Wu, C., Liu, J., Jing, X., Li, H., & Wu, L. (2017). Adaptive Fuzzy Control for Nonlinear Networked Control Systems. *IEEE Transactions on Systems, Man, and Cybernetics: Systems*, *47*(8), 2420-2430. https://doi.org/10.1109/TSMC.2017.2678760

X, W. L. (1994). Adaptive Fuzzy Systems and Control. *Design and Stability Analysis*. Repéré à https://cir.nii.ac.jp/crid/1572543024115001984

Xin, M., & Pan, H. (2010). Robust Control of PVTOL Aircraft with a Nonlinear Optimal Control Solution. *Journal of Aerospace Engineering*, *23*(4), 265-275. https://doi.org/10.1061/(ASCE)AS.1943-5525.0000039

Xing, Z., & Ai, J. (2023). Fault-Tolerant Control for Carrier-Based Aircraft Based on Adaptive Fuzzy Sliding-Mode Method. *Applied Sciences*, *13*(23), 12685. https://doi.org/10.3390/app132312685

Xiong, S., & Liu, H. H.-T. (2023). Low-Altitude Fixed-Wing Robust and Optimal Control Using a Barrier Penalty Function Method. *Journal of Guidance, Control, and Dynamics*, *46*(11), 1-6. https://doi.org/10.2514/1.G007501

Xiu, C., Liu, F., & Xu, G. (2018). General model and improved global sliding mode control of the four-rotor aircraft. *Proceedings of the Institution of Mechanical Engineers, Part I: Journal of Systems and Control Engineering*, *232*(4), 383-389. https://doi.org/10.1177/0959651817708066

Yamina, B., Georges, G., Ruxandra Mihaela, B., & Florian, T. (2017a). New Methodology for Optimal Flight Control using Differential Evolution Algorithms applied on the Cessna Citation X Business Aircraft – Part 2. Validation on Aircraft Research Flight Level D Simulator. *INCAS BULLETIN*, *9*(2), 45-59. https://doi.org/10.13111/2066-8201.2017.9.2.4

Yamina, B., Georges, G., Ruxandra Mihaela, B., & Florian, T. (2017b). New Methodology for Optimal Flight Control using Differential Evolution Algorithms applied on the Cessna Citation X Business Aircraft – Part 2. Validation on Aircraft Research Flight Level D Simulator. *INCAS BULLETIN*, *9*(2), 45-59. https://doi.org/10.13111/2066-8201.2017.9.2.4

Yan, B., Dai, P., Liu, R., Xing, M., & Liu, S. (2019). Adaptive super-twisting sliding mode control of variable sweep morphing aircraft. *Aerospace Science and Technology*, *92*, 198-210. https://doi.org/10.1016/j.ast.2019.05.063

Yau, H.-T., & Chen, C.-L. (2006). Chattering-free fuzzy sliding-mode control strategy for uncertain chaotic systems. *Chaos, Solitons & Fractals*, *30*(3), 709-718. https://doi.org/10.1016/j.chaos.2006.03.077

Yeager, J. C. (1998). *Implementation and Testing of Turbulence Models for the F18-HARV Simulation* (Rapport No. NASA/CR-1998-206937). Haipton, VA United States : Lockheed Martin Corp. Repéré à https://ntrs.nasa.gov/citations/19980028448

Yedavalli, Rama K. (2020). *Flight Dynamics and Control of Aero and Space Vehicles*. (S.l.) : Hoboken, N.J. : John Wiley & Sons. Repéré à https://www.wiley.com/en-ca/Flight+Dynamics+and+Control+of+Aero+and+Space+Vehicles-p-9781118934456

Yedavalli, R.K. (2022). *Title: « Flight Dynamics and Control of Aero and Space Vehicles » by Rama K. YedavalliTextbook Authorship Published By Wiley in 2020 : Aerospace Series; ISBN 9781118934425*. (S.l.) : (s.n.).

Yoo, B., & Ham, W. (1998a). Adaptive fuzzy sliding mode control of nonlinear system. *IEEE Transactions on Fuzzy Systems*, *6*(2), 315-321. https://doi.org/10.1109/91.669032

Yoo, B., & Ham, W. (1998b). Adaptive fuzzy sliding mode control of nonlinear system. *IEEE Transactions on Fuzzy Systems*, *6*(2), 315-321. https://doi.org/10.1109/91.669032

Yu, X., Fu, Y., Li, P., & Zhang, Y. (2018). Fault-Tolerant Aircraft Control Based on Self-Constructing Fuzzy Neural Networks and Multivariable SMC Under Actuator Faults. *IEEE Transactions on Fuzzy Systems*, *26*(4), 2324-2335. https://doi.org/10.1109/TFUZZ.2017.2773422

Yu, Zhilong, Li, Y., Lv, M., Pei, B., Xu, W., & Bu, X. (2024). Fixed-Time Adaptive Fuzzy Fault-Tolerant Attitude Control for Tailless Aircraft Without Angular Velocity Measurements. *IEEE Transactions on Fuzzy Systems*, *32*(4), 2458-2470. https://doi.org/10.1109/TFUZZ.2024.3356577

Yu, Ziquan, Li, J., Xu, Y., Zhang, Y., Jiang, B., & Su, C.-Y. (2023). Reinforcement Learning-Based Fractional-Order Adaptive Fault-Tolerant Formation Control of Networked Fixed-Wing UAVs With Prescribed Performance. *IEEE Transactions on Neural Networks and Learning Systems*, 1-15. https://doi.org/10.1109/TNNLS.2023.3281403

Yu, Ziquan, Xu, Y., Zhang, Y., Jiang, B., & Su, C.-Y. (2023). Fractional-order fault-tolerant containment control of multiple fixed-wing UAVs via disturbance observer and interval type-2 fuzzy neural network. *International Journal of Robust and Nonlinear Control*, *33*(17), 10257-1027. https://doi.org/10.1002/rnc.6577

Yu, Ziquan, Yang, Z., Sun, P., Zhang, Y., Jiang, B., & Su, C.-Y. (2023). Refined fault tolerant tracking control of fixed-wing UAVs via fractional calculus and interval type-2 fuzzy neural network under event-triggered communication. *Information Sciences*, *644*, 119276. https://doi.org/10.1016/j.ins.2023.119276

Yu, Ziquan, Zhang, Y., Jiang, B., Su, C.-Y., Fu, J., Jin, Y., & Chai, T. (2022). Enhanced Recurrent Fuzzy Neural Fault-Tolerant Synchronization Tracking Control of Multiple Unmanned Airships via Fractional Calculus and Fixed-Time Prescribed Performance Function. *IEEE Transactions on Fuzzy Systems*, *30*(10), 4515-4529. https://doi.org/10.1109/TFUZZ.2022.3154441

Yu, Ziquan, Zhang, Y., Liu, Z., Qu, Y., & Su, C.-Y. (2019). Distributed adaptive fractional-order fault-tolerant cooperative control of networked unmanned aerial vehicles via fuzzy neural networks. *IET Control Theory & Applications*, *13*(17), 2917-2929. https://doi.org/10.1049/iet-cta.2018.6262

Zareb, E. M., Nouibat, W., Bestaoui, Y., Ayad, R., & Bouzid, Y. (2019). Evolutionary Autopilot Design Approach for UAV Quadrotor by Using GA. *Iranian Journal of Science and Technology, Transactions of Electrical Engineering*, *44*. https://doi.org/10.1007/s40998-019-00214-6

Zeghlache, S., Djerioui, A., Benyettou, L., Benslimane, T., Mekki, H., & Bouguerra, A. (2019). Fault tolerant control for modified quadrotor via adaptive type-2 fuzzy backstepping subject to actuator faults. *ISA Transactions*, *95*, 330-345. https://doi.org/10.1016/j.isatra.2019.04.034

Zeghlache, S., Ghellab, M., & Bouguerra, A. (2017). Adaptive Type-2 Fuzzy Sliding Mode Control Using Supervisory Type-2 Fuzzy Control for 6 DOF Octorotor Aircraft. *International Journal of Intelligent Engineering and Systems*, *10*(3), 47-57. https://doi.org/10.22266/ijies2017.0630.06

Zeghlache, S., Kara, K., & Saigaa, D. (2015). Fault tolerant control based on interval type-2 fuzzy sliding mode controller for coaxial trirotor aircraft. *ISA Transactions*, *59*, 215-231. https://doi.org/10.1016/j.isatra.2015.09.006

Zhang, Q., & Liu, H. (2018a). Aerodynamic model-based robust adaptive control for close formation flight. *Aerospace Science and Technology*, *79*. https://doi.org/10.1016/j.ast.2018.05.029

Zhang, Q., & Liu, H. H. T. (2018b). UDE-Based Robust Command Filtered Backstepping Control for Close Formation Flight. *IEEE Transactions on Industrial Electronics*, *65*(11), 8818-8827. https://doi.org/10.1109/TIE.2018.2811367

Zhang, W., Jia, J., Zhou, S., Guo, K., Yu, X., & Zhang, Y. (2023). A Safety Planning and Control Architecture Applied to a Quadrotor Autopilot. *IEEE Robotics and Automation Letters*, *8*(2), 680-687. https://doi.org/10.1109/LRA.2022.3230593

Zhang, X., Wang, Y., Zhu, G., Chen, X., Li, Z., Wang, C., & Su, C.-Y. (2021). Compound Adaptive Fuzzy Quantized Control for Quadrotor and Its Experimental Verification. *IEEE Transactions on Cybernetics*, *51*(3), 1121-1133. https://doi.org/10.1109/TCYB.2020.2987811

Zhao, W., Duan, Y., Yu, Z., Qu, Y., & Zhang, Y. (2021). Integrated Guidance and Control for Autonomous Rendezvous of Unmanned Aerial Vehicle During Aerial Refueling. Dans *2021 International Conference on Unmanned Aircraft Systems (ICUAS)* (pp. 814-820). Athens, Greece : IEEE. https://doi.org/10.1109/ICUAS51884.2021.9476886

Zheng, X., & Yang, X. (2020). Improved adaptive NN backstepping control design for a perturbed PVTOL aircraft. *Neurocomputing*, *410*, 51-60. https://doi.org/10.1016/j.neucom.2020.05.065

Zhou, J., Yang, F., & Wang, K. (2016). Fuzzy Arithmetic on LR Fuzzy Numbers with Applications to Fuzzy Programming. *Journal of Intelligent and Fuzzy Systems*, *30*, 71-87. https://doi.org/10.3233/IFS-151712

Zhou, L., Liu, L., Cheng, Z., Wang, B., & Fan, H. (2020). Adaptive dynamic surface control using neural networks for hypersonic flight vehicle with input nonlinearities. *Optimal Control Applications and Methods*, *41*(6), 1904-1927. https://doi.org/10.1002/oca.2584

Zhou, R., Wang, T., Yu, Z., & Zhang, Y. (2023). Event-Triggered Finite-Time Sliding-Mode Fault-Tolerant Containment Control of Multi-UAVs with Actuator Faults. Dans *2023 6th International Symposium on Autonomous Systems (ISAS)* (pp. 1-6). Nanjing, China : IEEE. https://doi.org/10.1109/ISAS59543.2023.10164317

Zhu, Q., & Yang, Z. (2019). Dynamic recurrent fuzzy neural network-based adaptive sliding control for longitudinal automatic carrier landing system. *Journal of Intelligent & Fuzzy Systems*, *37*(1), 53-62. https://doi.org/10.3233/JIFS-179063

Zhuang, H., Sun, Q., Chen, Z., & Zeng, X. (2021). Robust adaptive sliding mode attitude control for aircraft systems based on back-stepping method. *Aerospace Science and Technology*, *118*, 107069. https://doi.org/10.1016/j.ast.2021.107069

Zohreh Nejad, E. E., Aillot, P., Henry, C., Ghazi, G., & Botez, R. M. (2024). Cessna Citation X Ground Speed Control using Deep Reinforcement Learning. Dans *AIAA SciTech 2024 Forum* (Vol. AIAA 2024-2152). Orlando, FL. https://doi.org/10.2514/6.2024-2152